

OXIDATION OF DNA BY LONG-RANGE CHARGE TRANSPORT

Thesis by
Megan Elizabeth Núñez

In Partial Fulfillment
of the Requirements
for the Degree of Doctor of Philosophy

California Institute of Technology
Pasadena, California

2002

(Submitted August 1, 2001)

Acknowledgements

First of all, I have to express my deepest gratitude to Jackie Barton for her infinite patience and good humor. I know I can be a bit *challenging* at times, but she never let on that she wanted to smack me, no matter how much I deserved it. She always managed to pick me up out of my despair when I just couldn't make things work, and damn it, she was right about pretty near everything. Best of all, she brought together in the Barton group a wonderful group of people and made a little family of us, which has been the best part of the last five years.

I also thank lots of people who helped me out during the last few years:

Dan Hall, for figuring out that guanines could be oxidized from a distance, for babysitting me during my first few months in the group (which I am sure was very trying), and for being a great role model and friend.

Pete Dandliker, for letting me in on the thymine dimer repair fun! Also for the work we did together on the experiments in chapter 3, of which Pete did the experiments for Figure 3.2 and Table 3.2.

Katie Noyes, the best SURF there ever was. She performed a lot of the experiments that laid the groundwork for chapters 4 and 5. I know she will be a fantastic scientist, even if she would rather be ethanol precipitating. And don't worry, no actual puppies were harmed in the making of these experiments.

Diego Gianolio in Larry McLaughlin's group at Boston College, for making lots of NDI-tethered oligonucleotides, and always so quickly and nicely. If only all collaborations worked so well!

William Greenberg in the Dervan labs, who helped me figure out how to make my triplexes stick.

David Vicic and Duncan Odom for defending Pete's and my thymine dimer work with some very nice and expediently done experiments, and for letting me help out a little.

Karolin Luger at Colorado State, for telling me that palindromic 146-mers cannot be expressed in bacteria and must be ligated from 73-mers. Also for encouraging me with her keen interest to keep going with the nucleosomes.

Dr. Gerald Holmquist for letting me come into his lab at the City of Hope, take over a bench, and spend 2 and 1/2 years (off and on) doing experiments, with lots of friendly encouragement and useful questions to ponder. Thanks also to Ning Ye, Shu-mei Dai, and Steven Bates for their technical assistance, and Timothy O'Connor for the Fapy/EndoIII enzyme mixture.

Harry Gray, Doug Rees, and Rich Roberts for being a very supportive and involved committee. I know that, at a school like Tech, their help and encouragement are *not* the norm, and I deeply appreciate it. Also Barbara Imperiali, who was also a very valuable member of my committee during my first two years here, and Carl Parker who has always been a font of biology wisdom.

The Howard Hughes Medical Institute for a predoctoral fellowship, and the NIH and National Institute for Cancer Research for funding my projects.

Maureen Renta, for all the millions of little things that she did for me, even though we both knew she didn't have to.

The wonderful staff in this department for all of their help in so many ways, especially Dian Buchness, Guy Duremburg, and Tom Dunn.

All the members of the Barton group family who left before me, variously friends, mentors, and idols, including Michelle Arkin, Sonya Franklin, Marilena Fitzsimons Hall, Ai Ching Lim, Brian Jackson, Tim Johann, Kitty Erkkila, Scott Rajski, and Brian Hudson.

Eric Stemp, for being a mentor, advisor, friend and all-around Big-Brother-I-Never-Had. Elizabeth Boon, for being so much fun to share lab space with for four years, and for being a great person to talk to. I hope she will come visit me at Oxy a lot. Duncan Odom, for his kind generous heart and a crazy wild laugh. Life will be very tame without him. Kimberly Copeland for never telling me to just shut up already, even though I deserve it; for always having a smile and never complaining. Also for reading so many manuscripts, and taking care of Zoe and Tiramisu. Chris Treadway for his sense of humor in the dark of night and wee hours of morning. Pratip Bhattacharya for being such a nice person. Tashica Williams for her fantastic spirit! And Greg Drummond and Sarah Delaney, for reminding me that although my friends might graduate and move away, there are always new friends around the corner.

David Bickar, for showing me how much *fun* biochemistry could be, and for treating me like a grownup (even if I wasn't quite yet).

Donna Ebenstein, Nicole Dennis, Karen Ye, Sonali Garg, Chris Neale, Lauren Mills, Jaimie Houghton, and my other Smith friends. Even though they live far away, they have always been a constant source of support and reassurance and a shoulder to cry on, as necessary.

Marcus Sarofim, the best roommate in the world. I would never have made it through graduate school without him.

Linda Columbus, for everything. We've come a long way, baby!

My wonderful family, for being always encouraging but never pushy; for telling me all along that I could do anything I wanted to, and letting me figure out for myself what that would be.

And MOST IMPORTANT OF ALL, my partner-friend-husband Ben. I don't know how I got so lucky, to find someone with so much love and kindness and patience. Thank you.

Abstract

Ever since the double helical structure of DNA was elucidated, it has been proposed that charge might move through the stacked base pairs of the double helix because of the electronic coupling of the π orbitals of the nucleotide bases with neighboring bases. Here it is demonstrated that electronic “holes” generated by a one-electron oxidation of DNA can result in permanent lesions on guanine bases up to 200 Å away from the intercalating oxidant as a result of such charge migration. Both rhodium and ruthenium complexes, covalently tethered to the 5' end of a double-stranded oligonucleotide and intercalated into the base stack, can with photoactivation promote oxidation of guanines in 5'-GG-3' sites over this distance. Since charges can move efficiently through the DNA oligonucleotides, it was important to characterize this reaction in more detail, and to extend observations of charge transport through DNA to larger and more complicated DNA assemblies that more closely mimic its structure *in vivo*.

Long-range oxidative damage to guanine doublets in DNA is shown to compete for oxidation with other reactions, such as the repair of thymine dimers. When both thymine dimer lesions and guanine doublets are present, both can be oxidized by a photoexcited rhodium complex, although each in lower yield than in the absence of the other. While the 5-GG-3' may represent the thermodynamically favored site for oxidative reaction, repair of the thymine dimer appears to be kinetically more favorable. Therefore electronic “holes” generated on genomic DNA might not of necessity cause DNA damage, but could also be funneled onto proteins or other oxidizable sites.

Using a variety of intercalating photooxidants targeted to a specific site on a restriction fragment by an appended triplex-forming oligonucleotide, the upper distance limits and sequence effects on long-range charge transfer through DNA

were examined. Charge migration occurs in both directions from the intercalator and on both DNA strands of the target, but the oxidation is significantly more efficient to the 3' side of the triplex, over 25-38 base pairs. When intercalators were tethered directly to the 5' terminus of the triplex-forming strand as opposed to the center, significant amounts of oxidative damage was generated only in the immediate vicinity of the intercalation site, suggesting that the base stack is distorted at the 5' end of the triplex region in the duplex/triplex junction. Targeting of photooxidative damage by triplex formation extends previous studies of long-range charge transport to significantly longer DNA sequences through a strategy that does not require covalent attachment of the photooxidant to the DNA being probed.

Within eukaryotic cells most DNA is packaged as nucleosome core particles, made up of ~146 base pairs of DNA wrapped around a core of histone proteins. Photoexcited rhodium complexes were also used to explore charge transport through DNA within these structures. Although histone proteins inhibit intercalation of a noncovalent rhodium complex, they do not prevent oxidation of 5'-GG-3' sites, the signature of oxidative charge transport through DNA. Furthermore, some of these sites are not directly accessible to a solution-bound oxidant due to histones in the major groove, and thus they must be oxidized from a distance. Therefore, although the structure of the nucleosome core particle generally protects DNA from damage from solution-borne molecules, it does not protect the DNA from charge transfer damage through the base pair stack. In support of this assertion, guanine bases within nucleosomal DNA were oxidized at a distance of over 23 base pairs from a covalently-tethered rhodium intercalator.

The environment within the cell nucleus contains a variety of other proteins and small molecules that could potentially influence the migration of

charge through DNA. Using the rhodium photochemistry, the oxidation of guanine by photoexcited rhodium complexes inside of nuclei from cultured human cells was examined and compared with the oxidative damage on bare genomic DNA. Oxidation occurs preferentially at the 5'-guanine of 5'-GG-3' sites, indicative of base damage by DNA-mediated charge transport chemistry. Moreover, oxidative damage occurs at protein-bound sites which are inaccessible to rhodium. Thus, on transcriptionally active DNA within the cell nucleus, DNA-mediated charge transport acts to induce base damage from a distance. Direct interaction of an oxidant is not necessary to generate a base lesion at a specific site within the nucleus.

All of these observations indicate that charges can migrate along DNA within the cell. These observations require a reconsideration of cellular mechanisms for DNA damage and repair, and present new avenues for exploration in the design of DNA-based drugs and therapies.

Table of Contents

Acknowledgements	page ii
Abstract	v
Table of Contents	viii
List of Figures	xiv
List of Tables	xviii

Chapter 1: Long-Range Charge Transfer as a Mechanism for DNA**Damage**

1.1 Deoxyribonucleic Acid	page 2
1.2 Types and Mechanisms of DNA Damage	5
1.3 Evidence for Charge Transport through DNA	16
1.4 Chemistry at a Distance	30
1.5 Mechanism of Charge Transport through DNA	39
1.6 DNA Charge Transport and Proteins	41
1.7 DNA Damage and Charge Transport in the Cell	45
1.8 References	47

Chapter 2: Long-Range Oxidative Damage to DNA

2.1 Introduction	56
2.2 Methods	57
2.2.1 Oligonucleotide Preparation	57
2.2.2 Preparation of Short Metal-Containing Oligonucleotides	58
2.2.3 Preparation of Long Metal-Containing Oligonucleotides by Enzymatic Ligation	59

2.2.4 Irradiation of Metal-Containing Oligonucleotides	59
2.3 Results and Discussion	61
2.3.1 Distance Dependence of Guanine Oxidation on Long DNA Duplexes	61
2.3.2 Long-Distance Oxidation by Ruthenium(III)	62
2.3.3 Long-Distance Oxidation by Photoexcited Rh(III)	66
2.3.4 Comparison of Oxidation by $^*\text{Rh(III)}$ and Ru(III)	70
2.3.5 Temperature Dependence of Long-Distance Oxidation	70
2.3.6 Mechanism of Electron Transfer through DNA	74
2.4 References	77

**Chapter 3: Oxidative Charge Transfer to Repair Thymine Dimers
and Damage Guanine Bases in DNA Assemblies
Containing Tethered Metallointercalators**

3.1 Introduction	80
3.2 Methods	81
3.2.1 Materials	81
3.2.2 Preparation and Characterization of Oligonucleotides Containing a Thymine Dimer	81
3.2.3 HPLC Assay for Thymine Dimer Repair	83
3.2.4 PAGE Assay for Oxidative Damage	83
3.3 Results and Discussion	84
3.3.1 Sequence Construction	84
3.3.2 Determination of Rhodium Metallointercalator Binding Site by Photocleavage	86

3.3.3 Repair of Thymine Dimers in Duplex DNA by *Rh(III)	89
3.3.4 Dimer Repair and Oxidative Guanine Damage by Rhodium in a Duplex Containing both a Thymine Dimer and a 5'-GG-3' Site	97
3.3.5 Repair of a Thymine Dimer by a Ru(III) Intercalator	99
3.3.6 Oxidation of Guanine by Ru(III) through an Intervening Thymine Dimer	101
3.3.7 Factors Governing Simultaneous Dimer Repair and Guanine Oxidation	108
3.3.8 Implications with respect to Biological Charge Transport Mediated by DNA	112
3.4 References	114

**Chapter 4: Long-Range Guanine Oxidation in DNA Restriction
Fragments by a Triplex-Directed Naphthalene Diimide
Intercalator**

4.1 Introduction	118
4.2 Methods	122
4.2.1 Oligonucleotide Preparation	122
4.2.2 Preparation of Restriction Fragments with Triplex Binding Sites	122
4.2.3 End-Labeling of Restriction Fragments	122
4.2.4 Triplex Annealing	123
4.2.5 Irradiation and Visualization of Samples	123

4.3 Results and Discussion	124
4.3.1 Intercalator-DNA Conjugates	124
4.3.2 Targeting Rh(phi) ₂ bpy ³⁺ to a Single Specific Sequence by Triplex Formation	124
4.3.3 Oxidation of 5'-GG-3' Sites in DNA Duplexes by Naphthalene Diimide Intercalators	137
4.3.4 Long-Range Oxidative Damage to Guanine by NDI in Restriction Fragments	141
4.3.5 Probing Triplex Structure Using Long-Range Charge Transfer	152
4.3.6 Long-Range Oxidation in Restriction Fragments	156
4.4 References	158
 Chapter 5: Oxidative Charge Transport in Nucleosomes	
5.1 Introduction	162
5.2 Methods	166
5.2.1 Isolation of Histones	166
5.2.2 Preparation of Palindromic 146-mer	169
5.2.3 Formation of Nucleosome Core Particles with 146-mer	172
5.2.4 Photoirradiation of Nucleosomes and Bare DNA with Rh(phi) ₂ DMB ³⁺	173
5.2.5 DNase I Footprinting	174
5.2.6 Nucleosome Core Particle Structures	174
5.3 Results and Discussion	175
5.3.1 Structure of the Nucleosome Core Particle and Sequence of the Nucleosomal DNA	175

5.3.2 Confirmation of the Structure of the Nucleosome Core Particle by DNase I Footprinting	177
5.3.3 Binding and Oxidation by Noncovalent Rh(phi) ₂ DMB ³⁺ on a 146-mer	182
5.3.4 Binding and Oxidation by Rh(phi) ₂ bpy ³⁺ Tethered to the 5' Termini of the 146-mer	190
5.3.5 Oxidation of Guanine Bases by Charge Transport through the Base Stack in Nucleosomal DNA	198
5.4 References	203
 Chapter 6: Evidence for Charge Transport in the Nucleus	
6.1 Introduction	206
6.2 Methods	
6.2.1 Photoirradiations with Rh(phi) ₂ DMB ³⁺ and Isolation of DNA	209
6.2.2 Denaturing Agarose Gel Electrophoresis	211
6.2.3 Ligation-Mediated PCR Amplification of DNA	212
6.3 Results and Discussion	216
6.3.1 Photoirradiation of Cells, Nuclei, and Bare Genomic DNA with Rh(phi) ₂ DMB ³⁺	216
6.3.2 Direct Photocleavage and Guanine Base Oxidation in the p53 Gene	223
6.3.3 Direct Photocleavage and Guanine Base Oxidation in the PGK Promoter Region	227
6.4 References	238

Chapter 7: Long-Range Oxidative Charge Transport through DNA:**Summary and Conclusions**

7.1 Summary and Conclusions	241
7.2 References	247

List of Figures

Chapter 1

1.1 B-form DNA.	page 3
1.2 The structure of DNA.	4
1.3 Structures of thymine base lesions induced by exposure of DNA to ultraviolet light.	7
1.4 Products of hydrogen abstraction from the ribose sugar.	11
1.5 Base lesions formed by hydroxyl radicals.	13
1.6 The Fenton reaction.	14
1.7 Octahedral metallointercalators used to examine DNA-mediated charge transport spectroscopically.	21
1.8 Structure of a phi complex of rhodium bound to a DNA oligonucleotide.	23
1.9 A DNA monolayer.	29
1.10 DNA oligonucleotide assembly containing an appended metallointercalator.	31
1.11 Phi complexes of rhodium damage DNA according to two distinct mechanisms.	32
1.12 Molecules proposed to oxidize guanine bases from a distance along DNA.	34
1.13 The flash-quench cycle.	36
1.14 Structures of proteins that modulate charge transfer through DNA.	44

Chapter 2

2.1 Sequence and synthetic strategy for a metallointercalator-tethered 63- base-pair assembly.	60
---	----

2.2 Oxidation of the 5' guanine of guanine doublets by ground-state Ru(III).	63
2.3 Oxidation of the 5' guanine of guanine doublets by photoexcited Rh(phi) ₂ bpy ³⁺ .	67
2.4 Distance dependence of long-range guanine oxidation by Ru(III) and *Rh(III).	71
2.5 Temperature dependence of long-range guanine oxidation.	73

Chapter 3

3.1 DNA assembly with Rh(phi) ₂ bpy ³⁺ covalently tethered.	85
3.2 Direct photocleavage and guanine base oxidation by a tethered rhodium intercalator in various DNA assemblies.	87
3.3 Long-range thymine dimer repair in a DNA assembly containing a tethered rhodium intercalator.	90
3.4 Long-range thymine dimer repair over an 8-fold range of concentrations.	92
3.5 Absence of dimer repair by a noncomplementary rhodium strand.	95
3.6 Absence of thymine dimer repair by a ruthenium intercalator.	102
3.7 Long-range guanine oxidation by Ru(III) in a DNA assembly containing a thymine dimer.	105
3.8 Proposed mechanisms for thymine dimer repair and guanine oxidation by an excited-state rhodium oxidant.	109

Chapter 4

4.1 Base triplex in triple helices with a pyrimidine motif.	120
4.2 Structures of intercalating photooxidants and oligonucleotide	

conjugates used in this study.	125
4.3 Sequence of the target restriction fragments.	127
4.4 Direct photocleavage at 313 nm of a restriction fragment by Rh(phi) ₂ bpy ³⁺ covalently tethered to a triplex-forming oligonucleotide.	129
4.5 DNase I footprinting of a 17-mer triplex-forming oligonucleotide bound to a restriction fragment.	132
4.6 Oxidation of a restriction fragment by a photoexcited rhodium intercalator covalently tethered to a triplex-forming oligonucleotide.	134
4.7 Oxidation of a short oligonucleotide duplex by noncovalent NDI.	138
4.8 Long-range oxidation of guanine bases by the triplex-directed NDI intercalator.	143
4.9 Oxidation of guanine bases on two target restriction fragments and a control fragment.	145
4.10 Oxidation of guanine bases on a target restriction fragment and a control fragment.	148
4.11 Histogram showing sites of significant base oxidation by triplex- directed NDI on target restriction fragments.	150

Chapter 5

5.1 Structure of the nucleosome core particle.	164
5.2 Denaturing SDS polyacrylamide gel of isolation of chicken erythrocytes.	170
5.3 DNase I digestion of duplex 1 with and without bound histone proteins.	178
5.4 Cleavage of histone-bound duplex 1 superimposed upon the crystal structure of the same sequence in the nucleosome core particle.	181

5.5 Direct strand scission and base oxidation by $\text{Rh}(\text{phi})_2\text{DMB}^{3+}$ on duplex 1 with and without histone proteins.	184
5.6 Direct strand scission and base oxidation by varying concentrations of $\text{Rh}(\text{phi})_2\text{DMB}^{3+}$ on duplex 1 with and without histone proteins.	187
5.7 Long-range oxidation of 5'-GG-3' sites by a covalently-tethered rhodium complex.	192
5.8 Long-range oxidation of 5'-GG-3' sites in the presence and absence of histone proteins at a range of temperatures.	196
5.9 Oxidation of guanine doublets in nucleosomal DNA by rhodium metallointercalators.	200
 Chapter 6	
6.1 Mechanisms of DNA photocleavage by $\text{Rh}(\text{phi})_2\text{DMB}^{3+}$.	208
6.2 LMPCR amplification of DNA.	213
6.3 Denaturing agarose gels for analysis of DNA cleavage efficiency.	218
6.4 Ligation-mediated PCR amplification of cellular, nuclear, and bare genomic DNA.	221
6.5 DNA damage promoted by photoactivated $\text{Rh}(\text{phi})_2\text{DMB}^{3+}$ on exon 5 of the p53 gene inside of isolated nuclei.	224
6.6 Assay for oxidation of guanine by a distance by $\text{Rh}(\text{phi})_2\text{DMB}^{3+}$ inside of isolated nuclei.	226
6.7 Sequence of a part of the upstream promoter region of PGK1.	228
6.8 LMPCR-amplified DNA cleavage after treatment of bare DNA or nuclei with rhodium and photoactivation.	230
6.9 Binding and base damage by a rhodium metallointercalator in the PGK promoter region.	233

List of Tables

Chapter 1

1.1 Studies of photoinduced electron transfer through DNA.	19
--	----

Chapter 3

3.1 Long-range thymine dimer repair in duplexes with tethered rhodium.	98
3.2 Long-range guanine damage in duplexes with tethered rhodium.	100

Chapter 5

5.1 Buffers for nucleosome isolation from chicken erythrocytes.	167
5.2 146-base-pair duplex assemblies formed by ligation of shorter oligonucleotides.	171
5.3 Sequences of half of palindromic DNA oligonucleotide assemblies.	176
5.4 Long-range guanine oxidation by covalently-tethered rhodium complexes.	194

Chapter 6

6.1 Ligation-mediated PCR primers.	214
------------------------------------	-----

Chapter 1

Long-Range Charge Transfer as a Mechanism for DNA Damage

1.1 Deoxyribonucleic Acid

Deoxyribonucleic acid (DNA) is our genetic material, used to store the information encoding all of our ribonucleic acids and proteins and to detail the instructions by which each of our cells is made and maintained (1). Unlike other cellular machinery and structural components such as proteins and lipids, which can be disposed of and replaced when damaged, the DNA “blueprint” cannot be replaced. Furthermore, once the sequence of the DNA has been changed, all of the products made from the DNA will also be changed. As a result, any modifications to DNA, intentional or otherwise, can have dramatic consequences for the fate of a cell or organism. Damage to DNA can lead to mutations, carcinogenesis, and cell death. Cells go to great lengths to protect DNA from modification and to repair damage when it occurs, but nonetheless, mutations happen. Because of the potentially dramatic effects of modifications to DNA, it is of great interest to study the mechanisms by which damage to DNA can occur.

The structure of DNA was first elucidated by Watson and Crick in 1953 (2). Although the structure of DNA can vary considerably based on the sequence and environment, the structure that they described, now called B-form DNA, is generally considered to represent the most common conformation of DNA (3). DNA *in vivo* is comprised of two linear polymer molecules bound in an antiparallel fashion to form a right-handed helix (Fig. 1.1). Each polymer is composed of repeating nucleotide units, each composed of a deoxyribose sugar, a phosphate moiety, and a nucleotide base, either thymine, cytosine, guanine, or adenine (Fig. 1.2). The repeating sugar-phosphate units form the external backbone of the helix, while the aromatic heterocyclic base pairs stack to form the core. The base pairing is highly specific, in that thymine pairs stably with only adenine and guanine with cytosine. Each base pair is stacked parallel to its neighbors, with an internuclear separation of approximately 3.4 Å and a relative twist of approximately 36°. The conformation of

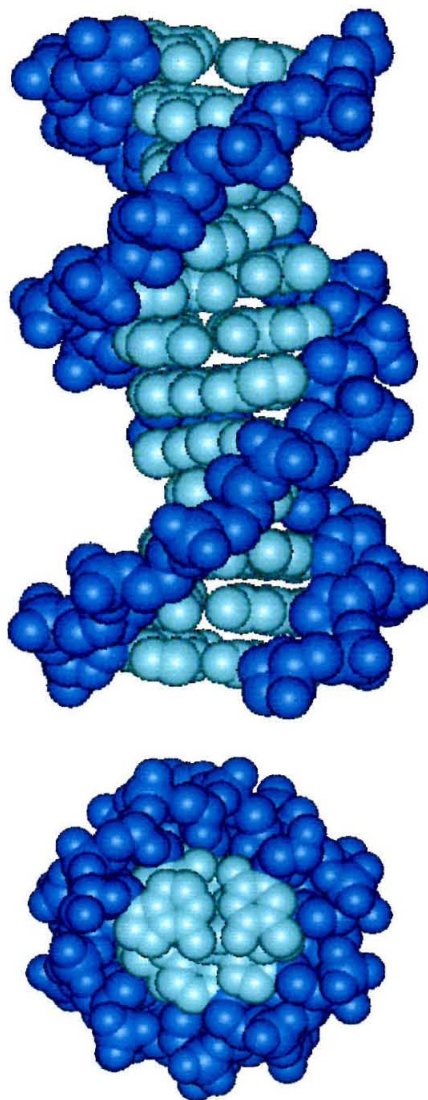


Figure 1.1: B-form DNA. The polyanionic sugar phosphate backbones are shown in blue and the heterocyclic, aromatic DNA base pairs in cyan. The base pairs are stacked on one another along the center of the helix with a 3.4 Å separation between neighboring base pairs and a 36° twist, giving a periodicity of 10 base pairs per turn of the helix. Two grooves are formed between the sugar phosphate backbone: the major groove, which is wide and shallow and contains specific functional groups contributed by the bases, and the minor groove, which is narrow and deep and predominantly hydrophobic in character.

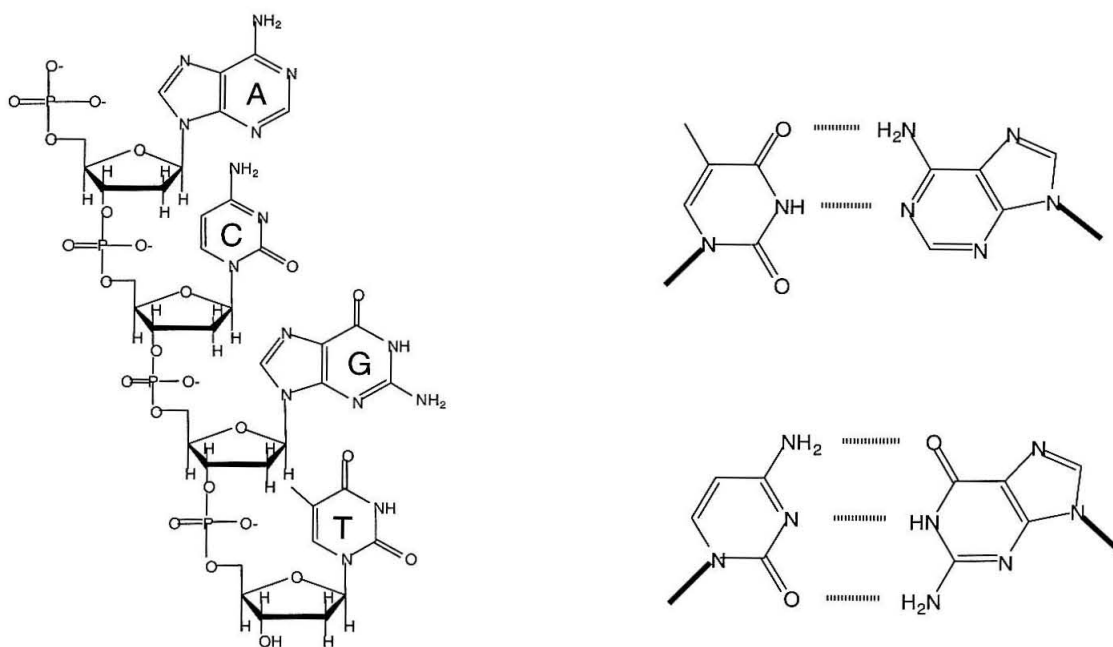


Figure 1.2: Structure of DNA. Individual DNA nucleotides, composed of a phosphate, a ribose sugar, and a nucleotide base, are connected by phosphodiester bonds to form a linear polymer (left). In B-form DNA, the two polymer strands are connected *via* specific hydrogen bonds between the base pairs. Thymine forms two hydrogen bonds with adenine (top right), and cytosine forms three hydrogen bonds with guanine (bottom right).

the nucleotides and the helical twist of the paired polymers generates two grooves between the backbones. The wider major groove contains along its bottom the functional groups projecting from edges of the nucleotide bases, and the deep, narrower minor groove is mostly hydrophobic.

This structure of DNA provides a simple picture of our genetic molecule. It is important to remember, however, that DNA does not quite look like this picture inside of living cells. The structure of DNA can vary based on sequence and environment. Some sequences, such as repeating 5'-TA-3' base steps, are inherently more flexible than others (4), and other sequences, such as poly-A tracts, can induce sharp bends in the DNA (5). Alternating GC sequences in the presence of high salt can revert to a left-handed Z-form helix (3). Furthermore, in humans, roughly three billion base pairs of DNA, or about 1 meter of DNA, are packaged into a nucleus roughly 50 μm in diameter (6). Several levels of compaction are necessary to fit the DNA into such a small space. Additionally, about half of the mass of the nucleus composed of proteins, including proteins to replicate, store, transcribe, and repair the DNA. These proteins bind to the DNA, changing its shape, stacking, and accessibility, among other parameters. It is within this more complicated and dynamic picture that we must examine the mechanisms of damage to DNA.

1.2 Types and Mechanisms of DNA Damage

Mutations to DNA can arise from a variety of sources, both endogenous and exogenous (1). The products of these alterations, especially base mismatches and modified bases, cause mistakes during transcription leading to mutant proteins, or more seriously cause mispairing during replication and permanent changes in the daughter DNA. Other DNA modifications, especially large covalent adducts and cross-links, are disruptive to transcription and replication, and may halt these processes altogether.

Spontaneous alterations to the DNA code in the absence of exogenous factors can result from accidental misincorporation, loss of bases, and deamination of bases (1). One of the most common sources of mutation is misincorporation, in which the wrong base can be accidentally misincorporated by a polymerase during the process of replication or repair, leading to a mismatched base pair (7). Although the correct base may be favored by only two or three kilocalories per mole, DNA polymerases are quite selective and generally contain a 3'->5' exonuclease activity as well, giving them error frequencies of only 1 base in a million or so as estimated in *E.coli*. A variety of accessory proteins and mismatch correction proteins are also available, further improving the fidelity of DNA pairing by several orders of magnitude. Loss of bases occurs by a spontaneous hydrolysis of the glycosidic linkage to the nucleotide base, leading to an abasic site (8). This base loss is faster at lower pH's and higher temperatures, and is faster for purines than pyrimidines and in single-stranded DNA than double-stranded DNA. Finally, the exocyclic amine groups of cytosine, adenine, guanine, and 5-methyl-cytosine can be lost spontaneously to generate uracil, hyoxanthine, xanthine, and thymine in the place of the original base. During replication or transcription, inappropriate bases can be placed opposite of these abasic sites and modified bases, generating permanent mutations of the base pair sequence.

Ultraviolet light is an exogenous source of damage to DNA. Although ultraviolet light below ~320 nm is absorbed by the ozone layer, the small bit of higher-energy light which does penetrate the atmosphere can modify DNA. Photoexcitation of DNA near its absorption maximum around 260 nm generates pyrimidine dimer lesions, in which adjacent pyrimidines become linked covalently by the formation of a cyclobutane ring between the 5,6 double bonds of each (Fig. 1.3) (9). Thymine-thymine dimers are the most common variety. There are multiple isomeric forms, four of which (*cis-anti*, *trans-syn*, *trans-anti*, and most commonly

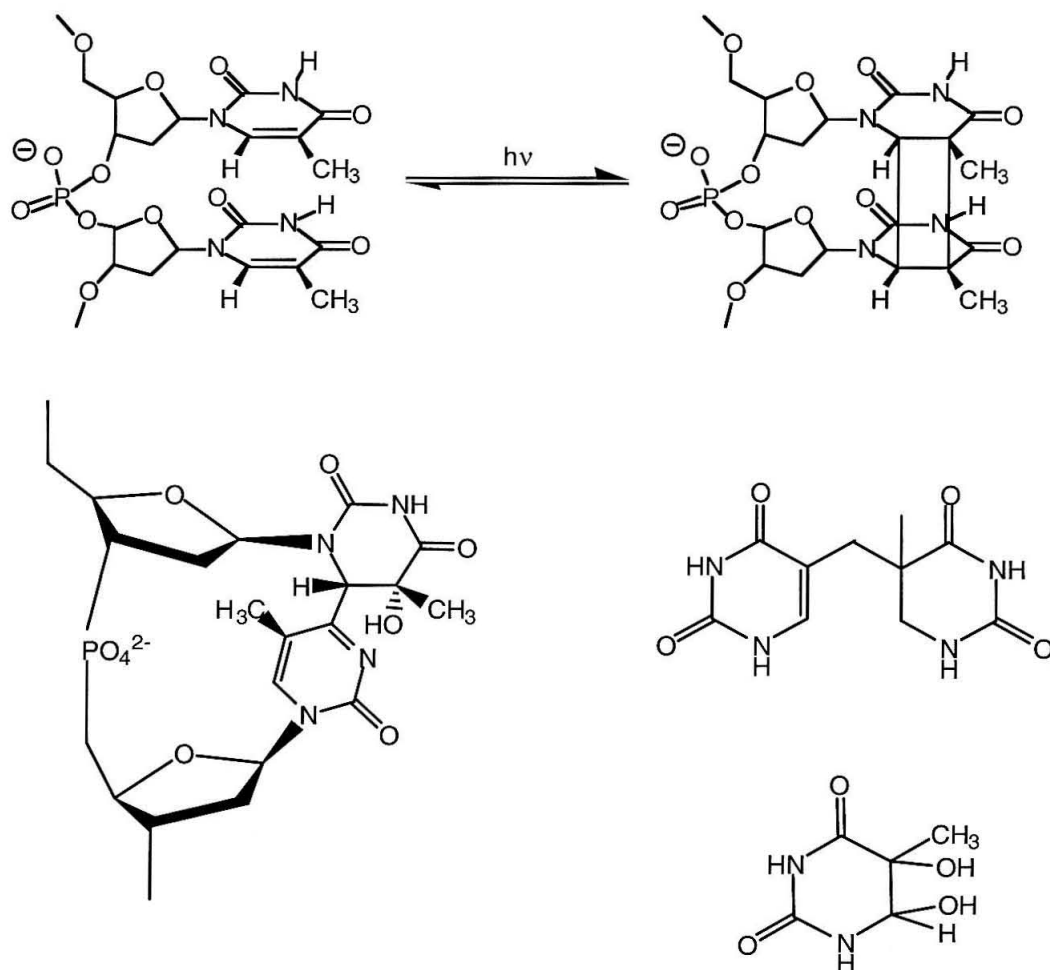
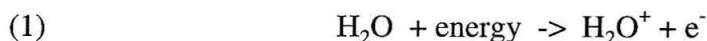


Figure 1.3: Structures of thymine base lesions induced by exposure of DNA to ultraviolet light. Cis-syn thymine cyclobutane dimer lesions (top) are one of the most common types of lesions, but 6-4 photoproducts (left), 5'-thyminylyl-5,6-dihydrothymine "spore" photoproducts (center right), and thymine glycol lesions (bottom right) also are generated by photoexcitation of DNA around 260 nm.

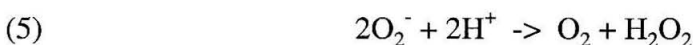
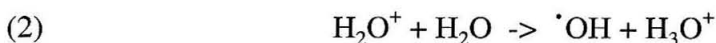
cis-syn) are favored due to the conformation of the DNA. A more distorted thymine dimer lesion, the (6,4) pyrimidine-pyrimidone photoproduct, can also be formed, as well as DNA-protein crosslinks, direct strand breaks, and a variety of minor lesions, such as thymine glycols, pyrimidine hydrates, and the “spore photoproduct” 5'-thyminyl-5,6-dihydrothymine (Fig. 1.3). Ultraviolet light at higher-energy wavelengths (193 nm) or at very high intensities can ionize the DNA bases directly, much like ionizing radiation (10). It should be noted, however, that *photoionization* processes are unlikely to be biologically relevant given the large atmospheric absorption at these wavelengths and the relatively low quantum yield of direct ionization relative to pyrimidine lesion formation.

Ionizing radiation is another exogenous source of DNA damage. X-rays and γ -rays generate damage on DNA either by ionizing DNA directly, or by ionizing other molecules which can then damage the DNA (11-12). Ionization of the DNA itself generates predominantly guanine cation radicals and cytosine anion radicals, due to the low ionization potential of guanine and the high electron affinity of cytosine, as well as base stacking and sequence effects and trapping via proton transfer across hydrogen bonds (13-16). Interestingly, since the energy of the ionizing radiation is assumed to be initially distributed randomly on the DNA, the localization of the cation radicals on guanine and the anion radicals on cytosine indicates that charges can move along the DNA, although it is not necessary that holes and electrons migrate over long distances to distribute themselves in this manner. At low temperatures (4-77K), electrons and holes have been proposed to migrate only a few bases before they become trapped, whereas at 200 K and above, charges to move over much longer distances, perhaps on the order of 75 base pairs (17,18). Charge migration is more efficient in double-stranded than single-stranded DNA (19, 20).

A large fraction of the ionizing radiation deposited on cells is absorbed by water, which abstracts electrons from water according to the following reaction:



Other reactive oxygen species (ROS), such as hydroxyl radical (21), peroxide, and superoxide can then be formed in reactions involving H_2O^+ and solvated electrons:



Hydroxyl and peroxide radicals propagate to generate other radicals by hydrogen abstraction through chain reactions:



where RH_2 can be a DNA base or sugar, a protein, lipid, or other molecule in the cellular milieu.

As a result of reactions with these various reactive oxygen species, a wide spectrum of products occurs due to treatment of DNA with ionizing radiation, including strand breaks, pyrimidine base lesions, and purine base lesions (11,22,23). Additionally, the excess electrons and holes can lead to a variety of damage products. The electrons and holes generated by direct ionization of the DNA bases can recombine, to generate no damage; be trapped by other oxidizing or reducing oxygen species, to form permanent base lesions; or abstract a hydrogen from a neighboring sugar, to generate a strand break. Single-strand breaks have been proposed to occur preferentially at guanine bases, due to the localization of the radical cation on guanine (24-26).

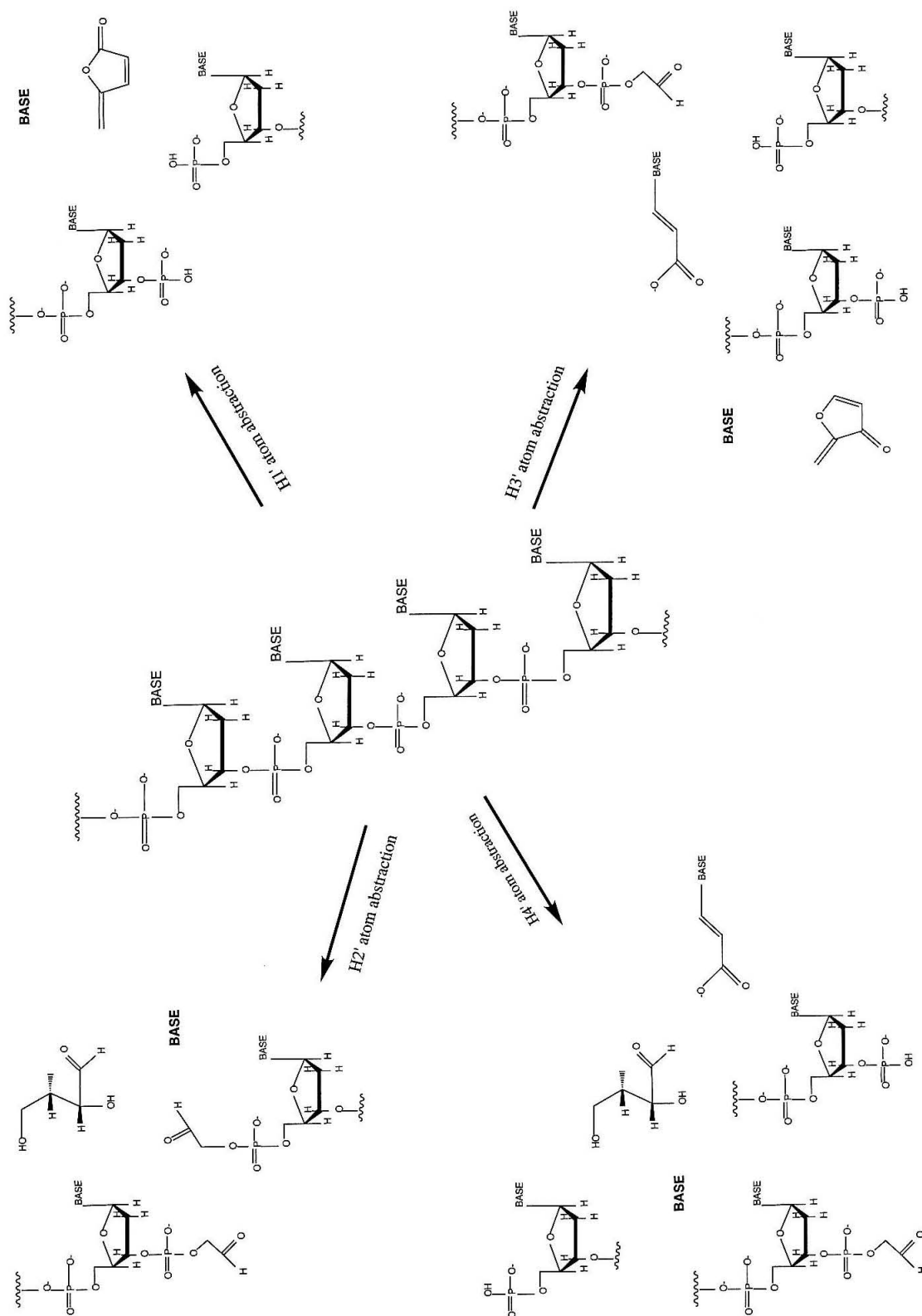
One of the most common sources of damage to nuclear DNA and other cellular macromolecules is ROS generated *endogenously* in the mitochondria as side products of oxygen reduction. DNA is generally inert to molecular oxygen because

this interaction is spin-forbidden, DNA being a singlet and molecular oxygen a triplet. However, DNA is quite reactive with radicals and singlet oxygen. Radical attack on the ribose residues of the DNA backbone leads to fragmentation of the sugar, loss of a base, or direct strand breaks with terminal sugar residues, depending on which hydrogen is abstracted (Fig. 1.4) (27). Hydroxyl radicals can also attack the DNA bases: attack on the C5-C6 thymine double bond subsequently generates thymine glycol, or on the C8 of guanine generates 8-hydroxyguanine (Fig. 1.5) (28). H_2O_2 , which is relatively inert by itself, can generate hydroxyl radicals in the presence of transition metal ions via the Fenton reaction (Fig. 1.6) (29). An imidazole ring-opened guanine derivative known as Fapy (2,6-diamino-4-hydroxy-5-formamidopyrimidine) and 8-hydroxyguanine are common products of peroxide treatment of DNA (Fig. 1.5). Singlet oxygen reacts predominantly with guanine bases, generating 8-hydroxyguanine (30).

A variety of small-molecule natural products and photosensitizers have also been shown to generate DNA damage. DNA can be covalently modified by a variety of electrophilic compounds to form unnatural base adducts (1). DNA is alkylated mono- or bifunctionally by reagents such as dimethyl sulfate, dimethyl nitrosamine, methylmethane sulfonate, and N-ethyl-N-nitrosourea at a variety of positions, especially the N7 of guanine and the N3 of adenine. Nitrogen mustards, cis-platin, and mitomycin, as well as the metabolically-activated aromatic amines and benzo[a]pyrene are examples of other electrophilic compounds which can covalently modify the DNA bases. The adducts formed are generally large and disruptive to normal processes on the DNA. (31-32).

DNA is also susceptible to modification by a variety of photoactivated small molecules (33). DNA photocleavage reagents can act by different mechanisms, including hydrogen abstraction from the ribose sugar, generation of ROS, singlet oxygen sensitization, and oxidation of the nucleotide bases by electron transfer (34),

Figure 1.4: Products of hydrogen abstraction from the ribose sugar. A variety of products can be formed, depending on which hydrogen is abstracted. The structure of the DNA (single- or double-stranded) and the presence or absence of oxygen can also influence the identity of the products (Adapted from 27).



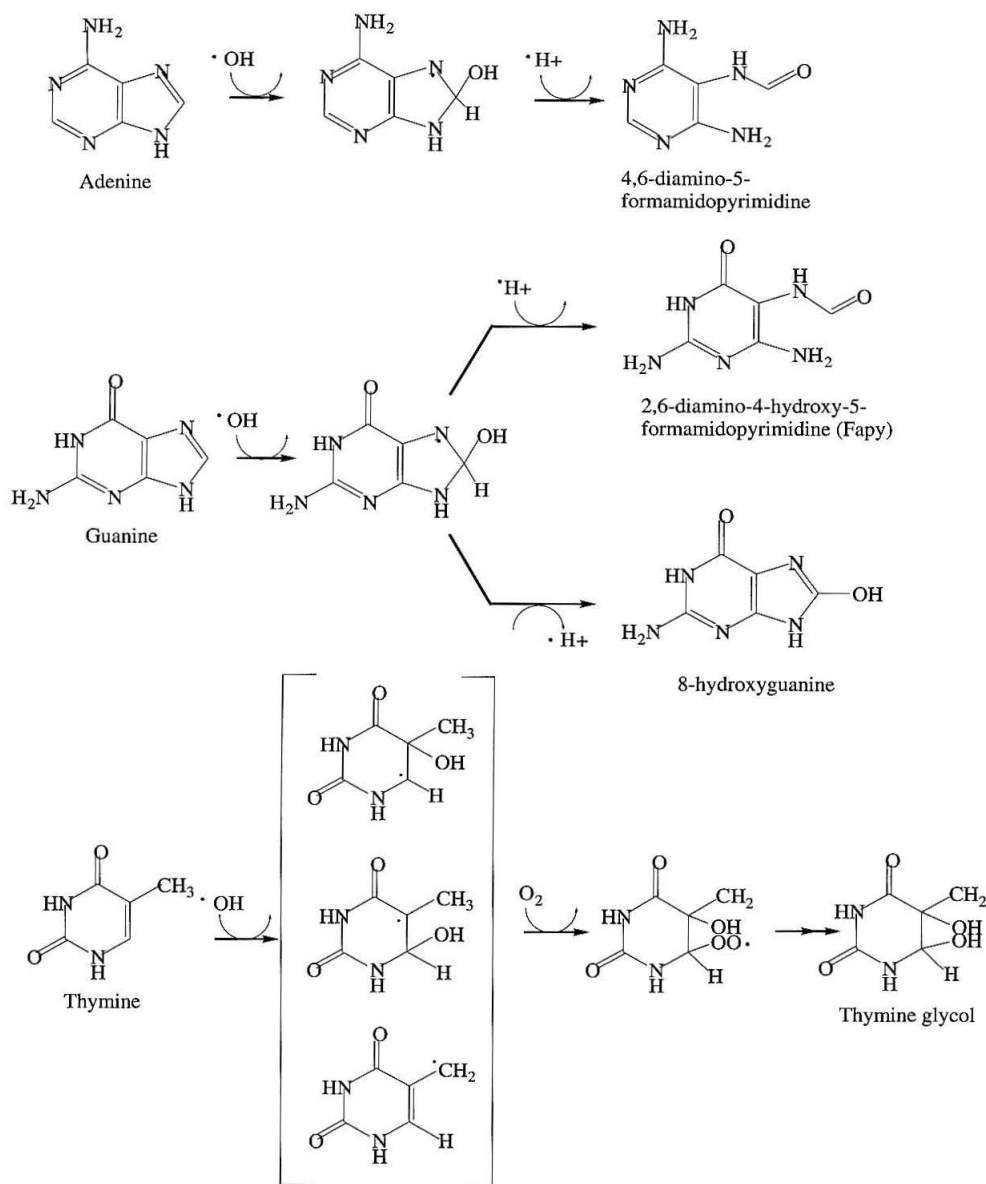


Figure 1.5: Base lesions formed by hydroxyl radicals. A variety of different lesions can be formed by hydroxyl radical attack on the DNA bases, some of which are shown here. The initial event generates a radical on the DNA base, which is trapped by an oxidation or a reduction of the base radical to form a stable, permanently-modified base.

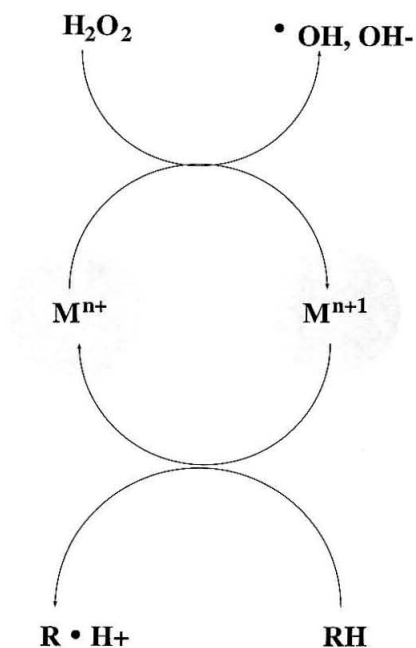


Figure 1.6: The Fenton reaction. Hydroxyl radicals are formed from hydrogen peroxide, catalyzed by transition metals. “R” can be any electron donor, commonly superoxide, ascorbate, or NADH.

and in fact many photocleavage reagents utilize more than one of the above mechanisms to damage DNA. Phi complexes of Rh(III), for example, can do both hydrogen abstraction and electron transfer chemistry (35). When irradiated at 313 nm, these Rh(III) metallointercalators undergo a ligand-to-metal charge transfer to form a phi cation radical, which can then abstract a hydrogen from a ribose at the binding site (36). The products of this reaction (a free base, a base propionic acid, and a 3' phosphoglycaldehyde group) are consistent with abstraction of the 3' hydrogen. When irradiated at 365 nm, some phi complexes of Rh(III) can also abstract an electron from bases on DNA, ultimately leading to the formation of permanent oxidized base lesions (35). Similarly, substituted anthraquinone molecules can damage DNA by hydrogen abstraction from a ribose sugar or electron transfer from guanine bases (37-39). Some polypyridyl ruthenium(II) complexes and porphyrin derivatives can generate singlet oxygen or oxidize DNA bases by electron transfer (40-42), while modified flavins can damage DNA by electron transfer and generation of ROS (43).

As detailed above, DNA can be modified in a staggering variety of ways, leading to any number of different kinds of damage lesions. Radicals can be generated on the DNA bases using ionizing radiation, high-energy ultraviolet light, reactive oxygen species, or photosensitizing oxidants. We describe here oxidative damage to DNA by long-range charge transport, wherein an electron is abstracted from the DNA at one place but damage is ultimately localized to a remote site. Given the number of different pathways in which a radical can be generated on the DNA bases, charge transport through DNA may in fact be a common mechanism by which DNA is damaged, although most experiments to date have explored charge transport with small DNA-binding molecules because it is easier to pinpoint the site of initial radical injection.

1.3 Evidence for Charge Transport through DNA

The question of whether double helical DNA provides an effective conduit for charge transport has fascinated scientists for forty years. In fact, Eley and Spivey said of DNA in 1962, "These paired base units are thus arranged like a pile of coins along the helix axis, and their interplane spacing of 3.4 Å is similar to that for graphite. It seemed, therefore, reasonable to suppose that a DNA molecule might behave as a one-dimensional aromatic crystal and show π -conductivity down the axis" (44). Therefore, the stacking of base not only confers stability to the polymeric assembly (3), but also may provide a basis for charge transport.

In the solid state, π -stacked arrays tend to be conductive along the stacking direction. Columnar stacks of planar aromatic heterocycles like porphyrins and phthalocyanins can conduct charge when fractional charges are generated on them by doping, electrochemistry, or pulse radiolysis (45-49). These solid-state π stacks display both high charge conductivity and a fast rate of electron transfer, with charge conductivities on the order of $10^{-6} \text{ m}^2/\text{Vs}$ and heterocycle-to-heterocycle hopping times faster than 1 ps. Conduction through these π -stacked arrays is dependent on the distance between heterocycles in the stack and upon the integrity of the π stack: longer heterocycle-to-heterocycle distances or increased disorder due to higher temperatures dramatically reduce conductivity. In contrast to these solid-state π stacks, double helical DNA provides a unique example of a π -stacked array in solution.

A diverse range of experiments has been carried out to probe the charge transport properties of DNA, but these experiments have yielded substantially differing conclusions. Physicists have tested the electrical conductivity of DNA, beginning with straightforward measurements carried out on ill-defined pellets, to more sophisticated studies on single molecules; their conclusions have ranged from DNA being an insulator to a quantum wire. Okahata *et al.* constructed films

containing aligned DNA molecules, and measured the current through the film when the DNA molecules aligned parallel or perpendicular to the electrodes (50). A large current which increased with increasing applied voltage was observed when the DNA molecules were aligned perpendicular to the electrodes, but almost no current was observed when the DNA was aligned parallel to the electrodes. Single-stranded DNA similarly did not conduct charge. These currents corresponded to a conductivity somewhat less than undoped conductive polymers such as polyacetylene. In contrast, Warman *et al.* measured the conductivity of hydrated, ionized DNA, and observed no conductivity except in the presence of a significant outer shell of water molecules, consistent with earlier results (51,52). They also observed no differences in conductance between samples in which the DNA was oriented parallel versus perpendicular to the electric field, from which they concluded that DNA was not a good medium for the conduction of charge. Fink and Schönenberger directly measured the conductivity of DNA ropes at least 600 nm long composed of a few DNA strands (53). They observed electrical current through these DNA molecules and determined the resistivity of the DNA, finding it to be comparable to other conducting polymers and good semiconductors. Porath *et al.* measured electron transport through individual, 10.4 nm-long pieces of dry double-stranded poly(dG)-poly(dC) molecules stretched between metal nanoelectrodes (54). At low applied voltage, the current was essentially zero, but large currents can be supported by the DNA at larger voltages. The dependence of the conductance upon voltage shows a series of peaks, possibly corresponding to the energy “bands” in DNA, and consistent with DNA being a large-bandgap semiconductor.

Radiation biologists observed that ionizing radiation selectively generates guanine radical cations and cytosine radical anions on DNA, consistent with charge migration through the DNA (11-26). Radical “traps” were introduced into the DNA to determine the distances over which these radicals could move along the DNA.

Estimates ranged from three (55) to twenty (56) or thirty (57) to two hundred (58) base pairs, depending on the choice of electron trap, and the technique and model employed.

The use of chromophores that bind to DNA to examine charge transfer through DNA spectroscopically provided a substantial advance in the field. The first systems involved donor and acceptor molecules bound non-covalently to the DNA. Marcus theory has been used to describe the rate k of electron transfer between two molecules

$$(7) \quad k = \left(\sqrt{4\pi^3 / h^2 \lambda k_B T} \right) H_{AB}^2 e^{-(\Delta G^*/RT)}$$

where H_{AB} is the matrix coupling element, λ is the reorganizational energy of the donor, acceptor and solvent, and ΔG^* is the free energy of activation (59). In this context, the inherent resistivity of a medium β has been gauged quantitatively as

$$(8) \quad H_{AB}^2 \propto e^{-\beta r}$$

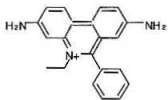
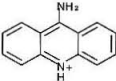
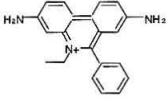
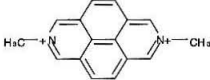
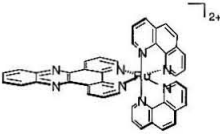
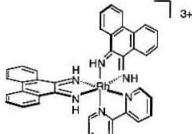
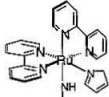
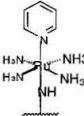
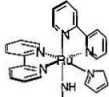
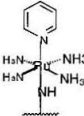
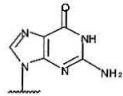
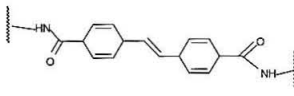
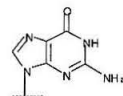
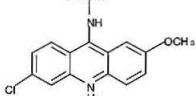
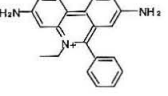
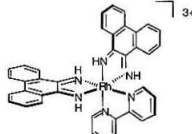
Therefore the rate of electron transfer is related to β as

$$(9) \quad k = k_0 e^{-\beta r}$$

where k_0 = a constant characteristic of the donor/acceptor pair, and r = the distance separating donor and acceptor. Using the relationship expressed in equation 9, the electron transfer rate as a function of donor-acceptor distance can be used experimentally to determine β , which reflects the ability of the DNA to conduct charge. Given that the parameter β is in the exponent of equation 9, small differences in β can represent very large differences in the efficiency of electron transfer. The average value of β for proteins is around 1.4 \AA^{-1} (60).

The classical intercalator ethidium has been used frequently as an electron donor in studies of DNA-mediated electron transfer (Table 1.1). Baguley and Le Bret observed that amsacrine could quench the fluorescence of intercalated ethidium without displacing it from the DNA (61). The authors concluded that this quenching must be due to electron transfer and not energy transfer because the donor emission

Table 1.1 Studies of photoinduced electron transfer through DNA.

Donor	Acceptor	Results	Reference
		Fast electron transfer between noncovalently-bound molecules.	(61)
		Slower electron transfer between noncovalently-bound molecules. Strong distance dependence assumed, giving $\beta=0.8 \text{ \AA}^{-1}$	(62)
		Very fast electron transfer at low donor-acceptor loadings (noncovalently-bound reactants).	(81,82)
		Efficient electron transfer over 40 Å (covalently-bound reactants). $\beta \leq 0.2 \text{ \AA}^{-1}$	(84)
		Slow electron transfer, on the order of proteins (covalently-bound reactants).	(85)
		Electron transfer dependent on distance (covalently-bound reactants). $\beta=0.64 \text{ \AA}^{-1}$	(87)
		Highly distance-dependent electron transfer (covalently-bound reactants). $\beta=1.4 \text{ \AA}^{-1}$	(89)
		Very fast electron transfer at all distances ($\beta=0.1 \text{ \AA}^{-1}$), with a decrease in quenching yield with increasing D-A distance.	(86)

spectrum and acceptor absorption spectrum do not overlap. Although the rate of quenching was too fast for them to measure and the donor-acceptor distances could not be determined, they did observe that quenching varied for different DNA sequences and for different acridine derivatives based upon their redox potentials. Brun and Harriman measured the rate of ethidium fluorescence quenching by intercalated DAP^{2+} (N,N'-dimethyl-2,7,-diazapyrenium dichloride) (62,63). The fluorescence decayed on the nanosecond timescale and could be fit to three exponentials, which the authors ascribed to quenching by acceptors located 3, 4, and 5 base pairs away. These rates and distances correspond to a β of 0.88 \AA^{-1} . However, there is no structural evidence that in fact the three exponentials correspond to these distances and not to three conformations of intercalators and DNA. In these cases both donor and acceptor molecules were intercalated into the DNA, but fluorescence quenching of DNA-bound ethidium has also been observed for nonintercalated molecules. Methyl viologen, which binds to the outside of the DNA helix electrostatically, can also quench ethidium fluorescence (64). The substantial increase in the quenching yield relative to the solution-phase reaction can be entirely accounted for by the effects of the DNA on diffusion, electrostatics, and excited-state lifetime. As a result, the DNA π stack appears to mediate the electron transfer reaction only when both donor and acceptor are intercalated. Atherton and Beaumont measured the rates of back-electron transfer from reduced Cu^+ ions bound to the exocyclic amines of guanine bases to ethidium and fit the rates to a β of 0.7 \AA^{-1} (65). However, these authors also assume that the three exponentials fit to the rate correspond to fixed, short donor-acceptor distances without structural conformation.

Transition metal complexes that associate with the DNA by intercalation have also been used as donors and acceptors. Metallointercalators are very well suited as probes of DNA-mediated electron transfer chemistry (Figure 1.7). The rich spectroscopy of dipyrrophenazine (dppz) complexes of ruthenium(II), exploited in

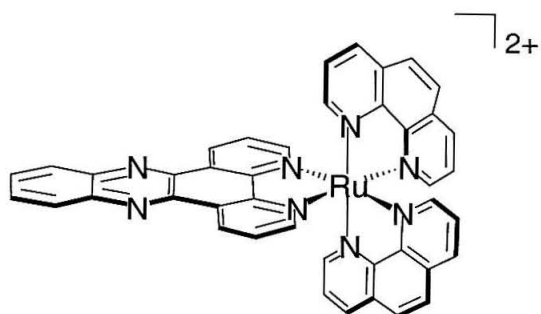
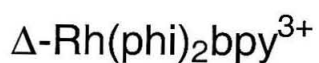
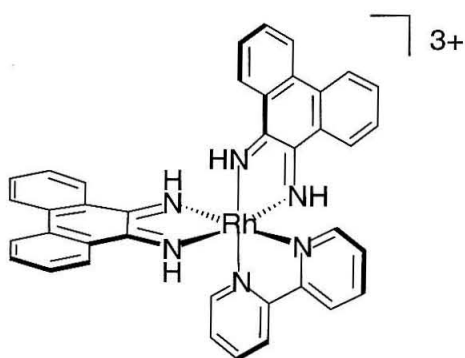


Figure 1.7: Octahedral metallointercalators used to examine DNA-mediated charge transport spectroscopically. The right-handed Δ isomers are shown. (phi = 9,10-phenanthrene quinone diimine; bpy = 2,2'-bipyridine; phen = 1,10-phenanthroline; dppz = dipyrido[3,2-a:2',3']phenazine).

developing luminescent DNA intercalators, provides a sensitive handle to monitor electron transfer to an electron acceptor (66). Although spectroscopically less interesting, the phenanthrene quinone diimine (phi) complexes of rhodium are good electron acceptors that can promote the oxidation of the DNA itself (35,67). Both metal complexes have also been valuable in the study of charge transfer through the base stack because each intercalates one heterocyclic, aromatic ligand into the DNA, which allows them to be electronically coupled into the π stack. This binding to DNA has been characterized in detail, using NMR spectroscopy and X-ray crystallography (68-70). The structures of the phi complexes of rhodium reveal deep intercalation of the phi ligand within the base stack, without apparent disruption or kinking of the neighboring base pairs (Fig. 1.8). The DNA around the binding site opens up to accommodate the metal complex with a base-pair-to-phi spacing of 3.4 Å. The metallointercalator resembles another base pair simply inserted within the stack. Similarly, these ruthenium complexes also intercalate into the π stack via their dppz ligands.

In addition to their major advantages as probes of DNA charge transport, octahedral metallointercalators have several other useful qualities (66,71). They bind avidly to DNA, with binding constants on the order of 10^7 M^{-1} (72,73). They are coordinatively saturated and substitutionally inert, so the metal center does not cross-link to the DNA bases, and due to their positive charges, they are soluble in water, which is critical for the study of DNA (74). They are chiral, which allows for shape-selection based on handedness corresponding to the right-handed DNA helix (75,76). Their ancillary ligands can be modified to change their sequence specificity, ability to intercalate, redox potentials, or to covalently attach them to DNA or peptides (77-80).

Using these metallointercalators, Barton and colleagues demonstrated fast electron transfer from a photoexcited $\text{Ru}(\text{phen})_2\text{dppz}^{2+}$ intercalator to $\text{Rh}(\text{phi})_2\text{bpy}^{3+}$

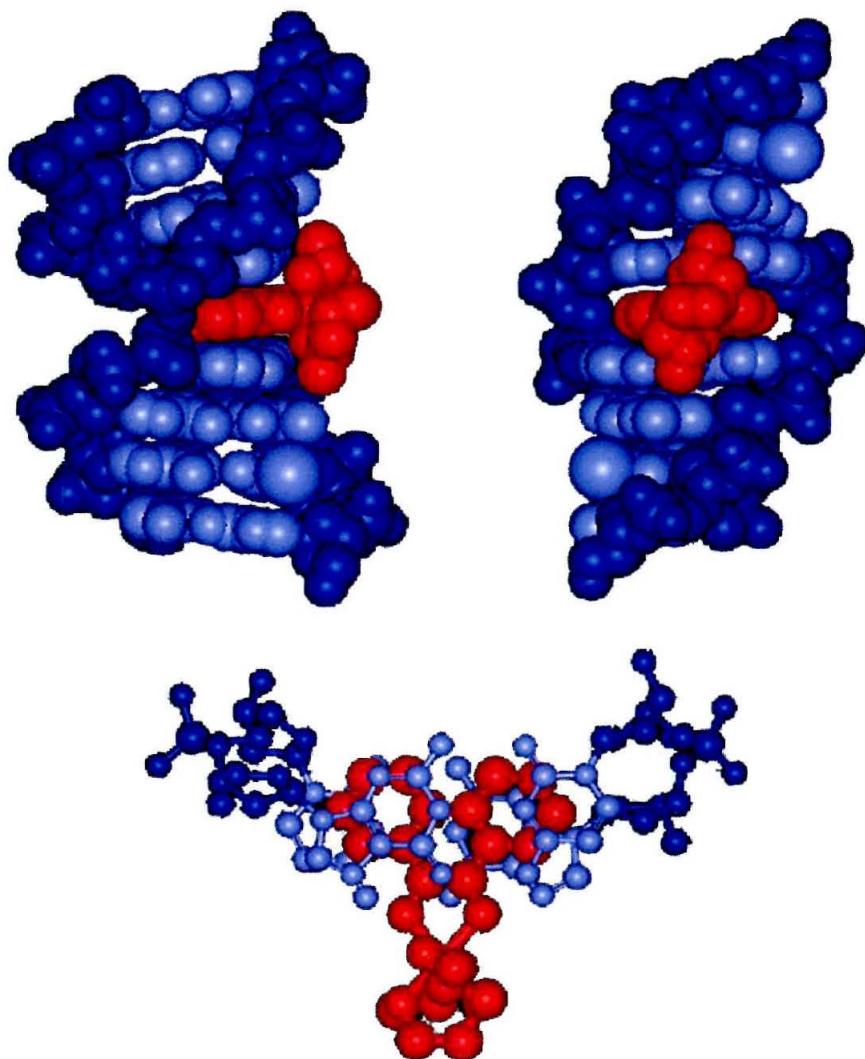


Figure 1.8: Structure of a phi complex of rhodium (red) bound to a DNA oligonucleotide (blue). The DNA is hardly perturbed by the intercalation of the metal complex. The phi ligand has significant overlap with the DNA base pairs, allowing for efficient electronic coupling into the DNA π stack (bottom).

or $\text{Rh}(\text{phen})_2(\text{phen})^{3+}$ on DNA with a rate faster than $3 \times 10^{10} \text{ s}^{-1}$ (81-82). This rate is independent of the loading of donor and acceptor onto the DNA and to the corresponding donor-acceptor distance, though the *yield* of electron transfer is sensitive to loading and distance. Assuming (in the absence of evidence for donor-acceptor clustering on the DNA helix) a random distribution of metal complexes, this rate would correspond to a $\beta < 0.2 \text{ \AA}^{-1}$. Interestingly, this group has recently shown using noncovalently-bound intercalators that quenching of $\text{Ru}(\text{phen})_2\text{dppz}^{2+}$ fluorescence by DNA-bound viologen acceptors occurs more slowly, on the nanosecond timescale, indicating that the structural and electronic properties of the donor and acceptor can affect the estimates for the efficiency of charge transfer through DNA (83).

All of these studies of electron transfer between noncovalently-bound donors and acceptors suffer from an inability to conclusively determine the distances over which charge is transferred. Recently, by constructing well-defined DNA assemblies containing donors and acceptors fixed at discrete sites on the helix, chemists have refined their approach to evaluating DNA as a molecular medium for electron transport, but as with earlier studies, measurements of DNA-mediated electron transfer in assemblies containing covalently-bound donors and acceptors also yielded conflicting results and very different estimated values of β (Table 1.1).

In the first example of electron transfer through DNA between fixed donors and acceptors, Murphy *et al.* demonstrated that the luminescence of a DNA-bound $\text{Ru}(\text{phen}')_2(\text{dppz})^{2+}$ complex is quenched by $\text{Rh}(\text{phen})_2(\text{phen}')^{3+}$ on *at least* the picosecond timescale (84). This luminescence quenching occurs over 40 \AA between the two metal complexes covalently tethered to either end of a 15-base-pair duplex oligonucleotide, giving an estimated β below 0.2 \AA^{-1} . Notably, the ruthenium luminescence is not quenched by a rhodium complex covalently attached to a different duplex oligonucleotide, demonstrating that this quenching reaction occurs

intramolecularly. Furthermore, the rate of quenching of the covalently tethered $\text{Ru(phen)}_2\text{dppz}^{2+}$ by groove-bound $\text{Ru(NH}_3)_6^{3+}$ is slow, and similarly, covalently-tethered non-intercalating Ru(phen)_3^{2+} is quenched slowly by a covalently-tethered non-intercalating Rh(phen)_3^{3+} , demonstrating that the intercalation of both donor and acceptor into the π stack of DNA is a critical component of the fast quenching. This quenching was identified as an electron transfer reaction due to the large thermodynamic driving force for such a reaction and the lack of spectral overlap between donor and acceptor metallointercalators.

Meade and Kayyem also examined the DNA-mediated electron transfer, using two ruthenium complexes that were not intercalated into the DNA π stack (85). They constructed an eight-base pair oligonucleotide duplex with a $\text{Ru(bpy)}_2(\text{im})^{3+}$ acceptor attached to the 5' terminal deoxyribose moiety at one end and a $\text{Ru(NH}_3)_4(\text{py})^{2+}$ donor at the other, and determined that the rate of electron transfer between metal centers was on the order of 10^6 s^{-1} . This rate corresponds with a value of $\beta > 1 \text{ \AA}^{-1}$, on the order of proteins.

DNA-mediated electron transfer was examined further by Barton and coworkers in DNA assemblies containing tethered ethidium and rhodium intercalators (86). Photoinduced quenching of the DNA-bound ethidium emission was monitored in assemblies prepared of increasing DNA length. The rate of electron transfer again is faster than 150 picoseconds, and the decrease in yield with increasing donor-acceptor distance, characterized by a slope of 0.1 \AA^{-1} , is quite small. The data were interpreted with a model in which direct donor-acceptor electron transfer is fast at all distances, but is exquisitely sensitive to subtle dynamic motions of base pair stacking between the reactants and the base pairs, and between neighboring base pairs themselves. Hence, as the number of intervening base pairs increases, the probability of a destacking event increases, leading to a decrease in overall yield of electron transfer. Measurements of electron transfer through a DNA assembly

containing a single base mismatch at the central position in the oligomer demonstrated its sensitivity to perturbations in the base pair stack. The introduction of a CA mismatch, which causes a local perturbation in the DNA stack, significantly diminishes the overall yield of electron transfer. These results not only underscore the exquisite sensitivity of DNA-mediated electron transfer to stacking, but also demonstrate that the *path* for electron transfer between the two intercalators is through the base pair stack.

Lewis *et al.* measured the rate of electron transfer in stilbene-capped hairpins (87,88). The stilbene moiety fluoresces strongly in hairpins containing six A-T base pairs, but its fluorescence is quenched in a distance-dependent manner by the presence of even one G-C base pair. Both the yield and rate of stilbene quenching drop off sharply with distance. The rate constants for the decay of the stilbene singlet as a function of guanine-stilbene distances between 1 and 4 base pairs were used to arrive at a β of $0.64 \pm 0.1 \text{ \AA}^{-1}$. Interestingly, the absorption and fluorescence maxima of the linker chromophore is shifted only modestly on integration into DNA hairpins, and no hypochromism or circular dichroism is induced by its introduction, indicating that the electronic structure of the stilbene is not strongly perturbed by its flanking base pair. In this case, some interaction with the base pairs occurs, resulting in a coupling with the π stack which is intermediate between that of two sugar-linked extrahelical ruthenium complexes, and between two intercalators. Clearly this is the case because although no hypochromism in the stilbene chromophore is evident, some stacking with the proximal base pair probably occurs to facilitate quenching by guanine and, correspondingly, an intermediate value of β is obtained.

Fukui and Tanaka measured the distance dependence of charge transfer between an acridine moiety attached to the DNA backbone in the middle of an oligonucleotide duplex and guanine bases within that duplex (89). The fluorescence

quenching of the acridine moiety by guanine has a very strong dependence on the acridine-guanine distance, and the rate of quenching is fairly slow (10^5 - 10^8 s⁻¹ for non-adjacent guanine bases), from which they estimate a β of around 1.5 \AA^{-1} . This very large value of β may be due to several factors. The structure of the acridine-oligonucleotide duplex is unknown, and therefore slow electron transfer may be due to a lack of intercalation and coupling into the π stack (90,91). Alternatively, Giese, Michel-Beyerle and colleagues have observed that spontaneous relaxation of the acridine chromophore is more rapid than electron transfer when the guanine base is not directly adjacent to the chromophore, introducing a large error into an estimate of β (92).

Electron transfer modulated by the dynamics of π stacking has been supported by recent ultrafast measurements of the photooxidation of deazaguanine by tethered ethidium in a family of DNA assemblies (93). In this case, the rate of electron transfer between the modified base and the intercalator is faster than 150 ps, and the yield of quenching decreases with a weak dependence on increasing distance. Transient absorption experiments reveal two components to the photooxidation. The electron transfer occurs on the timescale of 5 ps over distances of 10-17 \AA for the fully aligned assembly. A second component to the charge transfer, which occurs on the 70 ps timescale, correlates with the timescale for motion of the intercalated ethidium within its binding site.

In order to remove the effects of intercalator binding to the DNA upon the measured rate of electron transfer, Kelley and Barton examined the rate of electron transfer between guanine and fluorescent base derivatives (94,95). This base-base electron transfer system is an excellent model for the migration of charge *within* DNA. For photoinduced electron transfer from guanine to ethenoadenine, which is not well stacked in the DNA helix, $\beta = 1.0 \text{ \AA}^{-1}$. In contrast, $\beta = 0.1 \text{ \AA}^{-1}$ for the interstrand electron transfer to 2-aminopurine, which is well-stacked and hydrogen

bonded to the opposing thymine. The intrastrand reaction occurred too fast to measure, but it has a β of probably less than 0.4 \AA^{-1} . Notably, the measure of β also varied based upon the electron donor, with slower rates and concomitantly larger β values being measured for 7-deazaguanine relative to guanine.

We propose that these disparate descriptions of the ability of DNA to mediate the transfer of charge can be reconciled by considering the mode through which donors and acceptors are coupled, or not coupled, into the DNA π -stack. A β characteristic of the σ -bonded sugar phosphate backbone is obtained from the assembly in which metals are coordinated to the sugar positions on the helix, in which no electronic coupling between the metals and the DNA π stack would be expected to arise (85). Aromatic, heterocyclic intercalators and modified bases are generally well-coupled into the DNA π stack, and the rate of electron transfer is high and β is small (82,84,86,93-95). When the electronic coupling between donor, acceptor, and intervening base pairs is intermediate, such as in the case of the stilbene moiety attached to the DNA hairpin (87,88), the rate of the electron transfer and the estimated value of β are also intermediate. Driving force also appears to play a role which is difficult to assess given the potentially large effects on ET of small structural changes in chromophore or DNA. Certainly these differing results point to a need for detailed structural analysis of all systems, and for continuing systematic studies as a function of distance, sequence, driving force, and structure.

DNA electron transfer has also been measured through electrochemical studies on DNA bound to a gold surface (96,97) (Fig. 1.9). Studies employing a covalently-bound intercalator, daunomycin, as the redox probe, showed no significant change in electrochemistry as a function of distance between the daunomycin and the gold surface. However, the introduction of an intervening mismatch into the DNA radically diminishes long-range electron transfer to the intercalator. These results provide independent evidence for the sensitivity of DNA-

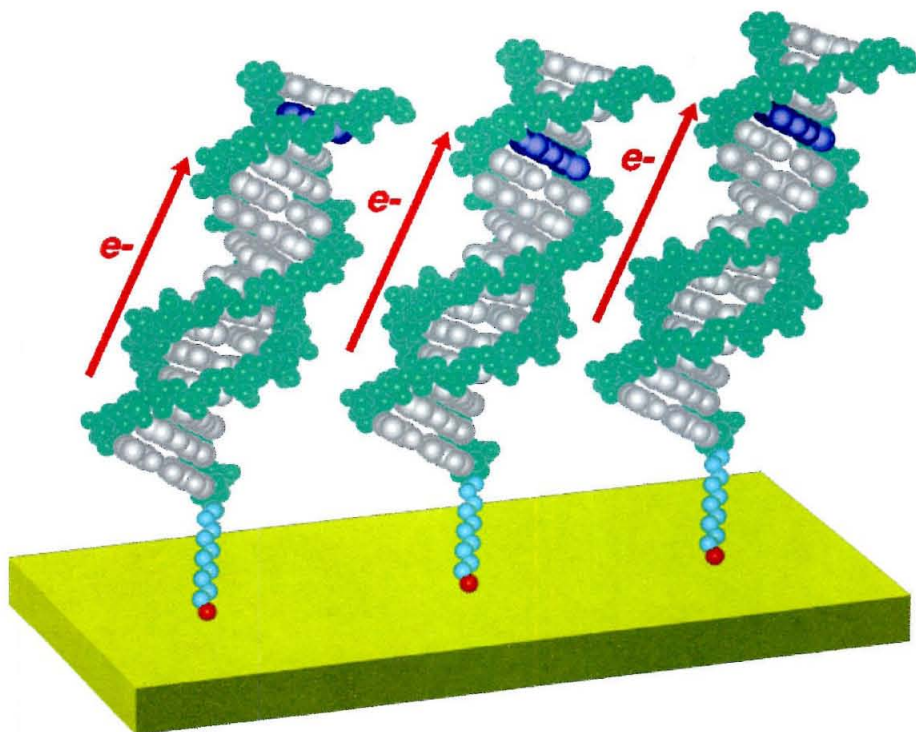


Figure 1.9: A DNA monolayer. Oligonucleotides bound to a gold surface *via* an alkane-thiol linker have been used to examine electron transfer through DNA. Intercalators bound to the DNA (blue) are reduced by electron transfer from the gold surface through the DNA π stack. Interruption of the base pair stack with a mismatched base pair decreases the amount of intercalator that is reduced.

mediated electron transfer to stacking and relative insensitivity to distance.

Furthermore, the efficiency of DNA-mediated electron transfer on these surfaces can be exploited to evaluate base stacking and detect single base mismatches in DNA.

1.4 Chemistry at a Distance

Not only can electron transfer mediated by the DNA be facile, but the π -stack can serve as a reactant in the electron transfer process. Radicals can migrate through the helix to react at a remote site from the oxidant. Oxidative damage to DNA *from a distance* was first demonstrated in an assembly containing a tethered rhodium intercalator as the photooxidant, spatially separated from 5'-GG-3' sites (Fig. 1.10) (35). Upon irradiation at 313 nm, phi complexes of rhodium(III) promote direct DNA strand cleavage, whereas irradiation at 365 nm yields oxidative damage to the DNA bases (Fig. 1.11). These damaged bases are then revealed as strand breaks by treatment with hot aqueous piperidine or base excision repair enzymes. This complex rhodium photochemistry is used to illustrate that binding and oxidation events occur in discrete locations, and thus guanine damage occurs at a distance from the metallointercalator.

Guanine bases are the target of long-range oxidation because they have the lowest potential of the four canonical nucleotide bases, as determined for nucleotides in acetonitrile (98,99). Within a double helix, a proton shift from guanine to cytosine in the base pair should further stabilize the radical on guanine. The 5'-G of 5'-GG-3' sites ("guanine doublets") had been earlier shown to be oxidized preferentially to 3' guanines or guanines flanked by other bases in electron-transfer reactions (100,101). This preferential oxidation of 5' guanines is thought to be due to the effects of stacking on the ionization potential of guanine, since in 5'-GG-3' sites the HOMO has been calculated to be located disproportionately on the 5' guanine of the doublet (102). Moreover, Foote and coworkers have proposed that upon oxidation

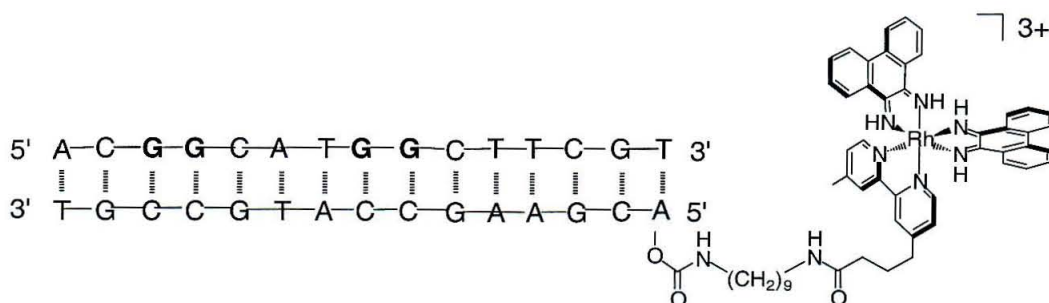


Figure 1.10: DNA oligonucleotide assembly containing an appended rhodium metallointercalator. This assembly was used to examine long-range oxidation of guanine doublets. The $\text{Rh}(\text{phen})_2\text{bpy}^{3+}$ complex is constrained by its tether to intercalate two or, at most, three base pairs in from the end of the helix.

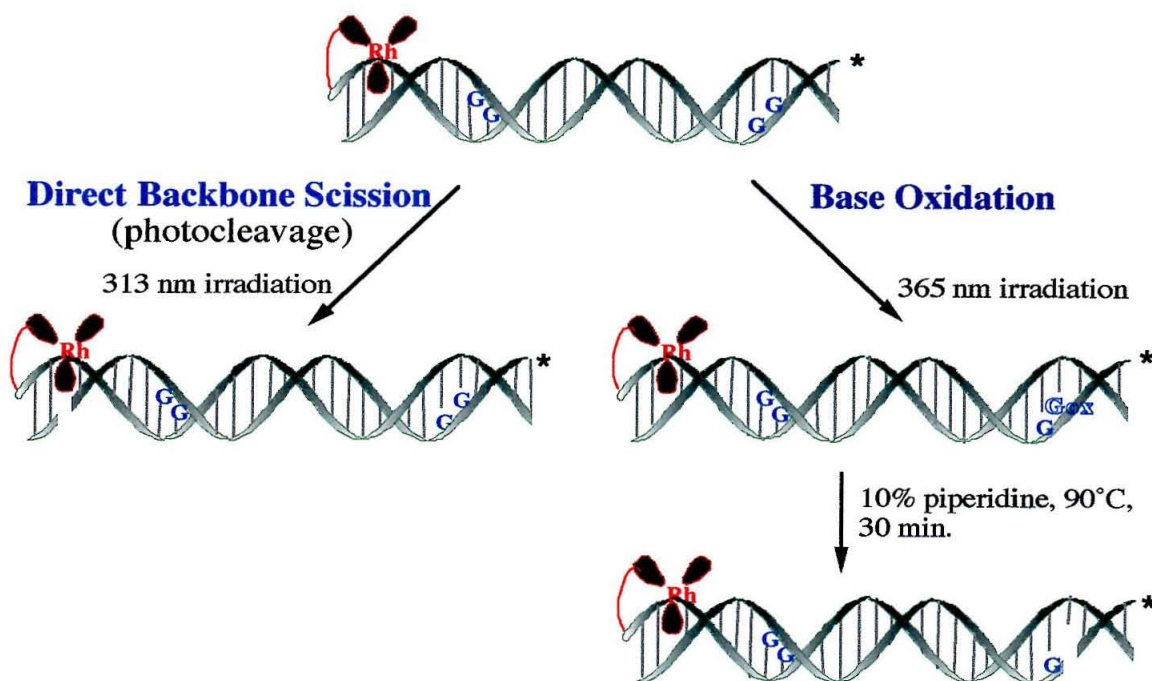


Figure 1.11: Phi complexes of rhodium damage DNA according to two distinct mechanisms. When irradiated at 313 nm, these rhodium complexes directly cleave the DNA sugar-phosphate backbone at the site of intercalation. When irradiated at 365 nm the complexes oxidize guanine bases, often at a distance from the intercalation site, in a reaction which is mediated by the DNA base pair stack. The oxidized guanine bases are converted to strand breaks by treatment of the DNA with hot aqueous piperidine.

the N7 of the 3' guanine, located directly below the center of the six-membered ring of the 5' guanine, would stabilize the radical on the 5' guanine. In the absence of guanine doublets, all single guanines are oxidized fairly equally (103).

As in electron transfer monitored spectroscopically, oxidative damage to DNA mediated by the base pair stack shows a shallow dependence on distance, but an exquisite sensitivity to stacking. Rhodium-tethered DNA assemblies were prepared containing two 5'-GG-3' sites with and without a bulged segment of DNA interrupting the π stack between the G doublets (104). Even though the sugar-phosphate backbone remained intact and the distance between the oxidant and the distal 5'-GG-3' site was shortened, insertion of the bulge yielded a significant diminution in oxidation of the G-doublet distal to the bulge. The efficiency of long-range oxidation of 5'-GG-3' sites in RNA/DNA hybrid oligonucleotides was shown to correlate with the degree of base stacking in these A-form helices (105). In DNA double crossover assemblies, where two closely-associated DNA double helices joined by their sugar-phosphate backbones are formed from four overlapping strands, oxidation of guanine doublets occurs in the base stack containing the rhodium intercalator, but not in the associated strand whose base stack is not electronically coupled to the intercalator (106). The dependence of long-range guanine oxidation on sequence and stacking will be discussed in more detail in chapters 2 and 4.

This ability to mediate long range charge transport is a characteristic of the DNA duplex, not the oxidant. Several oxidants have now been employed in experiments demonstrating long-range oxidation of guanine bases in DNA (Fig. 1.12). $\text{Ru(phen)}_2\text{dppz}^{2+}$ complexes, used to demonstrate DNA-mediated electron transfer spectroscopically, can also oxidize guanine bases at a distance through the DNA base stack (107). In this case, a ground state Ru(III) species is generated *in situ* by the flash-quench technique by quenching the photoexcited $^*\text{Ru(II)}$ species

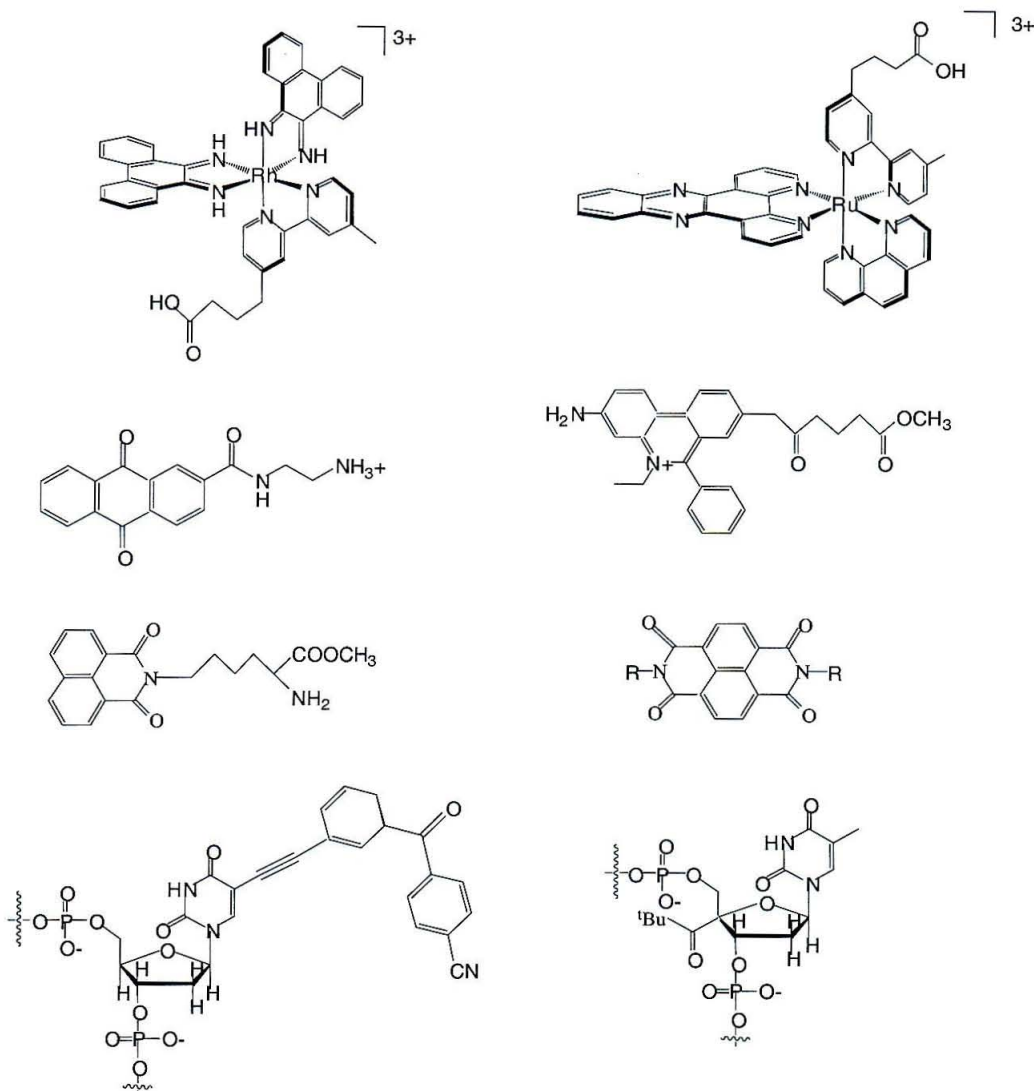


Figure 1.12: Molecules proposed to oxidize guanine bases from a distance along DNA. Clockwise, from top left: Rh(phi)₂bpy³⁺ (35), Ru(phen)(bpy')(dppz)³⁺ (107), ethidium (109), napthalene diimide (116), 4'-pivaloyl-modified deoxythymine (122,125), cyanobenzophenone-modified deoxyuridine (117-120), napthalimide (100,101), anthraquinone (38,111).

with a diffusible quencher such as ruthenium hexaamine, cobalt pentamine chloride, or methyl viologen (Fig. 1.13). The Ru(III) ground-state species is a powerful oxidant, capable of oxidizing guanine bases at a distance from the intercalation site. The guanine radical intermediate was observed directly by transient absorption spectroscopy (108). Interestingly, the yield of oxidized guanine correlates with the stability of the reduced quencher: unstable quenchers which decompose and are therefore not available to reduce the Ru(III) species back to the Ru(II) ground state (i.e., methyl viologen and cobalt pentamine chloride) produce high yields of oxidized guanine, whereas quenchers which can reduce the oxidant back to the ground state (i.e., ruthenium hexaamine) produce lower yields of oxidized guanine.

With photoactivation, the classic intercalator ethidium can also oxidize guanine bases at long range through the DNA base pair stack (109). When covalently tethered to the end of a 17-base pair oligonucleotide duplex and irradiated between 310 and 340 nm, ethidium intercalates near the end of the helix and oxidizes guanine doublets 17 and 44 Å away from the intercalation site. The amount of oxidization at both sites is roughly equal, demonstrating that the distance dependence of this charge transfer reaction is small. When irradiated at these wavelengths, ethidium also directly cross-links to bases at the intercalation site, allowing confirmation of the site of binding.

Photoexcited anthraquinone derivatives also oxidize guanine bases from a distance through DNA (110). Depending on the substituents, these anthraquinones can bind to DNA by intercalation, end-capping, or groove binding, and can damage DNA by hydrogen abstraction or electron transfer (39). End-capped and intercalated anthraquinones that access the DNA π stack oxidize 5' guanines of 5'-GG-3' sequences with a very weak dependence on distance, much like rhodium, ruthenium, and ethidium intercalators (111), but groove-binding anthraquinones that do not access the DNA π stack do not selectively introduce damage at these sites.

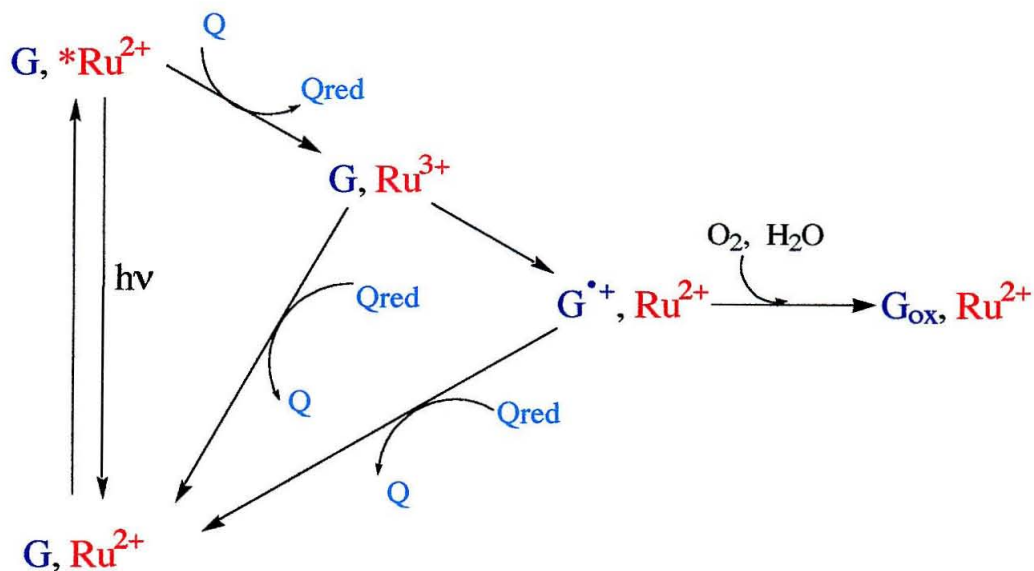


Figure 1.13: The flash-quench cycle. A ground-state Ru(III) oxidant is generated by photoexcitation of the ground state Ru(II) species, followed by quenching of the excited state. Common oxidative quenchers (Q) are methyl viologen, ruthenium hexaamine, and cobalt pentamine chloride. The Ru(III) species can then oxidize guanine bases to give a guanine radical intermediate, which when trapped by water or oxygen, generates a permanently-modified guanine base.

Intercalated anthraquinones have been used to examine the effects of stacking and structure on long-range guanine oxidation in a variety of systems (112-115).

Noncovalent naphthalimide and naphthalene diimide (NDI) intercalators were shown to oxidize 5' guanines of guanine doublets prior to the demonstration of long-range oxidation by rhodium complexes (100,101,116). Although it was assumed that guanine oxidation by NDI occurred at long range through the π stack, its mechanism was confirmed more recently using covalently-tethered NDI, as will be described in chapter 4.

Two other systems have also been developed for the examination of charge transport through DNA as measured by the oxidation of 5' guanines of guanine doublets. In both cases, the oxidant is not coupled into the base pair stack, and as a result, the reaction shows a very strong dependence on distance and sequence that is not apparent with intercalators. This distinct behavior indicates that some part of the charge transfer reaction may involve electron tunneling through σ bonds.

Alternatively, some other difference in the mechanism of guanine oxidation may distinguish these reactants from the intercalators. Saito *et al.* have shown that a cyanobenzophenone chromophore attached to a uracil nucleotide via an acetylene bridge can selectively oxidize guanine bases, but only in some sequence contexts (117-119). With many combinations of sequence flanking the modified uracil, virtually no guanine oxidation is observed. Not surprisingly, the addition of this benzophenone moiety destabilizes the oligonucleotide to which it is attached, indicating that it is probably not intercalated (120). Giese and coworkers have used strands modified with a pivaloyl moiety at the 4' position of a given deoxyribose sugar residue to generate, upon photolysis, a radical on the sugar (121,122). If a guanine base is located nearby in the sequence, it can be oxidized by the sugar radical, and in some cases the guanine radical can migrate a short distance before it is

trapped, but again the distances over which this reaction can occur are short and are highly dependent on the DNA sequence (123-125).

DNA-mediated charge transport can also promote another reaction from a distance: the repair of a thymine cyclobutane dimer lesion (Fig. 1.3a) (126). In a DNA assembly containing a centrally located thymine dimer and a remotely-appended rhodium intercalator, oxidation of the cyclobutane ring linking neighboring thymines cleanly triggers the cycloreversion reaction leading to quantitative repair. Intervening bulges diminish repair efficiency, indicating that the reaction is mediated by the DNA base stack. In contrast to studies of oxidative guanine damage by rhodium, thymine dimer lesion repair is less efficient with the covalently bound rhodium intercalator (at all distances) compared to repair with non-covalent rhodium, which we attribute this to the poor stacking of the non-aromatic thymine dimer within the helical stack. Although this system does not really provide a model for photolyase activity, as the enzyme repairs dimer lesions by photoreduction and likely not at a distance, it does demonstrate that the movement of charge through DNA may be used to trigger reactions at a distance besides the oxidation of guanine.

Interestingly, dppz complexes of ruthenium(III) were found to oxidize the 5'-GG-3' doublets efficiently but not to repair the thymine dimer lesion, as described in chapter 3. These metallointercalators are less potent oxidants than $\text{Rh}(\text{phi})_2\text{bpy}^{3+}$, and would not be expected, based upon their redox potentials in solution, to oxidize pyrimidines. Anthraquinones do not repair thymine dimer lesions, neither from a distance nor when bound noncovalently to an oligonucleotide duplex containing a lesion (127), yet naphthalene diimide intercalators can repair thymine dimer lesions, and from a distance (128). This discrepancy cannot be resolved based on an argument of redox potentials or poor stacking, since both are intercalators with potentials sufficient to oxidize guanine. It may be, however, that the charge transfer

reaction between the excited state anthraquinone and the thymine dimer lesion may violate spin-selection rules.

1.5 Mechanism of Charge Transport through DNA

Based upon the numerous experiments detailing electron transfer reactions monitored spectroscopically as well as oxidative chemistry at a distance, the debate concerning DNA electron transfer has evolved in the past few years to considerations of *how* rather than *whether* DNA-mediated charge transport proceeds.

One model describes the DNA bases as strongly electronically coupled, with the DNA π stack existing as a band of delocalized orbitals. Charges could be transferred through DNA by two different mechanisms consistent with this model (129,130). If the energy of the donor and acceptor molecules is significantly lower than that of the DNA bridge, it is expected that charge transfer through the DNA must occur by superexchange. In this case, the charge tunnels through the DNA bridge but does not actually occupy it. Ultrafast measurements of DNA electron transfer rates indicate that this mechanism wherein DNA serves only as a “virtual” bridge is unlikely, given that electron transfer rate seems relatively invariant with distance in the case of ruthenium-rhodium, ethidium-rhodium, ethidium-deazaguanine, and deazaguanine-deazaadenine donor-acceptor systems (84, 86, 93-95). As a consequence, β is not generally appropriate to mechanisms of DNA charge transport, although it may be empirically useful as a gauge of distance-dependence.

Alternatively, the donor and acceptor may be strongly coupled to each other through a low-lying bridge, such that the charge will transiently occupy the bridge as it is transferred (129,130). In this “molecular wire” mechanism, the charge transfer should be relatively insensitive to distance, but should be sensitive to dynamic interruptions in the base stack, consistent with the work of Kelley, Barton and coworkers (86, 93-95). A coherent charge transfer model does not, however,

explain the oxidation of guanine bases over distances of 200 Å, since it is unlikely that direct coupling could occur over > 50 base pairs (chapter 2).

At the other extreme is the proposal that charge transfer through DNA occurs by hopping (131-134). Arguing that the absorption spectrum of DNA polymers does not indicate extensive electronic coupling, Dee and Baur proposed in 1974 that localized holes, electrons, or singlet or triplet excitations could migrate through DNA by ultrafast hopping from base to base (131). Charges hop, with an equal chance of going forward or backward at each step, until trapped by vibrational relaxation. More recent permutations of the “hopping mechanism” have assumed that electron holes cannot hop onto pyrimidine bases due to their higher oxidation potentials. Having observed a strong distance dependence in oxidative damage in sequences lacking intervening G’s but a weaker dependence if these G “stepping stones” are available, Jortner, Giese, and coworkers have proposed a guanine-to-guanine hopping model for charge transport through DNA (132-133). Unfortunately, their guanine-guanine hopping model is inconsistent with efficient long-range guanine oxidation by rhodium intercalators through sequences containing only TA base pairs, as well as oxidative repair of thymine dimer lesions (126,135).

In this context, it is likely that the long range base oxidation chemistry involves a mixture of coherent transport and hopping. Charge transport over long molecular distances might best then be described as *domain hopping*, where charge is transiently delocalized over regions, gated by sequence-dependent DNA flexibilities, and hops occur from one delocalized region to the next. This proposal is consistent with the “phonon-assisted” polaron hopping model proposed by Schuster and colleagues (110, 111) and Rakhmanova and Conwell (136). The transient formation of polarons (regions of minor localized structural distortion associated with an electron or electron hole on the DNA) allows charge delocalization over regions of

sequence. Charge is transported by hops between these regions, and its movement is assisted by phonons (packets of vibrational energy).

It is possible that different mechanisms operate in different systems, depending on the energetics of the donor-acceptor pair, the electronic coupling of the donor-acceptor pair with each other and the intervening π stack, the possibility of back-electron transfer, the timescale of the trapping reaction, the sequence of the DNA, and a multitude of other factors.

1.6 DNA Charge Transport and Proteins

Charges have been shown definitively to move along DNA. In the cellular environment, DNA is intimately associated with a variety of proteins which serve to regulate replication and transcription as well as repair and package the DNA itself (6), making it important to examine the possible roles of proteins in a DNA-mediated charge transfer process. Using a variety of DNA-binding proteins, it was shown that protein binding to DNA can sensitively modulate charge transfer through the helix, depending on its effect on π stacking.

M.HhaI is a DNA methylase which, in binding its target site, flips out the cytosine for methylation and inserts a glutamine side chain, stabilizing a “gap” in the DNA π stack. Long range oxidative damage to guanine bases in DNA was examined as a function of *M.HhaI* binding to the sequence between the tethered rhodium oxidant and a distal 5'-GG-3' site (137). In binding to its target site, *M.HhaI* inhibits oxidative damage to DNA past the enzyme-induced gap. However, a mutant *M.HhaI* that inserts a tryptophan into the gap created by base flipping does not inhibit charge transfer on binding to DNA. In the mutant protein, the flat, aromatic tryptophan side chain takes the place of the missing DNA base, completing the π -stacked array needed to conduct charge through the helix.

The effect of other proteins on long-range charge transport has also been examined (Figure 1.14) (138). TATA-binding protein (TBP) generates two $\sim 90^\circ$ kinks on either end of its recognition site upon binding to DNA, seriously disrupting π stacking. As a result, TBP binding also disrupts long-range charge transfer through its binding site. *PvuII* restriction endonuclease and Antennapedia homeodomain protein, on the other hand, do not significantly distort the π stack on binding to DNA, and thus as a result do not inhibit long-range charge transfer. To the contrary, binding of either protein *increases* long-range guanine oxidation. The increase in charge transfer is proposed to be due to a restriction of dynamic motions of the DNA bases and a stiffening of the DNA helix, caused by protein binding, that facilitates charge transfer.

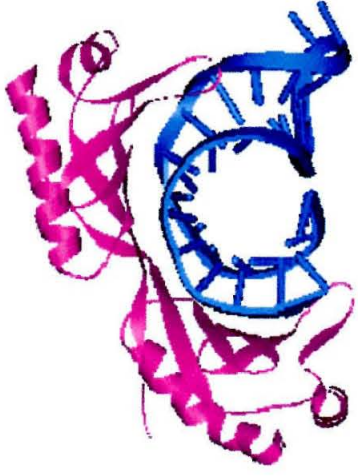
Since binding of transcription factors and other small proteins to DNA has been shown to modulate charge transfer through DNA *in vitro*, it is reasonable to assume that other proteins modulate charge transfer as well. The fundamental unit of DNA packing inside eukaryotic cells is the nucleosome core particle, in which ~ 150 base pairs of DNA is wrapped around an octamer of histone proteins. In addition to packaging DNA, the histone proteins are believed to serve both regulatory and protective functions. Given the ubiquity of the nucleosome, the potential involvement of the histone octamer in modulating charge migration through DNA is of significant interest, and will be discussed in chapter 5.

Furthermore, it is possible that proteins participate in charge transfer reactions on DNA as a mechanism for detecting dangerous stray radicals in the DNA base stack. Transient absorption spectroscopy has been applied to characterize electron transfer between small tripeptides (Lys-Trp-Lys) intercalated in DNA and $[\text{Ru}(\text{phen})(\text{bpy}')(\text{dppz})]^{3+}$, tethered to the DNA terminus (139). These results indicate that DNA-mediated charge migration between tryptophan and Ru occurs efficiently to produce the tryptophan radical. Similarly, when guanine bases are

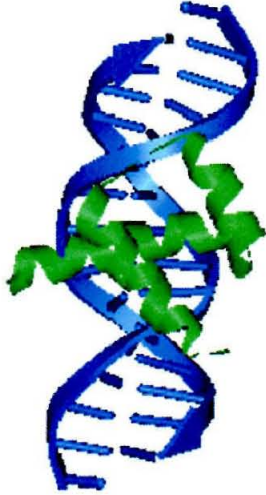
Figure 1.14: Structures of proteins that modulate charge transfer through DNA. *PvuII* endonuclease, TATA-binding protein, Antennapedia homeodomain, and *HhaI* methyltransferase were used to examine the effect of protein binding on long-range charge transfer to oxidize guanine bases at a distance (137,138). TATA binding protein significantly diminishes charge transfer through DNA, consistent with its tendency to generate strong kinks in its target DNA. *HhaI* methyltransferase, which flips a base out of the helix and inserts an aliphatic side chain into the gap, also diminishes long-range charge transport. All DNA-binding-proteins do not diminish long-range charge transport, however. A mutant *HhaI* protein that inserts an aromatic, heterocyclic tryptophan residue in place of the flipped-out base does not diminish long-range charge transport. *PvuII* endonuclease and Antennapedia homeodomain proteins generate no distortions to the DNA base pair stack, and as a result they do not diminish charge transport through the helix. In fact, they improve long-range charge transport, probably by stiffening the helix and reducing dynamic structural variations.



PvuII Endonuclease



TATA-Binding Protein



Antennapedia Homeodomain



HhaI Methyltransferase

oxidized at long range by ruthenium complexes in the presence of a site-specifically-bound *M.HhaI* mutant which inserts a tryptophan side chain into the DNA π stack, the tryptophan radical is observed (140). Thus a protein side chain might serve to funnel charges off of the DNA and onto damage-detecting proteins.

1.7 DNA Damage and Charge Transport in the Cell

Now that charges have been shown to move along DNA *in vitro*, new questions have begun to arise. Can charges move through DNA inside of cells? If so, over what kinds of distances? What kinds of permanent products are formed from hole/electron transfer on DNA? If charge transfer does not occur, what sequences, structures, proteins, or other factors prevent charge migration? (141) Is the movement of charges through DNA always associated with DNA damage, or can charge transport be used to carry out other long-range reactions, diagnose faulty DNA “wiring,” or to communicate across long distances? (142)

In the last several years we have begun to examine all of these issues, as will be elucidated in this volume. As detailed in chapter 2, we examined the distance limits for charge transfer and the effects of sequence and temperature. We compared the efficiency of thymine dimer repair and guanine damage *via* long-range charge transport to determine whether “hole” migration always leads to DNA damage, as shown in chapter 3. We extended our examination of the distance limits of charge transfer to restriction fragments, as described in chapter 4. Furthermore we developed a method for site-specific delivery of photooxidants to a single site on a DNA *in vitro*, which we hope to extend into cells to examine charge transfer across a gene from a single, specific site of damage. Chapter 5 accounts our examination of the effect of histone proteins on charge transfer. Finally, chapter 6 illustrates our first forays into the new field of DNA charge transfer inside the cell, experiments

where we demonstrate long-range guanine oxidation by photoexcited rhodium intercalators in *HeLa* nuclei.

1.8 References

1. E. Friedberg, G. Walker, W. Siede, *DNA Repair and Mutagenesis*, ASM Press, Washington, D.C (1995).
2. J.D. Watson, F.H. Crick, *Nature* (London) **171**, 737 (1953).
3. W. Saenger, *Principles of Nucleic Acid Structure*. Springer-Verlag, New York (1984).
4. R. E. Dickerson, *Nucleic Acids Res.* **26**, 1906 (1998).
5. D. Crothers, J. Drak, J.D. Kahn, S.D. Levene, *Methods Enzymol.* **212**, 3 (1992).
6. S. L. Wolfe, *Molecular and Cellular Biology*, Wadsworth Publishing Company, Belmont, California (1993).
7. A. Kornberg, T. Baker, *DNA Replication*, W. H. Freeman and Co., New York (1992).
8. T. Lindahl, *Nature* (London) **362**, 709 (1993).
9. A. Sancar, *Annu. Rev. Biochem.* **65**, 43 (1996).
10. H. Görner, *J. Photochem. Photobiol. B* **26**, 117 (1994).
11. P. O'Neill, E. M. Fielden, *Adv. Radat. Biol.* **17**, 53, (1993).
12. M. Symons, *J. Chem. Soc. Faraday Trans 1*, **83**, 1 (1987).
13. P. M. Cullis, J.D. Mc Clymont, M.E. Malone, A. N. Mather, I.D. Podmore, M.C. Sweeney, M. Symonds, *J. Chem. Soc. Perkin Trans. 2* **10**, 1695 (1992).
14. W. A. Bernhard, *J. Phys. Chem.* **93**, 2187 (1989).
15. M.D. Sevilla, D. Becker, M. Yan, S.R. Summerfield, *J. Phys. Chem.* **95**, 3409 (1991).
16. A.-O. Colson, B. Besler, M. D. Sevilla, *J Phys. Chem.* **96**, 9787 (1992).
17. M. Debije, M. Milano, W. Bernhard, *Angew. Chem. Int. Ed.* **38**, 2752 (1999).

18. Y. Razshazovskii, S. Swarts, J. Falcone, C. Taylor, M.D. Sevilla, *J. Phys. Chem. B* **101**, 1460 (1997).
19. M. Yan, D. Becker, S. Summerfield, P. Renke, M. D. Sevilla, *J. Phys. Chem.* **96**, 1983 (1992).
20. T. Melvin, S. Botchway, A. W. Parker, P. O'Neill, *J. Chem. Soc., Chem. Comm.* **6**, 653 (1995).
21. D. Becker, T. La Vere, M.D. Sevilla, *Radiation Res.* **140**, 123 (1994).
22. E. Gajewski, G. Rao, Z. Nackerdien, M. Dizdaroglu, *Biochemistry* **29**, 7876 (1990).
23. B. Sutherland, P. Bennett, O. Sidorkina, J. Laval, *Biochemistry* **39**, 8026 (2000).
24. P. M. Cullis, M. Malone, L. Merson-Davies, *J. Am. Chem. Soc.* **118**, 2776 (1996).
25. T. Melvin, S.W. Botchway, A.W. Parker, P.O'Neill, *J. Am. Chem. Soc.* **118**, 10031 (1996).
26. H. Sies, W. Schulz, S. Steenken, *J. Photochem. Photobiol. B* **32**, 97 (1996).
27. W. K. Pogozelski, T. D. Tullius, *Chem. Rev.* **98**, 1089 (1998).
28. C.J. Burrows, J.G. Muller, *Chem. Rev.* **98**, 1109 (1998).
29. J. Termini, *Mutation Res.* **450**, 107 (2000).
30. H. Seis, C. Menck, *Mutation Res.* **275**, 367 (1992)
31. S. Rajski, R. Williams, *Chem Rev.* **98**, 2723 (1998).
32. E. Jamieson, S. J. Lippard, *Chem. Rev.* **99**, 2467 (1999).
33. B. Armitage, *Chem. Rev.* **98**, 1171 (1998)
34. N. Paillous, P. Vicendo, *J. Photochem. Photobiol. B* **20**, 203 (1993).
35. D.B Hall, R.E. Holmlin, J.K. Barton, *Nature (London)* **382**, 731 (1996)
36. A. Sitlani, E.C. Long, A.M. Pyle, J.K. Barton, *J. Am. Chem. Soc.* **114**, 2302 (1992).

37. B. Armitage, C. Yu, C. Devadoss, G. Schuster, *J. Am. Chem. Soc.* **116**, 9847 (1994).
38. D. Breslin, G. B. Schuster, *J. Am. Chem. Soc.* **118**, 2311 (1996).
39. D. Breslin, J. Coury, J. Anderson, L. McFail-Isom, Y. Kan, L. D. Williams, L. A. Bottomley, G. B. Schuster, *J. Am. Chem. Soc.* **119**, 5043 (1997).
40. H.-Y. Mei, J. K. Barton, *J. Am. Chem. Soc.* **108**, 7414 (1986).
41. H.-Y. Mei, J. K. Barton, *Proc. Natl. Acad. Sci. USA* **85**, 1339 (1988).
42. D.T. Croke, L. Perrouault, M.A. Sari, J.-P. Battioni, D. Mansuy, C. Hélène, T. Le Doan, *J. Photochem. Photobiol. B* **18**, 41 (1993).
43. P. Herfield, P. Helissey, S. Giorgi-Renault, *Bioconj. Chem.* **5**, 67 (1994).
44. D.D. Eley, D.I. Spivey, *J. Chem. Soc., Faraday Trans.* **58**, 411 (1962).
45. T.J. Marks, *Science* **227**, 881 (1985).
46. J. G. Gaudiello, G. Kellogg, S. Tetrack, T. J. Marks, *J. Am. Chem. Soc.* **111**, 5259 (1989).
47. M. Almeida, J. Gaudiello, G. Kellogg, S. Tetrack, H. Marcy, W. McCarthy, J. Butler, C. Kannevuf, T. J. Marks, *J. Am. Chem. Soc.* **111**, 5271 (1989).
48. P. Schouten, J. Warman, M. De Haas, C. van Nostrum, G. Gelinck, R. Nolte, M. Copyn, J. Zwikker, M. Engel, M. Hanack, Y. Chang, W. Ford, *J. Am. Chem. Soc.* **116**, 6880 (1994).
49. P. Schouten, J. Warman, M. de Haas, M. A. Fox, H.-L. Pan, *Nature* **353**, 736 (1991).
50. Y. Okahata, T. Kobayashi, K. Tanaka, M. Shimomura, *J. Am. Chem. Soc.* **120**, 6165 (1998).
51. J.M. Warman, M. de Haas, A. Rupprecht, *Chem. Phys. Lett.* **249**, 319 (1996).
52. D. van Lith, J. M. Warman, M. de Haas, A. Hummel, *J. Chem. Soc., Faraday Trans. 1*, **82**, 2933 (1986).
53. H.-W. Fink, C. Schonenberger, *Nature (London)* **398**, 407 (1999).

54. D. Porath, A. Bezryadin, S. de Vries, C. Dekker, *Nature* (London) **403**, 635 (2000).
55. R. F. Anderson, K. Patel, W. Wilson, *J. Chem. Soc., Faraday Trans.* **87**, 3739 (1991).
56. A. Al-Kazwini, P. O'Neill, G. E. Adams, E. M. Fielden, *Radiat. Res.* **121**, 149 (1990).
57. A. Pezeshk, M. Symons, J. McClymont, *J. Phys. Chem.* **100**, 18562 (1996).
58. P. M. Cullis, J. McClymont, M. Symons, *J. Chem. Soc., Faraday Trans.* **86**, 591 (1990).
59. R. A. Marcus, N. Sutin, *Biochim. Biophys. Acta* **811**, 265 (1985).
60. H. B. Gray, W. R. Ellis, Jr., in *Bioinorganic Chemistry*, I. Bertini, H. Gray, S. Lippard, J. Selverstone Valentine, eds. University Science Books, Sausalito, California (1994).
61. B. C. Baguley, M. Le Bret, *Biochemistry* **23**, 937 (1984).
62. A.M. Brun, A. Harriman, *J. Am. Chem. Soc.* **114**, 3656 (1992).
63. A. Harriman, *Angew. Chem. Int. Ed.* **38**, 945 (1999).
64. P. Fromherz, B. Rieger, *J. Am. Chem. Soc.* **108**, 5361 (1986).
65. S. J. Atherton, P. C. Beaumont, *J. Phys. Chem.* **99**, 12025 (1995).
66. C. J. Murphy, J. K. Barton, *Meth. Enzymol.* **226**, 576 (226).
67. C. Turro, D. B. Hall, W. Chen, H. Zuilhof, J. K. Barton, N. Turro, *J. Phys. Chem.* **102**, 5708 (1998).
68. C. M. Dupureur, J.K. Barton, *Inorg. Chem.* **36**, 33 (1997).
69. B. P. Hudson, J. K. Barton, *J. Am. Chem. Soc.* **120**, 6877 (1998).
70. C.L. Kielkopf, K.E. Erkkila, B.P. Hudson, J.K. Barton, D. C. Rees, *Nature Struct. Biol.* **7**, 117 (2000).
71. T. W. Johann, J. K. Barton, *Phil. Trans. Royal Soc. (London)* **354**, 1706 (1996).

72. C. Hiort, P. Lincoln, B. Norden, *J. Am. Chem. Soc.* **115**, 3448 (1993).
73. K. Uchida, A.M. Pyle, T. Morii, J. K. Barton, *Nucleic Acids Res.* **17**, 10259 (1989).
74. A. M. Pyle, M. Y. Chiang, J. K. Barton, *Inorg. Chem.* **29**, 4487 (1990).
75. J. K. Barton, *Science* **233**, 727 (1986).
76. J. K. Barton, J. M. Goldberg, C. V. Kumar, N.J. Turro, *J. Am. Chem. Soc.* **108**, 2081 (1986).
77. A.M. Pyle, J.P. Rehmann, R. Meshoyrer, C.V. Kumar, N.J. Turro, J.K. Barton, *J. Am. Chem. Soc.* **111**, 3051 (1989).
78. A. M. Pyle, J. K. Barton, *Biochemistry* **33**, 12100 (1994).
79. N. Sardesai, S. Lin, K. Zimmerman, J.K. Barton, *Bioconj. Chem.* **6**, 302 (1995).
80. R. E. Holmlin, P. J. Dandliker, J. K. Barton, *Bonconj. Chem.* **10**, 1122 (1999).
81. C. J. Murphy, M. R. Arkin, N. Ghatlia, S. Bossmann, N. J. Turro, J. K. Barton, *Proc. Natl. Acad. Sci. USA* **91**, 5315 (1994).
82. M.R. Arkin, E.D.A. Stemp, R. E. Holmlin, J. K. Barton, A. Hörmann, E. Olson, P. F. Barbara, *Science* **273**, 475 (1996).
83. S. O. Kelley, G. Orellana, J. K. Barton, *J. Photochem. Photobiol. B* **58**, 72 (2000).
84. C.J. Murphy, M.R. Arkin, Y. Jenkins, N. Ghatlia, S. Bossmann, N.J. Turro, J. K. Barton, *Science* **262**, 1025 (1993).
85. T.J. Meade, J. Kayyem, *Angew. Chem. Int. Ed.* **34**, 352 (1995).
86. S. O. Kelley, R. E. Holmlin, E. D. A. Stemp, J. K. Barton, *J. Am. Chem. Soc.* **119**, 9861 (1997).
87. F. D. Lewis, T. Wu, Y. Zhang, R. Letsinger, S. Greenfield, M. Wasielewski, *Science* **277**, 673 (1997).

88. F. D. Lewis, R. Letsinger, M. Wasielewski, *Acc. Chem. Res.* **34**, 159 (2001).
89. K. Fukui, K. Tanaka, *Angew. Chem. Int. Ed.* **37**, 158 (1998).
90. K. Fukui, K. Tanaka, *Nucleic Acids Res.* **24**, 3962 (1996).
91. K. Fukui, K. Tanaka, M. Fujisuka, A. Watanabe, O. Ito, *J. Photochem. Photobiol. B* **50**, 18 (1999).
92. W. Davis, I. Naydenova, R. Haselsberger, A. Ogrodnik, B. Giese, M. Michel-Beyerle, *Angew. Chem. Int. Ed.* **39**, (2000).
93. S. O. Kelley, J. K. Barton, *Chem. Biol.* **5**, 413 (1998).
94. S. O. Kelley, J. K. Barton, *Science* **283**, 375 (1999).
95. C. Wan, T. Fiebig, S.O. Kelley, C. R. Treadway, J. K. Barton, A. H. Zewail, *Proc. Natl. Acad. Sci. USA* **96**, 6014 (1999).
96. S. O. Kelley, N. M. Jackson, M.G. Hill, J. K. Barton, *Angew. Chem. Int. Ed.* **38**, 941 (1999).
97. S.O. Kelley, E.M. Boon, J. K. Barton, N.M. Jackson, M.G. Hill, *Nucleic Acids Res.* **27**, 4830 (1999).
98. S. Steenken, S.V. Jovanovic, *J. Am. Chem. Soc.* **119**, 617 (1997).
99. S. Steenken, *Chem. Rev.* **89**, 503 (1989).
100. I. Saito, M. Takayama, H. Sugiyama, K. Nakatani, *J. Am. Chem. Soc.* **117**, 6406 (1995).
101. I. Saito, M. Takayama, *J. Am. Chem. Soc.* **117**, 5590 (1995).
102. H. Sugiyama, I. Saito, *J. Am. Chem. Soc.* **118**, 7063 (1996).
103. F. Prout, K. Houk, C. Foote, *J. Am. Chem. Soc.* **120**, 845 (1998).
104. D. B. Hall, J. K. Barton, *J. Am. Chem. Soc.* **119**, 5045 (1997).
105. D. T. Odom, J. K. Barton, *Biochemistry*, *in press*.
106. D. T. Odom, E. Dill, J.K. Barton, *Chem. Biol.* **7**, 475 (2000)
107. M. R. Arkin, E. D. A. Stemp, S. Coates Pulver, J. K. Barton, *Chem. Biol.* **4**, 389 (1997).

108. E. D. A. Stemp, M. R. Arkin, J. K. Barton, *J. Am. Chem. Soc.* **119**, 2921 (1997).
109. D. B. Hall, S.O. Kelley, J. K. Barton, *Biochemistry* **37**, 15933 (1998).
110. G. B. Schuster, *Acc. Chem. Res.* **33**, 253 (2000).
111. P. T. Henderson, D. Jones, G. Hampikian, Y. Kan, G. B. Schuster, *Proc. Natl. Acad. Sci. USA* **96**, 8353 (1999).
112. Y. Kan, G. B. Schuster, *J. Am. Chem. Soc.* **121**, 11607 (1999).
113. Y. Kan, G. B. Schuster, *J. Am. Chem. Soc.* **121**, 10857 (1999).
114. S. Gasper, G. B. Schuster, *J. Am. Chem. Soc.* **119**, 12762 (1997).
115. V. Sartor, P. T. Henderson, G. B. Schuster, *J. Am. Chem. Soc.* **121**, 11028 (1999).
116. S. Matsugo, S. Kawanishi, K. Yamamoto, H. Sugiyama, T. Matasuura, I. Saito, *Angew. Chem. Int. Ed.* **30**, 1351 (1991).
117. K. Nakatani, C. Dohno, I. Saito, *J. Am. Chem. Soc.* **121**, 10854 (1999).
118. K. Nakatani, C. Dohno, I. Saito, *J. Am. Chem. Soc.* **122**, 5893 (2000).
119. K. Nakatani, C. Dohno, I. Saito, *Tet. Lett.* **41**, 10041 (2000).
120. K. Nakatani, C. Dohno, I. Saito, *J. Org. Chem.* **64**, 6901 (1999).
121. A. Dussy, B. Giese, *Nucleosides Nucleotides* **18**, 1343 (1999).
122. E. Meggers, M. Michel-Beyerle, B. Giese, *J. Am. Chem. Soc.* **120**, 12950 (1998).
123. B. Giese, S. Wessely, M. Sporman, U. Lindemann, E. Meggers, M. Michel-Beyerle, *Angew. Chem. Int. Ed.* **38**, 996 (1999).
124. E. Meggers, A. Dussy, T. Schäfer, B. Giese, *Chem. Eur. J.* **6**, 485 (2000).
125. B. Giese, *Acc. Chem. Res.* **33**, 631 (2000).
126. P. J. Dandliker, R. E. Holmlin, J. K. Barton, *Science* **275**, 1465 (1997).
127. A. Dotse, E. K. Boone, G. B. Schuster, *J. Am. Chem. Soc.* **122**, 6825 (2000).

128. D. A. Vicic, D. T. Odom, M. E. Núñez, D. A. Gianolio, L. W. McLaughlin, J. K. Barton, *J. Am. Chem. Soc.* **122**, 8603 (2000).
129. D. Beratan, S. Priyadarshy, S. Risser, *Chem. Biol.* **4**, 3 (1997).
130. F. Grozema, Y. Berlin, L. Siebbeles, *J. Am. Chem. Soc.* **122**, 10903 (2000).
131. D. Dee, M. Baur, *J. Chem. Phys.* **60**, 541 (1974).
132. M. Bixon, B. Giese, S. Wessely, T. Langenbacher, M. Michel-Beyerle, J. Jortner, *Proc. Natl. Acad. Sci. USA* **96**, 11713 (1999).
133. J. Jortner, M. Bixon, T. Langenbacher, M. Michel-Beyerle, *Proc. Natl. Acad. Sci. USA* **95**, 12759 (1998).
134. Y. Berlin, A. Burin, M. Ratner, *J. Phys. Chem.* **104**, 443 (2000).
135. T. Williams, D. Odom, J. K. Barton, *J. Am. Chem. Soc.* **122**, 37 (2000).
136. S. V. Rakhmanova, E. Conwell, *J. Phys. Chem.* **105**, 2056 (2001).
137. S. R. Rajski, S. Kumar, R. J. Roberts, J. K. Barton, *J. Am. Chem. Soc.* **121**, 5615 (1999).
138. S. R. Rajski, J. K. Barton, *Biochemistry* **40**, 5556 (2001).
139. H.-A. Wagenknecht, E. D. A. Stemp, J. K. Barton, *Biochemistry* **39**, 5483 (2001).
140. H.-A. Wagenknecht, S. R. Rajski, M. Pascaly, E. D. A. Stemp, J. K. Barton, *J. Am. Chem. Soc.* **123**, 4400 (2001).
141. A. Heller, *Faraday Discuss.* **116**, 1 (2000).
142. S. R. Rajski, B. A. Jackson, J. K. Barton, *Mut. Res.* **447**, 49 (2000).

Chapter 2

Long-Range Oxidative Damage to DNA*

* Adapted from: M. E. Núñez, D. B. Hall, J. K. Barton, *Chem. Biol.* **6**, 85 (1998)

2.1 Introduction

As discussed in chapter 1, charge transport through DNA has been demonstrated spectroscopically, electrochemically, and biochemically. “Chemistry at a distance” was demonstrated first in an oligonucleotide assembly containing the tethered rhodium intercalator $\text{Rh}(\text{phi})_2\text{bpy}^{3+}$ and two 5'-GG-3' sites (1). The 5'-GG-3' sites were oxidized by the rhodium complex even when it was covalently tethered to one end of the DNA assembly at a distance of 10 or more base pairs away, corresponding to a distance for charge migration of 34 Å. Moreover, in a rhodium-modified DNA assembly containing two 5'-GG-3' sites, slightly greater oxidative damage was observed at the distal (34 Å) than the proximal site (17 Å), suggesting that over these distances, the yield of oxidative damage might be relatively insensitive to the distance of charge migration. This long-range reaction is, however, sensitive to the stacking of the intercalator into the helix, since the right-handed (Δ) isomer, which fits more deeply into the major groove of a right-handed DNA helix, generates more oxidized product than does the left-handed (Λ) isomer. Long-range oxidation is also sensitive to disturbances in the stacking generated by intervening bulges in DNA between the oxidant and the 5'-GG-3' site; large bulges which do not stack well into the helix (for example, the 5'-ATA-3' bulge) were shown to diminish the distal oxidation significantly (2).

Long-range charge transfer chemistry in DNA appears to be general and has now been demonstrated with a range of tethered oxidants. A tethered, intercalating ground-state ruthenium (III) species generated *in situ* was shown to oxidize guanine doublets over a comparable distance (3). When the only guanine doublet was replaced by a 5'-GC-3' sequence, damage was observed essentially equally at all the guanine sites. This observation underscored the notion that the radical could equilibrate over sites of equal oxidation potential on a time scale which was fast compared to the irreversible trapping reaction, which occurs on the μs to ms time

scale. Analogous long-range guanine damage was subsequently observed by photoexcitation of covalently bound anthraquinones, associated in a capped position on the duplex (4), as well as ethidium (5) and a uridine base modified with a cyano-benzophenone derivative (6). It is now clear that this long range oxidative damage to DNA is not simply a function of the oxidant employed but instead represents a unique feature of the DNA itself.

Given that charge migration can occur through DNA, it now becomes critical to establish those factors which control DNA-mediated charge transfer and ultimately lead to permanent base lesions. The distances over which charge transfer between guanine and an intercalator had been previously observed were between five and fifteen base pairs (17-51 Å), which are on the order of a single protein binding site. Here we examine whether charge transfer through DNA occurs over still longer distances, corresponding to promoter regions or perhaps through whole genes. Furthermore, in long pieces of DNA involving more than just a few intervening base pairs, issues of the sequence dependence upon charge transfer become much more important. Some sequences might better mediate charge transport than others, based upon their redox potentials and base stacking characteristics, so that we might envision traps, blocks, and bumps as well as regions of smooth sailing along the electronic DNA "pi-way." We have therefore begun to address the dependence on distance and sequence of DNA-mediated electron transfer from guanine to an intercalated photooxidant.

2.2 Methods

2.2.1 Oligonucleotide Preparation

Oligonucleotides were synthesized using phosphoramidite chemistry on an Applied Biosystems 394 DNA synthesizer with a dimethoxy trityl protective group on the 5' end. Oligonucleotides were purified on a Rainin Dynamax C18 column

by reversed-phase HPLC on a Waters HPLC and were deprotected by incubation in 80% acetic acid for 15 minutes. After deprotection, the oligonucleotides were purified again on the same C18 column by reversed-phase HPLC and were quantitated by UV-visible absorption spectroscopy on a Beckman DU 7400 Spectrophotometer using the following extinction coefficients for single-stranded DNA : $\epsilon(260\text{ nm, M}^{-1}\text{cm}^{-1})$ adenine (A) = 15,000; guanine (G) = 12,300; cytosine (C) = 7,400; thymine (T) = 6,700. Single strands were mixed with equimolar amounts of complementary strand and were annealed by gradual cooling from 95°C over 2 hours. DNA strands containing a phosphate group at the 5' end were prepared using the Chemical Phosphorylation Reagent (Glen Research) and were purified by HPLC without a dimethoxy trityl protective group.

2.2.2 Preparation of Short Metal-Containing Oligonucleotides

$\text{Rh}(\text{phi})_2(\text{bpy}')^{3+}$ and $\text{Ru}(\text{phen})(\text{bpy}')(\text{dppz})^{2+}$ ($\text{bpy}' = 4\text{-butyric acid-4'-methylbipyridine}$; $\text{phi} = 9,10\text{-phenanthrene quinone diimine}$; $\text{phen} = 1,10\text{-phenanthroline}$; $\text{dppz} = \text{dipyrido}[3,2\text{-a}:2',3']\text{phenazine}$) were prepared according to published procedures (7-9). Ruthenium and rhodium-tethered 17-base pair oligonucleotides were prepared according to published procedures (10) and were purified on a Rainin Dynamax C4 column by reversed-phase HPLC on a Hewlett-Packard 1050 HPLC. The diastereomeric strands were isolated and numbered according to the order of elution, and absolute configuration around the metal center was determined by circular dichroism based on the stereochemistry of the metal center (11). Purification of the rhodium-modified 28-mers was achieved by C18 reverse phase HPLC at 65°C (25 mM NH_4OAc , pH = 7, 0 to 15% CH_3CN over 30 minutes). A racemic mixture was used for all experiments with these constructs. The metal-conjugated oligonucleotides were quantitated using the following

extinction coefficients: for Rh-modified oligonucleotides, $\epsilon(390 \text{ nm}, \text{M}^{-1}\text{cm}^{-1}) = 19,000$; for Ru-modified oligonucleotides, $\epsilon(440 \text{ nm}, \text{M}^{-1}\text{cm}^{-1}) = 19,000$.

2.2.3 Preparation of Long Metal-Containing Oligonucleotides by Enzymatic Ligation

All ligations were performed using high-concentration T4 DNA ligase (New England Biolabs) in T4 DNA ligase buffer prepared without DTT. The metal-conjugated 63-mer was prepared by ligating a metal-conjugated 17-base pair oligonucleotide to a 46-base-pair oligonucleotide bearing a phosphate on the 5' end (Fig 2.1). First the 17-mer and the 46-mer were each annealed to their complementary oligonucleotides to create two duplexes with matching 6-base-pair sticky ends; then the two duplexes were mixed together with 10,000 units of high-concentration ligase and the solution was incubated at 14 °C overnight. The final solution contained 5 nmoles of the metallated duplex and 6 nmoles of the phosphorylated duplex in a 350 μL volume. The metal-conjugated 63-mer was separated from the smaller pieces by denaturing polyacrylamide gel electrophoresis in a 14% polyacrylamide gel. The band containing the longest oligonucleotide was identified by UV shadowing, extracted from the gel, and ethanol precipitated. The metal-conjugated 46-mer was prepared in the same manner.

2.2.4 Irradiation of Metal-Containing Oligonucleotides

Oligonucleotides were radioactively labeled by incubation with $\gamma\text{-}^{32}\text{P}\text{-ATP}$ and T4 polynucleotide kinase (12). The radiolabeled strands were purified by preparative gel electrophoresis in a 15% denaturing polyacrylamide gel, extracted, and purified by elution from a Nensorb 20 cartridge. For the metal-conjugated 63-base-pair assemblies, the labeled strands were annealed with complementary unlabeled metallated single strands at a concentration of 2 μM (strands) in 75 mM

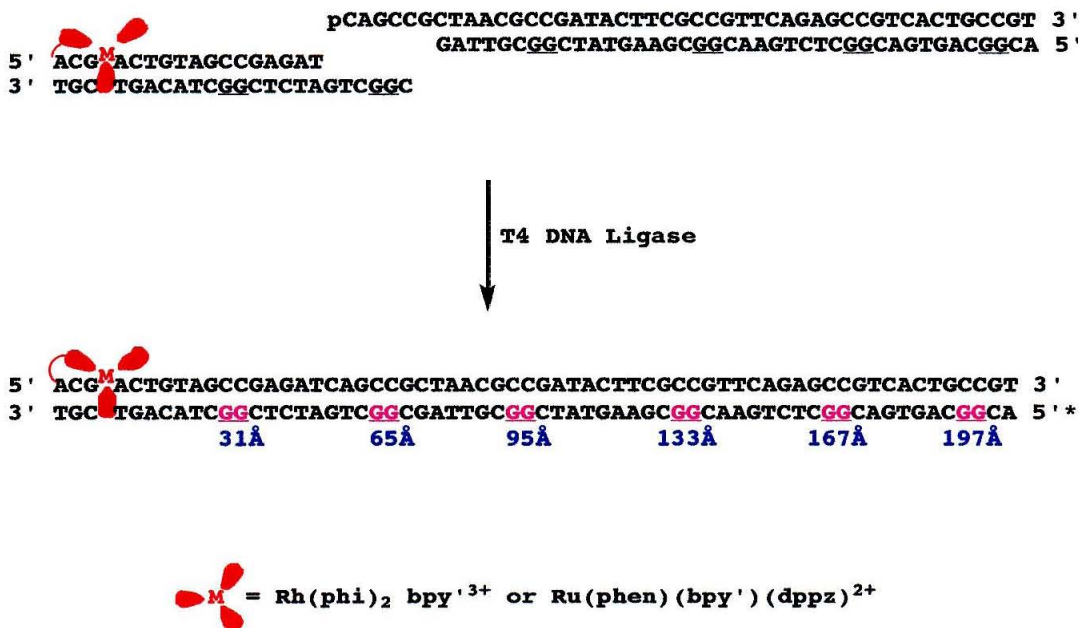


Figure 2.1: Sequence and synthetic strategy for a metallointercalator-tethered 63-base-pair assembly. The duplex assembly contains a tethered rhodium or ruthenium octahedral intercalator (red) and 6 guanine doublets spaced approximately 10 base pairs apart (magenta). The duplex was assembled from smaller oligonucleotides prepared by solid phase chemical synthesis, which were then enzymatically ligated using T4 DNA ligase. The 63-base strand containing the guanine doublets was 5' end-labeled with ³²P at the farthest end of the duplex from the metal, so the oxidation products on the bottom of each gel were produced by oxidation at the furthest end of the duplex from the rhodium or ruthenium.

Tris HCl (pH 8.0) as described above. For rhodium-containing 63-base-pair assemblies, 30 μ L aliquots were irradiated at 365 nm for 80-90 minutes on a 1,000 W Hanovia Hg-Xe arc lamp equipped with a monochromator. For ruthenium-containing 63-base-pair assemblies, 30 μ L aliquots were irradiated at 436 nm for 8-12 minutes with 40 μ M methyl viologen or for 1 hour without quencher. Control aliquots were not irradiated. All samples were treated with 10% piperidine for 30 minutes at 90°C, lyophilized, then analyzed by denaturing PAGE in a 14% gel. Cleavage of the labeled strand was measured by phosphorimagery using ImageQuant, v3.3 (Molecular Dynamics). The level of oxidation at individual guanine bases was determined by measuring the intensity of the band corresponding to that base as a fraction of the intensity of the whole lane. The fractional intensity of the corresponding band in the control lane was subtracted out to account for background levels of damage.

2.3 Results and Discussion

2.3.1 Distance Dependence of Guanine Oxidation on Long DNA Duplexes

We constructed a metallated 63-base-pair assembly containing several guanine doublets (Fig. 2.1). These duplexes contained one of two tethered octahedral metallointercalators, $\text{Rh}(\text{phi})_2\text{bpy}^{3+}$ or $\text{Ru}(\text{phen})(\text{bpy}')(\text{dppz})^{2+}$ (Fig. 1.7, 1.20). Excited-state rhodium(III) complexes may provide a model for oxidative damage *in vivo* by exogenous photosensitizers, while ground-state ruthenium (III) complexes could be considered analogous to solution-borne physiological oxidants such as hydroxyl radical. Of the six 5'-GG-3' sites contained in the assembly, the first 5'-GG-3' site was located 9 base pairs from the proposed intercalation site of the tethered metal and each of the others were located roughly 10 base pairs apart at 31, 65, 95, 133, 167, and 197 Å separation from the intercalation site. Each guanine doublet was flanked by cytosine on the 3' and 5'

sides. Since metallointercalator-tethered oligonucleotides longer than approximately 35 base pairs cannot be synthesized directly in good yield and in pure form, the metallointercalator-bound 63-mer duplexes were synthesized in pieces and then ligated together.

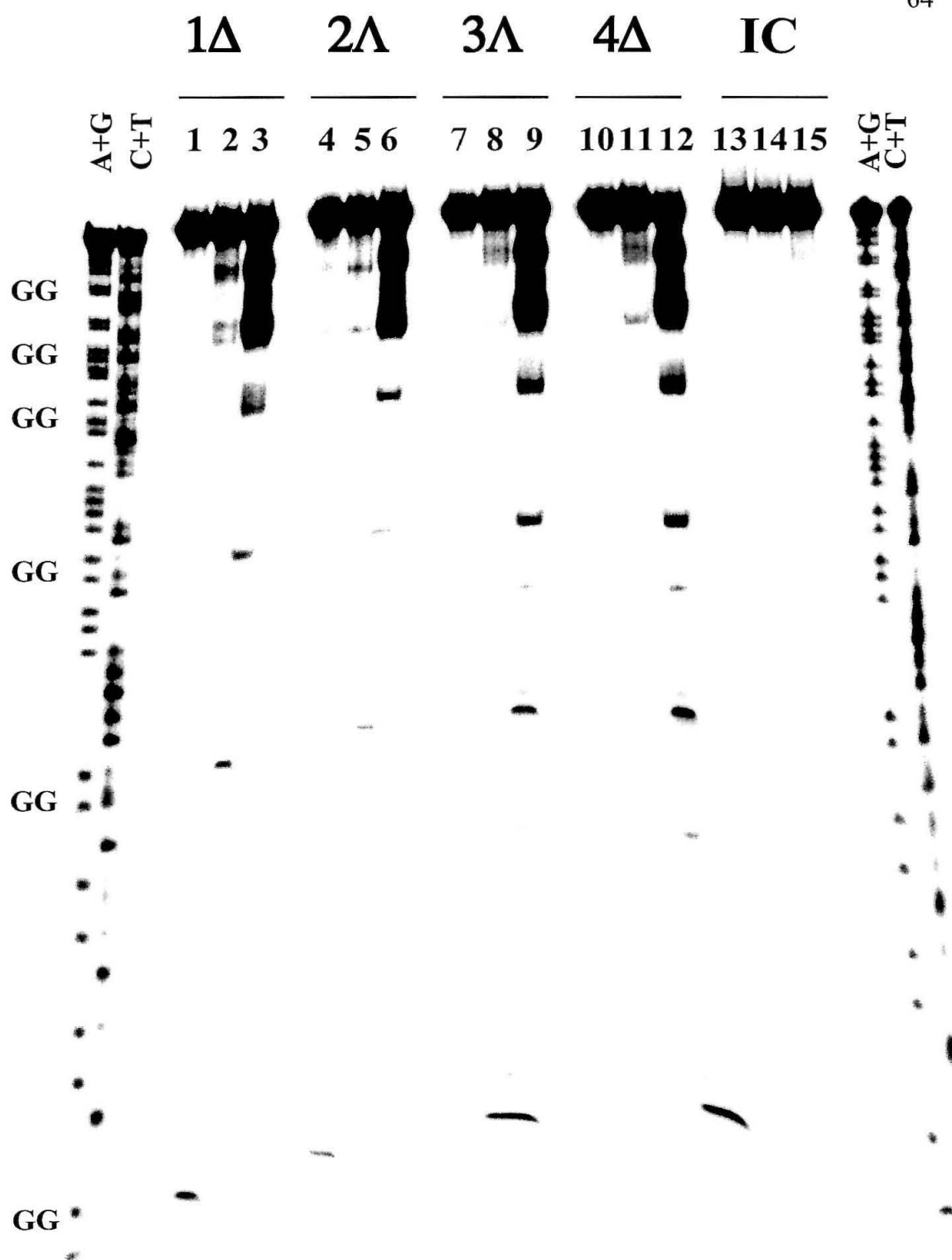
2.3.2 Long-Distance Oxidation by Ruthenium(III)

A 63-mer containing the tethered ruthenium(II) intercalator was constructed to examine the distance over which guanine oxidation could be observed with the ground state Ru(III) oxidant, generated by oxidative quenching of the photoexcited $^*Ru(II)$ by nonintercalating methyl viologen (3,16). As can be seen in Figure 2.2, oxidation at the 5' guanines of all 6 guanine doublets was observed after irradiation at 436 nm in the presence of methyl viologen. Hence, Ru(III) generated *in situ* can oxidize guanine doublets through almost 200 Å of the DNA π stack. It is noteworthy that long-range oxidation was only somewhat diminished with increasing distance over the range of separation of 100 to 200 Å from the intercalation site, but there was still appreciable base damage at these long intercalator-guanine distances.

The efficiency of guanine oxidation varied between all four diastereomeric metal-conjugated strands, with the 4 Δ isomer oxidizing guanine most efficiently and the 2 Δ isomer oxidizing guanine the least efficiently. This order of reactivity, 4 Δ > 1 Δ \approx 3 Δ > 2 Δ , agreed with previous studies indicating that the right-handed Δ isomers are better able to fit into the major groove, intercalate into the π stack, and oxidize nucleotide bases. In donor-acceptor systems using ruthenium intercalators, the efficiency of quenching followed the same order (17).

To demonstrate that oxidation 200 Å from the intercalation site is generated by electron transfer *through* the helix, it was important to establish that the reaction was intraduplex. First we demonstrated that the ruthenium complex is intercalated

Figure 2.2: Oxidation of the 5' G of guanine doublets by ground-state Ru(III). Each set of 3 lanes contains the following, respectively: a dark control (without irradiation); a ruthenium-tethered sample irradiated for an hour without quencher, which marks the site of ruthenium intercalation by singlet oxygen chemistry; and a ruthenium-tethered duplex irradiated for 10 minutes in the presence of methyl viologen to generate Ru(III) by flash-quench. All 6 guanine doublets were oxidized by the Ru(III) intercalator, with the largest amount of damage near the metallated end of the assembly (lanes 3, 6, 9, 12). The majority of the singlet oxygen damage occurred at one end of the duplex (lanes 2, 5, 8, 11), indicating that the metal was intercalated at the end of the duplex to which it was tethered. Note that singlet oxygen was also formed in the presence of quencher, but in very low yield on this time scale. The efficiency of oxidation depended on the diastereomer of the metal-conjugated strand. This order of reactivity, $4\Delta > 1\Delta \approx 3\Lambda > 2\Lambda$, agreed with previous studies indicating that the right-handed Δ isomers are better able to fit into the major groove and intercalate into the π stack. A mixture of assemblies containing those exclusively metallated but not radiolabeled, and those radiolabeled but lacking the tethered metal was irradiated to demonstrate that the reaction we observe occurs intra-duplex. Lanes 13-15 containing the intermolecular control (IC) samples show that the long-range oxidation was not due to intermolecular intercalation of the metal complex nor to a diffusible reactive species. The 2Λ diastereomer was used in the intermolecular control samples.



at the end of the duplex to which it is tethered. Irradiation of the ruthenium complex without methyl viologen leads to the sensitization of singlet oxygen, which is reactive only with guanine residues in the immediate vicinity of the intercalation site, given the limited lifetime and rate of diffusion of $^1\text{O}_2$ (3). When the ruthenium-tethered 63-base-pair assembly was irradiated without quencher, so as to generate damage with singlet oxygen, the damage was confined to one end of the duplex (lanes 2, 5, 8, and 11). This result was fully consistent with our assignment of the intercalation site to 2-3 base pairs from the end of the duplex based on molecular modeling. Low DNA concentrations were used in these experiments to disfavor interduplex intercalation. We expected metal intercalation to occur exclusively at the end of the duplex nearest the tether because of the rod-like biophysical behavior of short DNA oligonucleotides (18), and the singlet oxygen results supported the contention that the metallointercalator was bound only intraduplex.

In order to confirm more rigorously that the electron transfer reaction occurred intraduplex, we also examined guanine oxidation of a radiolabeled 63-base-pair assembly bearing no conjugated metal complex in the presence of an assembly with the same DNA sequence and a conjugated ruthenium complex but no radioactive label. These samples (lanes 13-15) showed little oxidation above background, indicating that the ruthenium complexes did not intercalate into assemblies other than the ones to which they were tethered and that the reactive species which oxidizes guanine was not diffusible. Importantly, this result also indicated that the oxidation that we observe is not due to a direct reaction of the DNA with the light used to photoexcite the metal complex. Therefore, oxidation of 5'-GG-3' sites in DNA by Ru(III) intercalators is mediated by the DNA duplex over a distance of 197 Å.

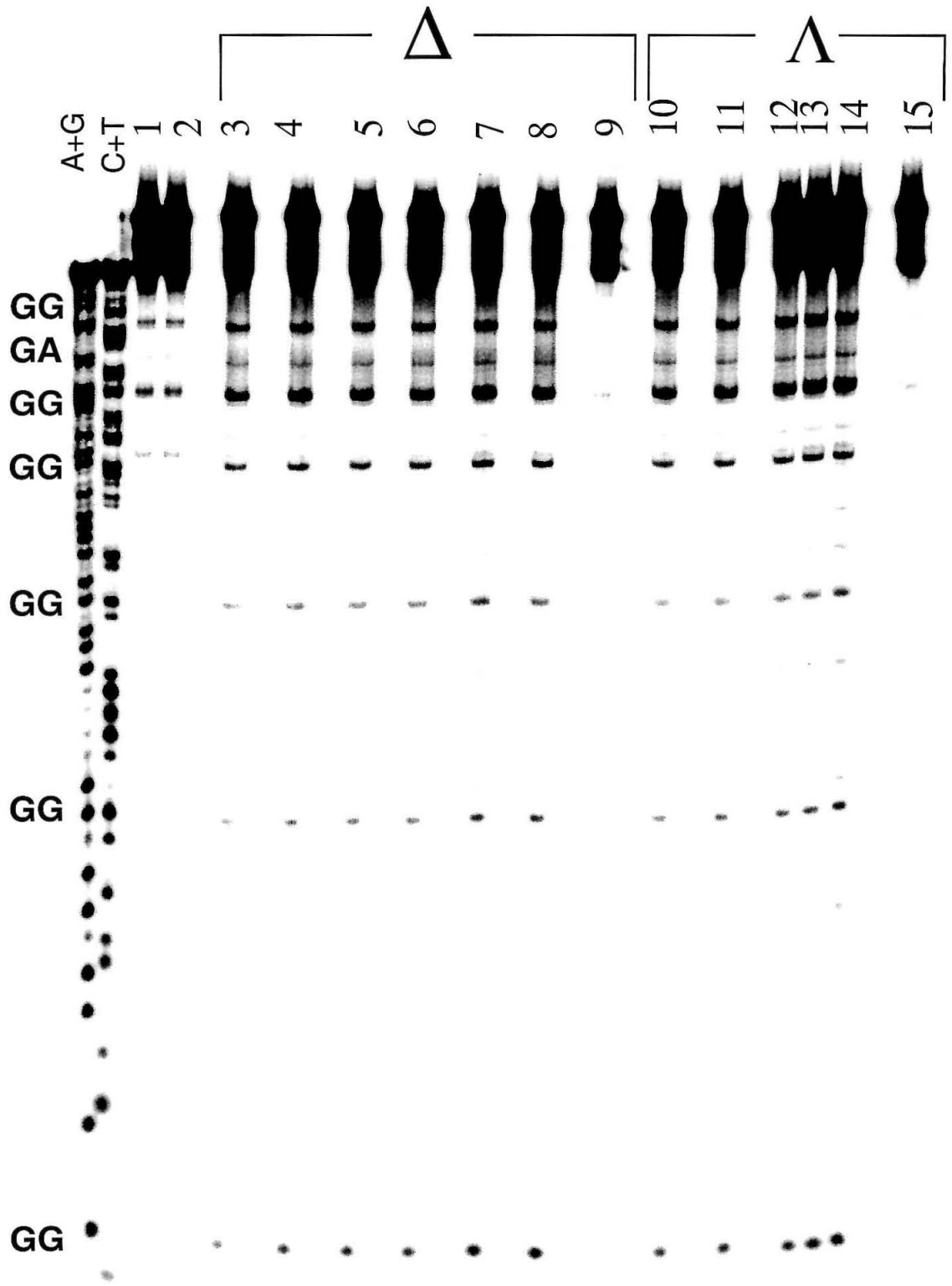
2.3.3 Long-Distance Oxidation by Photoexcited Rhodium(III)

A rhodium-tethered 63-base-pair assembly was also constructed in order to examine the distance over which oxidation by photoexcited rhodium can occur. With Rh(III), no diffusible quencher is required, since photoexcited $^*\text{Rh(III)}$ is a potent oxidant for DNA. This DNA assembly was identical to the ruthenium-tethered assembly except for the identity of the metallointercalator, which has not only a different metal center but different ligands and a higher redox potential (+1.6 V for Ru(III) vs. +2.0 V for $^*\text{Rh(III)}$) (3,19,20). Unlike Ru(III), which can oxidize only purines because of its potential, $^*\text{Rh(III)}$ can oxidize all of the DNA. After irradiation of the rhodium-conjugated 63-base-pair assembly at 365 nm and treatment with aqueous piperidine, approximately equal oxidation by both the Λ and Δ isomers of rhodium was observed at all 6 guanine doublets, 31, 65, 95, 133, 167, and 197 Å away from the putative intercalation site of the metal complex (Fig. 2.3). In addition to this guanine damage, some oxidative damage was observed also between the two proximal guanine doublets at a 5'-GA-3' site, which *ab initio* molecular orbital calculations have indicated is the next most easily oxidized site after 5'-GG-3' (21).

Irradiation of phi complexes of rhodium at 313 nm induces direct strand scission at the site of intercalation without piperidine treatment, providing an excellent marker for rhodium intercalation sites on DNA. Rhodium-tethered 63-base-pair assemblies were damaged extensively at the extreme 3' end of the strand but only minimally at the guanine doublets when irradiated at 313 nm (lanes 1,2), demonstrating that the rhodium complexes were intercalated near one end of the duplex and not within neighboring duplexes nor into the far end of the duplexes to which they were tethered.

We considered that multiple cleavage events on the same DNA duplex would complicate analysis of the distribution of oxidation, and therefore we

Figure 2.3: Oxidation of the 5' G of guanine doublets by photoexcited $\text{Rh}(\text{phi})_2\text{bpy}^{3+}$. Illustrated here are the phosphorimagery results for metallated duplexes after irradiation, piperidine treatment, and separation in a 14% denaturing polyacrylamide gel. The duplexes were radioactively labeled on the non-metallated strand. The metal was tethered to the far end of the assembly from the radioactive label (top of gel). Lanes 1 and 2 show the direct photocleavage by the metal complex (Δ and Λ isomers, respectively) resulting from irradiation at 313 nm for 10 minutes. In these samples, which were not piperidine treated, almost all of the cleavage is observed at the end of the assembly closest to the metal. The samples in lanes 3-15 were irradiated at 365 nm and piperidine cleavage to reveal the sites of guanine damage. Lanes 3-9 show the long-range oxidation of guanine doublets by the Δ -rhodium diastereomer over a range of time points (60, 70, 80, 90, 100, 110, and zero minutes, left to right), and lanes 10-15 show the same for Λ -rhodium diastereomer (60, 70, 80, 90, 100, zero minutes, left to right). The efficiencies of oxidation by the Λ and Δ isomers were approximately the same, so in later experiments mixtures of both isomers were used. The oxidation at all of the guanine doublets increased as a function of irradiation time. Irradiation conditions for all of the samples were 2 μM metal-tethered assembly, 75 mM Tris-HCl pH 8.3.



monitored the guanine oxidation at all of the doublets as a function of time. The amount of oxidation increased linearly as function of irradiation time for all six of the guanine doublets, indicating that multiple cleavage events on the same strand did not occur over the range of irradiation times used in this experiment. The possibility of multiple oxidation events at a single site caused by some preferential oxidation of 8-oxo-G formed in a separate oxidation event cannot be completely ruled out (22-26); however, this would require catalytic oxidation by the rhodium complex.

As in the case with the ruthenium-tethered assembly, the long-range guanine oxidation occurred intra-duplex. When an assembly with a conjugated rhodium complex but no radioactive label was irradiated in the presence of an assembly with the same DNA sequence labeled at the 5' end but bearing no metal, no oxidation was observed, which indicated that the reaction was intramolecular and therefore was mediated by the DNA duplex (data not shown).

Thus both excited-state rhodium and ground-state ruthenium intercalators can oxidize guanine bases through at least 200 Å of DNA. This overall distance for charge transport is not dissimilar to that found in the photosynthetic reaction center and across the mitochondrial electron transport chain (27). A distance of 200 Å through DNA furthermore corresponds to the distance between various conserved sites in a prokaryotic promoter or approximately 20 amino acids worth of genetic code. Thus DNA may offer an important macromolecular medium for the transmission of chemical information over long molecular distances within biological systems. Whether charges migrate in DNA over longer distances corresponding to eukaryotic genes, regulatory regions, or introns is a question that we are actively pursuing.

2.3.4 Comparison of Oxidation by *Rh(III) and Ru(III)

Both *Rh(III) and Ru(III) were both shown to oxidize DNA over at least 200 Å, and the patterns of oxidative damage by the two oxidants showed other similarities as well. Oxidation by both oxidants at the most distal guanine doublet was slightly higher than the oxidation at the two doublets which are located closer to the metal (Fig. 2.4). Oxidation at the guanine doublet nearest the end of an assembly generally is higher than at more proximal doublets (*I*), which may be due to better trapping of the guanine radical intermediate at the frayed ends of duplexes. Oxidation by both oxidants was strong in the 20-30 base pairs nearest the metal and dropped off gradually past that distance, a phenomenon which was not observed previously since all of the duplexes studied were shorter than 30 base pairs in length. Interestingly, the distribution of oxidized guanines generated by *Rh(III) and Ru(III) as a function of distance displayed one interesting difference. Although oxidation decreased gradually with distance from the metal in assemblies containing either intercalator, the rhodium complex was better able to oxidize guanine at longer distances from the intercalation site than was ruthenium. The difference in distance dependence could be caused by any of several factors, including the difference in intercalating ligand, the ease of back-electron transfer from the metal, or the difference in the redox potential of the photooxidant. The latter possibility would be consistent with a “hopping” model of charge transfer through DNA (*vide infra*) (28).

2.3.5 Temperature Dependence of Long-Distance Oxidation

The temperature dependence of guanine oxidation by rhodium over a range of physiologically relevant temperatures was also examined. Over this range of temperatures (5-35 °C), a 63-base-pair duplex should remain fully stacked. In general, the total amount of oxidized guanine generated by photoexcitation of

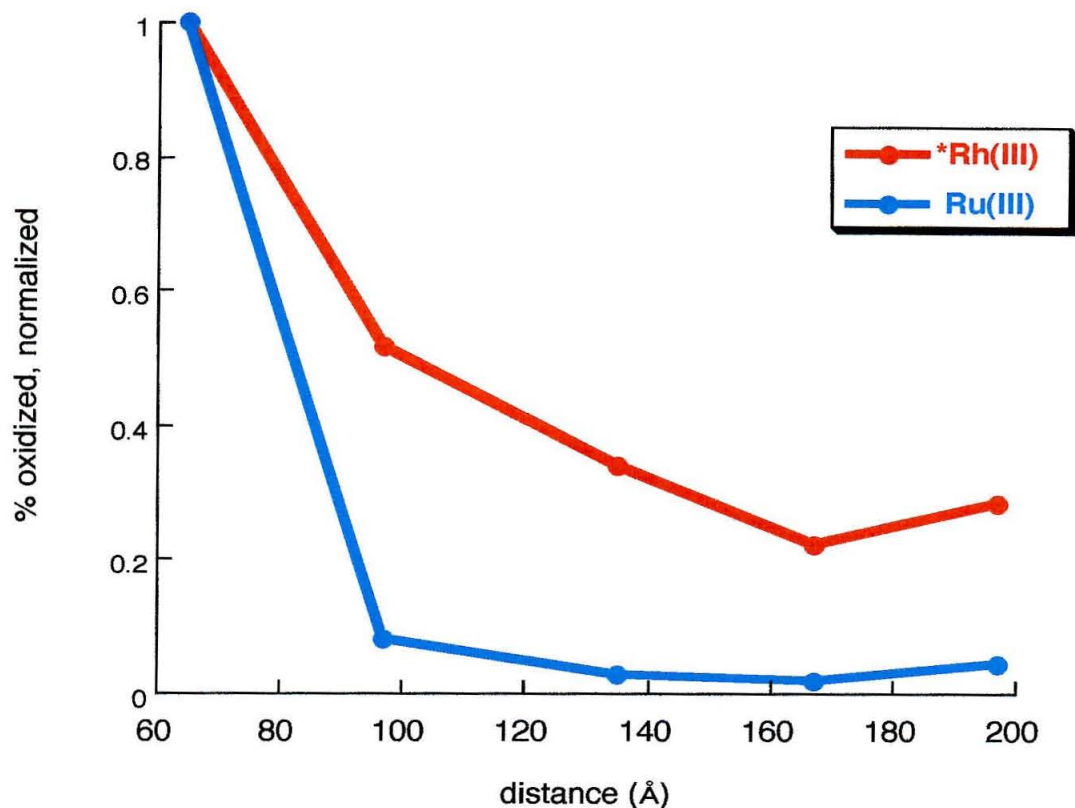


Figure 2.4: Distance dependence of long-range guanine oxidation by Ru(III) and *Rh(III). Ratios for the distal to proximal oxidation in the assemblies shown in Fig. 2.3 and Fig. 2.4 were compared for the ruthenium- and rhodium-tethered assemblies. The ratios at 60Å were used for normalization because the cleavage bands at shorter distances were intense and difficult to isolate for the purposes of quantitation. Oxidation of guanine by both tethered metallointercalators decreased as a function of distance. Interestingly, this distance dependence was more pronounced for ruthenium than for rhodium.

rhodium increased slightly with increasing temperature, likely reflecting an increased intercalation over this range of temperatures. More interestingly, the *distribution* of oxidized guanine products changed with increasing temperatures. The amount of oxidized guanine formed at the distal end of the duplex increased with increasing temperature, while the amount of oxidized guanine formed at the proximal end of the duplex decreased (Fig. 2.5). These two regions intersected at a distance of approximately 90 Å from the rhodium complex, where there was no change evident in oxidation over this temperature range. Although this crossover point corresponded to the center of the assembly, we determined that it was not location- but sequence-specific. The temperature dependence of oxidation in a 46-base-pair assembly (which was identical to the 63-base-pair assembly except for the last missing bases) contained a crossover point at the same sequence position, despite the fact that this point was no longer in the middle of the duplex (data not shown). Thus this crossover point did not represent a central node of an oscillating string model of DNA (29). Interestingly, the sequence at this position contained one of only three 5'-TA-3' sequences in the assembly. Since 5'-TA-3' is extremely flexible and frequently kinked due to the poor π overlap between bases (14), we propose that the 5'-TA-3' step might act as a temperature-sensitive "hinge." At low temperatures the hinge would be bent, blocking hole transfer to the end of the helix, while at increased temperatures the hinge would become more flexible, acquiring other conformations which were more amenable to charge transfer.

Our earlier studies had indicated that charge transfer through the DNA helix can be used to probe unusual DNA conformations in B-form Watson-Crick DNA such as bulges and mismatches in which the helical stacking is disrupted. The dependence of long-range guanine oxidation upon *dynamic* changes in the bending and flexing of the DNA now presents a new avenue for exploration of DNA-mediated electron transfer.

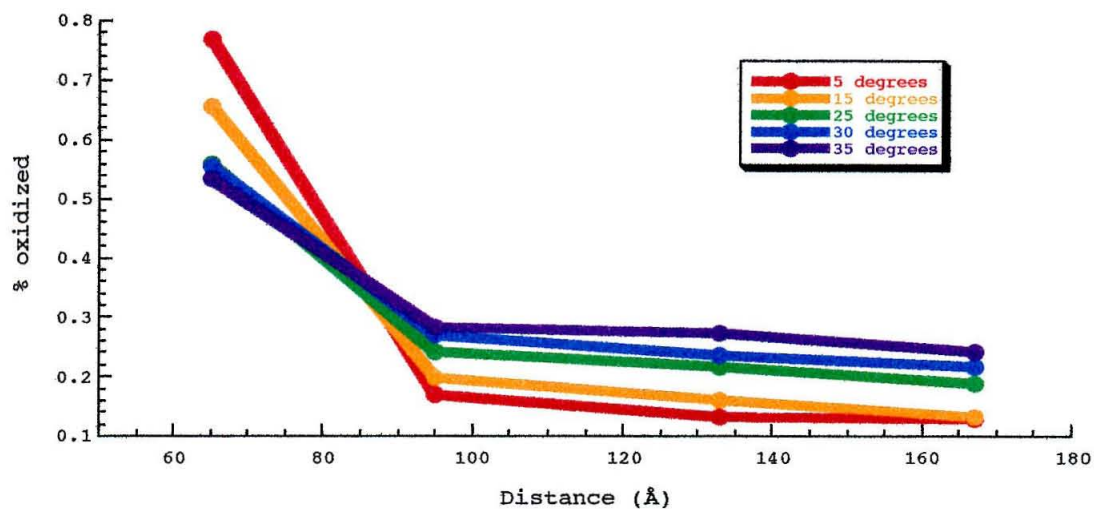


Figure 2.5: Temperature dependence of long-range guanine oxidation. The distance dependence of guanine oxidation by $^*\text{Rh(III)}$ decreased as a function of increasing temperature over the range of 5-35°C. Charge transfer was not affected by temperature at a point at which the lines cross, approximately 90 Å from the intercalation site of the metal.

2.3.6 Mechanism of Electron Transfer through DNA

As discussed in chapter 1, despite the enormous body of experimental work relating directly or indirectly to electron transfer through DNA, we still lack a theoretical framework which describes all of the observed data. In fact, several mechanisms may be operable in these different systems and over different distance regimes. The studies described here may be represented in the context of a "hopping" model of charge transfer through DNA (28). According to a hopping model, the electronic "hole" diffuses along the helix by hopping from base to base until it is trapped by vibrational relaxation at a site with a low oxidation potential, for example, in this case a 5'-GG-3' site. These pairs of nucleobase stepping stones have to be electronically coupled, but they do not necessarily need to be adjacent. Indeed, we consider that hopping may even occur between base domains over which charge is delocalized rather than between discrete base positions.

This general hopping mechanism could certainly be used to describe the data presented here. We may, for example, consider the dependence of long-range hole transfer on the identity of the intercalating metal. If we assume that the hole generated on DNA by *Rh(III) is more energetic than the hole generated by Ru(III) due to the difference in their reduction potentials (+1.6 V for Ru(III) vs. +2.0 V for *Rh(III) (17-20)), we would expect that relaxation and trapping of the hole might occur more rapidly (and therefore closer to the intercalation site) for Ru(III) than for *Rh(III). According to this model, the *Rh(III)-generated hole would also be more mobile because it could hop between any two bases (or base domains), whereas the Ru(III)-generated hole could hop only from purine to purine due to its lower potential. The hopping mechanism might also explain the shallow decrease in guanine oxidation which is observed with increasing distance, since some decrease in oxidation with distance would be expected as long as diffusion competes with vibrational relaxation and trapping. The increase in very long-range (i.e., >100 Å)

charge transfer at higher temperatures also favors a hopping model, since the electronic hole might use the extra thermal energy to offset vibrational relaxation and thus be able to diffuse further along the helix before it is trapped. Although far from decisive proof, these data provide some indication that the movement of charge through the helix can be described at least in part in the context of a hole-hopping mechanism.

In conclusion, charges generated on DNA by UV light, radicals, exogenous chemicals, and γ irradiation frequently lead to irreversible damage. It is unclear whether *in vivo* these charges can migrate along the helix over long distances, and, if so, how far they can migrate before they are trapped as a permanent lesion. In this study we examined the distance and sequence dependence of long-range oxidative charge transfer through DNA. These data establish that charge migration can occur and promote damage over very long molecular distances. We showed that oxidative charge transfer has a very shallow dependence on distance. Guanine oxidation via charge transfer is also not dependent on orientation or phasing along the helix relative to the metallointercalator, but it is sensitive to sequence, with multiple 5'-TA-3' steps being especially poor media for charge transfer. Moreover, we have shown that significant electron transfer occurs through the base stack of DNA oligonucleotides over distances of at least 200 Å. Furthermore, investigations of the temperature dependence of guanine oxidation and of oxidation through disturbances in the π stack illustrate that charge transfer is also sensitive to dynamic disturbances in the helical stacking through B-form DNA. These discoveries have important implications to the study of DNA damage and repair in biological systems. Indeed they show that changes in DNA generated in one location by radicals and oxidants can potentially cause damage at other locations far away in the genome. The longest distance over which guanine oxidation by photoinduced charge transfer through the helix can occur still remains to be shown, as does the

effect of DNA-binding by histones and other proteins upon charge transfer. It is possible that nature might use sequence-encoded DNA-mediated charge transfer as a means of signaling or, conversely, use sequence-dependent bending to generate "traps" for migrating charges around sequences which would be otherwise sensitive to damage. Whether long-range electron transfer reactions mediated by DNA occur in the cell and whether organisms have evolved a way to use electron transfer through the double helix to their advantage remains to be seen. Given the significant extent of DNA damage that can be generated through charge migration as well as the ability to modulate such long range damage by the intervening sequence, as seen here, it becomes important now to consider these potential reactions within the cell.

2.4 References

1. D.B. Hall, R.E. Holmlin, J.K. Barton, *Nature* **382**, 731 (1996).
2. D.B. Hall, J.K. Barton, *J. Am. Chem. Soc.* **119**, 5045 (1997).
3. M.R. Arkin, E.D.A. Stemp, S. Coates Pulver, J.K. Barton, *Chemistry and Biology* **4**, 389 (1997).
4. S.M. Gasper, G.B. Schuster, *J. Am. Chem. Soc.* **119**, 12762 (1997).
5. D.B. Hall, S.O. Kelley, J.K. Barton, *Biochemistry* **37**, 15933 (1998).
6. K. Nakatani, K. Fujisawa, C. Dohno, T. Nakamura, I. Saito, *Tetrahedron Lett.* **39**, 5995 (1998).
7. E. Amouyal, A. Homsy, J.C. Chambron, J. P. Sauvage, *J. Chem. Soc. Dalton Trans.* **6**, 1841 (1990).
8. P.A. Anderson, *et al.*, *Inorg. Chem.* **34**, 6145 (1995).
9. A.E. Friedman, J.-C. Chambron, J.P. Sauvage, N.J. Turro, J.K. Barton, *J. Am. Chem. Soc.* **112**, 4960 (1990).
10. R.E. Holmlin, P.J. Dandliker, J.K. Barton, *Bioconj. Chem.* **10**, 1122 (1999).
11. C.M. Dupureur, J.K. Barton, *Inorg. Chem.* **36**, 33 (1997).
12. J. Sambrook, E.F. Fritsch, T. Maniatis, *Molecular Cloning: A Laboratory Manual*, 2nd ed., Cold Spring Harbor Laboratory, New York (1989).
13. W. Saenger, *Principles of Nucleic Acid Structure*. Springer-Verlag, New York (1984).
14. R.E. Dickerson, In *Structure, Motion, Interaction and Expression of Biological Macromolecules. Proceedings of Tenth Conversation in Biomolecular Stereodynamics*, R. H. Sarma, M. H. Sarma, eds., pp. 17-36, Academic Press, Schenectady, N.Y. (1998).
15. R.E. Dickerson, *Nucleic Acids Res.* **26**, 1906 (1998).
16. E.D.A. Stemp, M.R. Arkin, J.K. Barton, *J. Am. Chem. Soc.* **119**, 2921 (1997).

17. R.E. Holmlin, R.T. Tong, J.K. Barton, *J. Am. Chem. Soc.*, **120**, 9724 (1998).
18. E. N. Trifonov, R.K.-Z. Tan, S.C. Harvey, In *Structure & Expression. Volume 3: DNA Bending and Curvature*, W.K. Olson, M.H. Sarma, R. H. Sarma, M. Sundaralingam, eds., pp. 243-253, Adenine Press, Schenectady, N.Y. (1987).
19. M.R. Arkin, P.F. *Science* **273**, 475 (1996).
20. C. Turro, A. Enenzahav, S.H. Bossmann, J.K. Barton, N.J.Turro, *Inorg. Chim. Acta* **243**, 101 (1996).
21. H. Sugiyama, I. Saito, *J. Am. Chem. Soc.* **118**, 7063 (1996).
22. C.J. Burrows, J.G. Muller, *Chem. Rev.* **98**, 1109 (1998).
23. G.W. Buchko, J.R. Wagner, J. Cadet, S. Raoul, M. Weinfeld, *Biochem. Biophys. Acta* **1263**, 17 (1995).
24. J. G. Muller, V. Duarte, R.P. Hickerson, C. J. Burrows, *Nucleic Acids Res.* **26**, 2247 (1998).
25. P. M. Cullis, M.E. Malone, L.A. Merson-Davies, *J. Am. Chem. Soc.* **118**, 2775 (1996).
26. F. Prat, K.N. Houk, C.S. Foote, *J. Am. Chem. Soc.* **120**, 845 (1998).
27. H.B. Gray, J. Winkler, In *Bioinorganic Chemsistry*. I. Bertini, H. Gray, S.J. Lippard, J.S. Valentine, eds. pp. 315-363, University Science Books, Mill Valley, California (1992).
28. D. Dee, M.E. Baur, *J. Chem. Phys.* **60**, 541 (1974).
29. S. R. Quake, H. Babcock, S. Chu, *S. Nature* **388**, 151 (1997).

Chapter 3

Oxidative Charge Transfer to Repair Thymine Dimers and Damage Guanine Bases in DNA Assemblies Containing Tethered Metallointercalators*

*Adapted from: P. J. Dandliker, M. E. Núñez, J. K. Barton, *Biochemistry* **37**,
6491 (1998)

3.1 Introduction

As described in the preceding chapters, we have employed metallointercalators tethered to one end of DNA assemblies to carry out chemical reactions at distant sites on the assemblies. Rhodium intercalators tethered to one end of a DNA duplex can induce oxidative damage specifically at the 5'-G of 5'-GG-3' sites located up to 200 Å away in the duplex in a reaction which is sensitive to the stacking of the intervening base pairs (1-3). Furthermore, a ground state ruthenium(III) oxidant generated *in situ* can also damage guanine bases from a distance (4,5).

Interestingly, long-range guanine base oxidation is not the only example of chemistry at a distance. Rhodium photooxidants tethered to DNA can promote the repair of thymine dimer lesions located at least 26-36 Å away in the DNA base stack via a long-range oxidative electron transfer process (6). The thymine cyclobutane dimer (T<>T) is a DNA lesion which results from a [2+2] photocycloaddition between adjacent thymine bases on the same polynucleotide strand (7). Bacteria use photolyase enzymes with bound flavin cofactors to repair the thymine lesion in a reductive catalytic cycle upon visible irradiation (8-12). The repair of thymine dimers triggered both oxidatively and reductively has been shown in model systems (13-19).

Here, we describe thymine dimer repair by photoexcited metallointercalators at long range through the DNA base stack in more detail. Additionally, we explore the relative reactivity of the thymine dimer and guanine doublet in a single duplex and allow sites to compete for trapping of the mobile charge. The guanine doublet and the thymine dimer are expected to localize a mobile charge to different extents: the oxidation potential of guanine is approximately +1.3V at neutral pH (20), while the standard oxidation potential of the thymine dimer is around +2.0 V (21-23). Furthermore, the trapped radical intermediates formed at the two sites have

distinctly different intrinsic lifetimes and stabilities. Hence, in an assembly containing both sites, it becomes interesting to explore their relative reactivities. Metallointercalators offer useful tools to probe this DNA-mediated charge transfer chemistry and more generally to begin to characterize radical migration through a DNA base pair stack.

3.2 Methods

3.2.1 Materials

Oligonucleotides were prepared as described in chapter 2. $\text{Rh}(\text{phen})_2\text{DMB}^{3+}$, $\text{Ru}(\text{phen})_2\text{dppz}^{2+}$ (dppz=dipyrido[3,2-a:2',3'-c]phenazine), $\text{Rh}(\text{phen})_2(\text{bpy}')^{3+}$ (bpy'= 4-butyric acid-4'-methylbipyridine), and $\text{Ru}(\text{phen})(\text{bpy}')(\text{dppz})^{2+}$ were prepared according to published procedures (24-26). Rhodium- and ruthenium-modified oligonucleotides were prepared according to published procedures (1,27). The electron transfer quenchers methyl viologen dichloride, $[\text{Ru}(\text{NH}_3)_6]\text{Cl}_3$, and $[\text{Co}(\text{NH}_3)_5\text{Cl}]\text{Cl}_2$ were purchased from Aldrich Chemical Company and used as received. Acetophenone was recrystallized thrice before use and stored at 4 °C in the dark.

3.2.2 Preparation and Characterization of Oligonucleotides Containing a Thymine Dimer

Thymine dimer formation in synthetic oligonucleotides was performed photochemically, using acetophenone as a triplet photosensitizer (66-67). Sequences contained only a single TT site, and no other adjacent pyrimidine bases. Aqueous solutions (1 mL) containing the oligonucleotide (~ 0.2 mM) and acetophenone (25 μM) were placed in an evacuable irradiation apparatus and rigorously degassed by freezing the sample, applying a vacuum, and slow thawing. This process was repeated six times for each sample. Solutions were irradiated *in*

vacuo for 4-6 h ($\lambda = 330$ nm) with a 1,000 W Hanovia Hg-Xe arc lamp equipped with a monochromator. Products were purified by HPLC on a Dynamax 300 Å C₁₈ reversed-phase column (10 mm ID x 25 cm L) from Rainin using a Hewlett-Packard 1090 HPLC. The strands eluted with a gradient of 50 mM CH₃COONH₄ (pH 6.5) / CH₃CN (~ 93:7 to ~ 89:11 over 30 min., flow rate = 3.5 mL min.⁻¹). In all cases, the desired thymine dimer-containing compound eluted ~ 2 min. before the unreacted starting material, and was formed as the major product. The product ratios are consistent with those previously reported and support the assignment of the major product as the *cis-syn* isomer (28). Conversion for 16-nucleotide strands ranged from 30 - 50%. Purity of the material was confirmed by analytical HPLC.

The presence and identity of the thymine dimer were confirmed using electrospray ionization-Fourier transform ion cyclotron resonance mass spectroscopy (ESI-FTICR MS), enzymatic digestion, and direct photoreversal to the normal oligonucleotide without the dimer. As expected, an oligonucleotide containing a repaired thymine dimer had a mass identical to that of the parent material as determined by electrospray ionization mass spectrometry. The theoretical mass of a 16-base-pair oligonucleotide with a repaired thymine dimer was 4929.8 (6), while the experimental mass of the repaired dimer strand was 4929.4. The identity of a thymine cyclobutane dimer can also be confirmed by direct photoreversal. Treatment of thymine dimer-containing DNA with 254 nm light, which is known to repair this type of lesion, afforded a compound with the same retention time as the original oligonucleotide (30). T4 DNA polymerase possesses 3' to 5' exonuclease activity which is blocked by the presence of a thymine dimer. Digestion of 5'-³²P-labeled thymine dimer strands with T4 DNA polymerase gave only products in which enzymatic cleavage was arrested at the site of thymine dimer incorporation. As expected, thymine dimer-containing DNA was

not susceptible to cleavage with hot piperidine, a treatment which is known to cleave DNA containing the pyrimidine-pyrimidone (6-4) photoproduct (31).

3.2.3 HPLC Assay for Thymine Dimer Repair

Complementary DNA strands were hybridized in aerated buffer containing 50 mM sodium chloride and 5 mM sodium phosphate, pH 8.0. Oligonucleotide duplexes (8 μ M) containing tethered Rh(phi)₂bpy³⁺ were irradiated at 365 nm for 1 and 3 h. For experiments with Ru(phen)₂dppz²⁺, oligonucleotide duplexes (8 μ M) containing Ru(phen)₂dppz²⁺ (8 μ M) and 10 equivalents of methyl viologen were irradiated at 436 nm for 2 and 5 min. Reaction mixtures were analyzed by HPLC on a Microsorb-MV C₁₈ reversed-phase column (4.6 mm ID x 25 cm L) from Rainin maintained at 65 °C, eluting with a gradient of 20 mM CH₃COONH₄ (pH 6.5) / CH₃CN (98:2 to 93:7 over 20 min., isocratic at 93:7 for 5 min., to 50:50 over 5 min., isocratic at 50:50 for 5 min.; flow rate = 1.0 mL min⁻¹). Under these conditions, the duplexes dissociate into single stranded components, each of which elutes from the column with a distinct retention time. Oligonucleotides (16-nucleotide) containing a thymine dimer eluted first (~ 11-12 min.), followed by the corresponding repaired strand (~ 15-16 min.), and the complement with tethered rhodium (~ 30 min.) Identity of the individual compounds was confirmed by co-injection with authentic material and, in one case, by isolation and electrospray ionization mass spectrometric analysis of the repaired strand. Thymine dimer repair was quantitated from peak areas in the chromatograms (normalized for differences in molar absorptivity at the detection wavelength, λ = 260 nm).

3.2.4 PAGE Assay for Oxidative Damage

Oligonucleotides were enzymatically phosphorylated (*) at the 5'-OH with γ -³²P-ATP according to a standard protocol (32). The product was incubated at 90

°C with 10% aqueous piperidine (0.100 mL) for 30 min., dried, and electrophoresed on a denaturing 20% polyacrylamide gel (0.8 mm thickness). Labeled product was located in the gel by autoradiography, excised, and extracted by incubation at 37 °C with 90 mM Tris-borate buffer (pH 8.3) containing 1 mM EDTA for 12 h. The mixture was filtered through an uncharged nylon-66 membrane, 0.45 µm pore size (Rainin), desalted on a Nensorb™ 20 cartridge, and freed of solvent *in vacuo*. Complementary DNA strands were hybridized in aerated buffer containing 5 mM sodium phosphate and 50 mM sodium chloride, pH 8.5. Oligonucleotide duplexes (8 µM) containing tethered Rh(phi)₂bpy'³⁺ were irradiated at 365 nm for 1 and 3 h, incubated at 90 °C with 10% aqueous piperidine (0.100 mL) for 30 min., dried, and electrophoresed on a denaturing 20% polyacrylamide gel. Cleavage of the labeled strand was quantitated by phosphorimagery using ImageQuant, v.3.3 software (Molecular Dynamics). Oxidation at individual bases was determined by measuring the intensity of the band corresponding to that base as a fraction of the intensity of the whole lane. The fractional intensity of the corresponding band in the control lane was subtracted out to account for background damage.

3.3 Results and Discussion

3.3.1 Sequence Construction

We designed and constructed a family of DNA duplexes containing a tethered rhodium intercalator, a 5'-GG-3' site, and a thymine dimer lesion (Fig. 3.1). The sequences vary with respect to the presence or absence of a 5'-GG-3' site and a thymine dimer lesion, as well as the relative position of the dinucleotides with respect to the tethered oxidant. Each of the assemblies possess an equivalent base composition (G/C and A/T content). The conserved 5'-...ATACGT-3' sequence at the tethered end provides a uniform DNA binding site for the metal

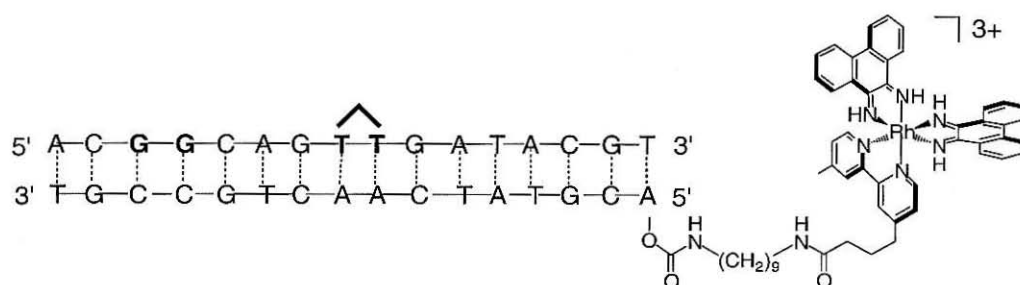


Figure 3.1: DNA assembly with $\text{Rh}(\text{phi})_2(\text{bpy}')^{3+}$ covalently tethered. The sequence at the intercalation site, the total AT/GC content, and the sequence around the surrounding the two oxidizable sites are the same in all of the assemblies.

complexes throughout the series. Bases immediately flanking the 5'-GG-3' and thymine dimer sites are also conserved in an effort to maintain structural uniformity at these sites from duplex to duplex.

3.3.2 *Determination of Rhodium Metallointercalator Binding Site by Photocleavage*

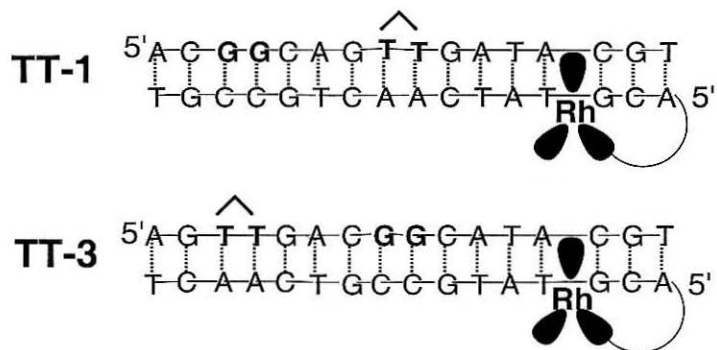
High energy (313 nm) photoexcitation of phi complexes of rhodium bound to DNA promotes direct strand cleavage in a reaction consistent with C3' hydrogen atom abstraction at ribose and subsequent strand scission at the intercalation site(s) (33-35). This direct photocleavage reactions permit us to determine the positions at which the metal complexes bind to the DNA duplex.

Metallated DNA duplexes containing a 5'-³²P-endlabel on the strand complementary to the rhodium-tethered strand were irradiated at 313 nm and electrophoresed on a denaturing polyacrylamide gel (Fig. 3.2). The primary cleavage, evident at the top of the gel, occurs at the first four bases, indicating that the rhodium is intercalated at the end furthest from the label (lanes 4, 8, 12, 16). Since the photocleavage reaction at high energy (313 nm), involving direct reaction at the sugar, generates no diffusible species, the multiple cleavage sites observed reflect multiple binding sites for the tethered rhodium. Thus intercalation is indicated up to four base steps from the end of the duplex, consistent with the flexibility and length of the tether.

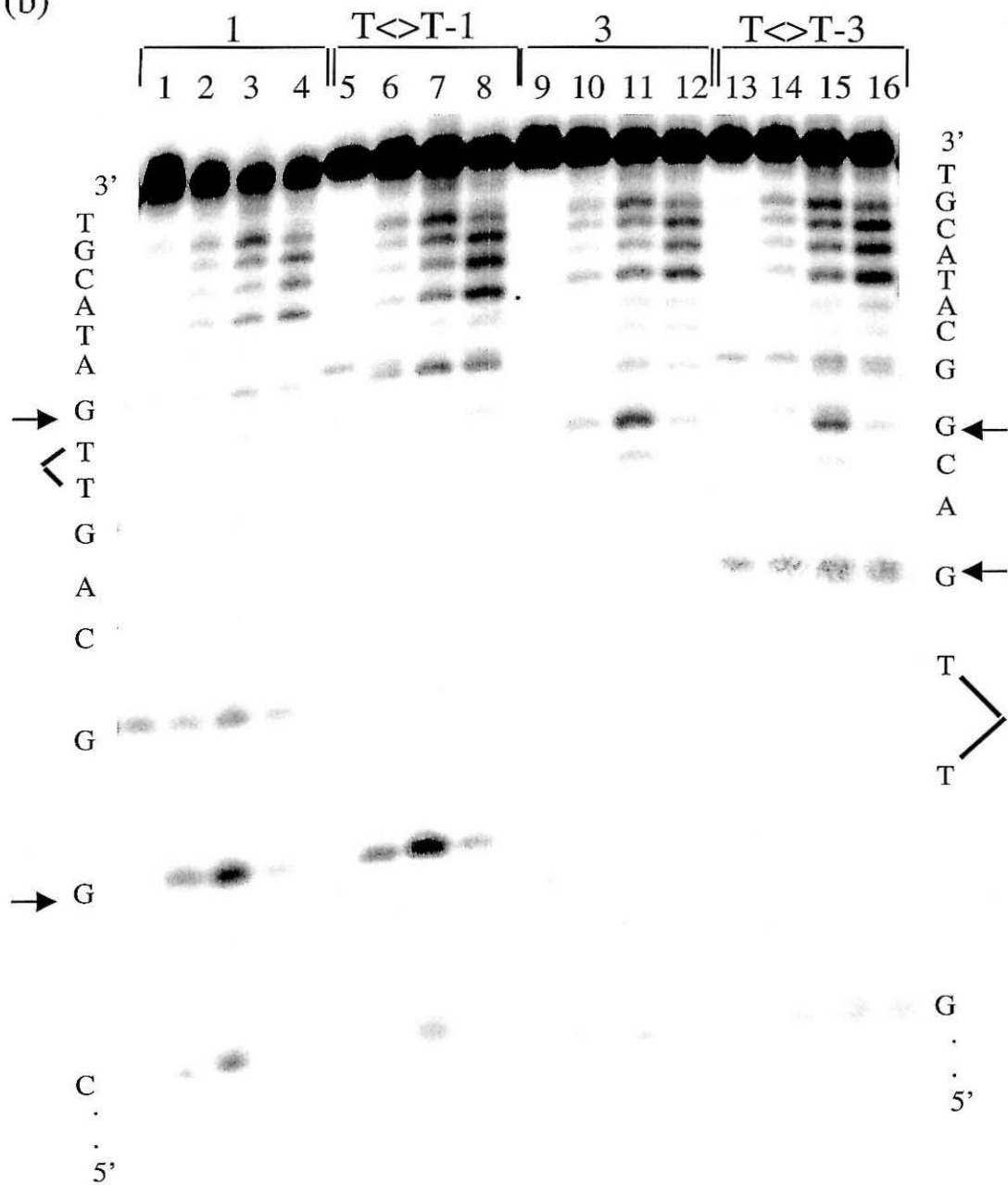
It is noteworthy that for the duplexes containing the thymine dimer, direct contact between the metal complex and the dimer is not required for repair. If Rh(phi)₂(DMB)³⁺ bound noncovalently to DNA is irradiated at 313 nm, photocleavage is seen throughout the duplex (data not shown). Furthermore, on the basis of the photocleavage results, tethering of rhodium to the end of the duplex precludes direct contact of the metal center with the thymine dimer.

Figure 3.2: Direct photocleavage and guanine base oxidation by a tethered rhodium intercalator in various DNA assemblies. (a) Sequence of the DNA oligonucleotide assemblies **1** and **3**. The presence of a thymine dimer in the DNA assembly is indicated by a “T<>T” in the name of the sequence. (b) Autoradiogram of **1**, **T<>T-1**, **3**, and **T<>T-3** after photoirradiation of the oligonucleotide duplex with tethered Rh(phi)₂bpy³⁺ and treatment with aqueous piperidine. Each set of four lanes contains the following samples: 0, 1, and 3 h irradiation at 365 nm or 20 min. at 313 nm, respectively. The number of the DNA oligonucleotide duplex assembly is shown at top. Horizontal arrows denote the 5'-G of 5'-GG-3' and the 3'-G of 5'-GTTG-3' sites, and the position of the thymine dimer lesion is denoted by triangular brackets.

(a)



(b)



For the sequences in Figure 3.2a, we calculate the distance from the intercalated rhodium to the thymine dimer to be approximately 19 Å (**T<>T-1**) and 36 Å (**T<>T-3**), measured through the DNA base stack from the third base step (the most probable intercalation site) to the center of the cyclobutane ring of the dimer. This assumes that the centroid-to-centroid stacking distance between adjacent base pairs is 3.4 Å.

3.3.3 Repair of Thymine Dimers in Duplex DNA by *Rh(III)

In assemblies containing both a tethered rhodium intercalator and a thymine dimer lesion, low energy (365 nm) excitation promotes the repair of the lesion triggered through long-range oxidative electron transfer. Thymine dimer repair was measured as a function of irradiation time by reversed-phase analytical HPLC at 65 °C (Fig. 3.3). Under these conditions the duplexes melt and each single-stranded oligonucleotide component elutes with a characteristic retention time. The rhodium-tethered strand is not evident in the HPLC traces shown in Figure 3.3 because it elutes much later in the gradient. No other products besides the dimer-containing strand and the repaired strand are formed in the repair reaction, as monitored by HPLC. We obtain quantitative conversion of the thymine cyclobutane dimer to the repaired strand containing two unmodified thymines in all cases. Repair requires the presence of both rhodium and light.

Thymine dimer repair yields were measured as a function of duplex concentration over a range of concentrations from 25 μM to 3 μM. Over this concentration range, the yield of repaired strand varied by approximately 17%. Figure 3.4 shows representative data and includes the full chromatogram with elution of the metallated strand. This range of concentrations was chosen to bracket the 8 μM duplex concentration used in these and previous dimer repair and guanine damage experiments. If the repair reaction were to proceed in a

Figure 3.3: Long-range thymine dimer repair in a DNA assembly containing a tethered rhodium intercalator. Shown are representative HPLC chromatograms at (a) 0, (b) 1, and (c) 3 h of irradiation ($\lambda = 365$ nm). The peaks correspond to the 16-nucleotide strands in which a thymine dimer is present (**T \diamond T-3**, elution time = 12.3 min.), or absent (**3**, elution time = 15.5 min.). The rhodium-modified oligonucleotide complement eluted at 29.9 min. and is not shown here. The absolute yield of repaired strand varies somewhat from experiment to experiment, depending upon irradiation.

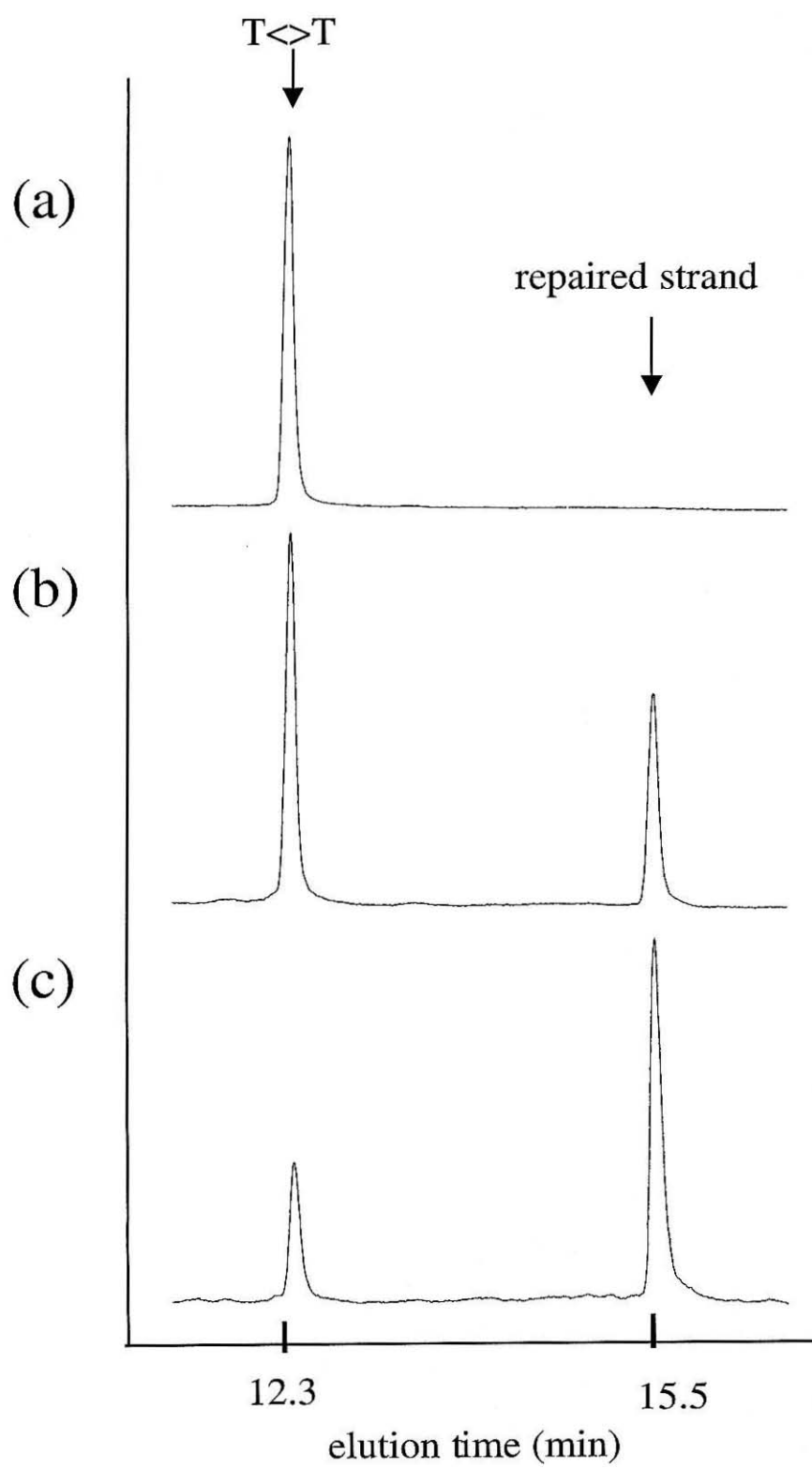
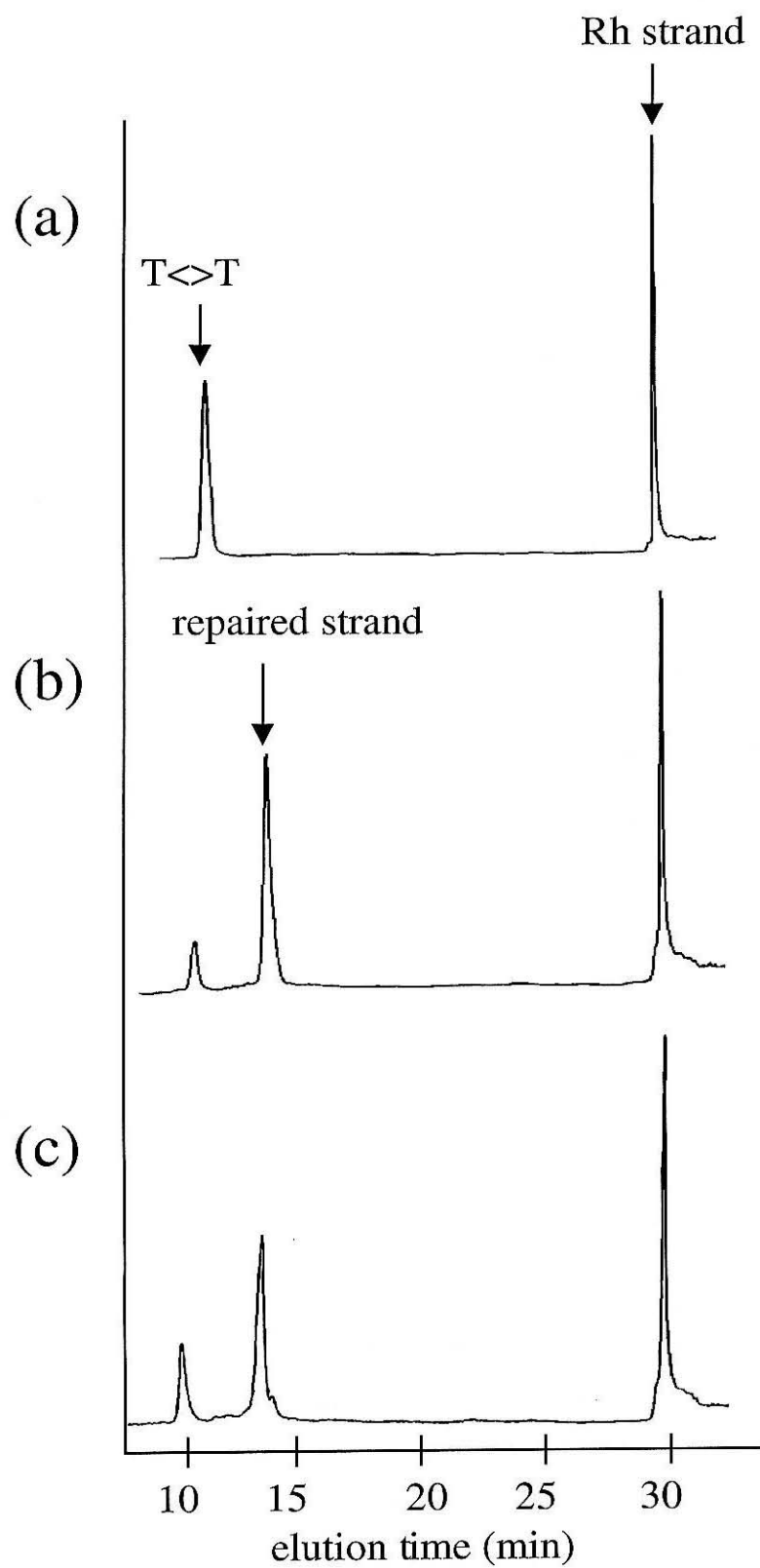


Figure 3.4: Long-range thymine dimer repair by a tethered rhodium intercalator over an 8-fold range of concentrations. Peaks in the HPLC chromatograms correspond to **T<>T-2** (elution time 10.2 min.), repaired strand **2** (elution time 13.2 min.) and the rhodium-tethered complementary strand (elution time = 29.4 min.). Samples shown here, which are representative of the set, correspond to the following: (a) dark control; (b) 25 μM rhodium and DNA duplex; (c) 6.25 μM rhodium and DNA duplex. All samples except the dark control were irradiated for 1 h at 365 nm. The levels of repair are as follows: 25 μM : $82 \pm 1\%$; 12.5 μM : $75 \pm 1\%$; 6.25 μM : $70 \pm 1\%$; 3.12 μM : $65 \pm 5\%$, where the error bars represent the error in the integration due to noise.

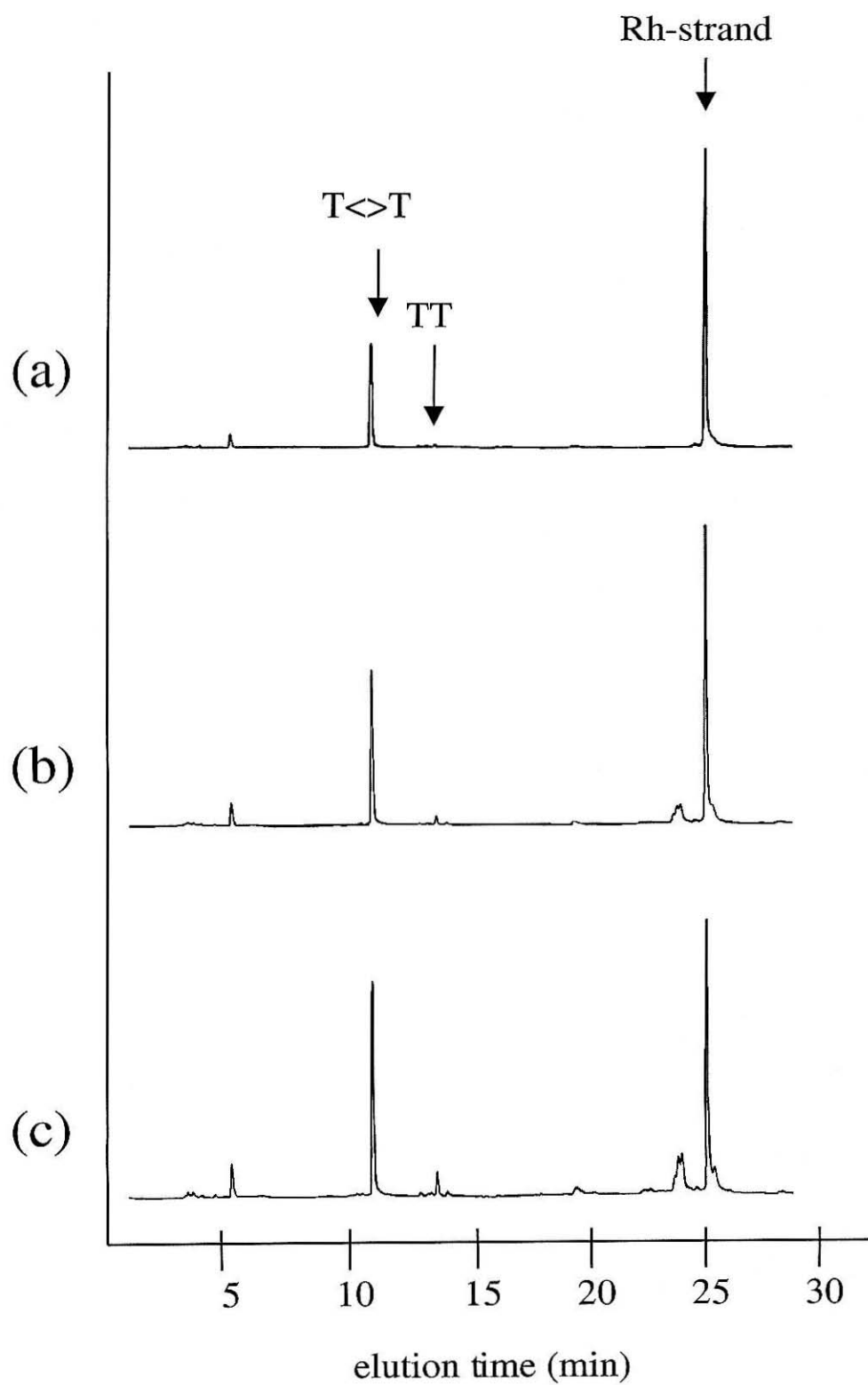


bimolecular fashion, assuming the interduplex repair efficiency to be comparable to that of nontethered $\text{Rh}(\text{phi})_2\text{DMB}^{3+}$, it would require that the repair efficiency change by more than 500% over the concentration range examined. That the reaction occurs intraduplex is also evident in comparing the repair efficiency in the rhodium-tethered duplex to that for repair of the duplex containing the thymine dimer by a separate rhodium-modified duplex lacking the dimer. We observe $\leq 5\%$ interduplex repair at a concentration of $8\ \mu\text{M}$.

DNA-mediated repair by charge transfer also requires that the intervening bases be paired. When a control solution containing a rhodium-modified strand ($8\ \mu\text{M}$) and a noncomplementary strand ($8\ \mu\text{M}$) containing a dimer was irradiated at $365\ \text{nm}$, essentially no repair is observed: after 1 h, 2% of the dimer strands were repaired; after 3 h, 6% were repaired (Fig. 3.5). The percent repair seen is comparable to the extent of dimer repair found upon irradiation without rhodium.

The data presented here indicate clearly that visible photolysis of rhodium intercalators bound to DNA can promote the repair of a thymine dimer lesion. An important issue with long-range thymine dimer repair by rhodium intercalators is whether the reaction is indeed mediated by the base pairs of the DNA double helix. One could imagine that the reaction proceeds instead in an interduplex fashion, with the rhodium complex from one duplex intercalating into a neighboring duplex at the site of the thymine dimer and initiating its repair. Several experiments rule out an interduplex reaction. Photocleavage reactions with $313\ \text{nm}$ light indicate that interduplex intercalation is negligible at duplex concentrations $\leq 25\ \mu\text{M}$. If the rhodium complexes intercalate into neighboring duplexes and repair the dimer in an intermolecular reaction, the photocleavage reactions at $313\ \text{nm}$ would show damage throughout the DNA strands. The photocleavage reactions instead indicate that intercalation occurs predominantly at the end of the duplex nearest to the tethered rhodium. Direct photocleavage studies of DNA duplexes containing a

Figure 3.5: Absence of dimer repair by a noncomplementary rhodium strand. A control solution containing a rhodium-modified strand (8 μM) and a noncomplementary strand (8 μM) containing a dimer was irradiated at 365 nm and only background repair is observed. Panel (a) shows the dark control sample which was not irradiated; the sample shown in panel (b) was irradiated for 1 h; the sample shown in panel (c) was irradiated for 3 h. The dimer strand (elution time =11 min.), the repaired strand (elution time =13 min.), and the rhodium-tethered strand (elution time =26 min.) are indicated by arrows. After 1h, 2% of the dimer strands were repaired; after 3 h, 6% were repaired.



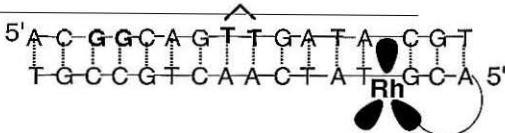
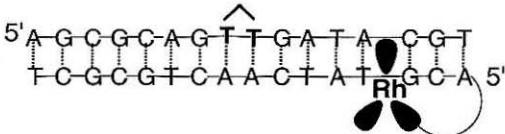
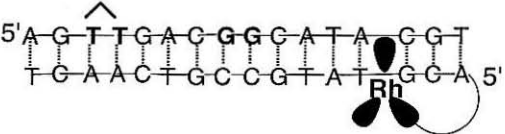
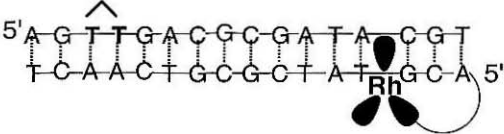
thymine dimer by non-covalently bound $\text{Rh}(\text{phi})_2\text{DMB}^{3+}$ also provide no indication of preferential intercalation neighboring the thymine dimer. Furthermore, if the repair reaction occurs in an interduplex fashion, the yield of repaired dimer would increase substantially as the concentration of the rhodium-tethered duplex was increased. Instead the level of repair observed as a function of concentration is consistent with an interduplex dimerization constant of $\leq 10^3 \text{ M}^{-1}$. Lastly, that the reaction occurs intraduplex is illustrated simply by the observation that little repair is detected in solutions containing duplexes with thymine dimers but no rhodium mixed with duplexes lacking a thymine dimer but with tethered rhodium. The rhodium intercalator must be bound to a DNA duplex containing the thymine dimer for the reaction to proceed.

3.3.4 Dimer Repair and Oxidative Guanine Damage by Rhodium in a Duplex Containing both a Thymine Dimer and a 5'-GG-3' Site

Because initial oxidation of a 5'-GG-3' site should be thermodynamically more favorable than oxidation of a thymine dimer, we considered the possibility that the guanine doublet would compete with the dimer for the migrating charge in duplexes containing both charge traps. Table 3.1 compares the dimer repair efficiency in four sequences with and without a guanine doublet. As expected, the presence of a 5'-GG-3' site within the duplex diminished the efficiency of thymine dimer repair, as evidenced by the smaller yields for **T<>T-1** compared to **T<>T-2** and for **T<>T-3** compared to **T<>T-4**. The same diminution in efficiency in the presence of a 5'-GG-3' doublet is evident in DNA assemblies containing tethered Λ rhodium, although the absolute yields of dimer repair were somewhat less for the Λ isomer (data not shown).

Oxidative base damage at the 5'-G of 5'-GG-3' sites in **1**, **T<>T-1**, **3**, and **T<>T-3** was monitored as a function of irradiation at 365 nm (Fig. 3.2).

Table 3.1: Long-range thymine dimer repair in duplexes with tethered rhodium

		Repair (%) ^a		Distance (Å) ^b	
		1 h	3 h	Rh- $\hat{\text{T}}\text{T}$	Rh-5'G
TT-1		75	93	19	37
TT-2		94	100	19	
TT-3		53	70	36	20
TT-4		90	100	36	

a Repair is expressed as the percentage of thymine dimer lesion repaired after 1 and 3 hr of irradiation. Samples containing 8 μM duplex were irradiated at 365 nm prior to analysis by HPLC. Repair efficiency is given for assemblies containing $\Delta\text{-Rh}$. Although the absolute accuracy of the measurements of thymine dimer repair can vary considerably from experiment to experiment due to combined error in sample preparation, irradiation, and HPLC analysis, the relative precision of these numbers is approximately 5-10%.

b Distances between Rh and the cyclobutane ring of the dimer and Rh and the 5' G of the 5'-GG-3' are based upon a 3.4 Å base-pair to base-pair separation and the intercalation positions shown schematically.

Oxidative damage is observed at the 5'-G of guanine doublets in sequences both with a dimer and without a dimer. Given that the rhodium intercalates next to the third base pair, oxidative damage is seen at a distance of 37 Å and 20 Å, respectively, from the tethered oxidant. In addition to damage at the 5'-G of 5'-GG-3' sites, we also observe oxidation at the 3'-G of the 5'-GT<>TG-3' tetrad only in the presence of dimer (lanes 5-7 and 13-15).

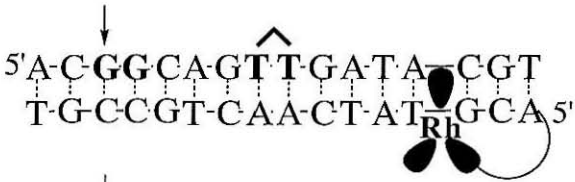
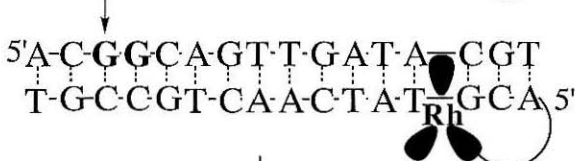
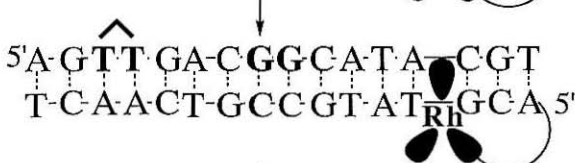
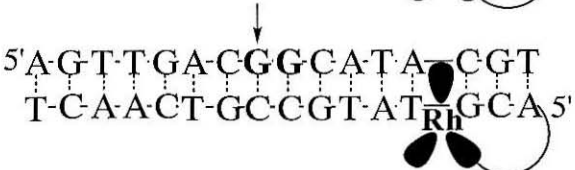
The amounts of damage at the 5'-G of the guanine doublets, quantitated by phosphorimagery, are given in Table 3.2. The presence of the thymine dimer produced a twofold diminution in oxidative damage in the corresponding assemblies, **T<>T-1** and **T<>T-3** relative to **1** and **3**, respectively. Analysis of these data is complicated by the thymine dimer repair which precedes or is concurrent with the oxidative damage. Over the first hour of irradiation, 50-70% of the thymine dimer lesions are repaired. That damage occurs at the 3'-side of the thymine dimer confirms that the dimer is present at least part of the time during the course of reaction.

The amount of guanine damage is twice as large when the 5'-GG-3' site is located distally from the intercalated rhodium (37 Å) than it is when the 5'-GG-3' site is located proximally (20 Å). As this preference is apparent both in the absence (**1** and **3**) and the presence (**T<>T-1** and **T<>T-3**) of the thymine dimer, it is not related to the dimer itself.

3.3.5 Repair of a Thymine Dimer by a Ru(III) Intercalator

Ru(III), generated *in situ* by irradiating Ru(phen)₂(dppz)²⁺ in the presence of groove-bound oxidative quenchers, can oxidatively damage 5'-GG-3' doublets (4,5). To determine whether Ru(III) could oxidatively repair a thymine dimer lesion, we prepared solutions containing a duplex with an identical sequence to **T<>T-1** (without tethered Rh), which contains both a centrally located thymine

Table 3.2: Long-range guanine damage in duplexes with tethered rhodium

		G Damage (%) ^a	
		<u>1 h</u>	<u>3 h</u>
TT-1		2	7
1		4	10
TT-3		1	4
3		1.5	5

^a Damage is expressed as the fraction of oligonucleotide (in percent) cleaved at guanine (site indicated by a vertical arrow) after 1 and 3h of irradiation. Samples containing 8 μ M duplex were irradiated at 365 nm and treated with aqueous piperidine prior to analysis by denaturing PAGE. Although the absolute accuracy of the measurements of guanine oxidation can vary by as much as 5% from experiment to experiment, the relative precision of these numbers is within 1%.

dimer and 5'-GG-3' site, and a duplex with an identical sequence to **T<>T-2** (without tethered Rh), in which the guanine doublet had been removed. The assemblies were irradiated in the presence of $\text{Ru(phen)}_2(\text{dppz})^{2+}$ and the oxidative quencher methyl viologen. Although on this time scale we observe significant thymine dimer repair by $\text{Rh(phi)}_2\text{DMB}^{3+}$, there was no evidence of thymine dimer repair by $\text{Ru(phen)}_2(\text{dppz})^{2+}$ (Figure 3.6). Several new signals appear in the chromatograms concomitant with a small decrease in the amount of the strand containing the dimer, probably corresponding to oligonucleotide products containing oxidized guanine bases. Guanines are known to be oxidized on this time scale, and the more heavily degraded strand corresponds to the strand containing the more easily-oxidized sites (4). The same results were obtained with the electron transfer quenchers $\text{Ru(NH}_3)_6^{3+}$ and $\text{Co(NH}_3)_3\text{Cl}^{2+}$ (data not shown). In the absence of quencher, the strands are not oxidized, and only a small amount of background repair occurs.

The Ru(III) species, generated *in situ* by oxidative quenching, promotes oxidative damage to DNA in a high yield reaction without repairing the thymine dimer lesion. With an estimated reduction potential of $E_{1/2}([\text{Ru}]^{3+/2+}) \sim +1.6\text{V}$ (36), Ru (III) is not sufficiently oxidizing to react with the thymine dimer. This conclusion is fully in line with estimates for oxidation of thymine dimer dinucleotides (9,22,23).

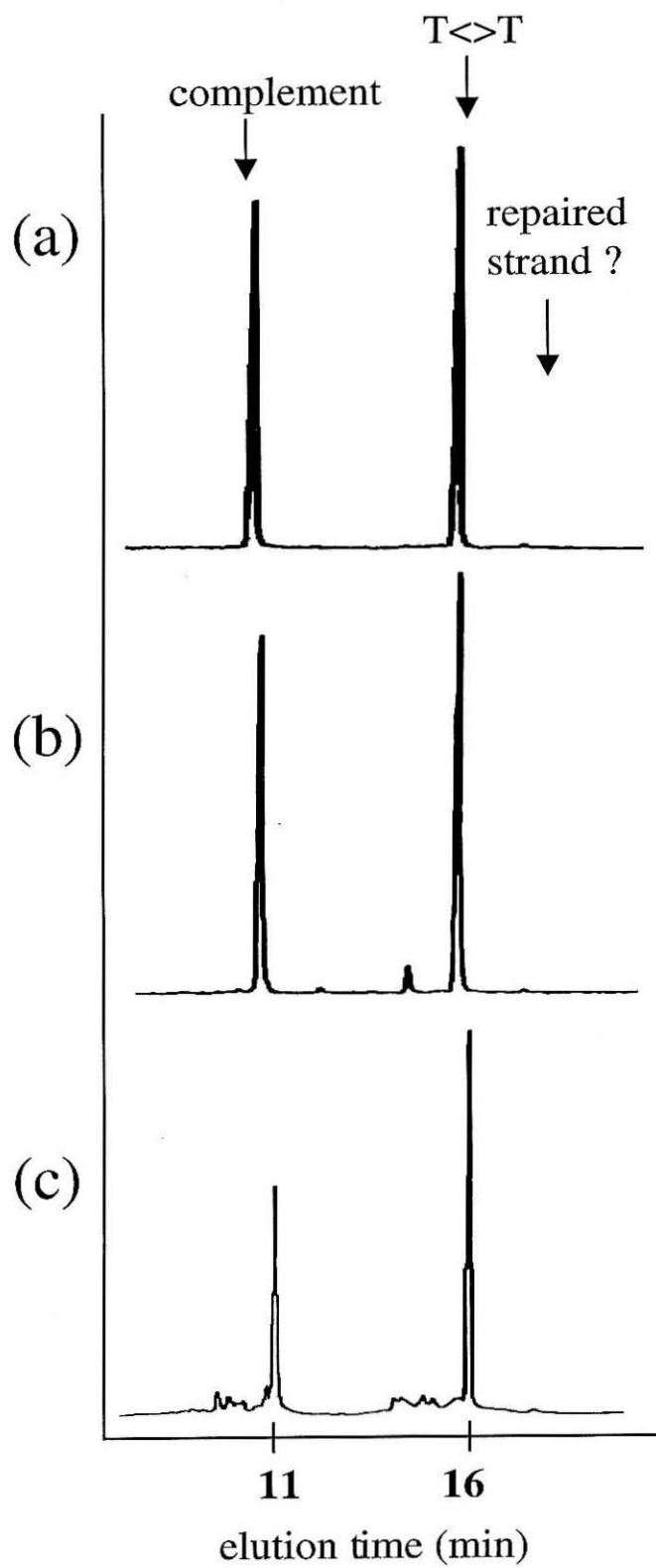
3.3.6 Oxidation of Guanine by Ru(III) through an Intervening Thymine Dimer

Since Ru(III) cannot promote the repair a thymine dimer, we can use ruthenium intercalators to probe whether the dimer generates a disruption in the π stack of the DNA duplex and how that disruption affects other electron transfer reactions. We prepared an oligonucleotide duplex containing tethered $\text{Ru(phen)(bpy')(\text{dppz})}^{2+}$, a centrally located thymine dimer site, and two 5'-GG-3'

Figure 3.6: Absence of thymine dimer repair using a ruthenium intercalator.

HPLC chromatograms for sequence **T<>T-1** without tethered rhodium are shown:

(a) dark control containing dimer-containing strand (elution time=16 min.) and the complementary strand (elution time=11 min.); (b) irradiation at 436 nm without quencher for 45 min.; (c) irradiation at 436 nm with 10 equivalents of methyl viologen for 2 min.

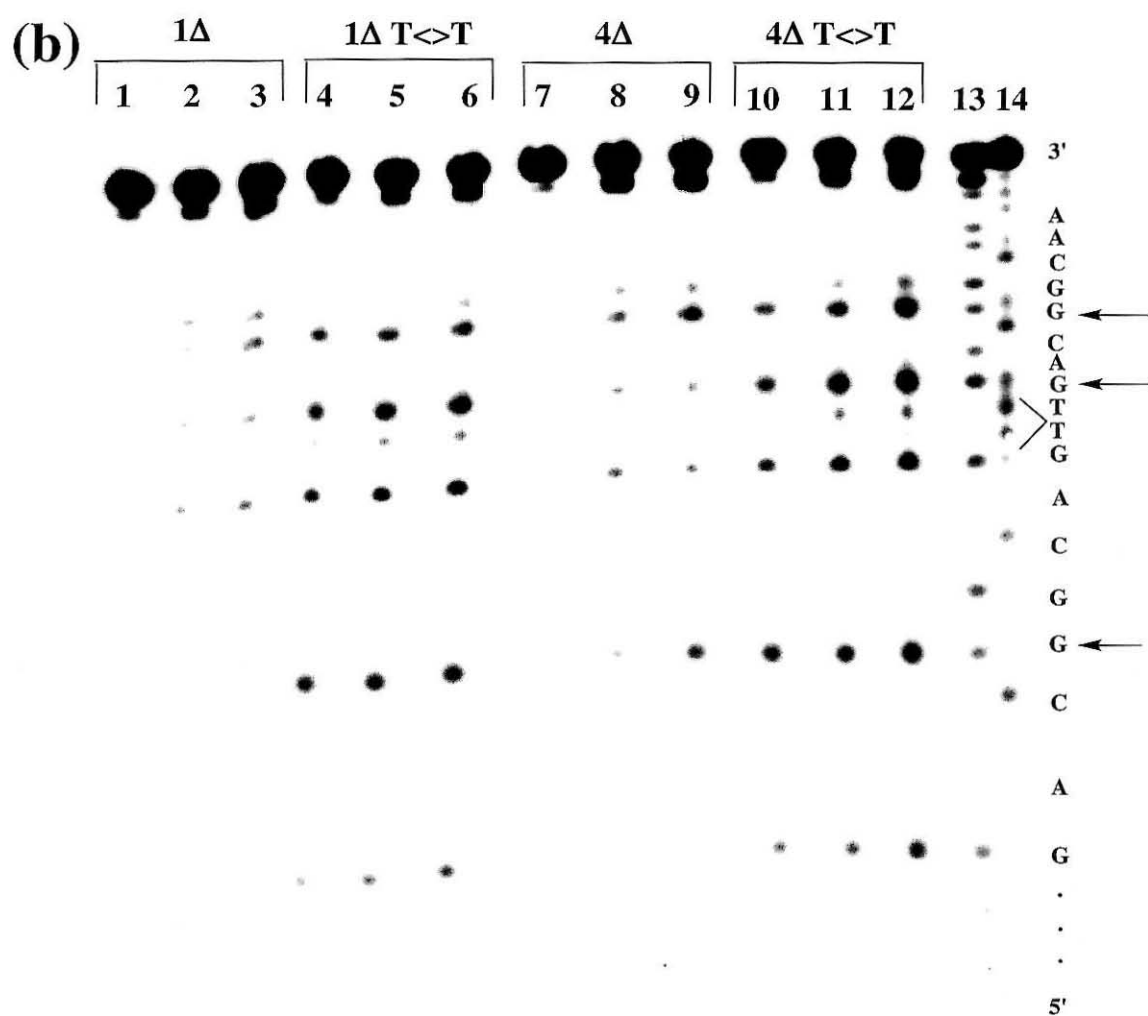
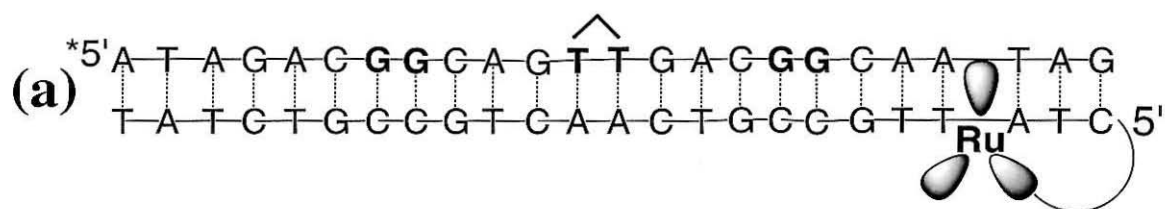


sites located either proximally (17 Å) or distally (51 Å) from the tethered photooxidant (Fig. 3.7a). This sequence is analogous to that used to examine the effects of a DNA bulge upon electron transfer, in which a disruption is placed in the middle of a duplex with a guanine doublet on either side and a metalointercalator tethered to one end (2). By quantitating the ratio of the damage at the two guanine doublets in the absence versus the presence of an intervening thymine dimer, we can evaluate the influence of the disruption upon electron transfer through the helix.

Assemblies containing tethered ruthenium intercalators were irradiated at 436 nm, treated with aqueous piperidine, and analyzed by denaturing PAGE. The 5'-G of both guanine doublets as well as the 3'-G of the 5'-GT<>TG-3' is damaged in all of the strands, as indicated by arrows (Fig 3.7b). As in irradiations with Rh-tethered sequences **T<>T-1** and **T<>T-3**, quantitation revealed increased damage at the 3'-G of the 5'-GT<>TG-3' in the presence of the dimer along with a concomitant decrease in the levels of damage at the 5'-G's of the guanine doublets. The ratio of the damage at a distal guanine doublet versus a proximal doublet was the same for duplexes containing or lacking a thymine dimer lesion for both Δ isomers of Ru(phen)(bpy')(dppz)²⁺.

We observed that the location of the dimer within the short pieces of duplex DNA affected the yield of dimer repair by the rhodium complex (Table 3.2). Placement of the thymine dimer distal (36 Å) from intercalated rhodium, as opposed to proximal (19 Å), reduces the repair efficiency. Although this might reflect the increased distance between the reactants, it is also possible that the effect of position in the duplex may be caused by thermodynamic destabilization and destacking near the dimer when it resides at the end of the assembly (**T<>T-3**, **T<>T-4**) rather than at its center (**T<>T-1**, **T<>T-2**). In smaller duplexes with the thymine dimer in the center of the helix, repair efficiency increases with

Figure 3.7: Long-range guanine oxidation by Ru(III) in a DNA assembly containing a thymine dimer. (a) Sequence **T<>T-5** with the location of the tethered ruthenium complex and the radioactive label indicated. (b) Autoradiogram of sequence **5** or **T<>T-5** irradiated with 10 equivalents of methyl viologen²⁺ at 436 nm. The designations 1 Δ and 4 Δ correspond to the absolute configuration around the metal center and the order of elution of the metallated strand by HPLC. Samples were: lanes 1-3, ruthenium isomer 1 Δ irradiated for 0, 30, and 60 seconds without a dimer; lanes 4-6, isomer 1 Δ irradiated for 0, 30, and 60 seconds with a thymine dimer; lanes 7-9, isomer 4 Δ irradiated for 0, 30, and 60 seconds without a dimer; lanes 10-12, isomer 4 Δ irradiated for 0, 30, and 60 seconds with a thymine dimer; lanes 13 and 14, Maxam-Gilbert sequencing lanes for A+G and C+T respectively. Horizontal arrows denote the 5'-G of 5'-GG-3' and the 3'-G of 5'-GTTG-3' sites. Position of the thymine dimer lesion is denoted by brackets. Note that the levels of piperidine-sensitive damage are higher in all of the lanes containing the dimer including the dark control lanes; this background damage, which appears to originate from the synthesis of the thymine dimer by irradiation with triplet sensitizer, is subtracted out in the quantitation.



increasing duplex length (6). We have observed that the efficiency of electron transfer is related to the stacking of the base pairs in the DNA duplex: disruptions in the DNA caused by bulges reduce thymine dimer repair efficiency and guanine oxidation on the far side of the disruption, presumably by disturbing electron transfer through that part of the duplex (2,6). Fraying at the ends of the duplex may disrupt stacking in a similar way, causing the diminution in repair efficiency for dimers located near the ends of the duplex.

Furthermore, the thymine dimer changes the chemical reactivity of bases in its vicinity. We noted that the 3'-G of the sequence 5'-GT<>TG-3' is preferentially oxidized by both rhodium and ruthenium in the presence of the thymine dimer, with a concomitant decrease in the damage at the 5'-G of 5'-GG-3' sites. The ratio of the damage at a distal guanine doublet versus a proximal doublet remains constant, however, indicating that putative structural perturbations introduced by the dimer do not block the migration of a charge *through* the helix. Since the structure of the thymine dimer within a duplex is still under debate (37-40), it is unclear whether the charge is transported through the strand opposite the dimer or through the dimer itself, given that the dimer would have to be stacked into the helix in order to be electronically coupled to the other bases. However, since the thymine dimer is not aromatic, it is unlikely that a nonaromatic ring would be well-coupled even if it were well-stacked. This increased sensitivity of the 3'-G to oxidation, relative to controls having identical base sequence but no thymine dimer (Fig. 3.2, 3.7), is reminiscent of increased sensitivity to long-range damage which we observed previously at single base mismatch sites (4). These data indicate that structural changes caused by the dimer either: i) increase the accessibility of the 3'-G of the 5'-GT<>TG-3' tetrad to molecular oxygen; ii) alter its redox potential; iii) increase the residence time of the excited electron hole at the site; iv) or some combination of these factors. Certainly the observation of preferential oxidation to one side of

the dimer reflects that some local structural distortion has occurred and that the distortion is asymmetric.

3.3.7 Factors Governing Simultaneous Dimer Repair and Guanine Oxidation

Because photolysis of the rhodium complex can promote both oxidative damage to DNA and the repair of a thymine dimer, we can examine how these two sites for oxidative reaction on DNA compete electronically within the DNA helix. Figure 3.8 summarizes the various competing reactions that are involved.

Photoexcitation of $\text{Rh}(\text{phi})_2\text{DMB}^{3+}$ at 400 nm gives rise to an intraligand charge transfer state on the phi with a reduction potential of $E_{1/2}([\text{Rh}]^{3+*/2+}) \sim +2.0$ V versus NHE (41), which is of sufficient potential to oxidize the thymine dimer. In contrast, ground-state Ru(III), with a less positive estimated reduction potential ($E_{1/2}([\text{Ru}]^{3+/2+}) \sim +1.6$ V versus NHE) (36), cannot oxidize the thymine dimer. This brackets the oxidation potential of the thymine dimer within a DNA duplex as +1.6 to 2.0 V. Thymine dimer repair by rhodium involves oxidation and collapse of the cyclobutane ring. Since we have demonstrated that catalytic amounts of rhodium, non-covalently bound, can be used to repair thymine dimers (6), we know that the oxidative repair of the dimer by rhodium is simply triggered by electron transfer. Also the lifetime of the dimer cation must be on the order (or shorter lived) than the reduced rhodium, which is known to undergo decomposition on the microsecond timescale. Chemically induced dynamic nuclear polarization (CIDNP) studies on thymine dimer model compounds reveal that the dimer cation radical intermediate has a lifetime < 200 ns, although the rate of the initial charge trapping event has not been bracketed (42). The presence of the surrounding DNA duplex may affect that lifetime, however.

Both $^*\text{Rh}(\text{III})$ and $\text{Ru}(\text{III})$ intercalators oxidize guanine selectively at the 5'-G of 5'-GG-3' sites. Although the electrochemical properties of guanine in duplex

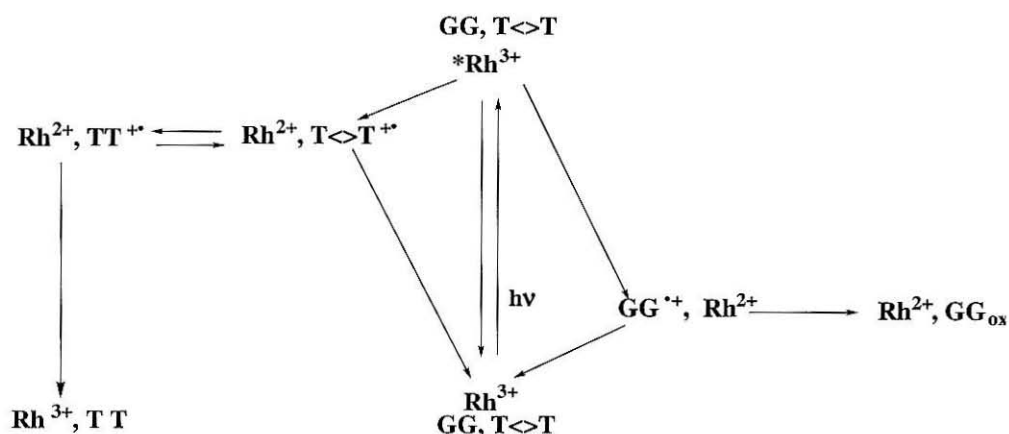


Figure 3.8: Proposed mechanisms for thymine dimer repair and guanine oxidation by an excited-state rhodium oxidant. When excited by light, the rhodium complex can oxidize guanine doublets or thymine dimers or return to the ground state. The oxidized thymine dimer radical cation intermediate can then undergo cycloreversion to a radical cationic form of the native thymines, which then oxidize the Rh^{2+} . The back reaction can also occur: the dimer radical cation intermediate can also oxidize the Rh^{2+} directly and return to the ground state. Alternatively, the 5'-G of the guanine doublet can be oxidized by ${}^*\text{Rh}^{3+}$. The oxidized guanine radical cation can then undergo a trapping reaction with water or oxygen to form 8-oxo-dG (G_{ox}), or the back reaction can occur. Transfer of the electronic hole between the dimer radical cation and the guanine and/or between the guanine cation radical and the dimer may also be possible, although the energetics make the latter unlikely (not shown).

DNA are not explicitly known, the oxidation potential of guanine was estimated by pulse radiolysis in neutral aqueous solution to be +1.29 V (20), which is less than the reduction potential of both ruthenium(III) and photoexcited rhodium(III). The quantum yield for oxidation by the "flash-quench" method with ruthenium complexes is higher than that for the direct photooxidation by the rhodium excited state, leading to a much higher yield of oxidized guanine in the same sequence over the same irradiation times. Although guanine oxidation is thermodynamically more favorable than thymine dimer repair, the former reaction involves multiple bimolecular reactions that trap the damage irreversibly. In fact the quantum yield of guanine oxidation is substantially lower than for dimer repair by tethered rhodium (5×10^{-8} versus at 365 versus 2×10^{-6} at 400 nm, respectively). Damage to guanine by metallointercalators is thought to proceed *via* initial oxidation of the base in ≤ 200 ns, giving the guanine cation radical which is quickly deprotonated to form the neutral guanine radical $[G^{\bullet}(-H)]$. The neutral guanine radical subsequently reacts with an oxygen source, likely O_2 , on the microsecond time or longer scale to form stable oxidation products (5). With both rhodium and ruthenium intercalators, the thermodynamics of the initial oxidation, lifetime of the guanine radical intermediate(s), rate of back electron transfer, and rate of oxygen trapping to provide damaged products can all potentially contribute to the damage yields.

In duplexes containing only thymine dimers, dimer repair occurs with high yield regardless of its location with respect to the metallointercalator. When the thymine dimer lesion and a guanine doublet are both present in an assembly containing tethered rhodium, the level of repair decreases. Clearly guanine oxidation is thermodynamically favored over dimer repair. The fact that dimer repair and guanine oxidation can compete for the mobile charge indicates that the charge is equilibrated across the entire duplex. The fact that the relative position of

the guanine doublet and the dimer lesion with respect to the oxidant does not affect the product outcome provides further evidence for this assertion. We have seen equilibration across the duplex before, by the formation of oxidized product by Ru(III) at all sites of equivalent oxidation potential in the absence of a guanine doublet "sink" (4).

In duplexes containing only guanine traps, oxidative damage and charge trapping occur at the most easily oxidized sites, independent of location with respect to the tethered oxidant (1-3). When both a thymine dimer and guanine doublet are present in an assembly containing tethered rhodium, the amount of oxidized guanine formed decreases. Although a diminution in the levels of guanine oxidation could in principle be caused by a destabilization in the helix induced by the dimer, we can eliminate this possibility because the amount of guanine oxidized by Ru(III) is not diminished by the presence of the thymine dimer. Therefore the thymine dimer must instead be depleting the system of the electronic holes which lead to the formation of oxidized guanine. Guanine oxidation is thermodynamically favored over thymine dimer repair by ~400 mV, which corresponds to an equilibrium constant for the equilibrium between oxidized guanine and oxidized dimer of 5×10^6 . The collapse of the dimer cation radical to two repaired thymines must occur faster than the trapping of the guanine cation radical by an oxygen source. What controls the formation of the two products is not then simply the thermodynamic difference between the guanine and the dimer but also the difference in lifetimes and reactivity between the guanine radical (μs - ms) and dimer cation radical intermediate (~200 ns). Furthermore, given that the order within the sequence does not affect the identity of the products, we may conclude that the equilibration must be faster than the trapping reactions of either the guanine radical or the dimer radical.

Our results therefore point to rapid equilibration of the oxidizing charge throughout the duplex on a timescale which is fast relative to the charge trapping event. Both hopping mechanisms and delocalized band models have been used to describe the movement of charges through DNA. In a hopping mechanism, an electron or electronic hole is localized on a particular base and migrates from base to base in discrete "hops," each hop independent of the previous one (43). The hopping rate is significantly faster than vibrational relaxation, allowing the charge to diffuse away from the site at which it is generated before it is trapped. When a hopping mechanism is used to explain the movement of the oxidizing charge across the duplex, one difficulty arises: how can an electronic hole hop *up* (energetically) to a thymine dimer from the neighboring bases, which have much lower oxidation potentials? We must invoke an excited electron or electronic hole with sufficient energy to oxidize all of the bases before relaxation in order for a hopping mechanism to describe our results, which clearly show the oxidation of both thymine dimers and guanine doublets located distal to the dimers. Alternatively, a delocalized band model may be considered to describe the equilibration of an oxidizing charge throughout the duplex. In this model, the DNA is described like other conducting polymers, with bands of many overlapping electronic states in the place of individual HOMOs and LUMOs into which electrons can be injected or from which electrons can be withdrawn. Perhaps some combination of hopping and delocalized band formation is needed in the development of models which accurately describe the migration of charges through DNA.

3.3.8 *Implications with respect to Biological Charge Transport Mediated by DNA*

Viewed classically, chemical modification of a particular DNA sequence in the genome requires direct contact between a sequence and the agent which carries out the chemistry. Here we demonstrate, however, that sequence-selective

chemical transformations of DNA can be induced remotely by charge transfer without direct physical contact between the oxidant and the reactive base(s) on the DNA. The reacting partner, the tethered metallointercalator, binds to DNA at a position spatially separated from the reactive 5'-GG-3' and thymine dimer sites, initiating chemistry at a distance. Moreover, the efficiency of one reaction is affected by the presence of the other, and different sites on the DNA duplex can compete for oxidation by a distant molecule. Although we now possess evidence for both long-range DNA damage and repair *in vitro*, later we pursue the question of whether analogous reactions occur in the cell, either as a mechanism for damage, or as a means of repair or signalling. Studies of the mechanisms of DNA damage by ionizing radiation and other sources have indicated that it is likely that electronic holes can migrate before settling on guanine (chapter 1). Irreversible, and potentially mutagenic, damage to guanine sites provides a reason why repair reactions or intracellular communication through the DNA base stack may be too hazardous for Nature to use. However, this work shows that even though guanine bases are energetically favored as the site of oxidation, other factors may govern what reaction ultimately occurs.

3.4 References

1. D.B. Hall, R.E. Holmlin, J.K. Barton, *Nature* **382**, 731 (1996).
2. D.B. Hall, J.K. Barton, *J. Am. Chem. Soc.* **119**, 5045 (1997).
3. M.E. Núñez, D. B. Hall, J. K. Barton, *Chem. Biol.* **6**, 85 (1998).
4. M.R. Arkin, E. D. A. Stemp, S. C. Pulver, J.K. Barton, *Chemistry and Biology* **4**, 389 (1997).
5. E. D. A. Stemp, M. R. Arkin, J. K. Barton, *J. Am. Chem. Soc.* **119**, 2921 (1997).
6. P. J. Dandliker, R. E. Holmlin, J. K. Barton, *Science* **275**, 1465 (1997).
7. A. Sancar, *Annu. Rev. Biochem.* **65**, 43 (1996).
8. T. P. Begley, *Acc. Chem. Res.* **27**, 394 (1994).
9. P. F. Heelis, R. F. Hartman, S. D. Rose, *Chem. Soc. Rev.* **24**, 289 (1995).
10. S.-T. Kim, A. Sancar, *Photochem. Photobiol.* **57**, 895 (1993).
11. A. Sancar, *Biochemistry* **33**, 2 (1994).
12. J. S. Taylor, *Acc. Chem. Res.* **27**, 76 (1994).
13. M. Charlier, C. Hélène, C. *Photochem. Photobiol.* **21**, 31 (1975).
14. C. Hélène, M. Charlier, *Photochem. Photobiol.* **25**, 429 (1977).
15. J. R. Jacobsen, A. G. Cochran, J. C. Stephans, D. S. King, P. G. Schultz, *J. Am. Chem. Soc.* **117**, 5453 (1995).
16. S.-T. Kim, R. F. Hartman, S. D. Rose, *Photochem. Photobiol.* **52**, 789, (1990).
17. S.-T. Kim, S. D. Rose, *J. Phys. Org. Chem.* **3**, 581 (1990).
18. T. Carell, R. Epple, V. Gramlich, *Angew. Chem. Int. Ed. Engl.* **35**, 620 (1996).
19. R. Epple, E.-U. Wallenborn, T. Carell, *J. Am. Chem. Soc.* **119**, 7440 (1997).
20. S. Steenken, S. V. Jovanovic, *J. Am. Chem. Soc.* **119**, 617 (1997).

21. P. F. Heelis, D. J. Deeble, S.-T. Kim, A. Sancar, *Int. J. Radiat. Biol.* **62**, 137 (1992).
22. C. Pac, J. Kubo, M. Tetsuro, H. Sakurai, *Photochem. Photobiol.* **36**, 273 (1982).
23. D. Wayner, in *Handbook of Organic Photochemistry*, J. C. Sca'iano, ed., pp 363-369, CRC Press, Boca Raton (1989).
24. E. Amouyal, A. Homsy, J. C. Chambron, J. P. Sauvage, *J. Chem. Soc. Dalton Trans.* **6**, 1841 (1990).
25. P. A. Anderson, *et al.*, *Inorg. Chem.* **34**, 6145 (1995).
26. A. E. Friedman, J.-C. Chambron, J.-P. Sauvage, N. J. Turro, J. K. Barton, *J. Am. Chem. Soc.* **112**, 4960 (1990).
27. R.E. Holmlin, P. J. Dandliker, J. K. Barton, *Bioconj. Chem.* **10**, 1122 (1999).
28. S. K. Banerjee, A. Borden, R. Christensen, J. E. LeClerc, C. W. Lawrence, *J. Bacteriol.* **172**, 2105 (1990).
29. S. K. Banerjee, R. B. Christensen, C. W. Lawrence, J. E. LeClerc, *Proc. Natl. Acad. Sci. USA* **85**, 8141 (1988).
30. J. K. Setlow, in *Current Topics in Radiation Research*, M. Ebert, A. Howard, eds. pp 197-248, North-Holland, Amsterdam (1966).
31. J. A. Lippke, L. K. Gordon, D.E. Brash, W. A. Haseltine, *Proc. Natl. Acad. Sci. USA* **78**, 3388 (1981).
32. J. Sambrook, E. F. Fritsch, T. Maniatis, *Molecular Cloning: A Laboratory Manual*, 2nd ed., Cold Spring Harbor Laboratory, New York (1989).
33. A. M. Pyle, E. C. Long, J. K. Barton, *J. Am. Chem. Soc.* **111**, 4520 (1989).
34. A. Sitlani, J. K. Barton, *Biochemistry* **issue**, 12100 (1994).
35. A. Sitlani, E.C. Long, A. M. Pyle, J. K. Barton, *J. Am. Chem. Soc.* **114**, 2303 (1992).

36. C. J. Murphy *et al.*, *Proc. Natl. Acad. Sci. USA* **91**, 5315 (1994).
37. M. G. Cooney, J. H. Miller, *Nucleic Acids Res.* **25**, 1432 (1997).
38. J. Kemmink *et al.*, *Nucleic Acids Res.* **15**, 4645 (1987).
39. J. S. Taylor, D. S. Garrett, I. R. Brockie, D. L. Svoboda, J. Telser,
Biochemistry **29**, 8858 (1990).
40. K. Miaskiewicz, J. Miller, M. Cooney, *J. Am. Chem. Soc.* **119**, 9156 (1997).
41. C. Turro, A. Enenzahav, S. H. Bossmann, J. K. Barton, N. J. Turro, *Inorg.*
Chim. Acta **243**, 101 (1996).
42. J. Kemmink, A. Eker, R. Kaptein, *Photochem. Photobiol.* **44**, 137 (1986).
43. D. Dee, M. E. Baur, *J. Chem. Phys* **60**, 541 (1974).

Chapter 4

Long-Range Guanine Oxidation in DNA Restriction Fragments by a Triplex-Directed Naphthalene Diimide Intercalator*

* Adapted from: M. E. Núñez, K. T. Noyes, D. A. Gianolio, L. W. McLaughlin, J. K. Barton, *Biochemistry* **39**, 6190 (2000).

4.1 Introduction

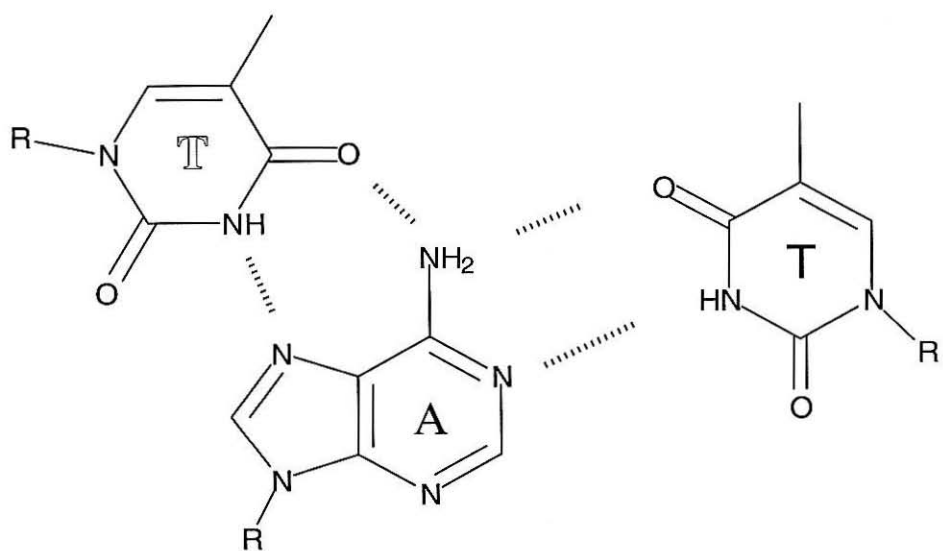
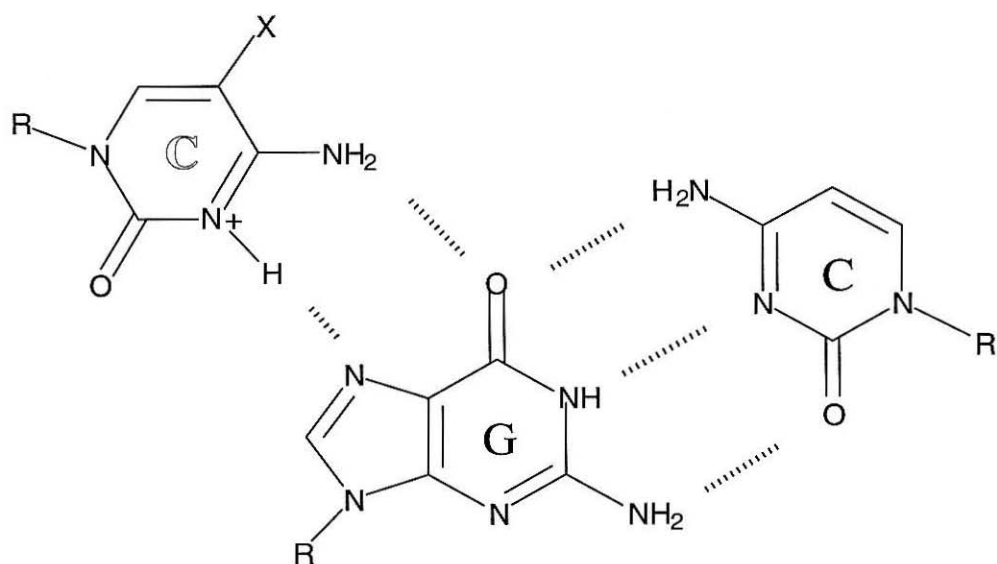
Having demonstrated that charge migration on oligonucleotide duplexes can yield permanent base lesions at distances of at least tens of base pairs from the damaging agent, we are interested in considering whether and how these holes might also migrate along DNA within the cell to distribute damage across the genome. This possibility holds implications both to the generation of damage on DNA and to its repair (*1*). In this context, it is important to determine the distance range for charge transport in natural DNA sequences, and to develop a system to study long-range charge transfer that does not necessitate covalent attachment of the photooxidant to the DNA of interest. In the experiments described here, we begin to explore this question by examining the distribution of damage along a DNA restriction fragment through the site-specific targeting of a intercalating photooxidant using oligonucleotide-directed triplex formation.

It has long been known that naphthalene diimide (NDI) molecules intercalate into DNA (*2-5*), and are potent electron acceptors (*6-9*). Matsugo *et al.* showed that hydroperoxy derivatives of naphthalene diimide molecules oxidize guanine with a preference for 5' guanines (*10*). It was later demonstrated that the related noncovalent naphthalimide molecule lacking the hydroperoxy groups exhibited the same preference for 5' guanines, and this preference was attributed to electron transfer chemistry (*11*). Recently the triplet excited state of photoexcited naphthalene diimide molecules were shown to oxidize nucleotides in aqueous solution, with oxidation of GMP being by far the most efficient (*12-13*). The reduction potential of the triplet excited state was estimated to be 1.8 V versus NHE, high enough to oxidize all of the nucleotide bases. In this study, we demonstrate that naphthalene diimide (NDI) intercalators covalently tethered to DNA sequences can oxidize guanine *at long range*, and we exploit the chemistry

of this intercalator to examine the limits of charge transfer in DNA restriction fragments.

Since the intercalating photooxidants used in this study, $\text{Rh}(\text{phi})_2\text{bpy}^{3+}$ and NDI, bind to DNA in a relatively sequence-neutral fashion (2, 14, 15), we attached them covalently to a second molecule which confers upon it sequence specificity, in this case a triplex-forming oligonucleotide (TFO). Triple helices are formed by the binding of a single-stranded oligonucleotide in the major groove of duplex DNA (16). These third strand oligonucleotides bind most tightly to sequences that contain only purines on one strand of the Watson-Crick duplex and only pyrimidines on the other. In the pyrimidine motif used in this study, an oligopyrimidine third strand binds parallel to the purine strand of the duplex, forming Hoogsteen hydrogen bonds between the duplex guanine and the protonated cytosine of the third strand ($\text{C}^+\bullet\text{GC}$), and between the duplex adenine and the thymine of the third strand ($\text{T}\bullet\text{AT}$) (Fig. 4.1). Triple helices have been shown to bind specifically to their target sequences on both short nucleotides and plasmid vectors, with association constants on the order of 10^7 M^{-1} depending on sequence, salt concentration, temperature, and pH (17-20). Intercalators such as acridine, NDI, benzopyridoindole, and benzopyridoquinoxaline covalently tethered to triplex-forming oligonucleotides stabilize the triplex considerably (21-29). Furthermore, molecules that react with DNA have been attached to a triple-helix-forming oligonucleotide and delivered site-specifically to their target, even on genomic DNA and inside of cells (30-37). Combining these methodologies, we attached intercalators to a 16-base-pair triplex-forming oligonucleotide, selectively targeted them to a single site on a restriction fragment, and determined the extent and pattern of base damage generated by these photooxidants on a DNA restriction fragment.

Figure 4.1: Base triples in triple helices with a pyrimidine motif. Base triples are formed by Hoogsteen hydrogen bonding between a thymine or protonated cytosine residue in the major groove and the Watson-Crick base pairs of double-stranded DNA ($X=H$ if cytosine, $X=CH_3$ if 5-methyl-cytosine). These Hoogsteen hydrogen bonds are highly specific for the target base pairs.



4.2 Methods

4.2.1 Oligonucleotide Preparation

Preparation of oligonucleotides with appended naphthalene diimides has been described (27-29). The synthesis and purification of $\text{Rh}(\text{phi})_2\text{bpy}^{3+}$ and of unmodified oligonucleotides has also been described in detail elsewhere (38).

4.2.2 Preparation of Restriction Fragments with Triplex Binding Sites

Triplex-binding oligonucleotides with *EcoRI* or *BamHI* sticky ends and 5' phosphate termini were synthesized by standard phosphoramidite chemistry on an Applied Biosystems DNA synthesizer. These strands were purified twice by HPLC, annealed, and ligated into the dephosphorylated *BamHI* site or *EcoRI* site of pUC19 by incubation with T4 DNA Ligase at 16°C overnight (New England Biolabs). This plasmid was transfected into commercially-available DH5 α competent *E. coli* (Life Technologies) by standard methods (39) and the cells were plated out on LB plates containing ampicillin, X-gal, and IPTG (Aldrich, Boehringer-Mannheim). Cultures were innoculated from separate clear colonies, and the plasmids were isolated (Qiagen) and sequenced by the Caltech DNA sequencing facility.

4.2.3 End-Labeling of Restriction Fragments

End-labeled restriction fragments were prepared by standard methods. Briefly, 20 μg of plasmid was cut with the first restriction enzyme, dephosphorylated using shrimp alkaline phosphatase (Boehringer-Mannheim), phenol-chloroform extracted and ethanol precipitated. Then the DNA was end-labeled using $\gamma^{32}\text{P}$ -ATP (ICN) and Polynucleotide Kinase (New England Biolabs) or $\alpha^{32}\text{P}$ -ddATP (Amersham) and Terminal Transferase (Boehringer-Mannheim). This DNA was again phenol-chloroform extracted and ethanol precipitated before being digested

with the second restriction enzyme. The desired fragment was isolated by nondenaturing polyacrylamide gel electrophoresis, identified by autoradiography, extracted by crushing-and-soaking in 10 mM Tris-HCl with 1 mM EDTA, and purified on a C18 minicolumn (Nensorb).

4.2.4 Triplex Annealing

The following mixtures were supplemented by the desired concentration of triplex-forming oligonucleotide. Rh triplexes: 50 MES buffer pH 5.75, 10 mM MgCl_2 , 1 mM spermidine chloride (Aldrich), 75 μM (base pair) calf thymus DNA (Boehringer-Mannheim) and the minimum amount of radiolabeled DNA required for visualization of the samples. NDI triplexes: "Wide Range" phosphate/citrate buffer (9.5 mM citrate and 12.5 mM phosphate) pH 5.6, 10 mM MgCl_2 , 1 mM spermidine chloride (Aldrich), 75 μM (base pair) calf thymus DNA (Boehringer-Mannheim), 1-2 molar equivalents of triplex-binding oligonucleotide, and the minimum amount of radiolabeled DNA required for visualization of the samples. The samples were allowed to equilibrate for at least 12 hours at 4°C and were irradiated at a controlled temperature.

4.2.5 Irradiation and Visualization of Samples

Samples (~30 μL) were irradiated at $11^\circ\text{C} \pm 1^\circ\text{C}$ at the desired wavelength on a 1000 W Hanovia Hg-Xe arc lamp equipped with a monochromator. After irradiation, the DNA was ethanol precipitated to remove multivalent cations. The DNA was then cleaved by incubation in 100 μL of 10% piperidine for 30 minutes at 90°C and dried *in vacuo*. Samples were analyzed by denaturing polyacrylamide electrophoresis on a 6% gel, followed by visualization and quantitation by phosphorimagery (ImageQuant by Molecular Dynamics).

4.3 Results and Discussion

4.3.1 Intercalator-DNA Conjugates

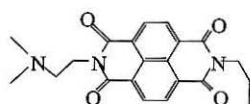
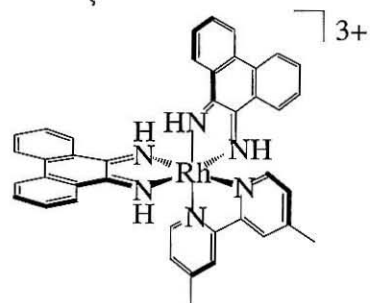
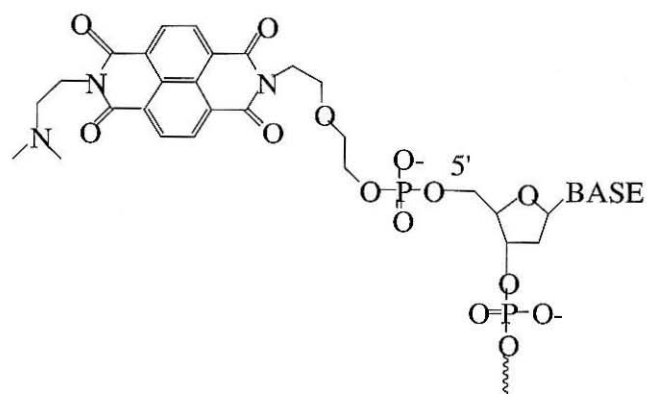
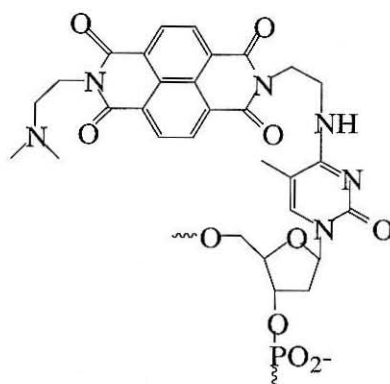
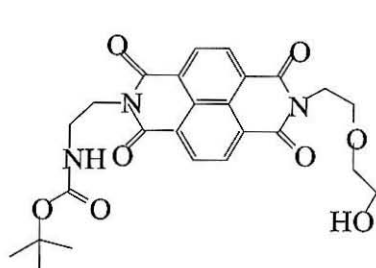
A 17-mer pyrimidine triplex-forming oligonucleotide was prepared with $\text{Rh}(\text{phi})_2\text{bpy}^{3+}$ appended to the 5' end of the sugar-phosphate backbone by a nine-carbon linker. Two naphthalene diimide (NDI) conjugates with a pyrimidine 16-mer oligonucleotide were also prepared for these studies. In the first, the intercalator was attached to the 5' end of the sugar-phosphate backbone through a short linker and a phosphodiester, and in the second, the intercalator was attached directly to the N4 amino group of a methylated cytosine base incorporated into the base sequence. These conjugates, along with $\text{Rh}(\text{phi})_2\text{DMB}^{3+}$ and protected, noncovalent NDI, are illustrated in Figure 4.2.

4.3.2 Targeting $\text{Rh}(\text{phi})_2\text{bpy}^{3+}$ to a Single Specific Sequence by Triplex Formation

Although $\text{Rh}(\text{phi})_2\text{bpy}^{3+}$ intercalates avidly into DNA, its binding is largely sequence-neutral (14,15). In order to confer sequence specificity to the intercalator, we tethered it to a pyrimidine triplex-forming oligonucleotide (TFO), and we incorporated a specific binding site at two locations within the plasmid pUC19 for the TFO to target (Fig. 4.3).

When the metallointercalator-TFO conjugate was incubated with a restriction fragment containing the target sequence, the rhodium complex was delivered to the target site and bound to the duplex adjacent to the triplex region. We established the binding site of the 5'-tethered rhodium complex by direct photocleavage of the sugar-phosphate backbone using irradiation with 313 nm (14, 40). Specific binding to the target site and concomitant photocleavage was observed from 8 μM down to less than 16 nM rhodium-triplex strand (Fig. 4.4). Furthermore, no nonspecific damage was observed, even at 8 μM triplex-forming

Figure 4.2: Structures of the intercalating photooxidants and oligonucleotide conjugates used in this study. At top left is the naphthalene diimide molecule in the noncovalent form. On the right is the cytosine-tethered naphthalene diimide molecule, which can be prepared as a phosphoramidite and incorporated into an oligonucleotide according to standard solid-phase methods (24). In the middle is the 5' tethered NDI, attached to the sugar-phosphate backbone through a 5-atom linker (25), and $\text{Rh}(\text{phi})_2\text{DMB}^{3+}$. On the bottom are shown two of the intercalator-oligonucleotide conjugates. "5" represents 5-methyl cytosine.



3' TTTCCT TTT TT5TCT T 5'



Figure 4.3: Sequence of the target restriction fragments. Only the part of the fragment flanking the target polypurine-polypyrimidine site is shown. The restriction fragments used in this study are in fact considerably longer than these sequences by approximately 200 base pairs. A 5' tethered and a base-tethered intercalator-TFO conjugate are also shown. Note that both TFO's can bind to both restriction fragments, since both sequences contain the identical target site and differ only their flanking sequence. "5" represents 5-methyl cytosine. The terms "5'side" and "3'side" refer to the direction along the duplex relative to the orientation of the third strand, and "PUR" and "PYR" refer to the purine-rich and pyrimidine-rich target duplex strands.

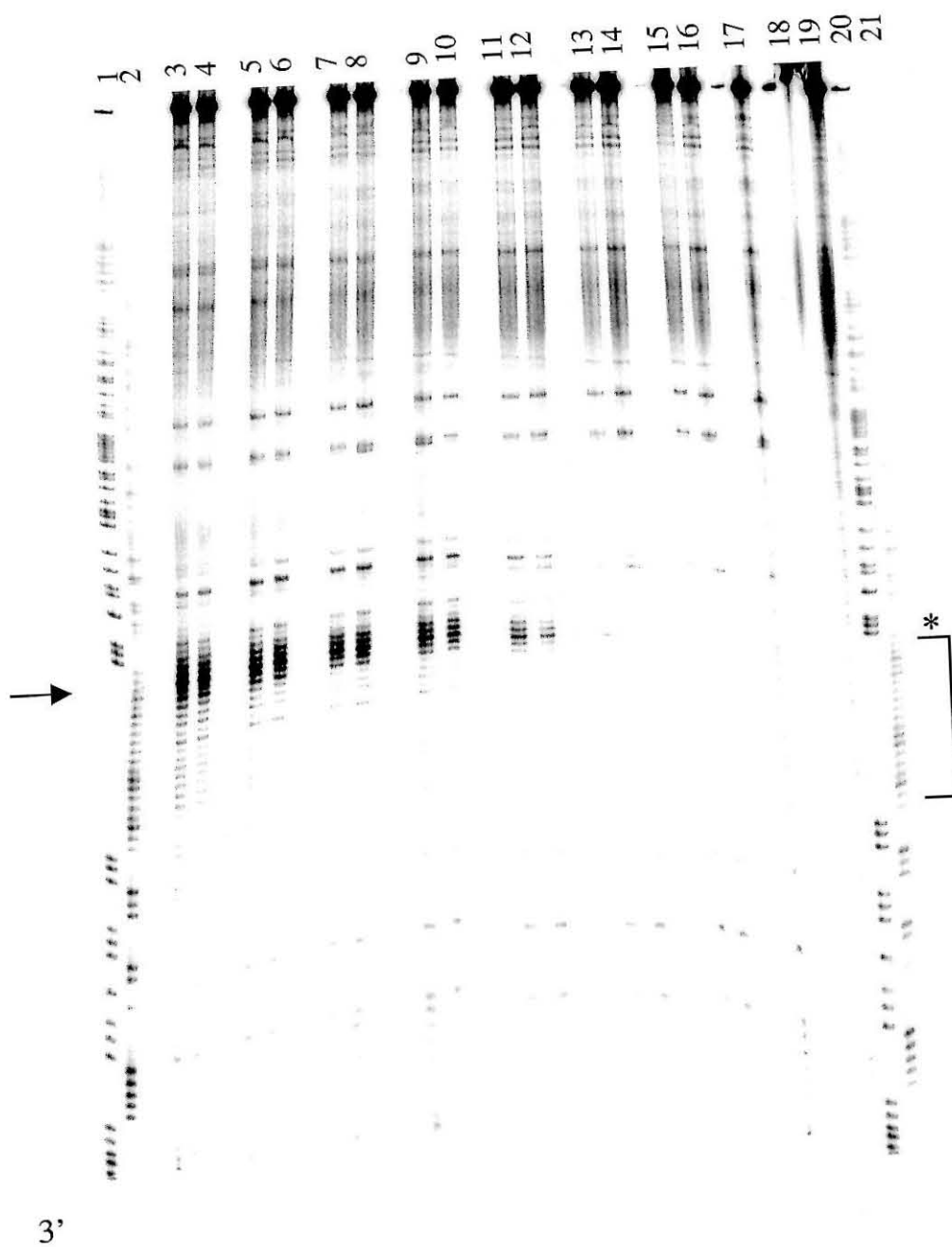
Sequence 1

5' GCAGGATCCCCGGGTACCGAGCTCGAATTCTTCCCTTTTTTCTCTTTTGAATTCACCTGGCCGTCGTTTACAAACGTCGTG3' Pyr
 3' CGTCCTAGGGGCCCCATGGCTCGAGCTTTAAGAAAGGAAAAAGAGAAAACCTTAAGTGACCCGGCAGCAAAAATGTTGCAGCAC5' Pur
 3' TTT55TTTTTTTTT5T5TTT 5' Rh 5' side TFO

Sequence 2

5' TGCCTGCAGGTCGACTCTAGAGGGATCCAGTTTCCCTTTTTTCTCTTTTACGACTGTAGCCGAGATCAGCCGCTAACGCCG3' Pyr
 3' ACGGACGTCCAGCTGAGATCTCCCTAGGTCAAAGGAAAAAGAGAAAATGCTGACATCGGCTCTAGTCGGCGAATTCGGGC5' Pur
 3' TTTCCCTTTTTTT5TCTT 5' NDI 5' side TFO

Figure 4.4: Direct photocleavage at 313 nm of a restriction fragment by $\text{Rh}(\text{phi})_2\text{bpy}^{3+}$ covalently tethered to a triplex-forming oligonucleotide. The polypurine strand containing sequence 1 is shown. Samples contained the following amounts of Rh-TFO, in lanes **3-17**, respectively: 8 μM , 4 μM , 2 μM , 1 μM , 500 nM, 250 nM, 125 nM, 63 nM, 32 nM, 16 nM, 8 nM, 4 nM, 2 nM, 1 nM, 0 nM. Maxam-Gilbert purine-specific sequencing reactions were loaded in lanes **2** and **21**, and pyrimidine-specific sequencing reactions in lanes **1** and **20**; lane **18** is a light control and lane **19** is a dark control. The designed binding site is indicated by a bracket and the binding site of the appended metal by an asterisk. The arrow points to the site of direct photocleavage by the photoexcited metallointercalator.



oligonucleotide. That the triplex-forming oligonucleotide was bound to the target site and not elsewhere on the restriction fragment at a concentration of $\sim 1 \mu\text{M}$ was confirmed by DNase I footprinting experiments, in which a clear footprint was observed in the triplex region in both the absence and presence of tethered metallointercalator (Figure 4.5). These DNase I footprints were used to determine approximate binding constants for the triplex forming oligonucleotides. Interestingly, the presence of the rhodium intercalator does not appear to improve the binding constant of the TFO, in contrast to other intercalators (21-29).

Having established that the 5'-Rh-tethered-TFO binds specifically to its target site, we irradiated the conjugate with its target restriction fragment and observed piperidine-sensitive damage in the same region as the direct photocleavage. However, we observed little or no long-range damage (Fig. 4.6). All of the DNA damage occurs in the vicinity of the binding site, in contrast to that seen repeatedly on oligonucleotide duplexes (40-42). Based on the lack of long-range charge transfer and the binding constant that was not improved by the presence of intercalator, we proposed that the metal complex was not well-intercalated into the duplex DNA. To improve the intercalation we systematically changed the length of the tether, the orientation of the linker ligand, the composition of the buffer, the chirality of the metal center, and the sequence of the putative intercalation site. In addition, we examined base oxidation by a 5'-tethered $\text{Ru}(\text{phen})(\text{bpy}')(\text{dppz})^{3+}$ complex and by tethered ethidium. In all cases we observed the same pattern of damage, in which all of the base damage is localized to the duplex-triplex junction at the 5' end of the triplex (not shown).

It has been shown previously that polypyrimidine triplex-forming strands can be used to deliver a variety of small molecules to long DNA duplexes (21-37). In the present study, we observed, using DNase I footprinting and exploiting the direct strand-scission chemistry of the phi complexes of rhodium, that a

Figure 4.5: DNase I footprinting of a 17-mer triplex-forming oligonucleotide bound to a restriction fragment. As the concentration of triplex decreases, nonspecific cleavage by the DNase I at the binding site of sequence 1 increases because of increased access to the radiolabeled duplex DNA by the enzyme. The location of the triplex-binding site is indicated by a bracket. Maxam-Gilbert A+G and C+T sequencing lanes are shown at left in lanes **1** and **2**. Samples contained the following amounts of unmodified TFO, in lanes **4-21**, respectively: 16 μM ; 8 μM ; 4 μM ; 2 μM ; 1 μM ; 500 nM; 250 nM; 125 nM; 62.5 nM; 31 nM; 15.5 nM; 8 nM; 4 nM; 2 nM; 1 nM; 0.5 nM; 0.25 nM; none. Lane **3** contained no DNase I.

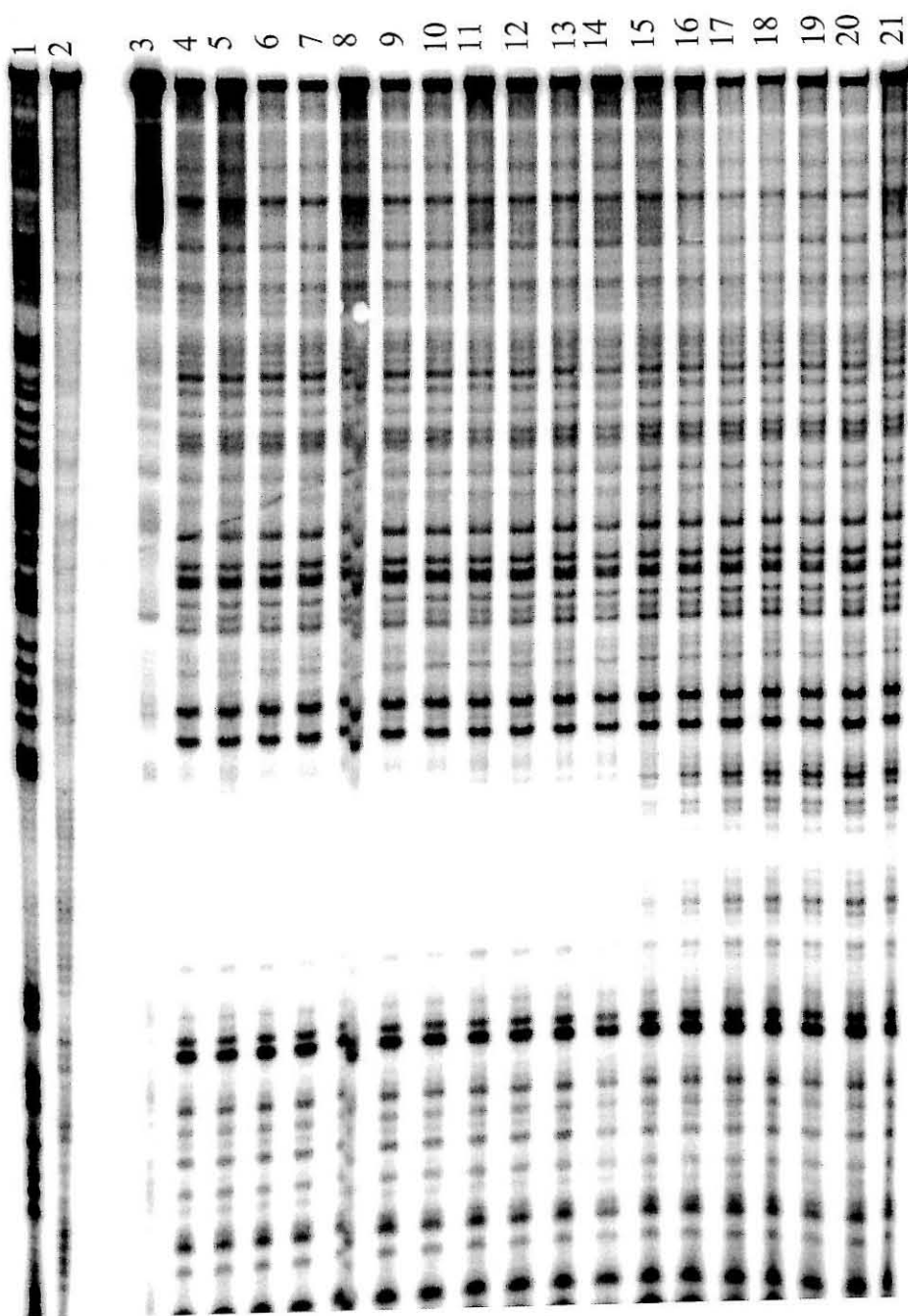
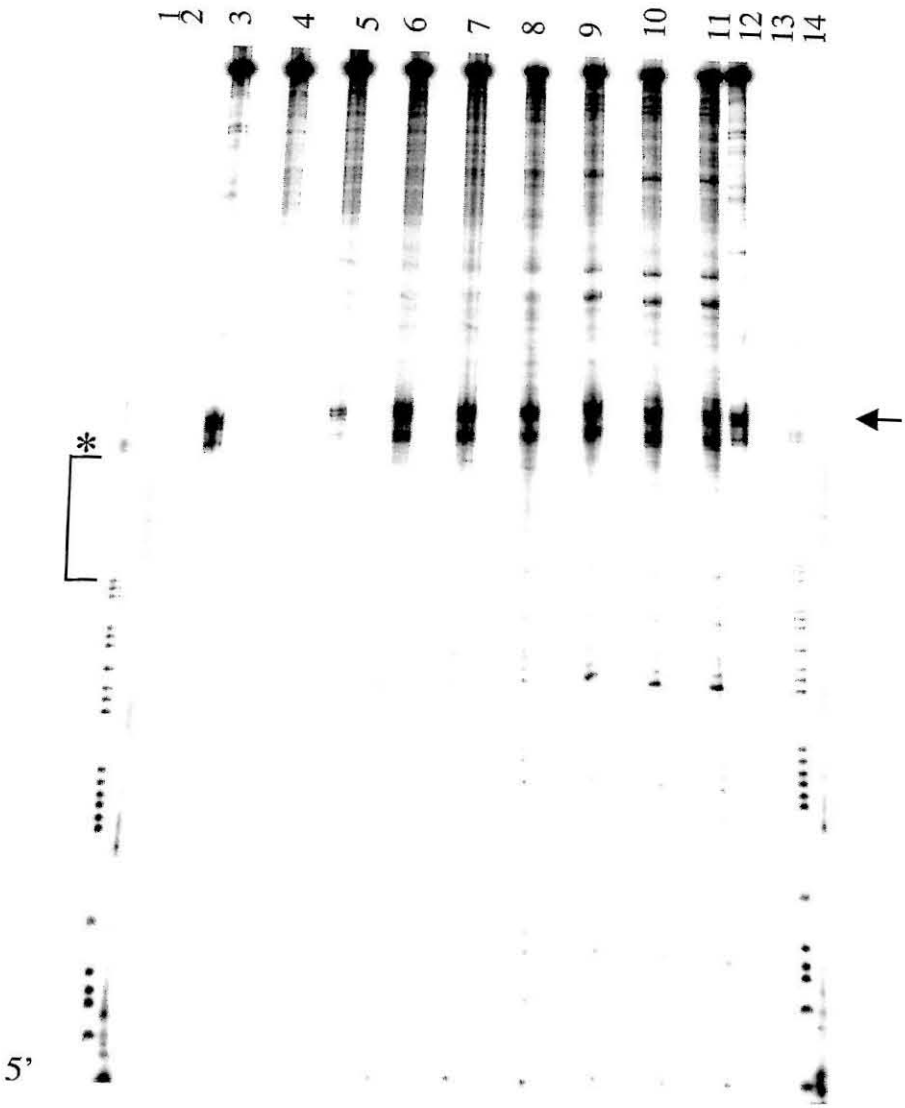


Figure 4.6: Oxidation of a restriction fragment by a photoexcited rhodium intercalator covalently tethered to a triplex-forming oligonucleotide. Minimal long-range damage on the pyrimidine strand of sequence 1 is observed at a range of irradiation times: lanes **4-11**, irradiation at 365 nm for 0, 15, 30, 45, 60, 75, 90, 120 min., respectively. However, the TFO is bound to its designed site, as demonstrated by the direct photocleavage at 313 nm, lanes **3** and **12**. The site of oxidation is indicated by an arrow, while the designed TFO binding site is marked by a bracket with an asterisk indicating the binding site of the metallointercalator.



pyrimidine TFO can deliver a 5' appended rhodium intercalator to a specific site within a ~250 bp restriction fragment (Fig. 4.4, 4.5). When we irradiated these samples at 365 nm to initiate long-range damage to guanine, however, we observed damage only locally (Fig. 4.6). It was therefore apparent that the metallointercalator, delivered by triplex formation, was not well-coupled into the π stack of the restriction fragment. Interestingly, systematic changes to the intercalator and the intercalation site were insufficient to improve the electronic coupling. There are several reasons which might explain this phenomenon. It is possible that the octahedral metallointercalators are mostly intercalated into or stacked on the end of the third strand of the triple helix, orientations which might not be expected to lead to good charge transfer through duplex DNA. However, this would not explain the efficient direct photocleavage, which requires the metal complex be intimately associated with the sugar-phosphate backbone of the duplex. One might also consider that the metallointercalator might not be well-intercalated into the duplex for thermodynamic reasons, due to the large entropic cost of orienting the intercalator and linker, but this is inconsistent with the behavior of this same linker and intercalator in duplex DNA. A third possibility is that the stacked base pairs of the triplex do not permit long-range charge transfer; however, this does not explain the absence of charge transfer in the duplex region.

Since we could not determine whether the absence of long-range damage was due to poor intercalation by the octahedral complexes or to an unusual structure in the DNA duplex, we examined next whether a planar, extremely hydrophobic, organic intercalating photooxidant, covalently attached to the terminus of the sugar-phosphate backbone or to a methylated cytosine embedded in the oligonucleotide sequence, might promote long range charge transport in restriction fragments using the triplex-directed binding methodology.

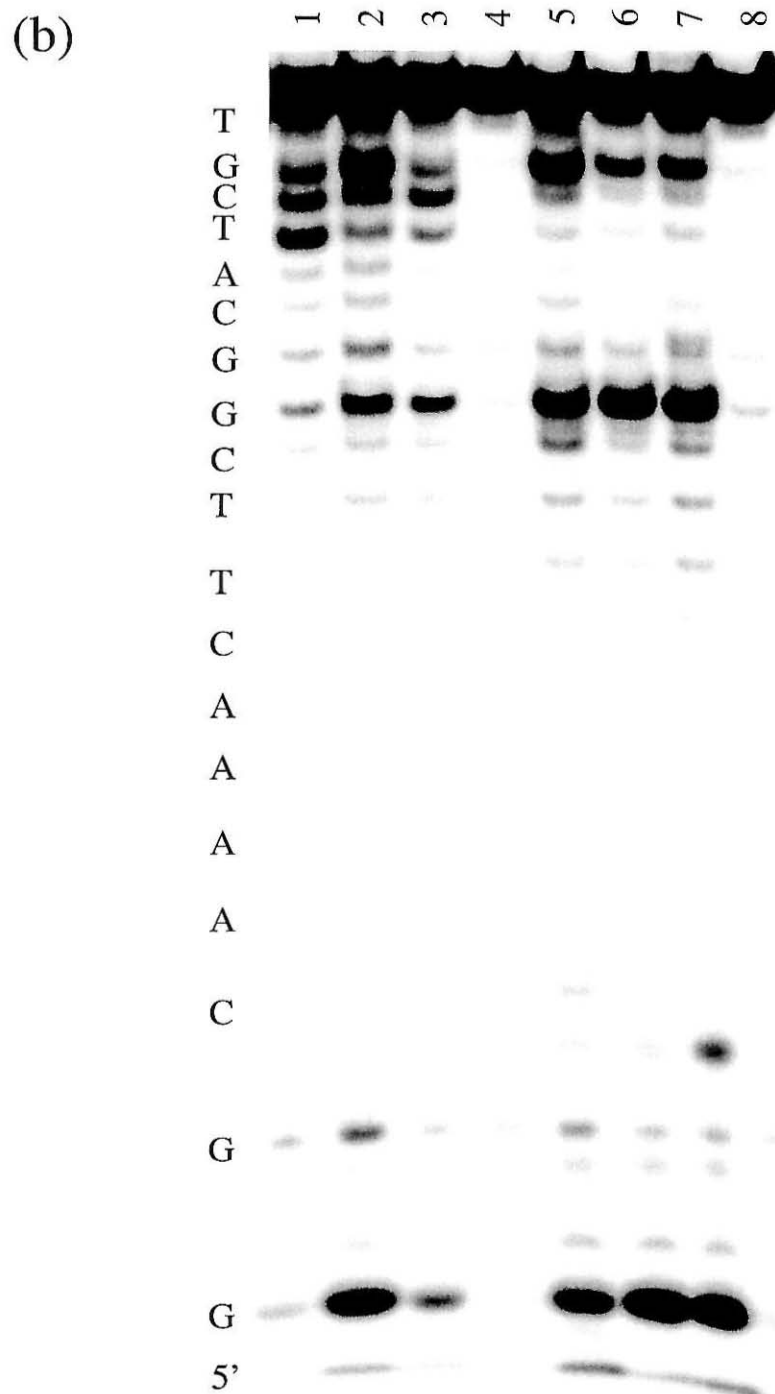
4.3.3 Oxidation of 5'-GG-3' Sites in DNA Duplexes by Naphthalene Diimide Intercalators

We examined first photooxidation on a 22-base pair oligonucleotide duplex by noncovalent naphthalene diimide (Fig. 4.7a). The target sequence contained two 5'-GG-3' sites. Selective oxidation at the 5' guanines of both guanine doublets was observed when the mixture was irradiated at 313, 340, and 365 nm but not 400 nm (Fig. 4.7b). Base damage was revealed upon cleavage of the DNA at the lesion with hot aqueous piperidine. Some oxidation was also observed at a single guanine positioned near the end of the sequence. We compared this oxidative damage to that generated by photoexcited $\text{Rh}(\text{phi})_2\text{bpy}^{3+}$ covalently tethered to the 5' end of the same duplex, and we found that the oxidation pattern was strikingly similar to that generated by noncovalent NDI. Both preferentially oxidize the 5' guanine of 5'-GG-3' steps, a characteristic "signature" of electron transfer. When both oxidants were present simultaneously, the amount of damage generated at guanines was diminished but not eliminated, which may be due to oxidation of NDI by photoexcited $\text{Rh}(\text{phi})_2\text{bpy}^{3+}$.

It seems likely that oligonucleotide-tethered naphthalene diimide molecules can oxidize guanine at long range by charge transport through the DNA base stack, since (a) they can intercalate into DNA and thus access the π stack, and (b) they have a potential sufficient to oxidize guanine bases. Almost 20 years ago, it was shown spectroscopically and viscometrically that naphthalene diimides bind to DNA by intercalation (4). Later work revealed that alkylamino-substituted diimides intercalate by a threading mechanism in which one of the substituents must slide between the base pairs (3). This binding mode results in a DNA binding affinity on the order of other planar, aromatic intercalators, such as ethidium, but with association and dissociation kinetics that are considerably slower. More recently, it was shown that this favorable stacking interaction with

Figure 4.7: Oxidation of a short oligonucleotide duplex by noncovalent NDI. (a) Sequence of the 22-base-pair duplex oligonucleotide. The rhodium intercalator is tethered to the 5' end of the top strand, indicated by an "X," where applicable. (b) Piperidine-sensitive base damage generated by covalently tethered $\text{Rh}(\text{phi})_2\text{bpy}^{3+}$ and noncovalent NDI. Lane **1**: Rh-22mer, irradiated at 313 nm to reveal the location of intercalation. **2**: Rh-22-mer, irradiated at 365 nm to initiate long-range oxidative base chemistry. **3**: Rh-22mer + noncovalent NDI, irradiated at 365 nm. **4**: Rh-22mer dark control. **5**: 22-mer +noncovalent NDI, irradiated at 313 nm. **6**: 22-mer + noncovalent NDI, irradiated at 340 nm. **7**: 22-mer + noncovalent NDI, irradiated at 365nm. **8**: 22-mer + noncovalent NDI, irradiated at 400 nm. Samples contained 2.5 μM duplex and 2.5 μM NDI, if applicable, in 35 mM Tris-HCl pH 8.3 with 10 mM NaCl. All samples were irradiated for one hour at room temperature.

(a) X-5' ACGATGCCGAAGTTTTGCCGAT 3'
 3' TGCTACGGCTTCAAAACGGGCTA 5'-³²P



DNA can be exploited to stabilize triplex formation (27). NDI hairpin linkers can be used to stabilize duplex and triplex formation by end-capping, as shown by the increased melting temperatures relative to the same hairpins with hexaethylene glycol linkers. Furthermore, NDI intercalators attached to cytosine residues within a triplex-forming strand can dramatically improve the melting temperature of a triplex (28). Similar NDI conjugates incorporated at the 3' or 5' termini (or both) of the third strand give rise to increased triplex stability, presumably as the result of intercalation into the base pairs of the target duplex (28,29). This extensive evidence of the intimate association between NDI and the DNA base pairs confirms that they are well coupled into the DNA base stack and hence effective participants in charge transport chemistry.

Photoexcited naphthalene diimides are powerful oxidants, estimated to have a reduction potential around 1.8 V versus NHE (12,13). They have been used recently in several model studies of electron transfer between tethered donor and acceptor molecules model studies (5-9). Based on a careful photophysical characterization of NDI in solution and the somewhat contradictory evidence for guanine oxidation by related molecules available in the literature, Aveline *et al.* proposed the following mechanism for the interaction of NDI with DNA (43): upon photoexcitation at 355 nm, the excited singlet species can produce hydroxyl radicals or undergo a rapid intersystem crossing to the excited triplet species. The excited-state triplet can then oxidize another NDI molecule or some other available electron donor or generate singlet oxygen. In our system, the hydroperoxy group which forms hydroxyl radicals is absent, and on average only one NDI molecule is present per duplex, eliminating two of these possible reaction pathways. The best available electron donor in the native DNA duplex is guanine. We propose that irradiation of NDI in our system leads to oxidation of guanine or the generation of singlet oxygen. In oligonucleotide duplexes and

restriction fragments irradiated with noncovalent NDI, we observe oxidation of guanine with a strong preference for 5' guanines of 5'-GG-3' doublets (Fig. 4.9,4.10). This damage pattern is consistent with electron transfer processes but is inconsistent with damage from singlet oxygen (40,44).

4.3.4 Long-Range Oxidative Guanine Damage by NDI in Restriction Fragments

Having demonstrated that an intercalator can be delivered to a specific site on our designed restriction fragments by covalent attachment of a triplex-forming oligonucleotide, we then explored whether NDI might be applied to examine the distance range and sequence effects for charge transfer in a restriction fragment. With the 5'-tethered NDI triplex-forming oligonucleotide, oxidative damage occurred predominantly at the intercalation site, just as we had observed with $\text{Rh}(\text{phi})_2\text{bpy}^{3+}$ appended to the 5' terminus of the pyrimidine third strand (not shown). To improve the electronic coupling of the intercalator into the duplex π stack, we constructed a new NDI-tethered triplex-forming oligonucleotide with the naphthalene moiety attached to an internal cytosine residue. In this new construct, the intercalator clearly binds at a different location and possibly with a different geometry than the 5'-appended intercalators. The sequence of the 16-mer pyrimidine strand with the internal NDI was similar to that of the 5'-tethered NDI conjugate, except for the placement of the NDI intercalator and replacement of 5-methyl cytosine by cytosine for synthetic reasons (Fig. 4.3). The same target sequences were used as well, since all of the TFO's were designed to target one site.

With the internally-tethered NDI, we observed strong oxidation at a distance of approximately 100 Å from the site of intercalation in both directions and along both duplex strands in the restriction fragments containing the target site (Figs. 4.8-4.10). Damage occurred almost exclusively at the 5' guanines of 5'-

GG-3' and, to a lesser extent, 5'-GA-3' sites. Furthermore, the naphthalene-induced damage at guanine occurred with high efficiency, since most of the duplex DNA was cleaved within ~10 minutes of irradiation. Minimal background damage was observed in the control sequences lacking the TFO binding site. The pattern of oxidative damage promoted by the triplex-directed naphthalene diimide intercalators on both restriction fragments is summarized in Figure 4.11.

More specifically, on the polypyrimidine strand of the restriction fragment containing sequence 2 (the duplex strand complementary to the polypurine TFO target strand), we observe strong guanine oxidation at the 5' guanine of a 5'-GG-3' site 33 base pairs (112 Å) away from the NDI-tethered cytosine, 3' to the triplex region (Figs. 4.8, 4.11). Guanine oxidation is also observed at a 5'-GGG-3' triplet ~20 bp away and, to a lesser extent, at two intervening single guanines. Weaker oxidation beyond that point probably occurs as well, although it is difficult to quantify relative to background damage. No guanine oxidation is evident in the triplex region, since the sequence on this strand is composed entirely of pyrimidines. No oxidative base damage occurs to the 5' side of the triplex region either; although several 5'-GG-3' sinks are present in this region, all are located on the complementary strand. The absence of oxidative damage either within or 5' to the triplex region was confirmed on another restriction fragment containing sequence 2 that was radiolabeled at a different restriction site (not shown).

On the target polypurine strand of sequence 2 (Fig. 4.9, 4.11), the strongest oxidation is observed at a guanine doublet 15 bp removed from the binding site on the 3' side of the triplex, with weaker damage observed at the 5'-GG-3' site within the triplex and at other single guanine sites. There is also strong damage at a distal guanine doublet located ~38 bp from NDI, as judged from the intense band of small fragments at the bottom of the gel. The location

Figure 4.8: Long-range oxidation of guanine bases by the triplex-directed NDI intercalator. Oxidation of guanine bases on the pyrimidine target strand of sequence 2 and a control fragment from pUC19. Lanes **1 & 2, 9 & 10** are Maxam-Gilbert A+G and C+T sequencing lanes. Samples in lanes **3-8** and **11-16** were irradiated for different lengths of time at 365 nm, as follows: 0 min., 1 min., 2 min., 5 min., 10 min., 15 min. The region 3' to the triplex is shown toward the top of the gel, and the 5' region toward the bottom. The location of the triplex-forming target site is indicated by a bracket, and the putative intercalation site is indicated by an asterisk. Arrows point to the sites of significant base oxidation by the NDI-tethered TFO. Minimal damage is observed in the pUC19 control fragment that does not contain a binding site.

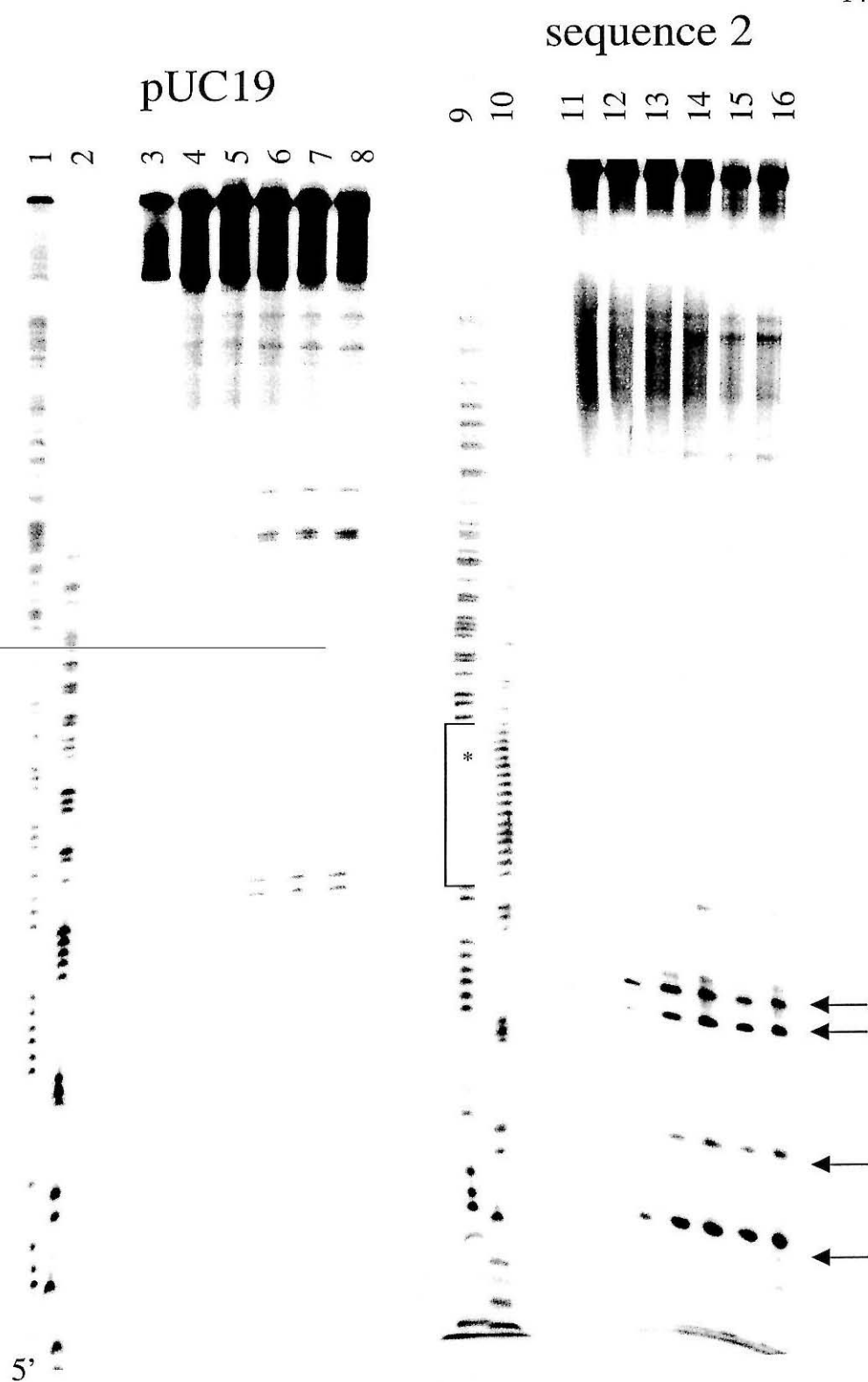
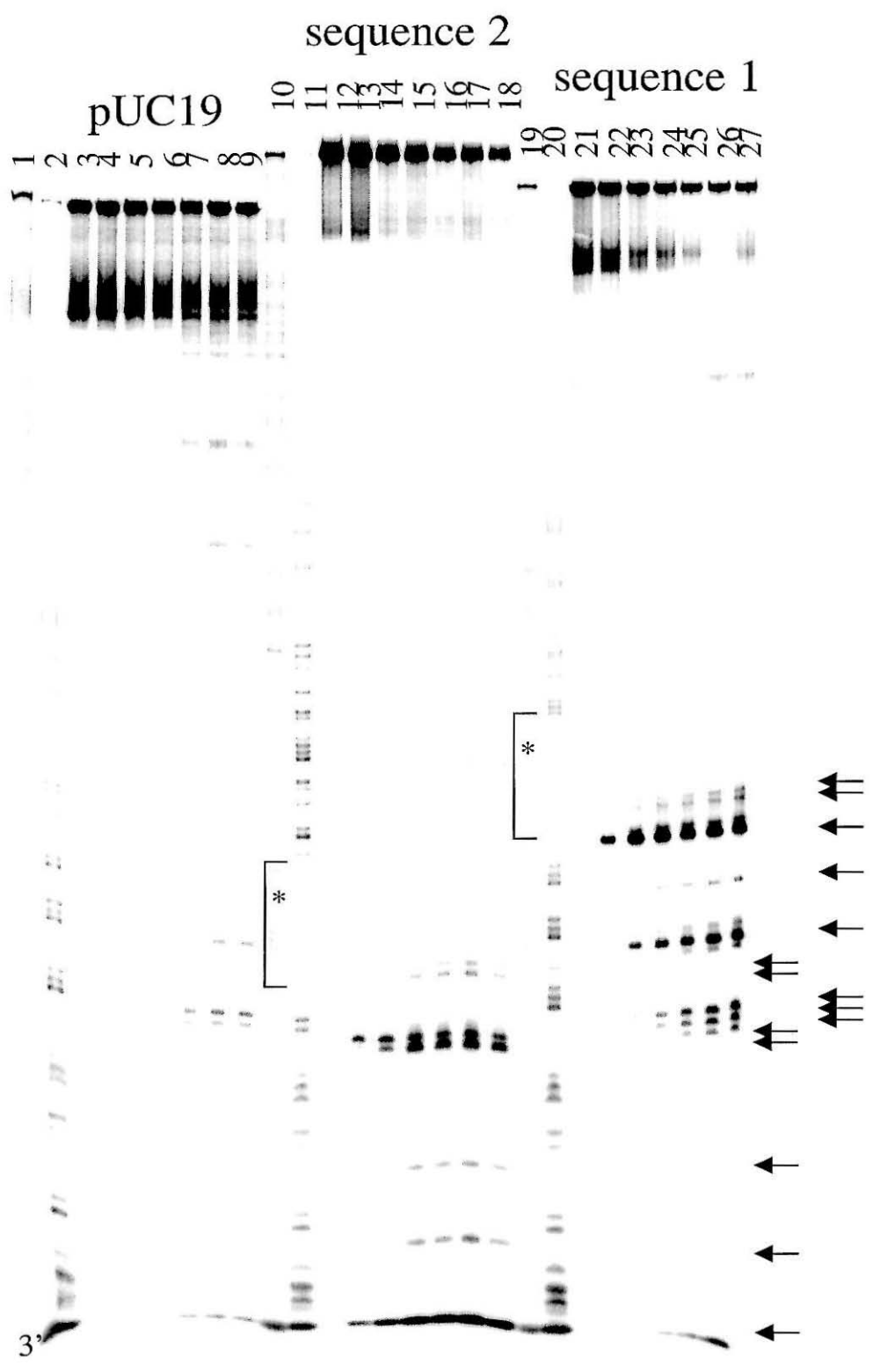


Figure 4.9: Oxidation of guanine bases on the purine strand and the pUC19 control fragment. Target sequences 1 and 2 are shown. Lanes **1 & 2, 10 & 11, 19 & 20**: Maxam-Gilbert A+G and C+T sequencing lanes. Lanes **3-9, 12-18, 21-27** show samples irradiated at 365 nm for varying lengths of time, as follows: 0 min, 1 min., 2 min., 4 min., 7 min., 10 min., 15 min., respectively. The region 5' to the triplex is shown toward the top of the gel, and the 3' region toward the bottom. The location of the triplex-forming target site is indicated by a bracket, and the putative intercalation site is indicated by an asterisk. Arrows at the right point to damage in the fragment containing sequence 2; arrows at the far right point to damage in the fragment containing sequence 1. Only minimal damage is observed in the pUC19 control fragment that does not contain a binding site.



and sequence of this distal cleavage site was confirmed on another restriction fragment containing sequence 2 radiolabeled at a different restriction site (Fig. 4.10, 4.11).

Because the intense cleavage 3' to the triplex region masked any other concurrent damage further up on the gel, we isolated a slightly different restriction fragment containing sequence 2 and radioactively labeled it at the opposite side of the triplex-forming region (Fig. 4.10, 4.11). In this case we observed significant oxidative damage on the polypurine strand within the triplex region itself. The strongest piperidine-exposed cleavage occurred at the guanine doublet immediately adjacent to the triplex region at the 3' triplex-duplex junction (15 bp away from the intercalated NDI). Less damage was observed at the guanine doublet within the triplex region and at the guanine immediately adjacent to the intercalator itself. Minimal oxidation was observed at the guanine doublets 16 and 26 base pairs away that are 5' to the triplex region.

By comparison, on the target polypurine strand of a restriction fragment containing sequence 1, extremely intense oxidation occurs at a guanine base immediately adjacent to the 3' end of the triplex region, 12 bases away from the NDI-tethered cytosine (Fig. 4.9, 4.11). Fairly strong damage is also seen at the 5' guanine of a 5'-GG-3' site 24-25 bases from the intercalator, and at a 5'-GGGG-3' site 31-34 bases from the intercalator. The 5'-GG-3' site inside of the triplex region also appears to be somewhat damaged. However, it is difficult to quantify any of the damage within or 5' to the triplex region since most of the strands are cleaved in more than one place, and only the shortest piece which retains the radioactive end-label appears on the gel. On the polypyrimidine strand of a restriction fragment containing sequence 1, the NDI intercalator oxidizes the guanine base immediately adjacent to the triplex on the 5' end (data not shown). This guanine at the duplex-triplex junction is very heavily oxidized. It appears

Figure 4.10: Oxidation of guanine bases on a target restriction fragment and a control fragment. The purine strand of a target fragment containing sequence 2 and the pUC19 control fragment are shown. Maxam-Gilbert sequencing lanes are not shown due to poor color contrast. Samples in lanes **1-8** and **9-16** were irradiated at 365 nm for varying lengths of time, as follows: 0 min., 1 min., 2 min., 4 min., 6 min., 8 min., 10 min., 12 min., respectively. The region 5' to the triplex is shown toward the bottom of the gel, and the 3' region toward the top. The location of the triplex-forming target site is indicated by a bracket, and the putative intercalation site is indicated by an asterisk. Arrows at the left point to damage on the fragment containing sequence 2. Background damage is observed in the pUC19 control fragment.

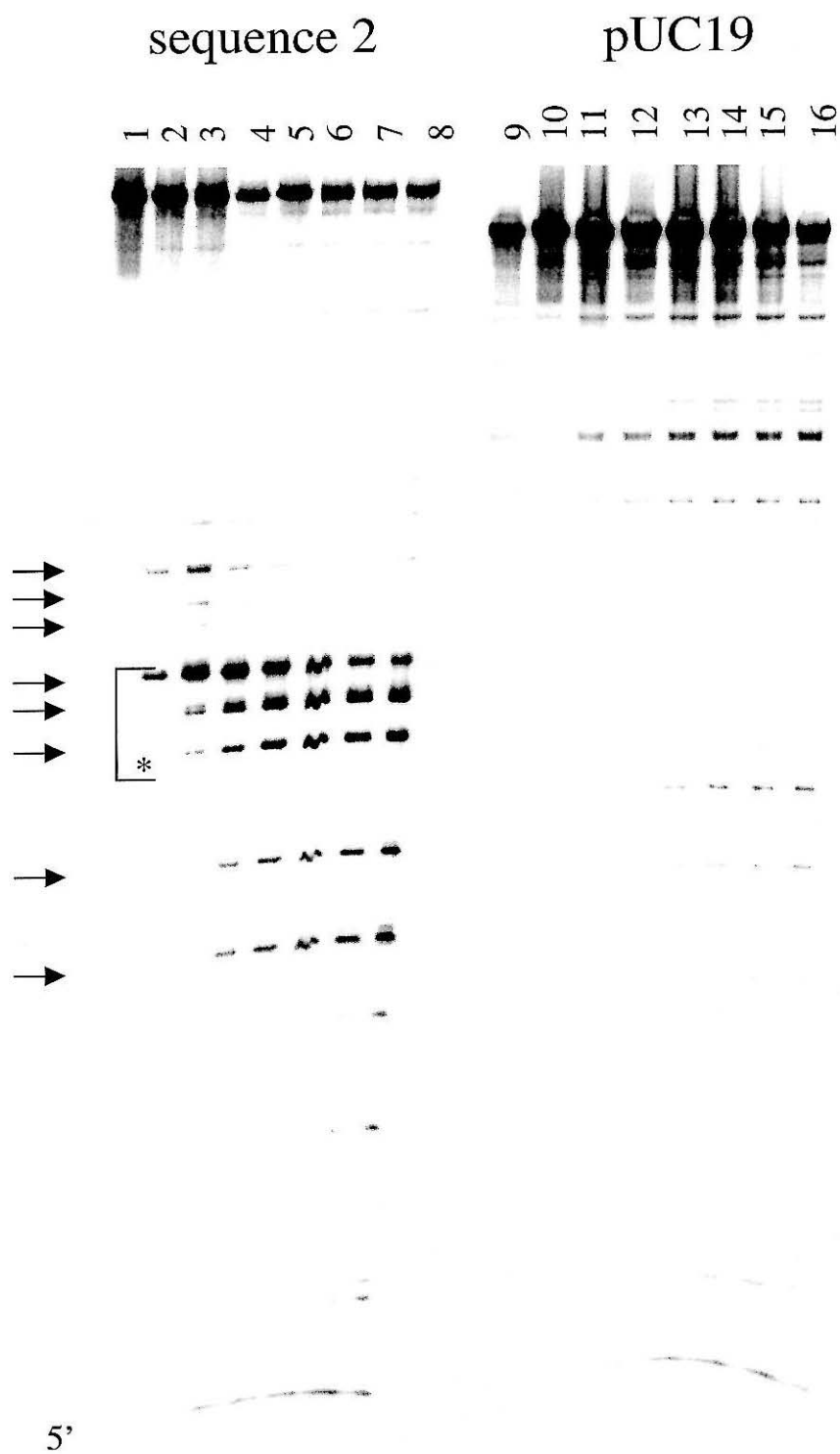


Figure 4.11: Histogram showing sites of significant base oxidation by triplex-directed naphthalene diimides on target restriction fragments. The sizes of the arrows reflect the relative amounts of damage generated at various guanine bases, although such measurements are merely an approximation since the data from several different gels were combined to make this histogram. Base oxidation is observed almost exclusively at guanine bases of 5'-GG-3' or 5'-GA-3' sites, which is characteristic of electron transfer damage through the π stack. Minimal oxidation is observed 5' to the triplex region containing sequence 2. It is unclear whether significant oxidation is observed 5' to the triplex region of containing sequence 1 due to the large amounts of oxidized guanine generated at other guanine bases, which mask damage in this region on the gel. The triplex-forming strand is shown adjacent to the target polypyrimidine strand to make space for the arrows.

that no other bases 5' to the triplex region are oxidized, although this absence of oxidation could not be confirmed by labeling at another restriction site, as no other restriction sites were available 5' to the triplex region. On this polypyrimidine strand of sequence 1, the NDI intercalator also oxidizes a 5'-GGG-3' site ~30 bp from the intercalator to the 3' side of the triplex and two intervening single guanine bases.

We have observed that some of the NDI-tethered oligonucleotides, in sharp contrast to metallointercalator-tethered oligonucleotides, can aggregate and can also bind nonspecifically at concentrations where all of the specific target sites are saturated. Furthermore, NDI-oligonucleotides are subject to some photodecomposition when irradiated in oxygen. Therefore it was critical in each system to test for any possibility of intermolecular reactions or non-specific binding. In the case of our internally-tethered NDI triplex-forming oligonucleotides, we observed little or no damage in the pUC restriction fragments which lack a specific binding site (Figs. 4.9, 4.11). This control indicates that neither free NDI, potentially generated by photodecomposition, nor stray NDI-TFO is binding nonspecifically to the restriction fragment. Moreover, it is apparent that the distribution of damage around the triplex site is markedly asymmetrical (Fig. 4.11), further evidence that a model in which NDI is released and diffuses away cannot explain the long-range damage that we observe.

4.3.5 Probing Triplex Structure Using Long-Range Charge Transfer

The NDI intercalator, delivered specifically to a single site, was used to probe the structure of triplex regions and examine long-range charge transport in restriction fragments. We have shown that long-range charge transfer initiated by photoexcited $\text{Rh}(\text{phi})_2\text{bpy}^{3+}$ could be used to probe the structure of DNA-protein complexes; charge transfer through the base stack is diminished upon binding of a

protein which disturbed π stacking in a base-flipping reaction (45). Here charge transport through the base stack initiated by photoexcited NDI yields insights into the structure of the triplex region and its effect upon neighboring duplex regions. We observe that in general charge moves through the triplex region to the duplex, resulting in significant oxidation at a distance from the intercalation site, which lies within the triplex (Fig. 4.11). Consequently, it is clear that the bases within the triplex region are well-stacked with each other and with the duplex region to the 3' side. This conclusion is consistent with NMR solution structures of intramolecular triplex hairpins showing base stacking (albeit neither B- nor A-form) (46-48).

In contrast to the large amounts of oxidative damage on the 3' side of the triplex site, oxidation to the 5' side of the triplex is minimal. This becomes important to consider in the context of observations that very little long range oxidation is observed with 5' appended oxidants, including $\text{Rh}(\text{phi})_2\text{bpy}^{3+}$, $\text{Ru}(\text{bpy}')(\text{phen})(\text{dppz})^{2+}$, ethidium, and NDI. Similar results have been reported previously with a 5'-appended flavin TFO (49). Thus it appears that the triplex region is not well stacked with the duplex region to the 5' side, i.e., that there is a junction in between the two regions where the bases do not overlap. The junction effect is directional, in that the duplex-triplex stacking on the 3' side appears to be effective and on the 5' side appears to be poor. This hypothesis explains why several 5'-tethered intercalators do not oxidize guanine bases at long range, but an internally-tethered NDI can do so.

The observation that the duplex-triplex region is poorly stacked is actually also consistent with previous results which showed poor charge transfer through 5'-TA-3' steps (42). 5'-pyr-pur-3' steps provide poor paths for charge transport, because there is very little π overlap between the pyrimidine and purine base pairs, theoretically reducing coupling and surely increasing the probability of

kinked structures and dynamic bending (50). In contrast, 5'-pur-pyr-3' steps display significantly more overlap due to the helical twist of the DNA. A 5'-pyr-pur-3' step is present at the 5' duplex-triplex junction in both plasmid 1 and 2, whereas a 5'-pur-pyr-3' step exists at the 3' junction, leading us to expect a more continuous transition between triplex and duplex at the 3' junction than at the 5' end. It is reasonable to assume that the poor stacking at this 5'-pyr-pur-3' step is exacerbated by the differences in the base stacking between the duplex and triplex regions. Obviously, it is important not to over-emphasize this effect, since both sequences abound with 5'-pyr-pur-3' steps which do not appear to reduce charge transfer significantly. Any discontinuity in the base-base stacking at the duplex-triplex junction is generated by the unusual stacking in the triplex region which does not overlap well with the bases of the duplex region, and the discontinuity may be merely exacerbated or localized by the inherent poor stacking of 5'-pyr-pur-3' step. The information concerning stacking at duplex-triplex junctions gleaned from this charge transport study is especially valuable in light of the fact that little or no structural information about such junctions is available currently (51). Indeed, measurements of charge transport provide a novel and sensitive probe of DNA stacking and dynamics.

Clearly, less oxidative damage arises within the triplex region compared to the distal duplex region. It has been proposed that this reduced yield of oxidized guanine within a triplex could be due to i) the effect of reduced oxygen accessibility and trapping, ii) the effect of altered stacking on the redox potentials and charge stabilization of guanine doublets, or iii) the effect of protonated cytosine bases on the electronic structure of the guanine bases (52). The first suggestion is almost certainly true, given that the major groove is occupied by the triplex-forming strand and ordered water molecules, which must reduce oxygen accessibility. Since the stacking of the bases is not substantially altered compared

to that in canonical B-form DNA (46-48), and since the differences in potential generated by stacking interactions are likely to be small (53), it is unlikely that the oxidation potential could be perturbed sufficiently to grossly disturb guanine oxidation in the triplex region; it may account for a small fraction of the diminution. The third proposal is also plausible, but the effect of a protonated third strand should be experimentally distinguishable from the other possibilities by comparing charge transfer through purine versus pyrimidine triplexes.

In and around the triplex region, guanine bases on both strands of the duplex are damaged. This observation is especially interesting when we consider that in the triplex region, between 17 and 20 continuous purine bases are found on one strand and the complementary continuous string of pyrimidines on the other. That guanine bases on both strands are damaged implies that migrating charges can move from one strand of the duplex to the other, we have previously observed interstrand charge transfer in spectroscopic studies (54). Alternatively, our results may imply that charges can move through long stretches of pyrimidine bases as well as through purine bases, since significant damage is observed on the pyrimidine duplex strand.

These results and their implications to the structure of a DNA triplex appear to be fairly consistent with recent work of Kan *et al.* on guanine oxidation by anthraquinones on short oligonucleotide triplexes (52). However, our system in which the NDI chromophore is delivered to a restriction fragment by a TFO offers important new insights. Since oxidation in the NDI-triplex system was monitored on both the polypurine and polypyrimidine strands of the duplex, we can assess charge transport through polypyrimidine sequences. Furthermore since our experiments exploited restriction fragments instead of short oligonucleotide duplexes, the ability of the NDI-TFO to find its target site within a long genomic sequence was established. Most importantly, the targeting of guanine damage in

restriction fragments with random DNA sequences by triplex formation provides a strategy to probe long-range charge transfer and base oxidation in genomic DNA, a critical issue in assessing the physiological consequences of DNA-mediated electron transfer.

4.3.6 Long-Range Oxidation in Restriction Fragments

Using specific triplex formation as a means to deliver a photooxidant to a specific location on a long DNA duplex, we have now observed charge transfer to damage guanines at long range, over roughly 25-38 bp in each direction, or approximately 70 bp total. The triplex delivery system allows us to examine for the first time charge transfer to damage guanine on both strands of the DNA duplex, confirming that oxidized guanine is generated on both strands with a similar distance range for its distribution. This distribution of oxidized bases seen here provides an example of the distance range for charge transport in a random sequence restriction fragment. This range appears to be about half of what we had previously observed on a synthetic oligonucleotide construct (52). However here the charge can migrate in two directions, which should on average cut in half the signal at the distal sites, and the weaker damage is more difficult to measure due to background from nonspecific binding and the possible distribution of very long-range damage among many distal sites. Base damage is therefore seen to be distributed over about 70 bp (~ 235 Å). Alternatively, it is possible that charge transfer is slightly diminished on restriction fragments, which are longer and therefore more flexible than oligonucleotides. Regardless, this distance distribution for charge transport is roughly comparable to what we have observed previously in one direction on oligonucleotides. It is interesting to consider whether this distance, roughly equal to one loop around a nucleosome, may therefore represent the distance regime to consider for chemical communication using DNA-mediated charge transport (55).

Naphthalene diimide intercalators are efficient long-range DNA photooxidants. When covalently tethered to a triplex-forming oligonucleotide, they can be delivered to a single specific site on a restriction fragment. Triplex-directed NDI intercalators were used to demonstrate that charges can migrate through genomic DNA over 25-34 bp in both directions down the helix and along both duplex strands, to generate permanent base lesions. The potential now exists to examine long-range charge transport in a variety of biological systems including supercoiled plasmids, mammalian chromosomal DNA, and even inside of cells, to examine the biological relevance and implications of DNA-mediated charge transport *in vivo*.

4.4 References

1. S. R. Rajski, B. A. Jackson, J.K. Barton, *Mut. Res.* **447**, 49 (2000).
2. Z.-R. Liu, K.H. Hecker, R. L. Rill, *J. Biomol. Struct. Dyn.* **14**, 331 (1996).
3. F. A. Tanious, S.-F. Yen, W. D. Wilson, *Biochemistry* **30**, 1813 (1991).
4. S.-F. Yen, E. J. Gabbay, W. D. Wilson, *Biochemistry* **21**, 2070 (1982).
5. R. S. Lokey *et al.*, *J. Am. Chem. Soc.* **119**, 7202 (1997).
6. J. L. Sessler *et al.*, *J. Org. Chem.* **63**, 7370 (1998).
7. Q. Tan *et al.*, *J. Phys. Chem. B* **101**, 5214 (1997).
8. H. Levanon *et al.*, *J. Am. Chem. Soc.* **120**, 6366 (1998).
9. L.L. Miller, K. R. Mann, *Acc. Chem. Res.* **29**, 417 (1996).
10. S. Matsugo *et al.*, *Angew. Chem. Int. Ed. Engl.* **30**, 1351 (1991).
11. I. Saito, *et al.*, (1995) *J. Am. Chem. Soc.* **117**, 6406 (1995).
12. J. E. Rogers, L. A. Kelly, *J. Am. Chem. Soc.* **121**, 3854 (1999).
13. J. E. Rogers, S. J. Weiss, L. A. Kelly, *J. Am. Chem. Soc.* **122**, 427 (2000).
14. A. Sitlani, J. K. Barton, *Biochemistry* **33**, 12100 (1994).
15. K. Uchida, A. M. Pyle, T. Morii, J. K. Barton, *Nucleic Acids Res.* **17**, 10259 (1989).
16. W. Saenger, *Principles of Nucleic Acid Structure*. Springer-Verlag, New York, New York (1984).
17. H. E. Moser, P. B. Dervan, *Science* **238**, 645 (1987).
18. S. Strobel, P.B. Dervan, *Science* **249**, 73 (1990).
19. W. Greenberg, P. B. Dervan, *J. Am. Chem. Soc.* **117**, 5016 (1995).
20. G. C. Best, P. B. Dervan, *J. Am. Chem. Soc.* **117**, 1187 (1995).
21. U. Asseline, N. T. Thuong, C. Hélène, *New. J. Chem.* **21**, 5 (1997).
22. K. R. Fox, *Nucleic Acids Res.* **22**, 2016 (1994).
23. K. R. Fox, *FEBS Lett.* **357**, 312 (1995).
24. B.-W. Zhou, E. Puga, J. Sun, T. Garestier, C. Hélène, *J. Am. Chem. Soc.* **117**, 10425.
25. G. C. Silver *et al.*, *Bioconj. Chem.* **8**, 15 (1997).

26. G. C. Silver *et al.*, *J. Am. Chem. Soc.* **119**, 263 (1997).
27. S. Bevers, T. O'Dea, L. McLaughlin, *J. Am. Chem. Soc.* **120**, 11004 (1998).
28. D. Gianolio, L. McLaughlin, *J. Am. Chem. Soc.* **121**, 6334 (1999).
29. D. Gianolio, J. Segismundo, L.W. McLaughlin, *Nucleic Acids Res.* **28**, 2128 (2000).
30. P. B. Dervan, *Nature* **359**, 87 (1992).
31. C. Giovannangeli, L. Perrouault, C. Escudé, N. Thuong, C. Hélène, *Biochemistry* **35**, 10539 (1996).
32. M. Grigoriev *et al.*, *J. Biol. Chem.* **267**, 3389 (1992).
33. D. Oh, P. Hanawalt, *Nucleic Acids Res.* **27**, 4734 (1999).
34. F.-X. Barre *et al.*, *Proc. Natl. Acad. Sci. USA* **97**, 3084 (2000).
35. M. Grigoriev *et al.*, *Proc. Natl. Acad. Sci. USA* **90**, 3501 (1993).
36. A. Majumdar *et al.*, *Nature Gen.* **20**, 212 (1998).
37. G. Wang, D. Levy, M. Seidman, P. Glazer, *Mol. Cell. Biol.* **15**, 1759 (1995).
38. M. Núñez, S. R. Rajski, J. K. Barton, *Meth. Enzymol.* **319**, 165 (2000).
39. J. Sambrook, E. F. Fritsch, T. Maniatis, *Molecular Cloning: A Laboratory Manual*, 2nd ed. Cold Spring Harbor Laboratory, New York (1989).
40. D. B. Hall, R. E. Holmlin, J. K. Barton, *Nature* **382**, 731 (1996).
41. D. B. Hall, J. K. Barton, *J. Am. Chem. Soc.* **119**, 5045 (1997).
42. M. Núñez, D. B. Hall, J. K. Barton, *Chem. Biol.* **6**, 85 (1999).
43. B. M. Aveline, S. Matusgo, R. W. Redmond, *J. Am. Chem. Soc.* **119**, 11785 (1997).
44. C. J. Burrows, J. G. Muller, *Chem. Rev.* **98**: 1109 (1998).
45. S. R. Rajski, S. Kumar, R. J. Roberts, J. K. Barton, *J. Am. Chem. Soc.* **121**, 5615 (1999).
46. I. Radhakrishnan, D. J. Patel, *Biochemistry* **33**, 11405 (1994).
47. M. Tarköy, A.K. Phipps, P. Shultze, J. Feigon, *Biochemistry* **37**, 5810 (1998).
48. I. Radhakrishnan, D. J. Patel, *Structure* **2**, 17 (1994).

49. C. Frier, J.-F. Mouscadet, J.-L. Décout, C. Auclair, M. Fontecave, M. *Chem. Comm.* **22**, 2457 (1998).
50. R. E. Dickerson, (1998) *Nucleic Acids Res.* **26**, 1906 (1998).
51. S. Rhee, Z. Han, K. Liu, T. Miles, D. R. Davies, *Biochemistry* **38**, 16810 (1999).
52. Y. Kan, G. B. Schuster, *J. Am. Chem. Soc.* **121**, 10857 (1999).
53. H. Sugiyama, I. Saito, *J. Am. Chem. Soc.* **119**, 617 (1996).
54. S. O. Kelley, J. K. Barton, *Science* **283**, 375 (1999).
55. M. Bixon *et al.*, *Proc. Natl. Acad. Sci. USA* **96**, 11713 (1999).

Chapter 5

Oxidative Charge Transport in Nucleosomes

5.1 Introduction

In our efforts to determine whether DNA charge transport is a biologically relevant phenomenon, we have determined that charge transport can occur over tens of base pairs on oligonucleotides and restriction fragments to affect DNA damage. However, DNA inside of cells is not only long, it is also intimately associated with a variety of proteins which serve to regulate replication and transcription as well as repair and package the DNA itself (1). Therefore, it is critical for us to examine the roles of proteins in altering the structure of DNA when attempting to determine the relevance of DNA-mediated charge transport inside of living cells.

In studies of DNA charge transport using oligonucleotides, it has been demonstrated that binding of a variety of proteins to DNA can sensitively modulate charge transport through the helix, depending on their effects on the stacking of the DNA base pairs (Fig. 1.14). *M.HhaI* is a DNA methylase which, in binding its target site, flips out the cytosine for methylation and inserts a glutamine side chain, stabilizing a “gap” in the DNA π stack (2). As a result of the gap, *M.HhaI* inhibits oxidative damage to DNA past its binding site. However, a mutant *M.HhaI* that inserts a tryptophan into the gap created by base flipping does not inhibit charge transport on binding to DNA, presumably because the flat, aromatic tryptophan side chain of the mutant protein takes the place of the missing DNA base, completing the π -stacked array needed to conduct charge through the helix. TATA-binding protein (TBP) generates two $\sim 90^\circ$ kinks on either end of its recognition site upon binding to DNA, seriously disrupting π stacking and long-range charge transport (3). *PvuII* restriction endonuclease and Antennapedia homeodomain protein do not significantly distort the π stack on binding to DNA, and as a consequence do not inhibit long-range charge transport (3). To the contrary, binding of either protein somewhat *increases* long-range

guanine oxidation, presumably because the proteins restrict the dynamic motions of the DNA bases and a stiffening of the DNA helix, facilitating charge transport.

The fundamental unit of DNA packing inside eukaryotic cells is the nucleosome core particle, in which ~150 base pairs of DNA are bound around an octamer of histone proteins (1). These particles are then assembled into higher-order structures, stabilized by other histone- and non-histone-proteins, in order to further compact the DNA so as to fit into the nucleus. In addition to packaging DNA, the histone proteins are believed to serve both regulatory and protective functions. Given the ubiquity of the nucleosome, the potential involvement of the histone octamer in modulating charge migration through DNA is of significant interest.

The structure of a nucleosome core particle has been determined for a histone octamer and a 146-base-pair palindromic DNA sequence (4). In this structure, the DNA is highly bent as it is wrapped 1.65 times around the outside of the histone octamer, forming a “superhelix” with a diameter around 42 Å (Fig. 5.1). The overall twist of the base pairs is 10.2 bp per turn, in contrast to the 10.5 bp per turn observed in solution, although there is considerable variability between different positions on the core particle. The combination of the base pair twist and the superhelix winding gives an overall *overwinding* of nucleosomal DNA compared to DNA in solution. The bending and relative mobility of the DNA are also heterogeneous in response to local histone-DNA interactions. Some regions of the DNA are highly kinked while others are quite straight. Exposed sections of the DNA are flexible and mobile and histone-bound sections of the DNA are dynamically restricted.

The fact that DNA-histone contacts are nonspecific does not imply that all DNA sequences bind equally well to form a core particle. Clearly, those sequences that are inherently more flexible or that contain correctly-phased bends

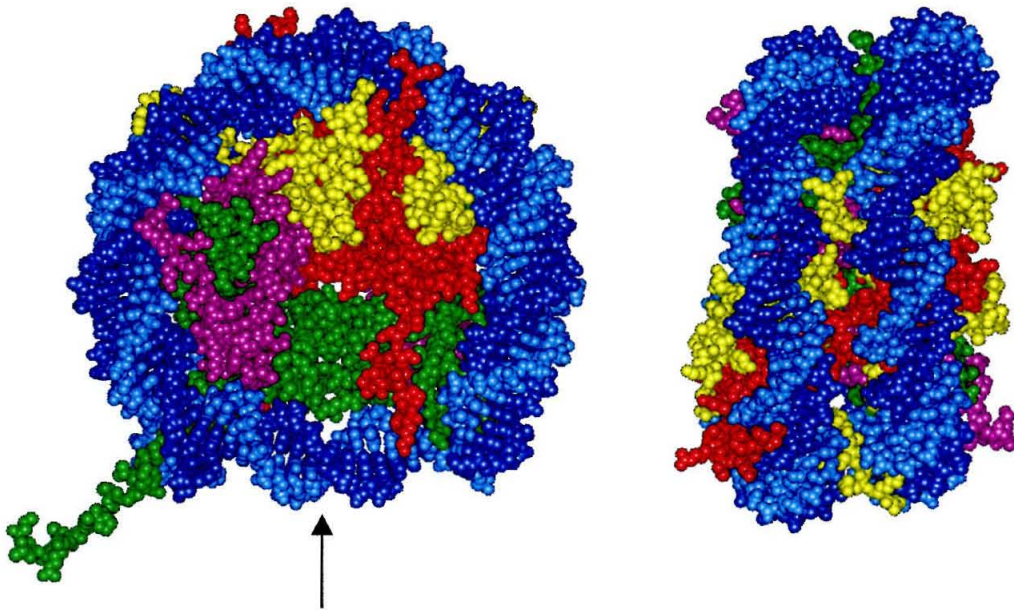


Figure 5.1: Structure of the nucleosome core particle. 146 base pairs of DNA (blue and cyan) are wrapped one-and-two-thirds times around an octamer of histone proteins (4,8). In order to wrap around the histones, the DNA is heterogeneously bent and overwound. The octamer is composed of two each of histones 2A (red), 2B (yellow), 3 (green), and 4 (purple), which bind nonspecifically to the DNA by a variety of electrostatic, hydrogen-bonding, and nonpolar interactions. The twofold rotational symmetry axis through the center of the nucleosome core particle is indicated by the arrow at the left.

will bind the histone octamer more readily than other sequences (5-7). It has been observed that A-T base pairs are preferred where the minor groove faces inwards toward the histone core and G-C pairs are preferred where the major groove faces inwards, because these base pairs bend more readily in that direction. As a result, placement of certain sequences can impart a rotational orientation upon the nucleosome core particle. In the case of this DNA for which the nucleosome core particle structure was solved, the 146-base-pair sequence contains 12 known nucleosome phasing regions which predispose it to form a single, stable conformation with the histone octamer (8).

Since a range of different DNA sequences needs to be accommodated by the histone octamer, the interactions between the protein core and the DNA are generally nonspecific and largely electrostatic (1,4). Therefore, the surface of the octamer has an overall positive charge, in contrast to the negative charge of the DNA polyanion. Interestingly, in addition to hydrogen bonds between arginine side chains in the minor groove and DNA backbone phosphates, other stabilizing interactions include hydrogen bonds between phosphates and main-chain amide nitrogen atoms as well as interactions between phosphates and helix dipoles (4). Extensive nonpolar contacts between the protein and deoxyribose groups, and hydrogen bonds and salt links between phosphates and other protein side chains also help to stabilize the protein-DNA interaction. Although some side chains do protrude into both grooves, they make very few contacts with bases.

Here we examine guanine oxidation by rhodium intercalators in nucleosome core particles to determine the effect of DNA packaging on long range charge transport through the base pair stack. Given that the DNA in the core particle is overwound, bent, and in some places dynamically restricted, binding of DNA to histones in this structure might serve to protect nucleosomal DNA from long-range oxidative damage. Alternatively, such packaging might

decrease the flexibility of the base stack, providing a unique and isolated medium to facilitate charge transport through the DNA base pair stack.

5.2 Methods

5.2.1 *Isolation of Histones*

Nucleosome core particles were isolated from chicken blood as described by Lutter (9) and Drew and Calladine (5), with minor alterations (10). Whole chicken blood, collected in sodium citrate, was obtained from Pel Freez Biologicals. 500 mL of blood in citrate buffer was centrifuged at 5000 x g for 10 minutes at 4°C to pellet the erythrocytes; the clear yellowish supernatant, containing plasma and buffer, was discarded. Three times the pellet was resuspended in cold solution **X** (Table 5.1) and recentrifuged to clean the cells. White blood cells were removed from the top of the pellet with a pipette. The pellet of whole cells was resuspended gently in 500 mL of cold solution **L** in order to lyse the cell membrane, and the resulting slurry was centrifuged for 3 minutes at 5000 x g. The supernatant, which was dark red due to the hemoglobin contained in the erythrocytes, was removed with a pipette attached to an aspirator and discarded. The pellet, containing the nuclei, was gently resuspended in cold solution **X** and re-centrifuged at 5000 x g for 3 minutes. The nuclei were rinsed repeatedly in this manner (resuspend the pellet in solution **X**, centrifuge, discard supernatant) until the hemoglobin was gone and the pellet was white. The washed nuclei in the pellet were then resuspended in cold solution **N** and centrifuged for 3 minutes at 5000 x g, and the supernatant was discarded. Half of the pellet was stored in 50% glycerol/ 50% solution **N** at -20°C for later purification. The remainder was gently resuspended in solution **N** at a concentration of ~ 5 mg/mL (this corresponds to ~ 50 AU/mL at 260 nm).

Table 5.1: Buffers for nucleosome isolation from chicken erythrocytes

Buffer A: 15 mM Tris HCl, 60 mM KCl, 15 mM NaCl, 0.15 mM spermine, 0.5 mM spermidine, pH 7.5.

Solution X: Buffer A, 0.34 M sucrose, 2.0 mM EDTA, 0.5 mM EGTA, 0.2 mM phenylmethylsulfonyl fluoride (PMSF)*, 1.0 mM benzamidine*, 15 mM β -mercaptoethanol*, pH 7.5.

Solution L: Solution X, 0.1% Nonidet p40, pH 7.5.

Solution N: Buffer A, 0.34 M sucrose, 0.2 mM PMSF*, 15 mM β -mercapoethanol*, pH 7.5.

Solution R: 10 mM Tris-HCl, 0.2 mM EDTA, 0.2 mM PMSF*, pH 8.0.

Solution S: 0.63 M NaCl, 20 mM Tris-HCl, 0.2 mM PMSF*, 0.2 mM EDTA, pH 7.5.

Solution D: 10 mM Tris-HCl, 0.2 mM PMSF*, 0.2 mM EDTA, pH 7.5.

*added fresh before use

After isolation of the nuclei, CaCl_2 was added to a concentration of 1 mM and the solution was incubated for 3 minutes at 37°C. Micrococcal nuclease (Boehringer-Mannheim) was added to a concentration of 40 U/mL to break the DNA up into smaller pieces. The nuclei were digested for 5 minutes, after which time the digestion was stopped by addition of EDTA to 2 mM. The mixture was centrifuged for 10 minutes at $\sim 5\text{--}8000 \times g$, the supernatant was discarded, and the pellet was resuspended in solution **R** to half of the previous volume. The low salt concentration of this solution lysed the nuclear membrane and releases everything into solution. The solution was poured gently into a 1 L erlenmeyer which was in turn placed in an ice bucket full of ice. The ice bucket and erlenmeyer were placed on a shaker in the cold room to shake *gently* overnight in order to bring the chromatin into solution. The cloudy off-white solution was centrifuged for 10 minutes at $\sim 5\text{--}8000 \times g$. In this case, the pellet (containing nuclear debris) was discarded and the supernatant (containing chromatin) was retained. Contrary to published procedures, only a modest fraction of the chromatin ($\leq 30\%$) went into solution. Using centricon vials (Amicon, Inc.) the solution was concentrated to 1/3 volume.

The solution was kept on ice as 4 M NaCl was added dropwise to a final concentration of *exactly* 0.65 M. This solution was then applied to a 1.5 cm x 60 cm Sepharose 4B (Sigma) size exclusion column preequilibrated with solution **S**. The sample eluted in this buffer after a couple of hours. Fractions were collected and their UV-visible spectra were determined. The fractions containing nucleosome core particles eluted early, due to their large size, and displayed a strong absorbance at 260 nm and a weaker absorbance below 230 nm; later fractions had a much weaker absorbance at 260 nm. The histone-containing fractions were dialyzed against solution **D** and were concentrated using a centricon vial (Amicon, Inc). This product was then evaluated by 18% SDS-

polyacrylamide gel electrophoresis and compared to commercially-purified histones (Fig. 5.2), roughly quantitated using a Coomassie protein assay (Pierce, Inc.), and used for reconstitution with labeled oligonucleotides. The product that was not needed immediately was stored at -20°C in 50% solution **D** and 50% glycerol with 0.02% sodium azide. These fractions were dialyzed against 1X TE (10 mM Tris-HCl, 1 mM EDTA, pH 7.5) and concentrated using centricon vials before use.

5.2.2 Preparation of Palindromic 146-mer

DNA sequences used in these experiments were based upon those used by Luger *et al.* for their structure of the nucleosome core particle (3,11), and are shown in Table 5.2. Oligonucleotides were prepared by standard phosphoramidite chemistry with 5' phosphate groups as applicable, and purified once by reverse-phase HPLC, as described (12). The oligonucleotides were desalted using Sep-Pak cartridges (Waters, Inc.), followed by phosphorylation as applicable with T4 Polynucleotide Kinase (New England Biolabs) in ligase buffer, treatment with hot aqueous piperidine, and purification by preparative denaturing agarose gel electrophoresis.

To synthesize duplex **1**, strand "2" was first radiolabeled at its 3' terminus using five of the following reaction mixtures: 2 μL DNA (50-500 pmoles); 10 μL α - ^{32}P -ddATP (50 μCi , Amersham); 1 μL Terminal Transferase enzyme (Boeringer-Mannheim); 10 μL terminal transferase 5X buffer; 5 μL CoCl_2 ; 22 μL dH_2O ; 50 μL total volume, incubated at 37°C for 1.5 hours. Samples were ethanol precipitated to remove free label, treated with hot aqueous piperidine, and purified on an 8% denaturing agarose gel. After crushing and soaking to elute the DNA from the gel (13), the radiolabeled "2" was purified by Sep-Pak. Duplex **1** was prepared by mixing 12 μM strand "1," 10 μM strand "2," and all of the

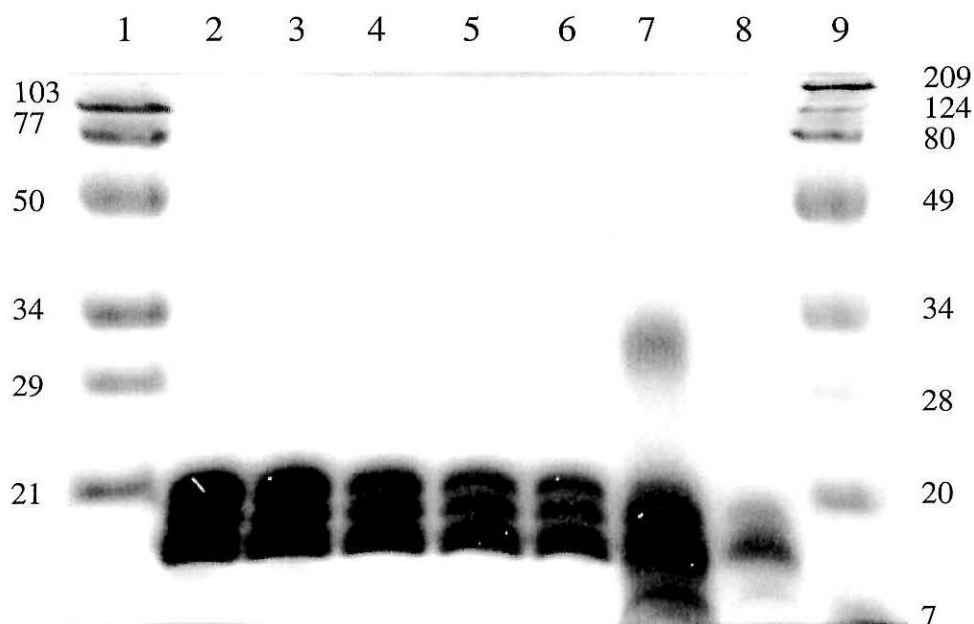


Figure 5.2: Denaturing SDS polyacrylamide gel of isolated chicken erythrocyte histones. Lanes **1** and **9** are molecular weight standards whose values are indicated at the side of the gel. Lanes **2-6** are samples of isolated chicken erythrocytes (serial dilutions from 3mg/mL stock), and lanes **7-8** are samples of commercially-available histones (Sigma). Note that our isolated histones are more pure than the commercially available proteins, which cannot assemble to form histone octamers. The published molecular weights of the histone proteins are: H2A, 14 kDa; H2B, 13.7 kDa; H3, 15.3 kDa; H4, 11.3 kDa; H1/H5, 21.5 kDa, total assembled nucleosome core particle, ~200 kDa (38).

Table 5.2: 146-base-pair duplex assemblies formed by ligation of shorter oligonucleotides[†]

Duplex 1

5' ATCAATATCCACCTGCAG¹TTCTACCAAAAGTGTA²TTGGAAACTGCTCCATCAAAAGGCATGTT¹CAGCTGAATTCAGCTGAACATGCCCTTTTGATGGAGCAGTTTCCAAATACACTTTTGGTAGAACTGCAGGTGGATATTGAT3' *
 *3' TAGTTATAGGTGGACGTC²GAAGATGGTTTTCACATAAAACCTTTGACGAGGTAGTTTTCGTACAAGTCGACTTAAAGTCGACTTGTACGGAAAAC¹TACCTCGTCAAAAGGTTTATGTGAAAACCATCTT¹GGACGTCACCTATAACTA5'

Duplex 1-Rh

Rh5' ³ EATCAATATCCACCTGCAG⁴TTCTACCAAAAGTGTA⁴TTGGAAACTGCTCCATCAAAAGGCATGTT²CAGCTGAATTCAGCTGAACATGCCCTTTTGATGGAGCAGTTTCCAAATACACTTTTGGTAGAAACTGCAGGTGGATATTGAT3' *
 *3' TAGTTATAGGTGGACGTC²GAAGATGGTTTTCACATAAAACCTTTTGACGAGGTAGTTTTCGTACAAGTCGACTTAAAGTCGACTTGTACGGAAAAC⁴TACCTCGTCAAAAGGTTTATGTGAAAACCATCTT³GGACGTCACCTATAACTA⁵' Rh

Rh-ligation primer: 5' CTCTTGGTAGAACCTGCAGGTGGATATTGAT 3'

Duplex 2

Rh5' ³ EATCAATATCCACCTGCAG⁵TTCTACCAAAAGTGTA⁵TTGGAA⁶CTGCTCCATCAAAAGGCATGTT⁶CAGCTGAATTCAGCTGAACATGCCCTTTTGATGGAGCAG⁶TTCCAAAGTACACTcTTGGTAGAACTGCAGGTGGATATTGAT3' *
 *3' TAGTTATAGGTGGACGTC⁶GAAGATGGTT⁶GTCACAT⁶GTACCTT⁵GGACGAGGTAGTTTTCGTACAAGTCGACTTAAAGTCGACTTGTACGGAAAAC⁵TACCTCGTCAAAAGGTT⁵GAATGTGAAGAACCATCTT³GGACGTCACCTATAACTA⁵' Rh

Rh-ligation primer: 5' CTCTTGGTAGAACCTGCAGGTGGATATTGAT 3'

* Radioactive label

[†] Bases changed from original sequence of Luger *et al.* are indicated by lower case/bold/underline. Numbers in italics correspond to the short oligonucleotides that were annealed to make duplexes 1, 1-Rh, and 2-Rh.

radiolabeled strand “2” with 10 X ligase buffer in 100 μ L total volume. Strand “1” and “2” were annealed by heating to 90°C and cooling gradually to ambient temperature, and were ligated to form the double-stranded, palindromic 146 mer by incubation with high-concentration T4 DNA ligase (New England Biolabs) at 17°C overnight.

To synthesize duplex **1-Rh** containing a tethered rhodium complex, short rhodium-tethered oligonucleotide “3” was prepared and purified as described (14). The rhodium-tethered 17-mer “3” was ligated to a phosphorylated 59-mer “4” to make a rhodium-tethered 76-mer “3+4” using the rhodium ligation primer shown in Table 5.2, and this product was purified by denaturing gel electrophoresis, both as described (15, chapter 2). The long, single-stranded, rhodium-tethered oligonucleotide “3+4” was then desalted using Sep-Pak cartridges and dried *in vacuo*. Strand “2” was radiolabeled at its 3’ terminus and gel purified as above. Duplex **1-Rh** was then prepared by mixing 12 μ M strand “3+4,” 10 μ M strand “2,” and all of the radiolabeled strand “2” with 10 X ligase buffer in 100 μ L total volume. Strands were annealed by heating to 90°C and cooling gradually to room temperature, and were ligated to form the double-stranded, palindromic 146 mer by incubation with high-concentration T4 DNA ligase (New England Biolabs) at 17°C overnight.

Duplex **2-Rh** was prepared in the identical manner as duplex **1-Rh** using oligonucleotides “5” and “6” and rhodium-tethered oligonucleotide “3.”

5.2.3 Formation of Nucleosome Core Particles with 146-mer

Nucleosome core particles were formed on the 146-mers by the salt exchange method (16). To one half of the ligation mixture, histones and salt were added in 7 reaction mixes as follows: 25 μ L histone stock solution (~3mg/mL); 5 μ L 10X dilution buffer + β -mercaptoethanol, 12.5 μ L 4M NaCl, 7.5 μ L 146-mer

ligation mix, in 50 μL total volume. The solution was incubated at room temperature for one hour. 16.5 μL of 1X dilution buffer (20 mM Tris-HCl pH 8.0; 1 mM EDTA, 1 mM β -mercaptoethanol) was added after every hour for three hours. Then, 100 μL of 1X dilution buffer was added every 15 minutes for an hour. When the total volume of each reaction reached 500 μL , the solutions were incubated for 1 hour at 37°C. The volume was reduced to < 20 μL using microcon filters (Amicon, Inc.), and was purified on a 5% nondenaturing acrylamide gel along with the half of the ligation sample to which no protein had been added. The 146-mer and the 146-mer with histones were clearly resolved from each other and from unligated single- and double-stranded 73-mers by electrophoresis for approximately 5 hours at 200 V at ambient temperature. Bands containing the desired samples were excised and the DNA or DNA-protein complexes were eluted into 1X TE by the crush-and-soak method (13). The solution was filtered through 0.45 μm filters to remove large pieces of gel and was dialyzed against 1X TE to remove running dye, borate, and acrylamide monomers. After concentrating this sample using microcon filters, it was used for DNase I footprints, photoirradiations, or Maxam-Gilbert sequencing reactions.

5.2.4 Photoirradiations of Nucleosomes and Bare DNA with $Rh(\phi)_2\text{DMB}^{3+}$

Samples (30 μL) containing radioactively-labeled 146-mer with or without bound histone proteins and 10 μM noncovalent rhodium complex (where applicable) were irradiated for up to 2 hours using a 1,000 Hg-Xe arc lamp equipped with a monochromator (Oriel). Samples were maintained around 12°C during irradiation to prevent evaporation. The volume of the stock solution was adjusted to contain a sufficient amount of radioactive label for visualization on the gel after purification, and was estimated to contain ~50-100 nM 146-mer DNA.

After irradiation, samples were incubated with 50 µg/mL proteinase K in 0.5% SDS for 1.5 hours at 37°. After digestion, the samples were treated with 10% piperidine at 90°C for 30 minutes and dried *in vacuo*. All samples, including those irradiated at 313 nm, were treated with piperidine to break DNA-protein crosslinks. Each sample was resuspended in 100 µL TE, extracted with phenol and chloroform, and ethanol precipitated before analysis on a 7% denaturing polyacrylamide gel. Gels were quantitated by phosphorimager using ImageQuant (Molecular Dynamics) and Excel (Microsoft).

5.2.5 DNase I footprinting

Samples containing radioactively-labeled 146-mer with or without bound histone proteins were treated with DNase I (17). Samples (30 µL) were incubated with varying concentrations of DNase I and 1.25 mM CaCl₂ or MgCl₂ for 2 minutes (no histones) or 5 minutes (with histones) before the reaction was stopped by the addition of 35 µL of stop solution (5.8 M ammonium acetate, 28 mM EDTA, 220 µM bp calf thymus DNA). After thorough mixing, 80 µL of 1% SDS were added. This mixture was extracted with phenol and chloroform and precipitated with ethanol and ammonium acetate before analysis on a 7% denaturing polyacrylamide gel.

5.2.6 Nucleosome Core Particle Structures

Coordinates of the nucleosome core particle were downloaded from the protein data bank (<http://www.rcsb.org/pdb>), files 1aoi (4) and 1eqz (8). Structures were examined using Web Lab Viewer Pro (Accelrys, Inc.).

5.3 Results and Discussion

5.3.1 *Structure of the Nucleosome Core Particle and Sequence of the Nucleosomal DNA*

A radioactively-labeled 146-mer oligonucleotide, duplex **1**, was used to determine whether charges can migrate through DNA bound to histones as a nucleosome core particle (Table 5.3). This sequence was selected because it forms a stable nucleosome core particle with a single rotational and translational setting, whose structure with recombinant frog and purified chicken histone proteins has been solved crystallographically (4,8). Significantly, the DNA sequence of duplex **1** is palindromic, which means that both strands are identical when read from the 5' to the 3' direction. Additionally, it means that both halves of the sequence, from the termini to the center, are identical. In the crystal the 146-mer binds to the C2-symmetric histone octamer with the center of the palindromic sequence almost aligned with the rotational symmetry axis of the octamer. Therefore, for the purposes of this study we can assume that the two halves of the DNA structure are also identical. Structures shown here display only one half (73 bp) of the sequence, corresponding to ~0.8 turns around the nucleosome core particle from the DNA terminus to the center.

In designing these experiments, only one base pair was changed from the sequence used previously (4) in each half of duplex **1**, in order to add a 5'-GG-3' site by which to monitor long-range charge transport to oxidize DNA bases (Table 5.3). As a result, the sequence contains seven 5'-GG-3' sequences in each half of the palindrome that (in the absence of guanine triplets) are expected to be the most easily oxidized sites on the duplex. These 5'-GG-3' sites are numbered as GG1 through GG7 from the terminus of the sequence to the center. Because of the palindromic nature of the sequence, the full 146-base-pair duplex actually contains fourteen 5'-GG-3' sites, seven on each identical strand. When viewed on

Table 5.3: Sequences of half of palindromic DNA oligonucleotide duplexes[†]

Duplex 1	
5' ATCAATATCCACCTGCA ³ <u>GG</u> TTCTACCAAAAGTGTATT ⁵ GGAAACTGCTCCATCAAAA ⁷ GGCATGTTTCAGCTGAA...	
*3' TAGTTATAGGT ¹ GGACGTC ² CAAGAT ⁴ GGTTTTCACATAAACCTTTGACGAG ⁶ GGTAGTTTCCGTACAAGTCGACTT...	↑
Duplex 1-Rh	
Rh5' tATCAATATCCACCTGCA ³ <u>GG</u> TTCTACCAAAAGTGTATT ⁵ GGAAACTGCTCCATCAAAA ⁷ GGCATGTTTCAGCTGAA...	
*3' TAGTTATAGGT ¹ GGACGTC ² CAAGAT ⁴ GGTTTTCACATAAACCTTTGACGAG ⁶ GGTAGTTTCCGTACAAGTCGACTT...	↑
Duplex 2-Rh	
Rh5' tATCAATATCCACCTGCA ³ <u>GG</u> TTCTACCAAGAGTGTACTT ⁵ GGAAcCTGCTCCATCAAAA ⁷ GGCATGTTTCAGCTGAA...	
*3' TAGTTATAGGT ¹ GGACGTC ² CAAGAT ⁴ GGTT ⁴ CTCACAT ⁸ GAACCTT ⁶ GGACGAG ⁶ GGTAGTTTCCGTACAAGTCGACTT...	↑ ↑ ↑ ↑

* Radioactive label

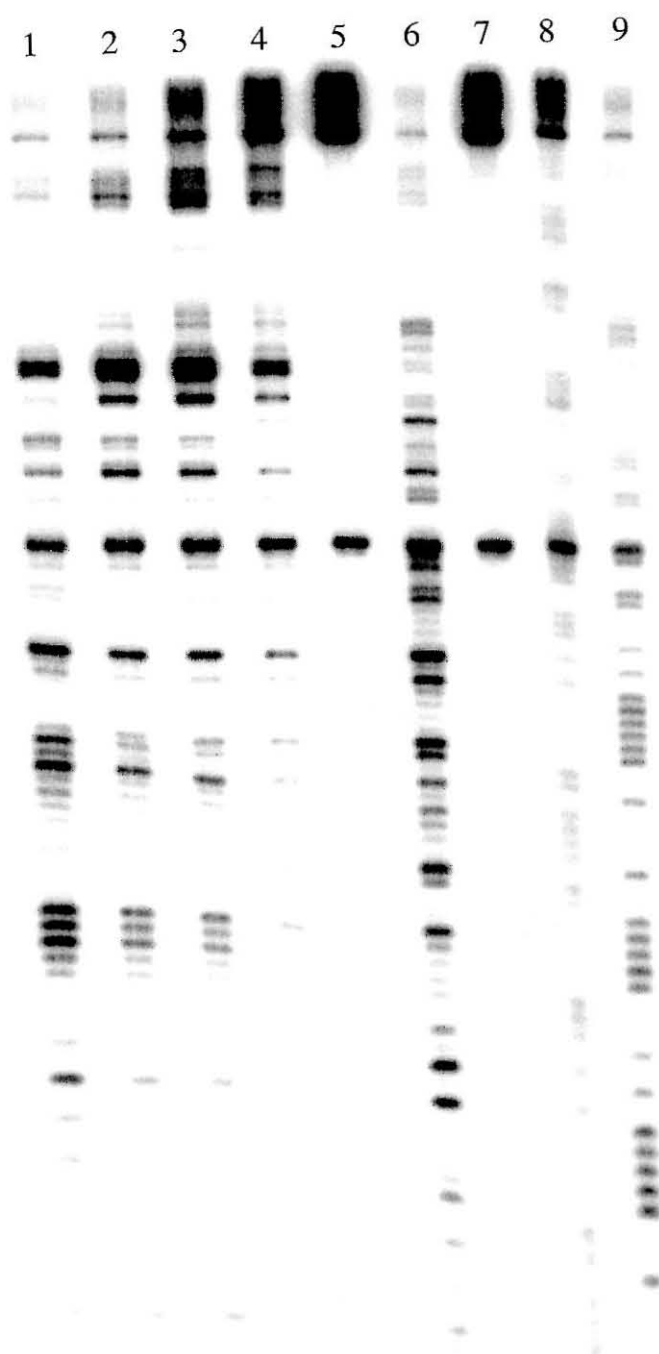
[†] Bases changed from original sequence of Luger *et al.* are indicated by lower case/underline and dark grey arrows. Red numbers correspond to the 5'-GG-3' sequences; corresponding 5'-GG-3' sequences on the other half of the palindrome are numbered identically.

a denaturing polyacrylamide gel, all seven 5'-GG-3' sites can potentially be seen in the order GG1, GG2, GG4, GG6, (center), GG7, GG5, GG3 from the radiolabeled 3' terminus at the bottom of the gel to the 5' terminus at the top.

5.3.2 *Confirmation of the Structure of the Nucleosome Core Particle by DNase I Footprinting*

Histone octamers can be exchanged from one piece of DNA to another by incubation with high concentrations of salt (i.e., 1M NaCl) followed by dilution or dialysis (16). Salt exchange from purified chicken DNA to duplex **1** resulted in the formation of one species with a larger molecular weight than the parent 146-mer as determined by non-denaturing gel electrophoresis (not shown). This larger species was isolated from the gel. DNase I footprinting was used to determine whether the histone proteins were bound specifically to the 146-mer to form a nucleosome core particle with the same structure as that elucidated crystallographically (4,8). Samples lacking histone proteins are cleaved more quickly and using a lower concentration of DNase than are samples with histones (Fig. 5.3). This slower cleavage is one indication that the 146-mer is bound to the histones and thus protected by them from cleavage. Slower cleavage by DNase I could be due to competition for DNase I by contaminating chicken DNA; however, studies with the same concentrations of nucleosome core particles that were *not* exchanged onto the target radiolabeled DNA indicate that the protective effect of the histone proteins is largely due to their binding to the DNA. More interestingly, the pattern of DNase I cleavage on the histone-bound 146-mer displays regions of periodic protection from and accessibility to DNase I (Fig. 5.3). This pattern is distinct from the pattern of enzyme cleavage on the bare 146-mer, which is more random. The distinct pattern of periodic cleavage is characteristic of DNA in nucleosome core particles and not to DNA with

Figure 5.3: DNase I digestion of duplex **1** with and without bound histone proteins. Lanes **1-5** have bound histone proteins, while lanes **6** and **7** do not; lanes **8** and **9** are Maxam-Gilbert purine- and pyrimidine-specific sequencing lanes, respectively. DNase I was added to each sample in the following amounts: lane **1**, 2.5 Units; lane **2**, 0.5 U; lane **3**, 0.25 U; lane **4**, 0.05 U; lane **5**, no enzyme; lane **6**, 0.05 U; lane **7**, no enzyme. The band at the center of the gel, present in all lanes, is due to incomplete ligation to form the 146-mer. Details of the digestion are explained in the Methods section. Note that bare DNA is cut more readily than histone-bound DNA, and that the pattern of cleavage by the DNase I enzyme in the presence of bound histone proteins is distinct from the pattern of cleavage in the absence of proteins.



randomly-bound histones. Furthermore, the pattern indicates uniform phasing of the DNA relative to the protein. This uniform phasing is expected, given the fact that this sequence contains 12 phased positioning sequences (8). On longer pieces of DNA, it is possible to have several species with the same rotational phasing but different translational orientations. However, since this radiolabeled DNA is only 146 base pairs in length (the minimum length of DNA required to bind entirely around a histone octamer), it is reasonable to expect one predominant form with the 146-mer bound (relatively) symmetrically to the histones to form a core particles. The presence of a single predominant form is also consistent with the results of the gel shift assay.

The pattern of DNase I cleavage can also be used to determine where the minor groove faces outward into the solution and becomes accessible to the enzyme, and where the minor groove faces inward toward the histone protein and is protected from the enzyme (17). These cleavage patterns can then be mapped to the DNA in the crystal structure to establish whether the two views of the histone-bound 146-mer DNA agree (Fig. 5.4). Regions of duplex 1 that are *hypersensitive* to DNase I correspond to places where the minor groove bends outward into the solution, whereas regions of duplex 1 that are *hyposensitive* to DNase I frequently correspond to places where the minor groove faces inward toward the histone octamer or where histone tails or side chains bind in the major groove. Interestingly, the DNase cleavage in some regions of the sequence is unchanged, indicating that the accessibility or reactivity of some stretches of the DNA sequence are not affected by the binding to the histone proteins. Although the DNase footprinting alone does not provide a clear picture of the core particle, it is fairly consistent with that provided by the crystal structure. This structural information is very useful because it not only tells us that our DNA is bound in a

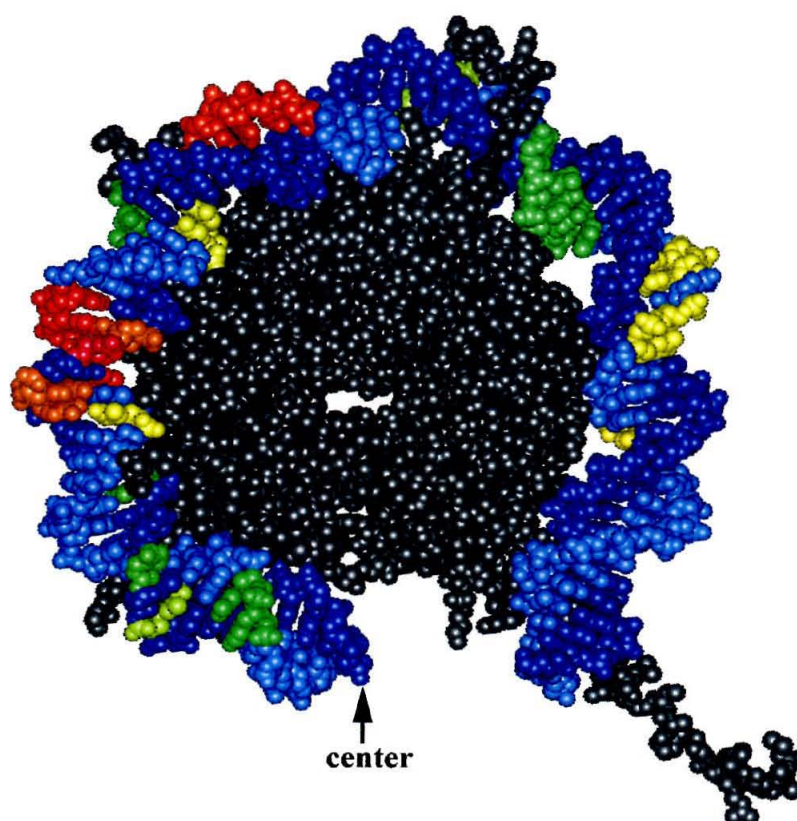


Figure 5.4: Cleavage of histone-bound duplex **1** superimposed upon the crystal structure of the same sequence in a nucleosome core particle (PDB structure 1aoi). The histone octamer is colored grey; one-half of the 146-mer palindromic DNA is shown in a range of colors. Blue and cyan regions were not cut by the enzyme in either the presence or absence of histones; yellow regions were cut by the enzyme fairly equally in the presence or absence of histones. Red and orange regions were *hypersensitive* to DNase I when duplex **1** was bound to the histones; green regions were *hyposensitive* to DNase I. Estimates of cleavage intensities are approximate and are based upon samples in which the total amount of cleavage was roughly equal. Since the enzyme cleaves bare DNA much more readily than protein-bound DNA, histone-bound samples were incubated for a longer time period and with more DNase I enzyme than bare DNA samples.

nucleosome core particle, but it allows us to examine the accessibility of particular reactive sites (*vide infra*).

The structures of duplex **1-Rh** and **2-Rh** containing tethered rhodium intercalators could not be examined similarly using DNase I footprinting because the rhodium-tethered oligonucleotides cannot be extracted with phenol and chloroform. However, gel shift experiments indicate that a single histone-bound species is formed by nucleosome exchange (not shown).

5.3.3 Binding and Oxidation by Noncovalent $\text{Rh}(\text{phi})_2\text{DMB}^{3+}$ on a 146-mer

As described in earlier chapters, $\text{Rh}(\text{phi})_2\text{DMB}^{3+}$ binds avidly to DNA by intercalation and reacts with DNA according to two distinct mechanisms. With irradiation at 313 nm, phi complexes of rhodium cleave the sugar-phosphate backbone at their intercalation site, allowing determination of where they are bound (18,19). This complex binds DNA with very little sequence preference, and thus photoirradiation at 313 nm yields a broad distribution of cleavage sites. In contrast, when irradiated at 365 nm, the rhodium complex preferentially oxidizes the 5' guanine of 5'-GG-3' sites. When spatially separated from the 5'-GG-3' sites, the rhodium complex can oxidize guanine bases by a long-range reaction that is mediated by the DNA base stack (20). The oxidized guanine base products, which probably include 8-oxo-guanine, imidazalone, and oxazalone derivatives, are converted to direct strand breaks upon incubation of the DNA with hot aqueous piperidine. Under certain reaction conditions the distinction between these two reactions is not always sharp. Treatment of samples that have been photocleaved by rhodium at 313 nm with hot aqueous piperidine reveals some photooxidation at 5'-GG-3' sites, and at high rhodium concentrations (>10 μM), photoexcitation at 365 nm leads to nonspecific DNA cleavage as well as guanine base oxidation. This overlap of reactivity depends in part upon the

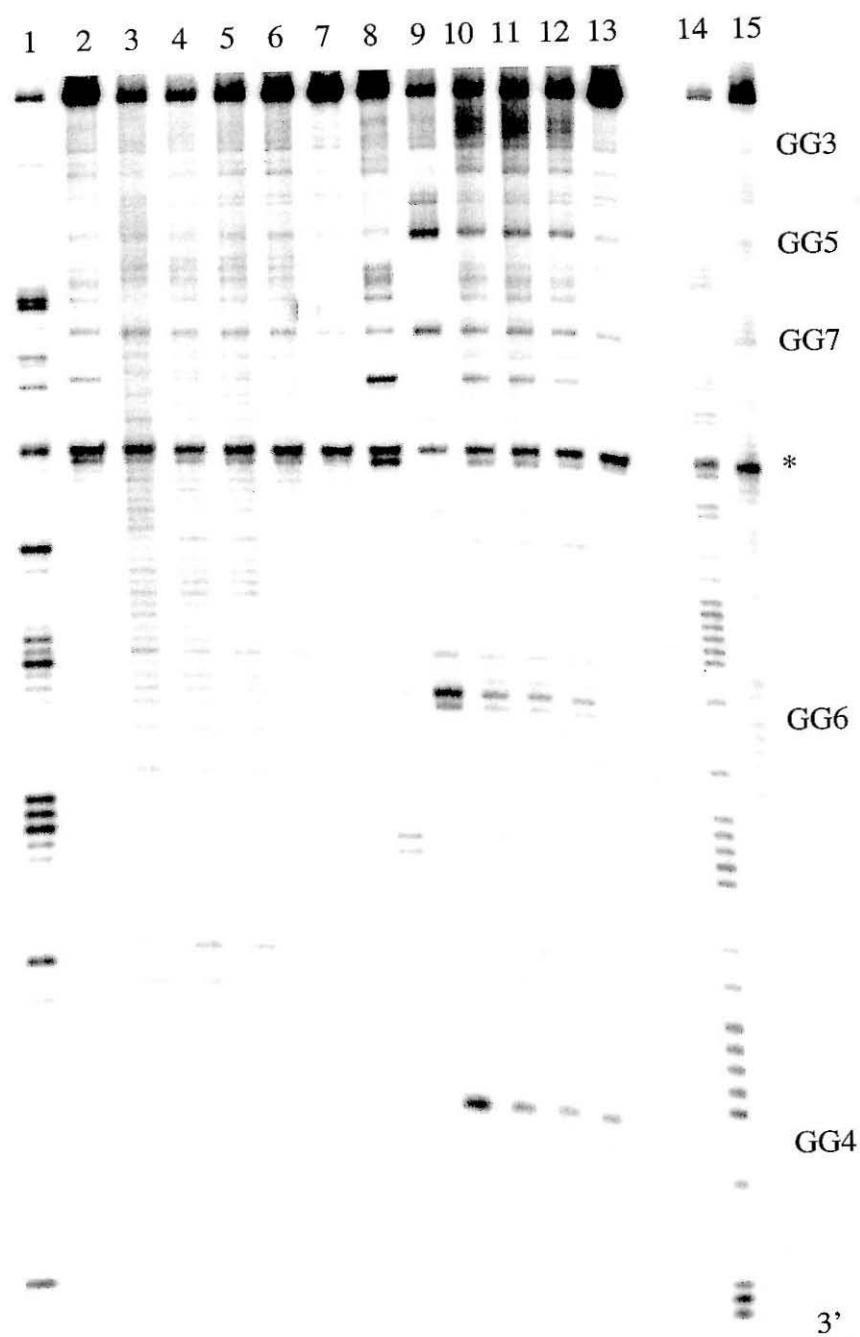
efficiency of reactions at high concentrations, and in part upon the fact that the light used for irradiation is dispersed over a range of wavelengths including the excitation wavelengths for both reactions.

Photoirradiation can also lead to DNA-protein crosslinks, either as a direct result of photoexcitation of the DNA or protein by the light source, or by an interaction between a base or sugar radical on the DNA (generated by the rhodium photoreactions) with the histone proteins (21). After photoirradiation, samples were treated with proteinase K and hot aqueous piperidine to break any DNA-protein crosslinks which may have been formed. The location of these cross-links would then be visualized by denaturing gel electrophoresis as direct strand breaks.

Duplex 1, both with and without bound histones, was incubated with 10 μM $\text{Rh}(\text{phi})_2\text{DMB}^{3+}$, and the mixture was irradiated at 313 nm to determine sites of direct strand cleavage where the metal complex binds. In the absence of histone proteins, the rhodium complex binds and cleaves throughout the oligonucleotide duplex 1 in a nonspecific fashion, as evident upon photoirradiation at both 313 nm and 365 nm (Fig. 5.5). This pattern of DNA damage is consistent with the fact that its concentration exceeds its nonspecific binding constant, and that the rhodium complex is present at high loading on the DNA.

When irradiated at 313 nm with the 146-mer oligonucleotide duplex 1 bound to histones as a nucleosome core particle, the rhodium complex cleaves the DNA much less extensively (Fig. 5.5), analogously to cleavage of these same nucleosome core particles by DNase I. What is especially interesting, however, is the *pattern* of direct DNA photocleavage. The distribution of rhodium photocleavage is not nonspecific, nor does it demonstrate a sequence specificity characteristic of $\text{Rh}(\text{phi})_2\text{DMB}^{3+}$ at lower concentrations (18,19). The photocleavage does not show a periodic pattern of protection and exposure similar

Figure 5.5: Direct strand scission and base oxidation by $\text{Rh}(\text{phi})_2\text{DMB}^{3+}$ on duplex **1** with and without histone proteins. DNA samples shown in lanes **1** and **8-13** are bound to histone proteins as a nucleosome core particle; DNA samples in lanes **2-7** are bare DNA without histone proteins. Lane **1** is sequence 1 bound to histone proteins as a nucleosome core particle and digested with 2.5 U of DNase I for 5 min. Samples were photoirradiated with 10 μM noncovalent $\text{Rh}(\text{phi})_2\text{DMB}^{3+}$ unless otherwise indicated, and all samples were treated 10% piperidine for 30 min. at 90°C after irradiation. Lane **2**: 10 min. at 313 nm without rhodium complex; **3**: 30 min. at 365 nm; **4**: 10 min. at 313 nm; **5**: 5 min. at 313 nm; **6**: 2 min. at 313 nm; **7**: no irradiation; **8**: 30 min. at 313 nm with no rhodium; **9**: 90 min. at 313 nm; **10**: 30 min. at 313 nm; **11**: 20 min. at 313 nm; **12**: 10 min. at 313 nm; **13**: no irradiation. Lanes **14** and **15** are Maxam-Gilbert pyrimidine-specific and purine-specific sequencing lanes, respectively. The band at the center of the gel, present in all lanes and indicated by an asterisk, is due to incomplete ligation to form the 146-mer.

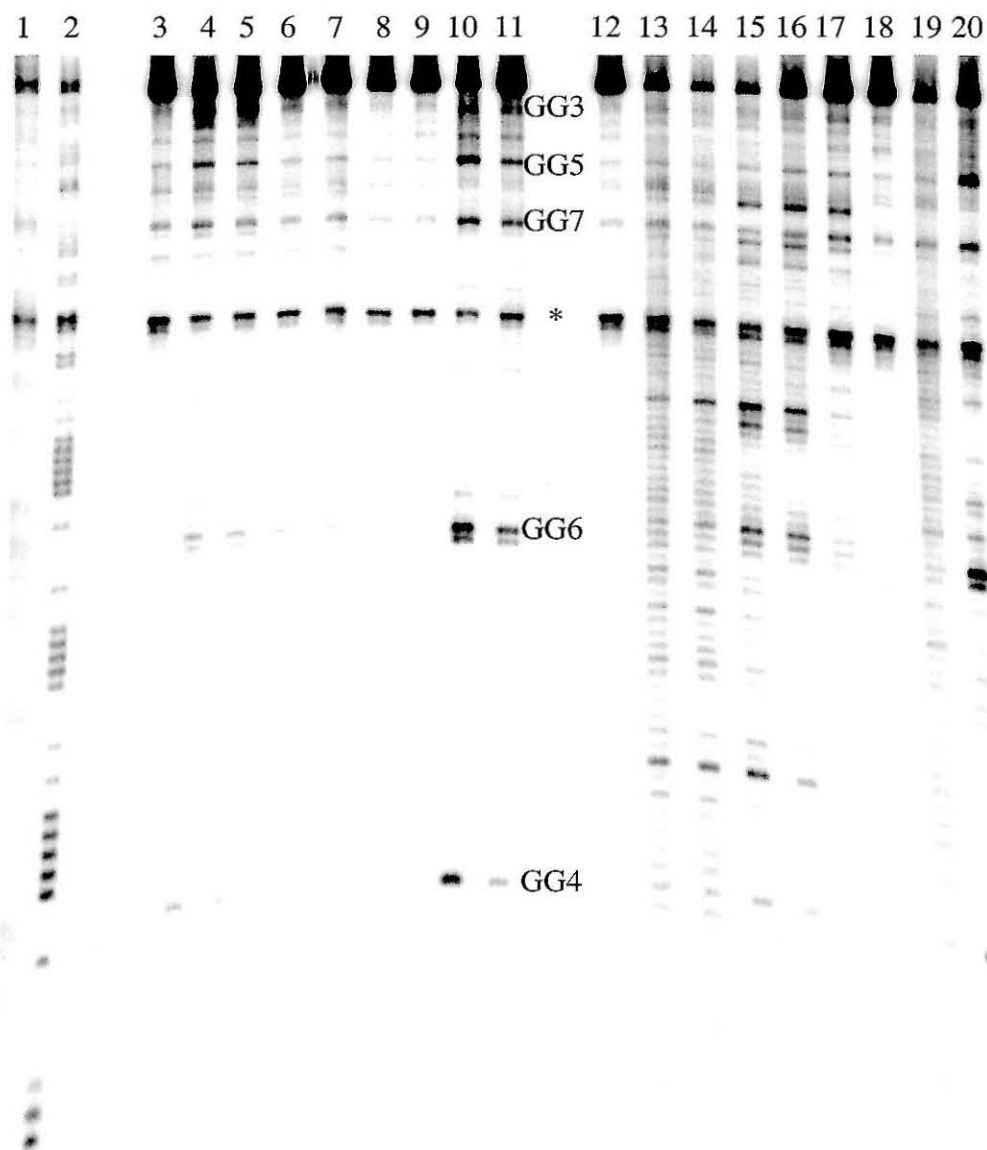


to cleavage by DNase I, hydroxyl radical, and micrococcal nuclease on nucleosome core particles. Instead, cleavage is observed exclusively at the 5' guanine of 5'-GG-3' sites (and at sites of direct photodynamic damage that are independent of rhodium). This damage pattern is the same, irrespective of irradiation at 313 nm or 365 nm.

To establish that the unusual patterns of cleavage were not due to rhodium concentration effects, we examined direct photocleavage and base oxidation in the same system by different concentrations of $\text{Rh}(\text{phi})_2\text{DMB}^{3+}$ between 10 μM and 100 nM (Fig. 5.6). On duplex **1** in the absence of histone proteins, the distribution of rhodium-induced DNA damage is fully consistent with previous studies. At a concentration of 10 μM the rhodium complex binds and photocleaves bare DNA nonspecifically at both 313 nm and 365 nm because the rhodium complex is present at a very high loading on the DNA. At 1 μM and lower concentrations, a weak sequence specificity in binding emerges (lanes 13-17). At 1 μM rhodium concentration, nonspecific cleavage at 365 nm is not evident, and charge transport damage is localized to 5'-GG-3' sites (lane 20). However, in a nucleosome core particle, the pattern of rhodium binding and direct strand scission at 313 nm on duplex **1** is distinctly different from that on bare DNA. Damage at both wavelengths is localized to the 5' guanine of 5'-GG-3' sites, which is the signature of charge transport damage through the DNA base pair stack.

The absence of relatively nonspecific direct strand scission at 313 nm in nucleosome core particles indicates that the structure of the core particle diminishes the ability of the noncovalently bound rhodium intercalator to bind to the DNA. Histone proteins are known to protect DNA from binding and cleavage by a variety of small molecules and proteins, such as hydroxyl radical, triple-helix-forming oligonucleotides, DNase I, micrococcal nuclease, and various

Figure 5.6: Direct strand scission and base oxidation by varying concentrations of $\text{Rh}(\text{phi})_2\text{DMB}^{3+}$ on duplex **1** with and without histone proteins. DNA samples shown in lanes **3-11** are bound to histones as nucleosome core particles. DNA samples in lanes **12-20** are bare DNA without histone proteins. Lanes **1** and **2** are Maxam-Gilbert purine-specific and pyrimidine-specific sequencing lanes, respectively. Lane **3**: 10 μM rhodium, no photoirradiation; **4**: 10 μM rhodium, 20 min. at 313 nm; **5**: 5 μM rhodium, 20 min. at 313 nm; **6**: 1 μM rhodium, 20 min. at 313 nm; **7**: 500 nM rhodium, 20 min. at 313 nm; **8**: 100 nM rhodium, 20 min. at 313 nm; **9**: no rhodium, 20 min. at 313 nm; **10**: 10 μM rhodium, 90 min. at 365 nm; **11**: 1 μM rhodium, 90 min. at 365 nm; **12**: 10 μM rhodium, no photoirradiation; **13**: 10 μM rhodium, 10 min. at 313 nm; **14**: 5 μM rhodium, 10 min. at 313 nm; **15**: 1 μM rhodium, 10 min. at 313 nm; **16**: 500 nM rhodium, 10 min. at 313 nm; **17**: 100 nM rhodium, 10 min. at 313 nm; **18**: no rhodium, 10 min. at 313 nm; **19**: 10 μM rhodium, 30 min. at 365 nm; **20**: 1 μM rhodium, 30 min. at 365 nm. All samples were treated with 10% piperidine for 30 min. at 90°C after photoirradiation. The band at the center of the gel, indicated by an asterisk, is due to incomplete ligation to form the 146-mer. 5'-GG-3' sites are indicated by numbers corresponding to Table 5.3.



intercalators (17,22-32). In nucleosome core particles, histone proteins directly block access to large sections of the major and minor grooves, and may electrostatically repel positively-charged DNA-binding molecules with their own substantial positive charge. Although it has been shown that molecules that bind in the major or minor groove can often bind to nucleosomal DNA wherever their binding sites are exposed on the solution face of the nucleosome (22,23,25,26), intercalators generally do not bind well to nucleosome core DNA and, where possible, bind instead to linker DNA (26-32). This exclusion of intercalators from the nucleosome core particle is thought to occur because the bound histone octamer clamps down on the DNA, preventing the DNA from unstacking and unwinding to accommodate the intercalator. Like ethidium and other intercalators, the rhodium complex probably intercalates preferentially near the end of the DNA duplex, since the DNA near the ends is more floppy and less tightly anchored to the protein than the DNA near the middle of the sequence (4). The rhodium complex could also intercalate near the middle of the sequence on DNA strands which contain a nick on one strand due to imperfect ligation, since related rhodium complexes bind preferentially at base mismatches and other sites of destabilized base stacking (33,34). Like other intercalators, the rhodium complex may also bind with lower frequency and affinity at other sites on the nucleosome core particle that display exposed major grooves and substantial flexibility. Bands due to photoinduced strand scission at 313 nm at intercalation sites near the end, at single-strand nicks, and at low-affinity sites would be difficult to observe on the denaturing acrylamide gel.

Notably, when our noncovalent rhodium intercalator is photoexcited in the presence of the nucleosome core particle, it selectively oxidizes all of the 5' guanines of 5'-GG-3' sites, despite the low accessibility of nucleosomal DNA. The prevalence of this damage on nucleosomal DNA indicates that charges can

move through the π stack even when that DNA is bound around a histone octamer. However, these experiments do not establish the distances over which the electronic “hole” can migrate, since we do not know for certain where the rhodium complex is bound.

5.3.4 Binding and Oxidation by $Rh(\phi)_2bpy^{3+}$ Tethered to the 5' Termini of the 146-mer

To determine the distances over which charges can migrate in nucleosomal DNA between 5'-GG-3' sites and intercalating oxidants whose positions are known, duplex **1-Rh** was constructed with the same DNA sequence as duplex **1**, plus a $Rh(\phi)_2bpy^{3+}$ complex covalently attached to each 5' end (Table 5.3). We have previously demonstrated that this complex is constrained by its diaminononane linker to intercalate 2 or 3 base pairs from the end of a DNA oligonucleotide duplex, from whence it can oxidize 5'-GG-3' sites over ~ 200 Å (15,20). This radioactively-labeled 146-base-pair oligonucleotide duplex **1-Rh**, modified with a tethered rhodium, was exchanged with histone octamers according to the same method as duplex **1**. Although the solubility of the resultant rhodium-tethered oligonucleotide precluded DNase I footprinting analysis, the behavior of this duplex by gel shift analysis was the same as duplex **1**. Given that the DNA sequence is identical to duplex **1** and the rhodium complexes are covalently attached to the termini, the structure of the nucleosome formed with duplex **1-Rh** is likely to be equivalent to that formed with duplex **1**.

Duplex **1-Rh** with or without bound histone proteins was photoirradiated at 313 nm and 365 nm (Fig. 5.7). In the *absence* of histone proteins, only oxidative base damage can be observed after irradiation at 313 nm, since the two symmetric termini of the 146-mer are lost from the bottom of the gel and compressed near the top. Significantly, however, no other direct cleavage is

observed, indicating that the metal complex is not binding to some other location in the sequence. With irradiation at both 365 nm and 313 nm and treatment with hot aqueous piperidine, oxidation is observed at GG1, GG2, GG3, and GG4, located 8, 11, 16, and 24 base pairs away from the closest intercalated metal complex, assuming an intercalation site 3 base pairs in from its site of covalent attachment. The oxidation occurs selectively at the 5' guanine of these 5'-GG-3' sites. No significant oxidation is observed at the other guanine doublets positioned further from the rhodium intercalation site, i.e., GG5, GG6, and GG7. Importantly, in the presence of bound histone proteins, the pattern of damage with irradiation at both wavelengths is identical to the pattern of damage in the absence of bound histone proteins. This observation indicates that the wrapping the 146-mer around a histone octamer to form a nucleosome core particle does not change the rhodium intercalation into this sequence nor the long-range charge transport through it (Table 5.4).

It is noteworthy that in this 146-base-pair sequence, no guanine oxidation is observed at guanine doublets GG5, GG6, and GG7, located 38, 48, and 56 base pairs away from the rhodium intercalator, even in the absence of bound protein. The absence of charge transport to oxidize guanine doublets over this distance contrasts with earlier observations with oligonucleotide duplexes (15,35). The result is, however, perhaps not surprising given that this sequence was designed to favor the bending of DNA so as to form stable nucleosome core particles. The oligonucleotide sequence contains a dozen phased nucleosome positioning sequences, designed to facilitate DNA wrapping around histones as a result of being intrinsically bent in the correct direction for binding to the circular surface of the octamer or by being particularly flexible (8, 5-7). Such static or dynamic disruptions in base pair stacking would be expected to diminish long-range guanine oxidation (2-3, 15, 36-37).

Figure 5.7: Long-range oxidation of 5'-GG-3' sites by a covalently-tethered rhodium complex. The oligonucleotide duplex assembly **1-Rh** varies from duplex **1** only in the presence of the covalently-tethered metallointercalator at each 5' end; the sequence of base pairs is the same as that of duplex **1**. The samples shown here contain the left-handed Λ isomer of the rhodium complex; results for the right-handed Δ isomer were the same. Samples shown in lanes **1-3** are bare DNA containing no added histone proteins; lanes **4-6** contain histone proteins bound as a nucleosome core particle. Lane **1**: no photoirradiation; **2**: 90 min. at 365 nm; **3**: 15 min. at 313 nm; **4**: no photoirradiation; **5**: 90 min. at 365 nm; **6**: 15 min. at 313 nm. All samples were treated with hot aqueous piperidine. Lanes **7** and **8** are Maxam-Gilbert pyrimidine-specific and purine-specific sequencing lanes, respectively. The band at the center of the gel, indicated by an asterisk, is due to incomplete ligation to form the 146-mer. 5'-GG-3' sites are indicated with numbers corresponding to Table 5.3.

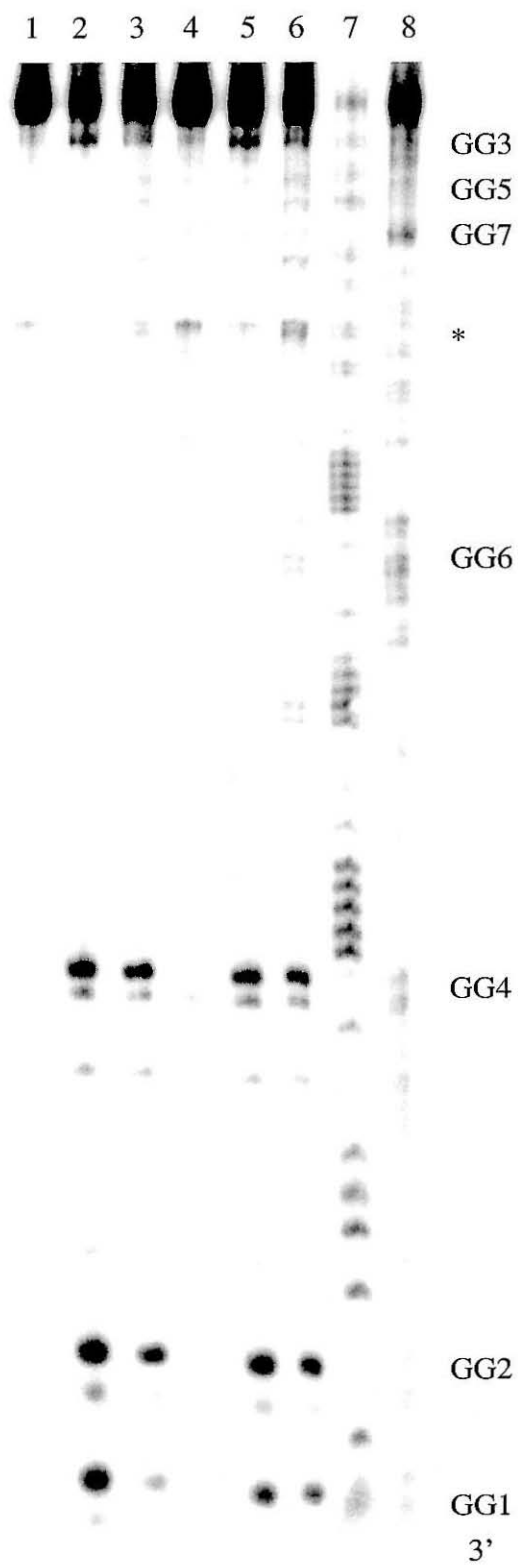


Table 5.4: Long-range guanine oxidation by covalently-tethered rhodium complexes[†]

Duplex 1-Rh, Bare	<p>Rh5' <u>₃</u>TATCAATATCCACCTGCAG<u>₃</u>TTCTACCAAAAGTGTA<u>₃</u>TTTGGAAACTGCTCCATCAAAA<u>₃</u>GGCATGTTTCAGCTGAA...</p> <p>*3' TAGTTATA<u>₃</u>GGTGGACGTC<u>₃</u>CAAGAT<u>₃</u>GGTTTTCACATAAAACCTTTGACGAG<u>₃</u>GGTAGTTTCCGTTACAAGTCGACTT...</p> <p>Red arrows indicate oxidation sites: 1, 2, 3, 4, 5, 6, 7.</p>
Duplex 1-Rh, NCP	<p>Rh5' <u>₃</u>TATCAATATCCACCTGCAG<u>₃</u>TTCTACCAAAAGTGTA<u>₃</u>TTTGGAAACTGCTCCATCAAAA<u>₃</u>GGCATGTTTCAGCTGAA...</p> <p>*3' TAGTTATA<u>₃</u>GGTGGACGTC<u>₃</u>CAAGAT<u>₃</u>GGTTTTCACATAAAACCTTTGACGAG<u>₃</u>GGTAGTTTCCGTTACAAGTCGACTT...</p> <p>Red arrows indicate oxidation sites: 1, 2, 3, 4, 5, 6, 7.</p>
Duplex 2-Rh, Bare	<p>Rh5' <u>₃</u>TATCAATATCCACCTGCAG<u>₃</u>TTCTACCAAGAGTGTA<u>₃</u>TTTGGAACTGCTCCATCAAAA<u>₃</u>GGCATGTTTCAGCTGAA...</p> <p>*3' TAGTTATA<u>₃</u>GGTGGACGTC<u>₃</u>CAAGAT<u>₃</u>GGTTCTCACATGAACCTTTGACGAG<u>₃</u>GGTAGTTTCCGTTACAAGTCGACTT...</p> <p>Red arrows indicate oxidation sites: 1, 2, 3, 4, 5, 6, 7, 8.</p>
Duplex 2-Rh, NCP	<p>Rh5' <u>₃</u>TATCAATATCCACCTGCAG<u>₃</u>TTCTACCAAGAGTGTA<u>₃</u>TTTGGAACTGCTCCATCAAAA<u>₃</u>GGCATGTTTCAGCTGAA...</p> <p>*3' TAGTTATA<u>₃</u>GGTGGACGTC<u>₃</u>CAAGAT<u>₃</u>GGTTCTCACATGAACCTTTGACGAG<u>₃</u>GGTAGTTTCCGTTACAAGTCGACTT...</p> <p>Red arrows indicate oxidation sites: 1, 2, 3, 4, 5, 6, 7, 8.</p>

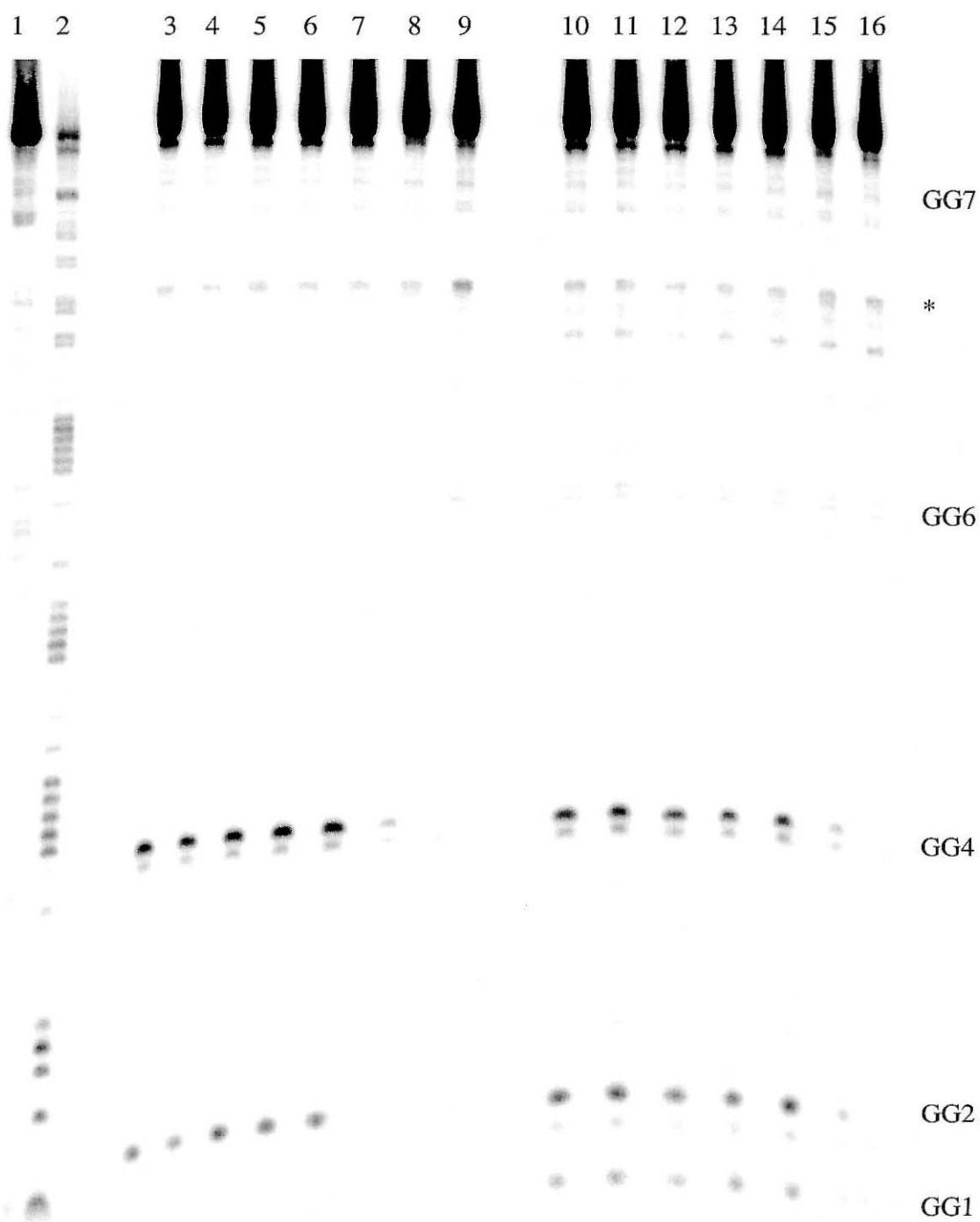
[†] Photoinduced oxidation of 5'-GG-3' sites (red) by covalently-tethered rhodium complexes is indicated by red arrows. The size of the red arrows indicates the extent of oxidation, to a first approximation. Fewer than 1% of strands are oxidized at GG5, GG6, GG7, or GG8.

Since we had previously observed an increase in long-range oxidative damage with increased temperature, we examined the guanine oxidation on duplex **1-Rh** in the presence and absence of histone proteins at various temperatures between 5°C and 35°C (Fig. 5.8). However, in this case, variations in temperature do not change the yield of long-range oxidation, nor do they change the patterns of guanine oxidation on duplex **1-Rh**. At none of these temperatures, in either the presence or absence of histone proteins, do we observe oxidation at the more distal 5'-GG-3' sites.

Subtle, temperature-independent differences in the pattern of guanine oxidation were caused by the binding of histone proteins in some experiments and can be seen here (Fig. 5.8). Oxidation at the GG1 site is slightly increased, whereas oxidation at the GG4 site is slightly diminished in the presence of bound histones compared to their absence. The very minor differences are seen between bare and histone-bound DNA may be due to mild disruptions in the base stack caused by bending of the DNA into a superhelix, lack of dynamic flexibility in the structure of the DNA when “clamped down” by protein binding, or local structure-dependent effects on charge localization and trapping of the radical species. What is striking is that, despite the multitude of factors which could potentially modulate long-range guanine oxidation, the pattern of oxidation is relatively unchanged by binding of the DNA to histone proteins as a nucleosome core particle.

We also attempted to increase the very long-range guanine oxidation (>30 bp) by making small changes in the DNA sequence to reduce its kinks and/or bendability in the absence of protein. Duplex **2-Rh** was constructed, in which three AT base pairs in *A-tract sequences* were changed to GC base pairs in each half of the palindromic sequence (Table 5.2). This base pair change also introduced a new 5'-GG-3' site into the sequence. Despite the changes in the

Figure 5.8: Long-range oxidation of 5'-GG-3' sites in the presence and absence of bound histone proteins at a range of temperatures. All samples contain duplex **1-Rh** with the right-handed Δ isomer of the rhodium metallointercalator. Lanes **1** and **2** are Maxam-Gilbert purine-specific and pyrimidine-specific sequencing lanes, respectively. Lanes **3-9** are samples containing bare DNA without histone proteins; samples in lanes **10-16** contain bound histone proteins. All samples were photoirradiated at 365 nm for one hour, unless otherwise indicated: Lane **3**: 5°C; **4**: 15°C; **5**: 22°C; **6**: 27°C; **7**: 35°C; **8**: 10 min. at 313 nm, 27°C; **9**: no photoirradiation; **10**: 5°C; **11**: 15°C; **12**: 22°C; **13**: 27°C; **14**: 35°C; **15**: 10 min. at 313 nm, 27°C; **16**: no photoirradiation. All samples were treated with hot aqueous piperidine. The band at the center of the gel, indicated by an asterisk, is due to incomplete ligation to form the 146-mer. 5'-GG-3' sites are indicated by numbers corresponding to Table 5.3.



sequence of the oligonucleotide, the pattern of guanine oxidation on duplex **2-Rh** was unchanged from the pattern on duplex **1-Rh**. In the absence of protein, oxidation is observed at GG1, GG2, GG3, and GG4, located 8, 11, 16, and 24 base pairs away from the closest intercalated metal complex. However, there is almost no oxidation at GG5, GG8, GG6, and GG7, located 37, 42, 48 and 56 base pairs from the intercalation site respectively (Table 5.4). As with duplex **1-Rh**, the binding of histone proteins makes very little change in the pattern of oxidation, except to very slightly favor oxidation of GG1 and slightly disfavor GG4. It is quite likely that more systematic and drastic changes in the DNA sequence would increase long-range charge transport to the other 5'-GG-3' sites in the absence of protein; however, these changes would also probably diminish the affinity of this sequence for the histone octamer and change the structure of the nucleosome core particle.

5.3.5 Oxidation of Guanine Bases by Charge Transport Through the Base Stack in Nucleosomal DNA

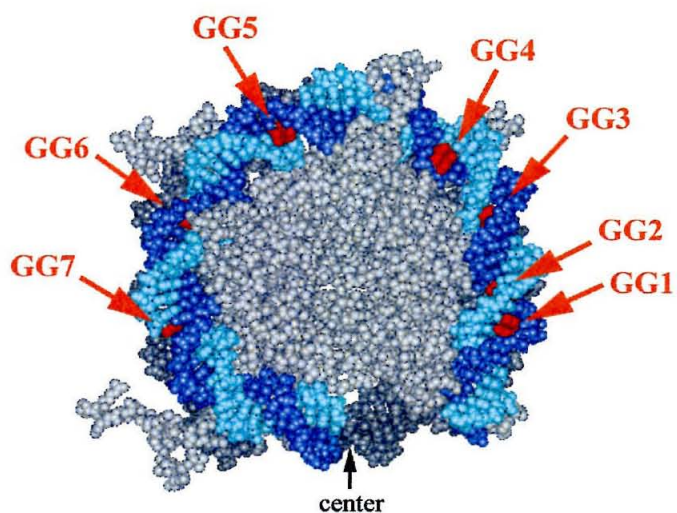
In this study we describe the oxidation of guanine doublets in nucleosome core particles by rhodium intercalators to determine the effect of DNA packaging on long range charge transport through the base pair stack. Given that the DNA in the core particle is overwound, bent, and in some places dynamically restricted, it was possible that binding of DNA to histones in this structure might serve to protect nucleosomal DNA from long-range oxidative damage. Alternatively, such packaging might provide a unique and isolated medium to facilitate charge transport through the DNA base pair stack. The base pair stacking seen in the crystal structure of the nucleosome core particle is relatively normal (i.e., B-form), and the binding of some proteins has previously been shown to increase long-range guanine oxidation by stiffening the helix (2,3).

The binding of histone proteins to a 146-base-pair oligonucleotide duplex to form a nucleosome core particle was observed to radically diminish binding of rhodium complexes to the DNA, consistent with previous research on ethidium and other intercalators. The structure of the nucleosome core particle is proposed to exclude intercalators by clamping down on the DNA and preventing the unwinding and destacking necessary for intercalation, causing the intercalators to bind preferentially to linker DNA and the termini of core DNA. Notably, despite its radically diminished binding, when our noncovalent rhodium intercalator is photoexcited in the presence of the nucleosome core particle, it selectively oxidizes all of the 5' guanines of 5'-GG-3' sites (Fig. 5.9). This pattern of damage is the signature of charge transport through the DNA base stack, indicating that although the DNA bound as nucleosome core particles is relatively protected from attack from small molecule intercalators by the histone proteins, it is still accessible to damage by long-range oxidation. When the rhodium complex is covalently tethered to the end of the DNA duplex, guanine doublets up to 24 base pairs away are oxidized through the base stack (Fig. 5.9). This long-range oxidation is not significantly modulated by binding of the DNA to histone proteins to form a nucleosome core particle. The kinks and flexibility of the DNA sequence alone, which dictates to some large degree its own nucleosomal packaging, have a much larger effect on the ability of charges to move through DNA than does binding to a histone octamer.

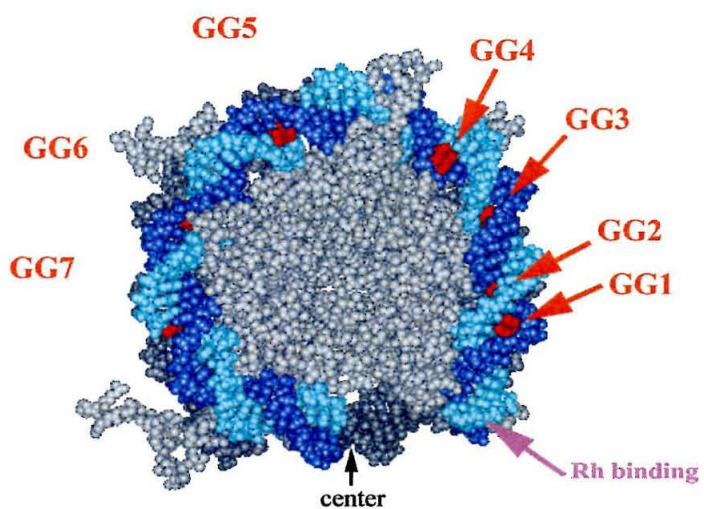
The long-range oxidation of guanine bases at sites made inaccessible to rhodium complexes by protein binding is consistent with our observation of the oxidation of guanine doublets and triplets in transcription factor binding sites in the PGK promoter within nuclei (chapter 6). Furthermore, these discoveries have important implications for damage to and repair of the genome *in vivo*, where much of the DNA is bound to nucleosome core particles. Although it has

Figure 5.9: Oxidation of guanine doublets in nucleosomal DNA by rhodium metallointercalators. One-half of the palindromic 146-base-pair sequence is shown in blue and cyan, with 5'-GG-3' sites highlighted in red and numbered according to Table 5.3. The other half of the DNA palindrome, which is identical to this half, and the histone octamer are shown in grey. On the top, although noncovalent rhodium complexes bind to duplex **1** less in the presence of histone proteins, they can oxidize the 5' guanine of all seven 5'-GG-3' sites when photoexcited at 313 or 365 nm (red arrows). This pattern of DNA damage is characteristic of long-range oxidation through the base-pair stack. The sites of rhodium binding, and therefore the distances over which charges can migrate, could not be determined in this system. On the right, covalently-tethered rhodium complexes intercalate into duplex **1-Rh** near the ends to which they are attached (purple arrow), oxidizing GG1, GG2, GG3, and GG4, corresponding to 5'-GG-3' sites 8, 11, 16, and 24 base pairs from the site of intercalation (red arrows). Guanine doublets near the center of the nucleosomal DNA (GG5, GG6, and GG7) were not oxidized either in the presence or absence of protein. Binding of histone proteins to form nucleosomes appears to have very little effect on long-range charge transport through DNA. (Picture adapted from PDB coordinates 1aoi, reference 4.)

Duplex 1 with Noncovalent Rhodium



Duplex 1-Rh with Covalently-Tethered Rhodium



been proposed that histones function to protect DNA in addition to packaging and regulating it, it appears that packaging of DNA as nucleosomes does not protect it from long-range damage through the base pair stack. As a result, damage generated on DNA may be spread from an initial exposed site to divergent distal sites within transcriptionally inactive regions of the DNA packaged within nucleosomes. Damage within nucleosomes is likely to be detected and repaired less readily than active and accessible regions of the genome, allowing for the persistence of damaged sites generated by long-range charge transport and the propagation of these damage events to form permanent mutations.

5. 4 References

1. B. Lewin, *Genes VII*, Oxford University Press, Oxford, England (2000).
2. S.R. Rajsiki, S. Kumar, R. J. Roberts, J. K. Barton, *J. Am. Chem. Soc.* **121**, 5615 (1999).
3. S. R. Rajsiki, J. K. Barton, *Biochemistry* **40**, 5556 (2001).
4. K. Luger, A. Mäder, R. Richmond, D. Sargent, T. Richmond, *Nature* **389**, 251 (1997).
5. H. Drew, C. Calladine, *J. Mol. Biol.* **195**, 143 (1987).
6. D. J. Fitzgerald, J. N. Anderson, *Nucleic Acids Res.* **26**, 2526 (1998).
7. T. E. Shrader, D. M. Crothers, *Proc. Natl. Acad. Sci. USA* **86**, 7418 (1989).
8. J. M. Harp, B. L. Hanson, D. E. Timm, G. J. Bunick, *Acta Cryst. D* **56**, 1513 (2000).
9. L. Lutter, *J. Mol. Biol.* **124**, 391 (1978).
10. R. D. Kornberg, J. W. LaPointe, Y. Lorch, *Meth. Enzymol.* **170**, 3 (1989).
11. K. Luger, T. J. Rechsteiner, T. J. Richmond, *Meth. Enzymol.* **304**, 3 (1999).
12. M.E. Núñez, S. R. Rajsiki, J. K. Barton, *Meth. Enzymol.* **319**, 165 (2000).
13. J. Sambrook, E. F. Fritsch, T. Maniatis, *Molecular Cloning: A Laboratory Manual*, 2nd ed. Cold Spring Harbor Laboratory, New York (1989).
14. R. E. Holmlin, P. J. Dandliker, J. K. Barton, *Bioconj. Chem.* **10**, 1122 (1999).
15. M. E. Núñez, D.B. Hall, J. K. Barton, *Chem. Biol.* **6**, 85 (1998).
16. J. J. Hayes, K.-M. Lee, *Methods* **12**, 2 (1997).
17. L. Lutter, *Meth. Enzymol.* **170**, 264 (1989).
18. A. Sitlani, E. C. Long, A. M. Pyle, J. K. Barton, *J. Am. Chem. Soc.* **114**, 2302, (1992).
19. K. Uchida, A. M. Pyle, T. Morii, J. K. Barton, *Nucleic Acids Res.* **17**, 10259 (1989).
20. D. B. Hall, R. E. Holmlin, J. K. Barton, *Nature (London)* **382**, 731 (1996).

21. K. Nguyen et al., *J. Am. Chem. Soc.* **122**, 3585 (2000).
22. M. Bellard, G. Dretzen, A. Giangrande, P. Ramain, *Meth. Enzymol.* **170**, 317 (1989).
23. I. Cartwright, C. Elgin, *Meth. Enzymol.* **170**, 359 (1989).
24. P. Brown, K. Fox, *Biochem. J.* **319**, 607 (1996).
25. J. M. Gottesfeld et al., *J. Mol. Biol.* **309**, 615 (2001).
26. J. T. Millard, *Biochimie* **78**, 803 (1996).
27. C. T. McMurray, K. E. van Holde, *Biochemistry* **30**, 5631 (1991).
28. C. T. McMurray, E. W. Small, K. E. van Holde, *Biochemistry* **20**, 5644 (1991).
29. J. B. Chaires, N. Dattagupta, D. M Crothers, *Biochemistry* **22**, 284 (1983).
30. P. Hagmar, S. Pierrou, P. Nielsen, B. Nordén, M. Kubista, *J. Biomol. Struct. Dyn.* **9**, 667 (1992).
31. L. Yu, I. Goldberg, P. Dedon, *J. Biol. Chem.* **269**, 4144 (1994).
32. K. Fox, personal communication.
33. B. A. Jackson, J. K. Barton, *J. Am. Chem. Soc.* **119**, 12986 (1997).
34. B. A. Jackson, V. Y. Alekseyev, J. K. Barton, *Biochemistry* **38**, 4655 (1999).
35. P. T. Henderson, D. Jones, G. Hampikian, Y. Kan, G.B. Schuster, *Proc. Natl. Acad. Sci. USA* **96**, 8353 (1999).
36. D. B. Hall, J. K. Barton, *J. Am. Chem. Soc.* **119**, 5045 (1997).
37. T. T. Williams, D. T. Odom, J. K. Barton, *J. Am. Chem. Soc.* **122**, 9048 (2000).
38. C. von Holt et al., *Meth. Enzymol.* **170**, 431 (1989).

Chapter 6

Evidence for DNA Charge Transport in the Nucleus

6.1 Introduction

DNA inside of cells can be damaged by a variety of agents to generate unnatural and potentially mutagenic base lesions (1). Modified or functionalized bases can be induced by direct ionization by high-energy X-ray and γ -ray sources, irradiation with UV light, interactions with reactive oxygen species, and reactions with a diverse set of small molecules, both therapeutic and carcinogenic. Studies of DNA-mediated charge transport have elucidated another possible mechanism for the generation of base lesions (2,3). A variety of methods have demonstrated that the stacked aromatic base pairs of DNA provide an efficient medium for charge transport, including oxidation of bases from a distance through the base pair stack (4,5). A metallointercalator covalently tethered to one terminus of an oligodeoxynucleotide duplex can oxidize 5'-GG-3' sequences up to 200 Å away (6,7). The efficiency of this long-range oxidation displays a very weak dependence on distance, but it is sensitive to coupling of the oxidant into the base pair stack and to the stacking of the intervening base pairs (2,8-10). Because of their well-characterized binding and photochemical properties, rhodium(III) complexes were first utilized to study oxidative DNA damage from a distance, but long-range oxidative damage has now been demonstrated using a variety of photooxidants, indicating that this reaction is characteristic of the DNA itself and is not a property of an unusual photooxidant. Photoactivation of naphthalimides, Ru(III) intercalators, ethidium, anthraquinones, and even sugar radicals have been shown to promote oxidative damage to 5'-GG-3' sites from a distance (11-16).

To examine whether charge migration through DNA occurs within the cell, isolated whole nuclei were incubated with a rhodium intercalator, $\text{Rh}(\text{phi})_2\text{DMB}^{3+}$ and then irradiated with ultraviolet light above ~320 nm. Phenanthrenequinone diimine (phi) complexes of rhodium bind to DNA avidly from the major groove by intercalation of the phi ligand into the base pair stack

(17) (Fig. 1.8). These complexes react with DNA according to two distinct mechanisms when irradiated between 300 and 400 nm (Fig. 6.1). They generate a frank strand break at the intercalation site, giving products consistent with the abstraction of the 3' hydrogen of the sugar by the metal complex (18). A variety of products, including 3' or 5' phosphates, free bases, base propenoic acids, and 3' phosphoglycaldehydes are formed without further treatment (Fig. 1.4). Since this reaction does not involve a diffusible intermediate, it can be used to determine precisely where the metal complex is bound. Phi complexes of rhodium can also oxidize guanine bases through a long-range reaction which is mediated by the DNA π stack (2,6). The oxidized guanine radical intermediates are trapped by oxygen or water to form a variety of irreversible products including 8-oxo-guanine, formamidopyrimidine, oxazalone, and imidazalone derivatives (19). These modified base products do not generally disrupt the sugar-phosphate backbone, but they can be converted to strand breaks with 5' phosphate termini by subsequent treatment with a mixture of the base-excision repair enzymes endonuclease III (EndoIII) and formamidopyrimidine DNA glycosylase (Fapy glycosylase). The hydrogen abstraction and long-range oxidation reactions can be isolated by excitation with specific wavelengths of light. However, when the metal complex is irradiated with both wavelengths of light simultaneously, as we have done here, a combination of products results. It is then possible to determine which bases are oxidized by looking at the *difference* between the cleavage events in the absence of Fapy glycosylase/EndoIII (frank strand breaks) and presence of Fapy glycosylase/EndoIII (base oxidation chemistry plus frank strand breaks).

Using ligation-mediated PCR (LMPCR), the pattern of base damage was determined for genes of interest. Preferential oxidation of 5' guanines of 5'-GG-3' doublets and other guanine multiplets is the characteristic signature of charge

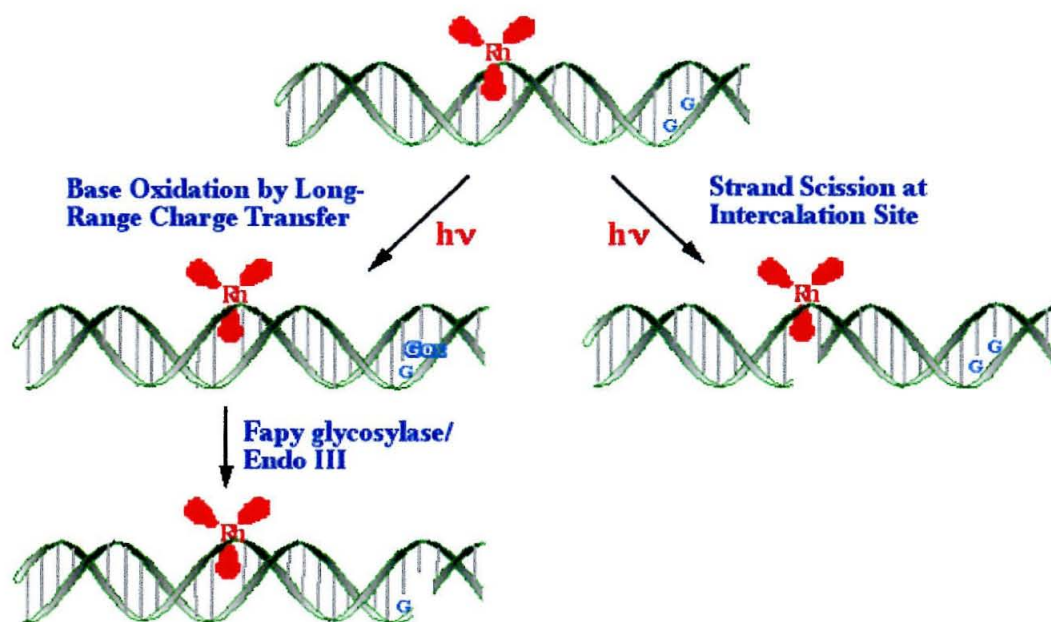


Figure 6.1: Mechanisms of DNA photocleavage by $\text{Rh}(\phi)_2\text{DMB}^{3+}$. Upon photoexcitation with near-ultraviolet light, the complex oxidizes the 5' guanine of 5'-GG-3' sites from a distance by long-range charge transfer through the DNA base pair stack. The damaged guanine bases that result from this oxidation are revealed by treatment with the base excision repair enzymes formamido-pyrimidine DNA glycosylase and endonuclease III (Fapy glycosylase/EndoIII). When the rhodium complex is photoexcited at higher energy, sugar phosphate backbone is cleaved directly at the site of intercalation. These frank strand breaks do not require enzyme treatment to be revealed. When the metal complex is irradiated with both wavelengths of light simultaneously, a combination of products results. It is then possible to determine which bases are oxidized by looking at the *difference* between the cleavage events in the absence of Fapy glycosylase/EndoIII (frank strand breaks) and presence of Fapy glycosylase/EndoIII (base oxidation chemistry plus frank strand breaks).

transfer through the DNA base stack, whereas oxidation of all guanines equally or reaction of other bases points to a different mechanism of damage (2,19). Guanine bases are oxidized preferentially because they have the lowest oxidation potential of the four canonical nucleotide bases (20), and a selectivity for 5' guanines of 5'-GG-3' sites arises from the effects of base stacking on the ionization potentials of the bases (21,22). Oxidation potentials increase across the series 5'-GGG-3' < 5'-GG-3' < 5'-GA-3' << 5'-GC-3', 5'-GT-3'.

6.2 Methods

6.2.1 Photoirradiations with $Rh(phi)_2DMB^{3+}$ and Isolation of DNA

Three classes of samples were prepared that were incubated with rhodium and irradiated: whole cells, nuclei, and bare genomic DNA. The isolation of first the nuclei and then the DNA was identical in all three cases, but the rhodium and light were applied at different points in the purification process.

To remove the red indicator dye from the cell culture medium, *HeLa* cells were first rinsed in Hank's medium without phenol red. The cells were then covered in Hank's medium without phenol red plus 90 μM $Rh(phi)_2DMB^{3+}$ and incubated for 1 hour at 37°C in the dark before photoirradiation for 2.5 hours on ice with an Oriel solar simulator and a 360 nm cutoff filter. Some cells were permeabilized by treatment for one minute with 0.05 % lysolecithin (Sigma Chemical Co.) in sterile medium before the rhodium incubation (23). "Light control" and "dark control" samples which lacked either irradiation or rhodium were prepared identically except for the exclusion of light or rhodium. Following irradiation, nuclei were isolated immediately.

Nuclei were isolated from *HeLa* cells as described (23). The medium was removed from the petri dish and the cells were incubated for 5 minutes in cold buffer A (where buffer A is 0.3M sucrose, 60 mM KCl, 15 mM NaCl, 60 mM

Tris-HCl pH 8, 0.5 mM spermidine, 0.15 mM spermine, 2 mM EDTA) plus 0.5% Nonidet. The cells were then scraped off of the plates with a sterile, disposal plastic cell scraper, and removed to a 50 mL conical centrifuge tube, in which the nuclei were pelleted by centrifugation for 5-10 minutes at 1000 x g. The solution containing the cell debris was discarded, and the pellet of nuclei was rinsed with 5 mL buffer A and recentrifuged. The rinse solution was also discarded. Nuclei which were irradiated at this stage were gently resuspended in 1 mL of buffer A with 33 μ M Rh(phi)₂DMB³⁺ and immediately photoirradiated on ice for 1 hour using an Oriel UV solar simulator and a 360 nm cutoff filter. "Light control" and "dark control" samples which lacked either irradiation or rhodium were also prepared. After irradiation, the nuclei were then pelleted by centrifugation. The pellets of nuclei were frozen in 1 mL buffer A at -70°C.

The polyamines spermine and spermidine were used in small amounts in the nuclear isolation buffer to maintain ionic strength. Although the presence of polyamines does not affect the *pattern* of protein footprints as measured using photoexcited rhodium complexes, oxidation of guanine bases is enhanced relative to the frank strand breaks and other background. Control samples lacking rhodium show no frank breaks or base oxidation, indicating that the polyamines are incapable of oxidizing the DNA themselves.

Genomic DNA was isolated from nuclei by resuspending the nuclei gently but thoroughly in 5 mL of buffer B (where B=150 mM NaCl, 5 mM EDTA, pH 7.8). 5 mL of buffer C (20 mM Tris-Cl pH 8, 20 mM NaCl, 20 mM EDTA, 1% SDS) were added to lyse the nuclei and release their contents into the solution. To the mixture was added 600 ug/mL of proteinase K and 100 ug/mL of RNase A with gentle swirling, and the solution was incubated at 37°C for 4 hours or longer (until clumps of cellular material were no longer visible). The DNA was extracted with Tris-saturated phenol and chloroform and ethanol precipitated

with 2.5 equivalents of ethanol and 200 mM NaCl. The DNA was pelleted, rinsed with 70 % ethanol, and allowed to air dry. The DNA was then allowed to resuspend gradually in 1X TE at 4°C overnight, without vortexing or pipetting to resuspend, and was then quantitated by UV-visible spectroscopy at 280 nm. Naked genomic DNA was suspended in TE to ~100 µg/mL with 33 µM Rh and irradiated for 1 hour without preincubation. “Dark control” and “light control” samples which lacked either Rh or irradiation were also prepared. After irradiation, DNA was ethanol precipitated to remove rhodium.

The DNA was treated with Fapy DNA glycosylase and endonuclease III to remove a variety of modified base lesions and breaks in the DNA backbone, generating 5' phosphate termini (24). 25 µg aliquots of DNA were incubated with 1000 ng of Fapy DNA glycosylase and 250 ng endonuclease III in 250 µL buffer N (50 mM Tris-HCl pH 7.6, 100 mM KCl, 1 mM EDTA, 0.1 mM DTT, 100 µg/mL BSA) at 37°C for at least 1 hour. The reaction was stopped by the addition of 100 µL of water and 50 µL of 0.8% SDS with mixing. The DNA was extracted with phenol and chloroform, and precipitated with 18 µL of 5M NaCl and 1 mL of 100% ethanol. The pellet was rinsed with 80% ethanol and air dried. The DNA was allowed to resuspend in 20 µL of 1X TE overnight at 4°C.

6.2.2 Denaturing Agarose Gel Electrophoresis

The strand break frequency was estimated by denaturing agarose gel electrophoresis utilizing glyoxal (25). The 0.7% agarose gel was prepared in 10 mM sodium phosphate pH 7 and run in the same buffer, which was constantly-recirculated to maintain its pH. The DNA was modified with glyoxal by incubation in the following mix at 50°C for 1 hour: 5µg DNA, 10 mM sodium phosphate pH 7, 1M glyoxal, 50% (v/v) DMSO, 20 µL final volume. Added to the DNA samples was 4 µL loading buffer (10 mM sodium phosphate pH 7, 50 %

glycerol, 0.25% bromophenol blue, 0.25% xylene cyanol). The gel was run at 50 V for 2.5 hours, and stained with 10 µg/mL acridine orange for 45 minutes.

6.2.3 Ligation-Mediated PCR Amplification of DNA

DNA samples and Maxam-Gilbert sequencing standards were amplified by LMPCR manually (26). Ligation-mediated PCR involves first a primer-extension step followed by ligation of a linker to the blunt ends of the DNA. PCR is then carried out using primers to the gene of choice on one end and to the linker on the other. A series of nested primers are used for these steps to increase the specificity of the amplification for the gene of choice (Fig. 6.2). Procedures for the amplification of the PGK promoter region are detailed below, and the primers are shown in Table 6.1 (27). Procedures for amplification of the p53 exon 5 are the same except for the sequence of the primers and the annealing temperatures.

The primer extension solution contained the following components (indicated concentrations are for the stock solutions, not for the final reaction solution): 1 µL of 1 µg/µL of DNA, 1 µL of 10X *Pfu* buffer, 0.8 µL of 2.5 mM dNTPs, 0.6 µL of 2 µM primer 1, 1.0 µL of 70% sucrose, 0.2 µL of *Pfu* “Turbo” polymerase, and 5.4 µL of dH₂O, in a final volume of 8.0 µL.

The samples were incubated on a thermocycler according to the following program: 95°C for 5 minutes, 60°C for 30 minutes, 75°C for 10 minutes.

The ligation reaction added a double-stranded linker piece to the blunt ends created by the enzyme digestion and primer extension: 0.46 µL of 1M Tris HCl pH 7.5, 1.02 µL of 100 mM MgCl₂, 0.32 µL of 1M DTT, 0.16 µL of 100 mM ATP, 0.78 µL of 1 mg/mL BSA, 1.6 µL of 20 µM linker, 1.7 µL of dH₂O, and 0.32 µL of 20 U/µL T4 DNA ligase, in 6.4 µL final volume. This ligation mixture was incubated at 17°C overnight.

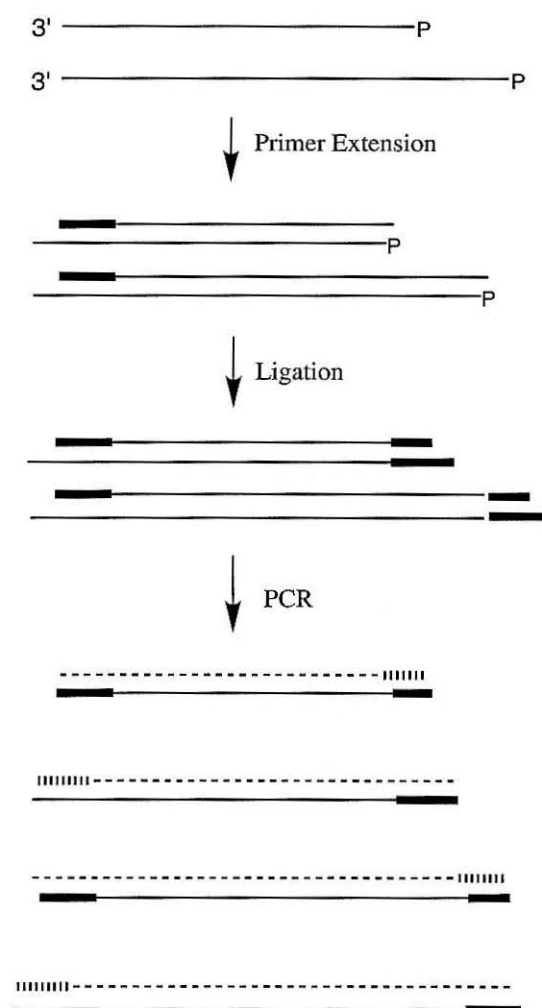


Figure 6.2: LMPCR amplification of DNA. DNA that has been cleaved chemically, photochemically, or enzymatically to create a 5' phosphoryl end can be amplified by this method. First, a double-stranded piece of DNA with a blunt end is produced by primer-extension, and a linker is ligated onto the blunt end of the DNA. PCR is then carried out using primers to the gene of choice on one end and to the linker on the other. A series of nested primers are used for the primer extension and PCR steps to increase the specificity of the amplification for a single gene.

Table 6.1: Ligation-mediated PCR primers

PGK Transcribed (Forward) Strand

1: 5'-CCTGGGTCTCGCACATTC-3'

2: 5'-GCACATTCTTCACGTCCGTTTCGCA-3'

3: 5'-CACGTCCGTTTCGCAGCGTCACC-3'

PGK Nontranscribed (Reverse) Strand

1: 5'-GGGAGAGAGGTCGGTGATT-3'

2: 5'-GGTGATTCGGTCAACGAGGGAG-3'

3: 5'-GGTCAACGAGGGAGCCGACTG-3'

p53 Nontranscribed Strand

1: 5'-TGGGGACCCTGGGCAA-3'

2: 5'-GCAACCAGCCCTGTCGTCTC-3'

3: 5'-CAACCAGCCCTGTCGTCTCTCC-3'

*Linker*5'-GCGGTGACCCGGGAGATCTGAATTC-3'
3'-CTAGACTTAAG-5'*Linker Primer*

5'-GCGGTGACCCGGGAGATCTGAATTC-3'

The DNA was then amplified by the polymerase chain reaction with a primer specific for the gene of interest and another specific to the linker: 1.0 μL of 70% sucrose, 0.67 μL of 10 X *Pfu* buffer, 0.4 μL of 25 mM dNTPs, 0.2 μL of 20 μM primer 2, 0.2 μL of 20 μM linker primer, 0.4 μL of *Pfu* turbo enzyme, and 0.6 μL of dH_2O , in a total volume of 3.5 μL . 3.5 μL of this mixture of PCR components was added to 8 μL of the previous ligation mix. The thermocycler program heated the samples according to the following protocol: 1 cycle: 2 min at 95°C, 2 min. at 64°C, 3 min. at 76°C. 18 cycles: 45 sec. at 95°C, 2 min. at 64°C, 3 min. at 76°C. 1 cycle: 10 min. at 76°C. 1 cycle: store at 6°C.

The samples were next treated with 1 μL of 1U/ μL exonuclease at 37 °C for 30 min. to remove leftover primers, followed by incubation at 72°C to kill the exonuclease.

Finally, the samples were PCR amplified with labeled nested primers. In this case, the label was an IR-fluorescing molecule, but a radioactive label might be used as well. The PCR reaction mix contained 1.0 μL of 70% sucrose, 0.35 μL of 10 X *Pfu* buffer, 1 μL of 20 μM *primer 3, and 1.15 μL of dH_2O , in a final volume of 3.5 μL . Samples were heated according to the following thermocycler program: 1 cycle: 2 min. at 95°C. 5 cycles: 45 sec. at 95°C, 3 min. at 66°C, 2 min. at 76°C. 1 cycle: 10 min. at 76°C. To this final reaction mix was added 3 μL of stop solution/running dye and 2 μL was loaded onto the gel.

The products were separated and visualized by denaturing polyacrylamide gel electrophoresis using a LI-COR DNA model 4200 automated sequencer (LI-COR, Inc., Lincoln, NB). The resulting data were analyzed using the “RFLP Scan” program (Scanalytics, Inc., Fairfax, VA), which allowed quantitation of the intensity of each band in each lane, and the resulting intensity values were imported into Microsoft Excel for processing. Data sets were normalized if necessary to account for uneven gel loading by multiplying each measurement in

one lane uniformly by a constant such that the total intensity of each lane (sum of all of the band intensities) was the same. Because the products of the cleavage reactions are amplified through a series of LMPCR steps, it is generally not feasible to combine the results of multiple manual experiments directly to obtain error bars (however, see 27). As a result each of the histograms shown in this paper illustrates the data from a single experiment. However, all of the experiments were repeated multiple times, both from the LMPCR step forward and also from the first DNA isolation and nuclear irradiation steps using new batches of *HeLa* cells, to assure that the patterns of frank strand breaks and base oxidation are reproducible.

Control samples were prepared for both naked and nuclear DNA lacking rhodium, UV-irradiation, or both. No bands appeared in these control lanes in the p53 region. PCR amplification of the PGK region showed five bands above background that were deleted from all data sets.

6.3 Results and Discussion

6.3.1 Photoirradiation of Cells, Nuclei, and Bare Genomic DNA with $Rh(\phi)_2DMB^{3+}$

Cells, nuclei, and bare genomic DNA were photoirradiated with $Rh(\phi)_2DMB^{3+}$ to determine if the patterns of DNA damage are the same in the cellular environment as in the test tube. Most important to us is the question of whether long-range charge transport can occur in the cell unimpeded by proteins and other nuclear components which might serve to protect DNA *in vivo* from damage. In order to answer this question, we first had to put the rhodium metallointercalator into the nucleus, which proved to be somewhat challenging. Although photoactivated rhodium complexes efficiently cut bare genomic DNA and DNA in isolated nuclei, very little DNA damage was induced by

photoactivated rhodium on DNA in cells when it was simply added to the medium and photoirradiated. Incubating cells with rhodium complex in the dark beyond one hour did not increase the amount of DNA cleavage, but photoirradiation for 2.5 hours resulted in more DNA cleavage than after 1 hour, although there was appreciable photodecomposition of the rhodium complex (as observed by the loss of orange color in the solution) at these long irradiation times. Even so, the amount of direct photocleavage was insufficient for LMPCR amplification (not shown). Consistent with the idea that the rhodium complex was unable to cross the plasma membrane to access the interior of the cell and the nucleus, permeabilization of the cells with lysolecithin before the rhodium incubation introduced a larger amount of rhodium- and light-dependent DNA damage.

The amount of direct photocleavage and enzyme-revealed base damage was assessed using denaturing agarose gel electrophoresis of purified genomic DNA (Fig. 6.3). On a denaturing agarose gel, long, relatively undamaged pieces of DNA run near the top of the gel, whereas shorter pieces generated by breaks in the sugar-phosphate backbone run near the bottom of the gel. The more strand breaks are present, the smaller the pieces of DNA. This analysis reveals that, in general, DNA treated with rhodium intercalators and light (whether as bare DNA, nuclear DNA, or cellular DNA) are cleaved more than control samples that were not photoirradiated or treated with rhodium. The "light-" and "dark control" samples were themselves cleaved no more than the completely untreated control samples. Clearly then the strand breaks which are observed are due to the rhodium photochemistry and not to direct interaction with the light source or a cellular response to the rhodium complexes. Nevertheless, nuclear and cellular DNA was less efficiently cleaved by the metallointercalator than bare DNA, resulting in larger and less uniformly-sized pieces. Samples containing photoexcited rhodium that were not treated with a mixture of Fapy glycosylase

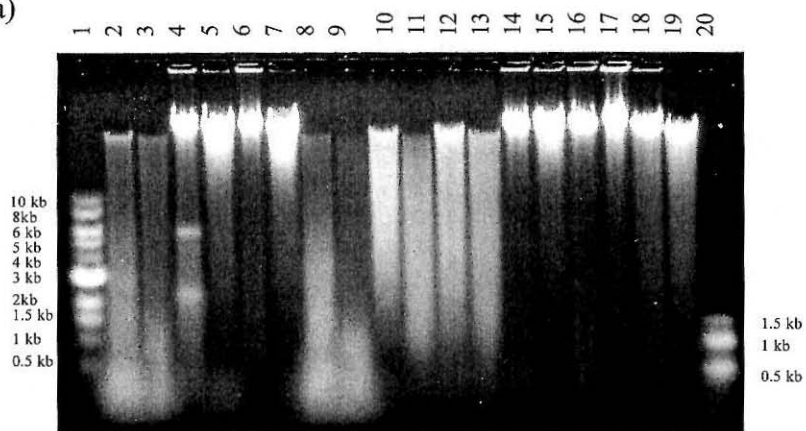
Figure 6.3: Denaturing agarose gels for analysis of DNA cleavage efficiency.

Sample names indicate the stage in the purification process in which the samples were incubated with rhodium and/or photoirradiated. “Dark control” samples were incubated with rhodium but not photoirradiated; “light control” samples were photoirradiated by not incubated with rhodium. Details of the sample preparation are described in the text.

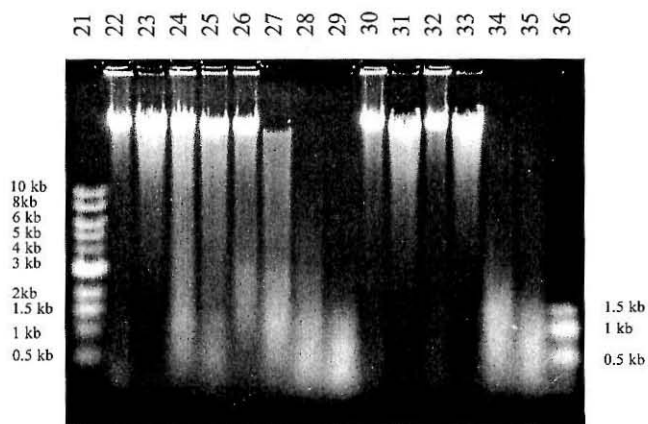
(a) Lane **1**: “1 kb ladder” size standard; **2**: cells; **3**: cells with Fapy/EndoIII; **4**: cells dark control; **5**: cells dark control with Fapy/Endo III; **6**: cells light control; **7**: cells light control with Fapy/EndoIII; **8**: cells (modified filter); **9**: cells (modified filter) with Fapy/EndoIII; **10**: nuclei with polyamines; **11**: nuclei with polyamines and Fapy/EndoIII; **12**: nuclei without polyamines; **13**: nuclei without polyamines with Fapy/EndoIII; **14**: nuclei dark control; **15**: nuclei dark control with Fapy/EndoIII; **16**: nuclei light control ; **17**: nuclei light control with Fapy/EndoIII; **18**: nuclei without polyamines (modified filter); **19**: nuclei without polyamines (modified filter) with Fapy/Endo III; **20**: “100 bp ladder” size standard.

(b) Lane **21**: “1 kb ladder” size standard; **22**: no treatment control; **23**: no treatment control with Fapy/EndoIII; **24**: bare DNA 16 μM Rh; **25**: bare DNA 16 μM Rh with Fapy/EndoIII; **26**: bare DNA 8 μM Rh; **27**: bare DNA 8 μM Rh with Fapy/EndoIII; **28**: bare DNA 33 μM Rh; **29**: bare DNA 33 μM Rh with Fapy/EndoIII; **30**: bare DNA dark control; **31**: bare DNA dark control with Fapy/EndoIII; **32**: bare DNA light control; **33**: bare DNA light control with Fapy/EndoIII; **34**: bare DNA 16 μM Rh (modified filter); **35**: bare DNA 16 μM Rh (modified filter) with Fapy/EndoIII; **36**: “100 bp ladder” size standard.

(a)



(b)

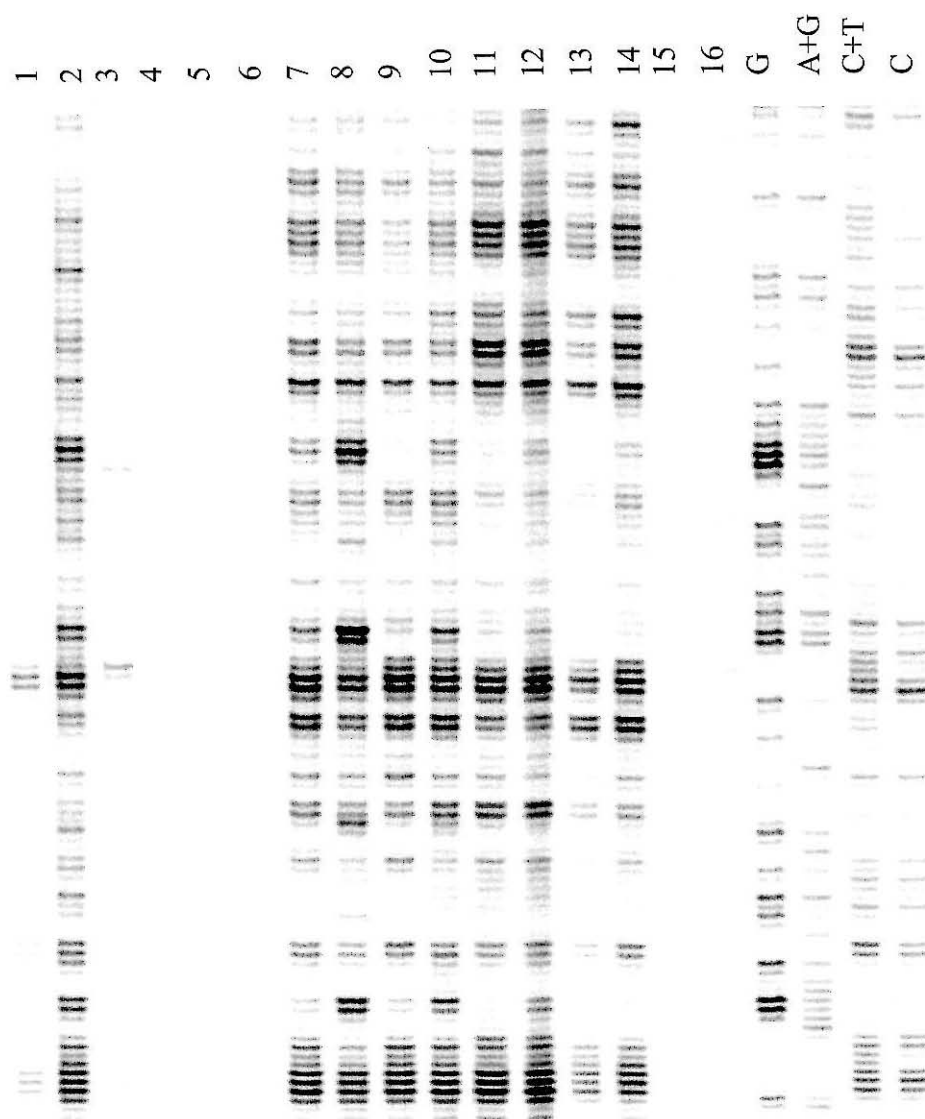


and endonuclease III repair enzymes showed a significant amount of damage, putatively direct photocleavage, despite the presence of one or two 360 nm band pass filters. These direct frank breaks were used to determine by LMPCR where on specific genes the metal complex was bound (*vide infra*). However, in general, treatment with a mixture of Fapy glycosylase and endonuclease III transformed the DNA into even smaller pieces, indicating that some damaged bases were also generated by the photoactivated rhodium complexes.

When amplified by ligation-mediated PCR, nuclear and bare DNA showed a pattern of direct frank breaks and enzyme-induced base damage (Fig. 6.4). The cellular DNA, however, showed almost no frank strand breaks when amplified by LMPCR, seemingly contrary to the results of the denaturing agarose gel which showed a large direct strand break frequency (26). The hydrogen abstraction reaction generates a variety of frank strand breaks with different termini, but only DNA breaks which have 5' phosphoryl ends are available for ligation and subsequent amplification by PCR. Therefore, it is possible that most of the $\text{Rh}(\text{phi})_2\text{DMB}^{3+}$ frank break sites generated intracellularly are not amplified and thus are not represented on the gels. Treatment of the cellular DNA with Fapy glycosylase and Endonuclease III followed by LMPCR, on the other hand, revealed a significant amount of damage which is not particularly sequence-specific, consistent with Fapy glycosylase/EndoIII trimming the different frank break termini down to 5' phosphoryl ends. This proposal stands somewhat in contrast to previous characterization of the products of rhodium hydrogen abstraction, which indicated that 5' ends generally maintain phosphoryl groups (Fig. 1.4, 28).

Interestingly, frank strand breaks with 5' phosphoryl ends must be generated in larger proportions on bare DNA and on nuclear DNA, since a strong LMPCR signal is observed in the absence of Fapy glycosylase/Endo III for these

Figure 6.4: Ligation-mediated PCR amplification of cellular, nuclear, and bare genomic DNA. Primers for the forward strand of the PGK promoter were used. “Dark control” samples were incubated with rhodium but not photoirradiated; “light control” samples were photoirradiated but not incubated with rhodium. Details of sample preparation are described in the text. Maxam-Gilbert sequencing lanes are shown at the right. Lane **1**: cellular DNA, **2**: cellular DNA with Fapy/EndoIII; **3**: cellular DNA, dark control; **4**: cellular DNA, light control; **5**: nuclear DNA, dark control; **6**: nuclear DNA, light control; **7**: nuclei with polyamines, **8**: nuclei with polyamines and with Fapy/EndoIII; **9**: nuclei no polyamines; **10**: nuclei without polyamines with Fapy/EndoIII; **11**: bare DNA (33 μ M Rh); **12**: bare DNA (33 μ M Rh) with Fapy/EndoIII; **13**: bare DNA (8 μ M Rh); **14**: bare DNA (8 μ M Rh) with Fapy/EndoIII; **15**: bare DNA dark control; **16**: bare DNA light control. Note that there are virtually no bands in the lane for cellular DNA treated with photoexcited rhodium but without Fapy/Endo III treatment, despite the fact that this DNA was cleaved by the metal complex (Fig. 6.3, lane 2), indicating that the products of rhodium photocleavage under these conditions may not have 5' phosphoryl ends. The light and dark control lanes are similarly virtually empty, demonstrating that both rhodium and light are necessary to cleave the DNA. Note also the similarity between the nuclear samples irradiated in the presence and absence of polyamines (lanes 7 and 9, and lanes 8 and 10), which differ only in the intensity of the bands at multiple guanine sites.



samples. Furthermore, the patterns of enzyme-revealed damage on bare DNA and nuclei, which are very similar to each other, are somewhat different from the damage pattern on cellular DNA. These distinctions are not related to DNA charge transport, since the damage under consideration is frank strand breaks generated by hydrogen abstraction; instead, it probably reflects the different products generated by hydrogen abstraction from the ribose sugar of DNA in the presence and absence of oxygen. Alternatively, the differences may reflect some greater amount of protein crosslinking in the cellular samples compared to the nuclear samples. Regardless of the cause, however, this twist of rhodium photochemistry complicates the analysis of rhodium binding and base damage by charge transport in cellular DNA, since the methods for determining rhodium binding, footprinting, and base oxidation rely on having a clear LMPCR signal both before and after treatment with Fapy glycosylase and endonuclease III. Therefore, we examined charge transfer in isolated nuclei as a model system for the native nuclear environment.

6.3.2 Direct Photocleavage and Guanine Base Oxidation in the p53 Gene

The damage induced by $\text{Rh}(\text{phi})_2\text{DMB}^{3+}$ and near-ultraviolet light in nuclear DNA was monitored first on exon 5 of the p53 gene. Some frank strand breaks are present across the exon, indicating that the rhodium complex intercalates throughout the DNA (Fig. 6.5a). As published previously, although the complex shows no high site-specificity, there is a minor preference for the pyrimidine-containing strand of a base pair (18,28,29). Treatment with the mixture of base excision repair enzymes Fapy glycosylase and EndoIII causes new bands to appear. The difference between DNA samples before and after Fapy glycosylase/EndoIII treatment represents the base damage (Fig. 6.5b). The

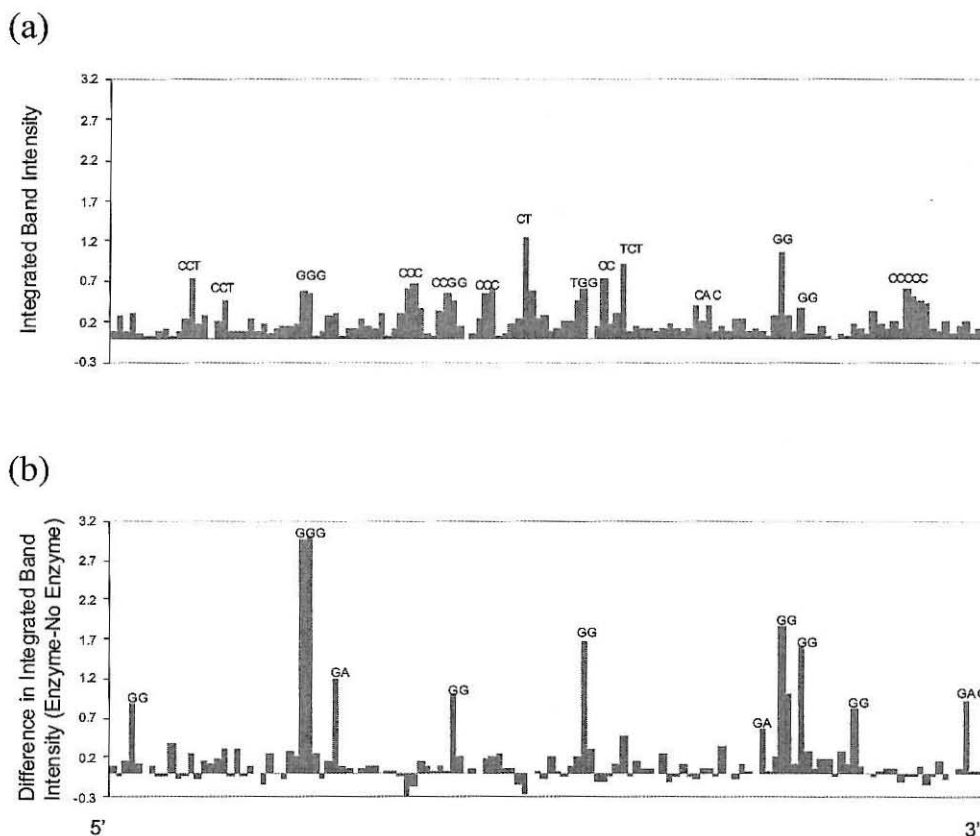


Figure 6.5: DNA damage promoted by photoactivated $\text{Rh}(\text{phi})_2\text{DMB}^{3+}$ on exon 5 of the p53 gene inside of isolated nuclei. (a) Frank strand breaks corresponding to the rhodium complex binding sites are shown. The complex binds in a fairly sequence-neutral fashion, although it prefers to cleave at the sugars of pyrimidines (25,30). About 25 bp are excluded from each end of the exon for clarity on the histogram. (b) Base damage is subsequently revealed by treatment with Fapy glycosylase/EndoIII base excision repair enzymes. The most heavily oxidized site is the sole 5'-GGG-3' site in this exon, followed by the 5'-GG-3' and 5'-GA-3' sites, fully consistent with oxidation by $\text{Rh}(\text{phi})_2\text{DMB}^{3+}$ from a distance through the DNA π -stack (38,39).

most heavily damaged positions are the 5'-GGG-3' trinucleotide and the 5'-GG-3' dinucleotides, followed in intensity by 5'-GA-3' dinucleotides, which follows the order of their oxidation potentials. This pattern is fully consistent with electron transfer damage. In addition, base damage occurs preferentially at the 5' guanines of these sites rather than at the 3' guanines or adenines. A 5' bias is characteristic of charge transfer damage but inconsistent with damage by singlet oxygen or other reactive oxygen species (19,21). The damage seen at guanine doublets and multiplets is not caused by the light source or any component of the buffer, as both frank strand breaks and oxidized bases are absent in the absence of rhodium.

Though the DNA damage generated inside of nuclei occurs at 5'-GG-3' sites, consistent with a DNA charge transfer reaction, these data do not firmly establish that base oxidation occurs from a distance. To explore the possibility of oxidative damage from a distance inside the nucleus, we examined a promoter region where rhodium binding should be selectively inhibited by the presence of transcription factors bound to the DNA (Fig. 6.6). If guanine doublets are oxidized at these sites where the rhodium complex cannot bind directly, then oxidative damage must occur by a long-range mechanism. Furthermore, the dual nature of the rhodium photochemistry can be used to demonstrate directly that intercalation and oxidation occur at spatially distinct sites. Direct backbone scission by phi complexes of rhodium has been used to footprint restriction enzymes and even distamycin, a small minor-groove-binding molecule, on restriction fragments (29). Conversely, long-range oxidation has been shown to occur through protein binding sites if the proteins do not disturb the DNA base stack (30).

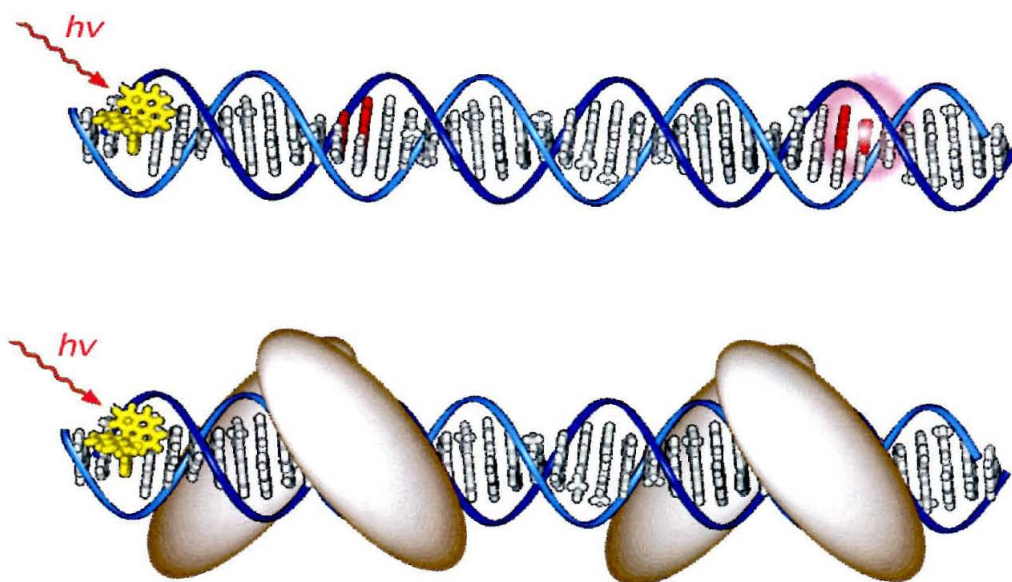


Figure 6.6: Assay for oxidation of guanine from a distance by $\text{Rh}(\text{phi})_2\text{DMB}^{3+}$ inside of isolated nuclei. To determine whether charge transfer can occur *at long range* on DNA inside of nuclei (top), the oxidation of guanines which are protected from direct access of the rhodium complex was monitored in the presence of stable DNA-binding proteins. Oxidation of these guanine sites must occur from a distance (bottom).

6.3.3 Direct Photocleavage and Guanine Base Oxidation in the PGK Promoter Region

Rhodium binding and oxidation were examined in the promoter region of the phosphoglycerate kinase gene (PGK1), for which the transcription factor binding pattern is well characterized (Fig. 6.7) and for which LMPCR primers and protocols are well-established (27,31). This region features two GC boxes, containing three consensus binding sites for the Sp1 zinc-finger transcription factor, as well as a CCAAT-sequence and region with reasonable homology to two transcription factor NF1 binding sites.

A comparison of the pattern and intensity of rhodium-induced frank strand breaks on naked DNA to that on DNA isolated from nuclei reveals clear footprints on the LMPCR sequencing gel. Rhodium binding and direct DNA backbone cleavage are diminished by the proteins bound to this promoter within the nucleus. In the NF1-like region, for example, the intensity of frank strand breaks is decreased noticeably on the transcribed strand, corroborating protein binding at this site (Fig. 6.8a, lanes 2-3). On the nontranscribed strand, frank strand breaks by rhodium are rare in the NF1-like region, both on rhodium-treated naked DNA and DNA isolated from nuclei, because this strand is purine-rich. Nevertheless, strong oxidative damage is apparent and is enhanced at the central 5'-GGG-3' site on the DNA isolated from rhodium-treated nuclei compared to naked DNA (Fig. 6.8b, lane 4).

Results of direct photocleavage and base oxidation by $\text{Rh}(\text{phi})_2\text{DMB}^{3+}$ in the PGK1 promoter are shown as histograms in Figures 6.8. Photofootprinting by the rhodium complex is evident when the intensity of frank strand breaks in the rhodium-treated naked DNA is subtracted from that of DNA isolated from rhodium-treated nuclei (Fig. 6.9a). The strong footprint in the NF1-like region is seen clearly (red). Interestingly, this footprint appears to be displaced by a few

Figure 6.7: Sequence of a part of the upstream promoter region of the PGK1 gene, showing regions of the promoter which reproducibly bind transcription factors, as revealed by DNase I and DMS footprinting followed by LMPCR (23,31). Red, green, and blue (and to a lesser degree, cyan) regions showed a decrease in cleavage by DNase I *in vivo*, whereas italicized bases flanking the protein binding sites showed increases in cleavage. PGK is an X-linked gene which is constitutively active in normal male cells and in one copy in normal female cells. Although *HeLa* cells are derived from female cells, they contain only active X chromosomes. Any copies of PGK are active and demonstrate transcription factor footprints (23).

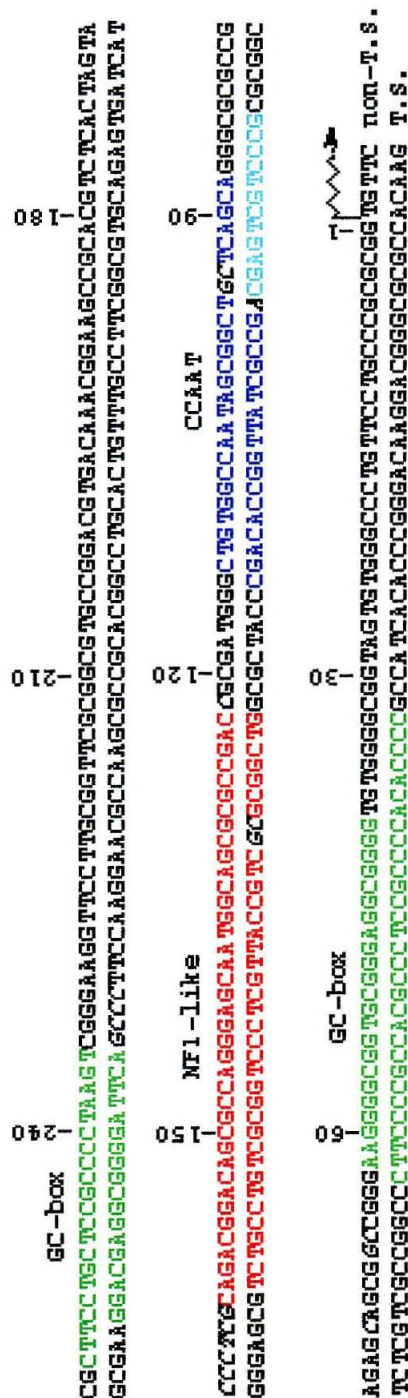
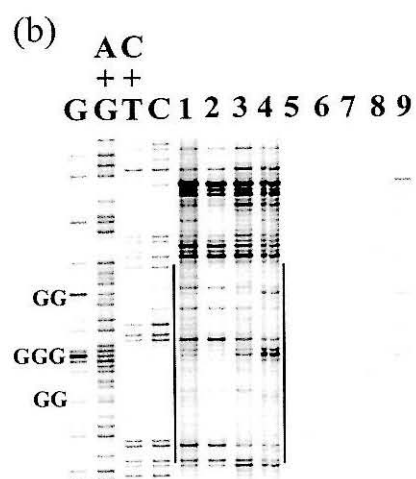
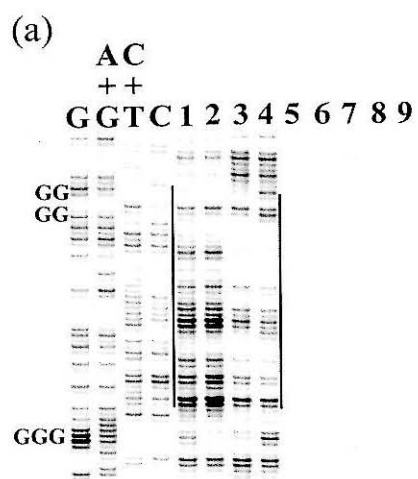


Figure 6.8: LMPCR-amplified DNA cleavage after treatment of bare DNA or nuclei with rhodium and photoactivation at the PGK promoter near the NF1-like binding site. (a) DNA cleavage on the **transcribed strand** (seq -113 to -175). The location of the bound protein as determined by DNase I is indicated by dark bracketed lines. Maxam-Gilbert sequencing lanes are shown at the right. All samples were treated with Fapy glycosylase/EndoIII, unless otherwise indicated. Lane 1: naked DNA, without Fapy glycosylase/EndoIII. 2: naked DNA. 3: nuclei. 4: nuclei, without Fapy glycosylase/EndoIII. 5: naked DNA without photoirradiation. 6: naked DNA without rhodium. 7: nuclei without photoirradiation. 8: nuclei without rhodium. 9: naked DNA without photoirradiation or rhodium. Note that there is a significant reduction in frank strand breaks between the naked DNA and nuclear DNA samples in the region of the NF1-like box (compare lanes 2,3), resulting in a footprint, and an increase in frank strand breaks flanking the NF1-like region toward the top of the gel. (b) DNA cleavage on the **nontranscribed strand** (seq -185 to -119). Lane 1: naked DNA without Fapy glycosylase/EndoIII. 2: naked DNA. 3: nuclei. 4: nuclei, without Fapy glycosylase/EndoIII. 5: naked DNA without rhodium or photoirradiation. 6: naked DNA without rhodium. 7: nuclear DNA without rhodium. 8: naked DNA without photoirradiation control. 9: nuclear DNA without photoirradiation. Note that although there are very few frank strand breaks in either the nuclear or naked DNA on this strand by which to establish protein binding (lanes 2,3), there is a strong enzyme-dependent band in the nuclear DNA lanes at the location of a 5'-GGG-3' site (lane 4).

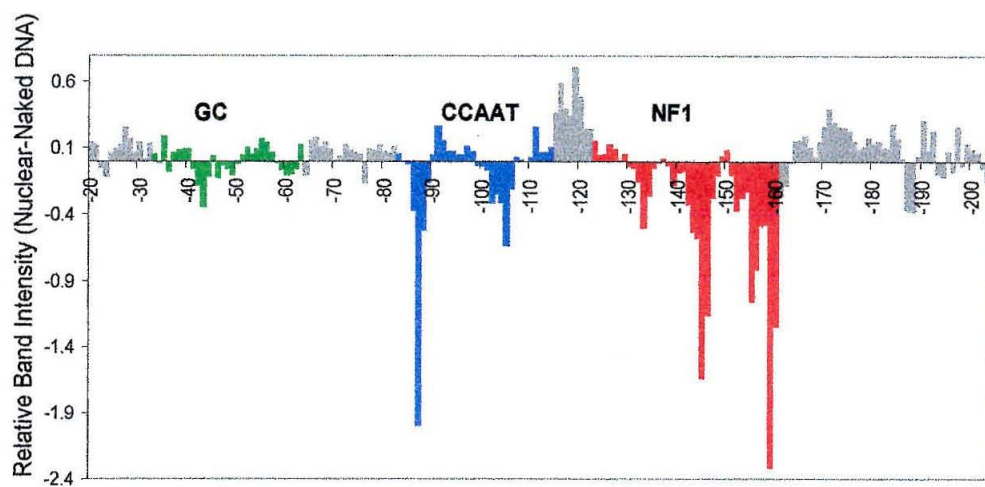


base pairs relative to that sequence footprinted using DNase I (23), and this shift is consistent with rhodium and DNase I binding and cleaving by different mechanisms and in different grooves of the helix (32). A significant decrease in frank strand breaks in nuclear DNA is seen also in the CCAAT box protein-binding region both on the transcribed strand (Fig. 6.8a) and the nontranscribed strand (not shown). It is noteworthy that frank strand breaks are increased in the region between the NF1-like and CCAAT box regions, indicating that rhodium intercalation is facilitated by binding of transcription factors to the DNA sequences flanking this region. Such a hyperreactivity has been seen previously (23,33). In the experiment illustrated here, only a weak footprint, at best, is seen at the GC-box proximal to the transcriptional start site (Fig. 6.9a-green); other cell preparations have shown more significant footprinting at this site. A strong footprint is also seen for the more distal GC-box, but on the complementary strand that contains mostly pyrimidines (not shown). As with the NF1-like box, in both GC boxes, frank strand breaks are seen preferentially on the cytosine-rich strand, which is characteristic of the rhodium complex.

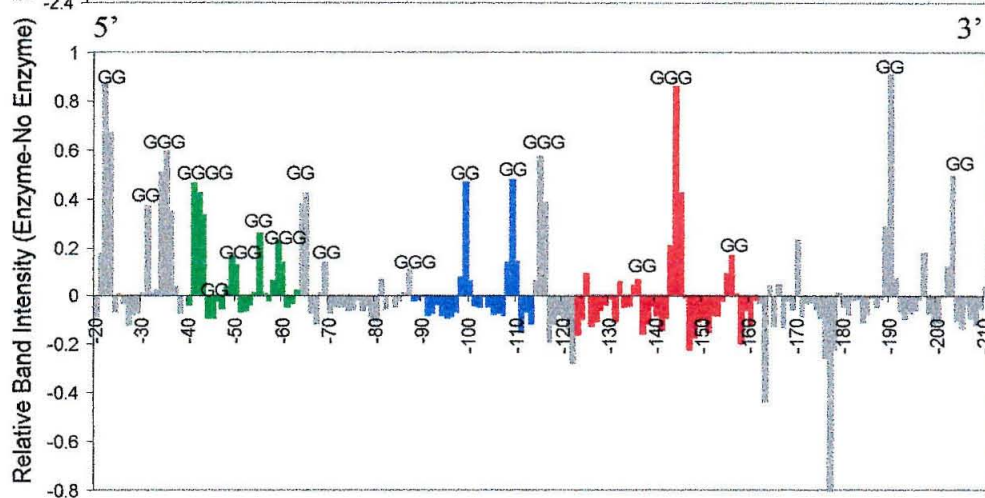
Importantly, despite the fact that rhodium binding is inhibited by transcription factors, significant oxidative base damage is still apparent. As seen earlier on the p53 exon, the base damage revealed by Fapy glycosylase/EndoIII treatment occurs at guanine multiplets (Fig. 6.9b). This 5'-GG-3' and 5'-GGG-3'-specific damage is fully consistent with a charge-transport mechanism for DNA damage in this region. Furthermore, the pattern of frank strand breaks indicates that rhodium binding is not uniformly distributed over the PGK promoter, yet guanine multiplets are damaged at sites footprinted for NF1, CCAAT, and the proximal GC box. Guanine multiplets are also preferentially damaged in the distal GC box on the complementary strand (not shown).

Figure 6.9: Binding and base damage by a rhodium metallointercalator in the PGK promoter region. (a) Difference between the frank strand breaks on the nuclear DNA and the naked DNA (transcribed strand). Colored regions correspond to the protein-binding domains (Fig 6.6). This difference histogram illustrates footprints in the transcribed strand at the CCAAT and NF1-like sequences and a “positive footprint” of increased sensitivity to rhodium binding/cleavage between the two proteins. (b) Base damage in nuclear DNA as revealed by Fapy glycosylase/EndoIII (nontranscribed strand). Guanine bases are preferentially oxidized, as in the p53 gene, and no footprints are apparent at the protein binding sites. (c) Plot of the intensity of all guanine damage in nuclear DNA expressed as a percentage of damage versus that on the bare DNA (nontranscribed strand), to compare directly the level of damage obtained within the nuclei versus that for DNA in the absence of bound protein. Damage to 5' guanines in guanine multiplets is enhanced in nuclei relative to naked DNA, but the small extent of damage at most of the *single* guanine sites and 3' guanines in nuclei is modestly diminished, especially in regions which are proposed to bind proteins. Since there appears to be no significant diminution in oxidation at protein binding sites, it appears that sites that are blocked from direct binding of the rhodium complex can be oxidatively damaged from a distance. Note that although both frank strand breaks at guanine and oxidative guanine base damage are represented in this histograms, the majority of the cleavage events are due to the latter reaction, especially at multiple guanine sites, due to the inherent sequence preferences of the two rhodium photoreactions.

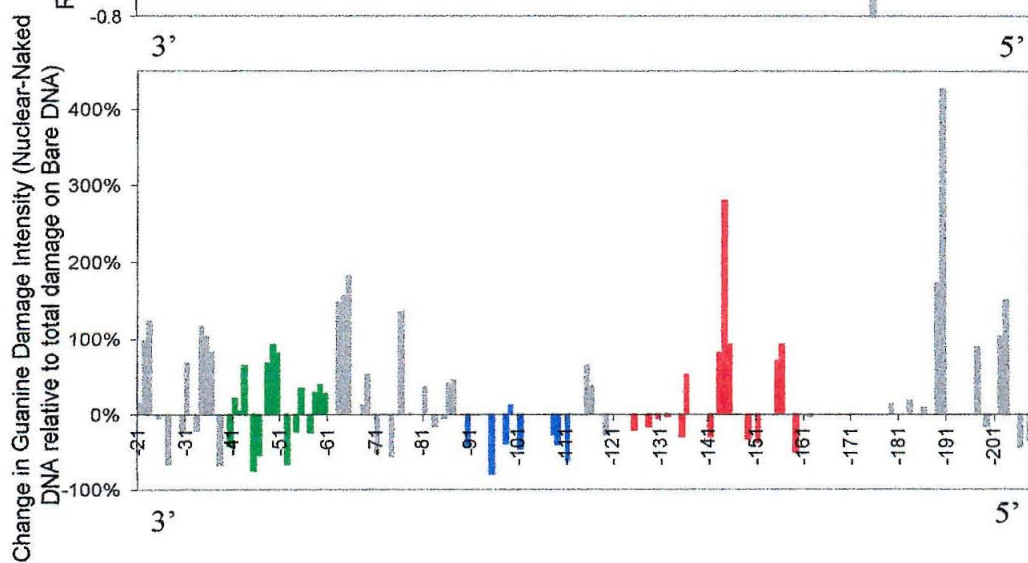
(a)



(b)



(c)



A plot of intensity of all guanine damage in nuclear DNA expressed as a percentage of damage versus that on the naked DNA can be used to compare directly the level of damage obtained within the nuclei versus that for DNA in the absence of bound protein (Fig. 6.9c). Damage to guanine multiplets is enhanced in nuclei relative to naked DNA, but the small extent of damage at most of the *single* guanine sites in nuclei is modestly diminished, especially in regions which are proposed to bind proteins. Within the NF1-like protein binding region, there is a small decrease in damage at single guanine sites, consistent with reduced rhodium binding and frank strand breaks in this region, but an increase in damage at the two 5'-GG-3' sites and a 300% increase in damage at the 5'-GGG-3' site. The strong oxidation at the 5'-GGG-3' site in the middle of this NF1-like binding sequence can be seen also clearly on the gel (Fig. 6.8b). This enhancement in long range oxidative damage with protein binding has been seen in studies of long range charge transport in the presence of DNA-bound proteins having the helix-turn-helix motif (30). Such enhancements may be due to the effects of increased rigidity in stacking on charge transport, or to changes in the trapping time of a radical intermediate. From these data it appears that long-range oxidative damage is favored over frank strand breaks inside of nuclei. Although it is possible that the favoring of one type of damage over another is a consequence of the experimental conditions, the overall similarity of the rhodium damage and the reproducibility of the damage under different experimental conditions indicates otherwise. This preference could result from a change in the type of base oxidation products in the nuclear environment, increased stiffening of the helix favoring long-range radical migration over short-range oxidation, or a slowing of the radical trapping time and increased radical equilibration time due to decreased oxygen accessibility to the helix caused by proteins and small molecules. Guanine damage within the CCAAT box and the proximal GC box also shows, in

general, an increase in the 5' guanines of guanine multiplets but a decrease in damage at 3' guanines or single guanines. Clearly, then, there is no significant diminution in oxidation across this promoter despite the presence of bound proteins. These data indicate that sites that are blocked from direct binding of the rhodium complex are nonetheless able to be oxidatively damaged. *Guanine oxidation therefore must occur through the DNA π stack from a distance.*

The distances over which this charge transport occurs cannot be established with certainty, given the many sites that are available to the rhodium complex. Nonetheless, the protein footprints are sufficiently large to conclude that guanine oxidation occurs from a distance of at least five or ten base pairs (17-34 Å) and possibly as far as thirty or more (100 Å). Establishing the upper distance limits of charge migration within the cell remains a goal.

Charge transport through DNA to effect oxidative damage at a distance has become well established (2-16). The data presented here extend DNA charge transport as a feasible mechanism for the generation of DNA base lesions within the cellular environment. DNA inside of cells is therefore susceptible to damage that arises from a remotely-bound site, indeed even at sites that are inaccessible directly as a result of protein binding. It will be worthwhile to examine known mutagens and therapeutic natural products to determine if they operate through a similar mechanism (34,35). It will also be important to determine whether organisms have evolved to protect their genomes from long range damage. Perhaps radical damage is funneled to or insulated from specific sites within the genome. We do not suggest based upon these data that radical migration occurs over megabase distances, and indeed studies on DNA restriction fragments would suggest that charge transport over those distances is not likely (10). One could, however, consider that segments throughout the genome may encode "sinks" for damage, and that other segments could serve as buffers as a result of local

sequence-dependent or protein-dependent structural deformations to protect critical regions. Certainly, the biological consequences and opportunities for DNA-mediated charge transport now require consideration.

6.4 References

1. E. C. Friedberg, G. C. Walker, W. Siede, DNA Repair and Mutagenesis. American Society for Microbiology Press, Washington DC (1995).
2. D. B. Hall, R. E. Holmlin, J. K. Barton, *Nature* **382**, 731 (1996).
3. S. M. Gasper, G. B. Schuster, *J. Am. Chem. Soc.* **119**, 12762 (1997).
4. S. O. Kelley, J. K. Barton (1998) in *Metal Ions in Biological Systems* (Sigel, A., and Sigel, H., Eds.) pp 211-249, Marcel Dekker, Inc., New York.
5. M. E. Núñez, J. K. Barton, *Curr. Op. Chem. Biol.* **4**, 199 (2000).
6. M. E. Núñez, D. B. Hall, J.K. Barton, *Chem. Biol.* **6**, 85 (1999).
7. P. T. Henderson, D. Jones, G. Hampikian, Y. Kan, G. B. Schuster, *Proc. Natl. Acad. Sci. USA* **96**, 8353 (1999).
8. D.B. Hall, J.K. Barton, *J. Am. Chem. Soc.* **119**, 5045 (1997).
9. S. R. Rajski, S. Kumar, R. J. Roberts, J. K. Barton, *J. Am. Chem. Soc.* **121**, 5615 (1999).
10. E. M. Boon, D. M. Ceres, T. G. Drummond, M. G. Hill, J. K. Barton, *Nat. Biotechnol.* **18**, 1096 (2000).
11. I. Saito, M. Takayama, H. Sugiyama, K. Nakatani, *J. Am. Chem. Soc.* **117**, 6406 (1995).
12. M. E. Núñez, K. T. Noyes, D. A. Gianolio, L. W. McLaughlin, J. K. Barton, *Biochemistry* **39**, 6190 (2000).
13. M. R. Arkin, E. D. A. Stemp, S. Coates Pulver, J. K. Barton, *Chem. Biol.* **4**, 389 (1997).
14. D. B. Hall, S. O. Kelley, J. K. Barton, *Biochemistry* **37**, 15933 (1998).
15. G. B. Schuster, *Acc. Chem. Res.* **33**, 253 (2000).
16. B. Giese, *Acc. Chem. Res.* **33**, 631 (2000).
17. C. L. Kielkopf, K. E. Erkkila, B. P. Hudson, J. K. Barton, D. C. Rees, *Nature Struct. Biol.* **7**, 117 (2000).

18. A. Sitlani, E. C. Long, A. M. Pyle, J. K. Barton, *J. Am. Chem. Soc.* **114**, 2302 (1992).
19. C. J. Burrows, J. G. Muller, *Chem. Rev.* **98**, 1109 (1998).
20. S. Steenken, S. V. Jovanovic, *J. Am. Chem. Soc.* **119**, 617 (1997).
21. H. Sugiyama, I. Saito, *J. Am. Chem. Soc.* **119**, 617 (1996).
22. F. Prat, K.N. Houk, C.S. Foote, *J. Am. Chem. Soc.* **120**, 845 (1998).
23. G. P. Pfeifer, A.D. Riggs, *Genes Dev.* **5**, 1102 (1991).
24. R. Drouin, H. Rodriguez, G.P. Holmquist, S.A. Ackman, in *Technologies for Detection of DNA Damage and Mutations*, G. Pfeifer, Ed. (Plenum Press, New York, 1996), pp 211-225.
25. R. Drouin, S. Gao, G.P. Holmquist, in *Technologies for Detection of DNA Damage and Mutations*, G. Pfeifer, ed., (Plenum Press, New York 1996) pp 37-43.
26. G.P. Pfeifer, R. Drouin, G.P. Holmquist, *Mut. Res.* **288**, 39 (1993).
27. S.-M. Dai, H.-H. Chen, C. Chang, A.D. Riggs, S.D. Flanagan, *Nature Biotech.* **18**, 1108 (2000).
28. A. Sitlani, J. K. Barton, *Biochemistry* **33**, 12100 (1994).
29. K. Uchida, A.M. Pyle, T. Morii, J.K. Barton, *Nucleic Acids Res.* **17**, 10259 (1989).
30. S.R. Rajski, J.K. Barton, *Biochemistry* **40**, 5556, (2001).
31. G. P. Pfeifer, R.L. Tanguay, S.D. Steigerwald, A.D. Riggs, *Genes Dev.* **4**, 1277 (1990).
32. T.D. Tullius, *Annu. Rev. Biophys. Biophys. Chem.* **18**, 213 (1989).
33. P.B. Dervan, *Science* **232**, 464 (1986).
34. H. Rodriguez, G.P. Holmquist, R. D'Agostino, Jr., J. Keller, S.A. Akman, *Cancer Res.* **57**, 2394 (1997).
35. H. Rodriguez, *et al.*, *J. Biol. Chem.* **270**, 17633 (1995).

Chapter 7

Long-Range Oxidative Charge Transport through DNA: Summary and Conclusions

7.1 Summary and Conclusions

The question of whether double helical DNA provides an effective conduit for charge transport has fascinated scientists since its structure was first elucidated. Eley and Spivey said of DNA in 1962, "These paired base units are thus arranged like a pile of coins along the helix axis, and their interplane spacing of 3.4 Å is similar to that for graphite. It seemed, therefore, reasonable to suppose that a DNA molecule might behave as a one-dimensional aromatic crystal and show π -conductivity down the axis" (1). That the stacking of base pairs not only confers stability to the polymeric assembly, but also may provide a basis for charge transport, has been examined using a diverse range of experiments, yielding substantially different conclusions (reviewed in 2,3). Physicists have tested the electrical conductivity of DNA, beginning with straightforward measurements carried out on ill-defined pellets, to more sophisticated studies on single molecules, and their conclusions have ranged from DNA being an insulator to a quantum wire. Radiation biologists observed that ionizing radiation selectively generates guanine radical cations and cytosine radical anions on DNA, consistent with charge migration through the DNA. The use of chromophores that bind to DNA to examine charge transfer through DNA spectroscopically provided a substantial advance in the field. In the first systems, involving donor and acceptor molecules bound non-covalently to the DNA, a variety of answers emerged about the ability of DNA to conduct charge. Later systems featured donors and acceptors bound covalently at fixed distances on defined oligonucleotide assemblies. Even in these systems the rates and efficiencies of electron transfer through DNA vary considerably, but in general the studies concluded that charges can migrate through DNA. The efficiency and rate of this charge transfer appears to depend on the contact of the donor and acceptor molecules with the DNA base pair stack. When there is good π -orbital overlap

between the DNA and the reactants, fast, efficient charge transfer is possible in a variety of systems.

Not only can electron transfer mediated by the DNA be facile, but the π -stack can serve as a reactant in the electron transfer process. Radicals can migrate through the helix to react at a remote site from the oxidant. Oxidative damage to DNA *from a distance* was first demonstrated in an assembly containing a tethered rhodium intercalator as the photooxidant, spatially separated from the sites of oxidation, 5'-GG-3' sites (4). As in electron transfer monitored spectroscopically, oxidative damage to DNA mediated by the base pair stack shows a shallow dependence on distance, but an exquisite sensitivity to stacking (5). This ability to mediate long range charge transport is a characteristic of the DNA duplex, not the oxidant, since a variety of different intercalators have been shown to oxidize guanine doublets from a distance (6-9).

It is within this context that the work described in this volume began. Work by physicists and radiation biologists indicated that charge transfer could happen on long DNA's, but the studies routinely used poorly characterized DNA's and examined its bulk properties. Alternatively, these scientists frequently examined the DNA in non-biological situations, such as in ice at very low temperatures, or under vacuum after drying. Other biologists looked at radiation damage in whole cells, but not with base pair resolution or with an ability to determine distances. Studies by chemists indicating that charges could move in DNA utilized well-characterized DNA in aqueous solution and fixed reactant distances, but the distances examined were short and the DNA was bare of any proteins or other small molecules native to the cell nucleus. Since charges had been demonstrated to move efficiently through DNA oligonucleotides, and since there was some indication that charge migration could occur on longer pieces of DNA as a result of some kinds of DNA damage, it was important to

characterize charge transport reactions in more detail, and to extend observations of charge transport through DNA from oligonucleotides to larger and more complicated but still well-defined DNA assemblies that more closely mimic its structure *in vivo*. We chose to examine the mechanisms of long-range oxidative damage to guanine bases in DNA within a more complicated and dynamic model of our genetic material.

First, we examined the distance dependence of long range charge transport using long oligonucleotides, demonstrating that electronic “holes” generated by a one-electron oxidation of DNA can result in permanent lesions on guanine bases up to 200 Å away from the intercalating oxidant as a result of such charge migration. Both rhodium and ruthenium complexes, covalently tethered to the 5' end of a double-stranded oligonucleotide and intercalated into the base stack, can with photoactivation promote oxidation of guanines in 5'-GG-3' sites over this distance. These studies also shed some light on the mechanism of oxidative charge transport through DNA. Excited-state rhodium metallointercalators are better able to oxidize distal guanine bases than are ground-state ruthenium oxidants, hinting that the characteristics of the intermediate generated on the DNA may depend on not only the DNA itself but the oxidant as well. The efficiency of long-range oxidation of guanine doublets was also seen to depend on temperature, probably via the effects of changing temperature on the flexibility of DNA in solution.

The upper distance limits and sequence effects on long-range charge transfer through DNA were examined further using a variety of intercalating photooxidants targeted to a specific site on a restriction fragment by an appended triplex-forming oligonucleotide. Charge migration occurs in both directions from the intercalator and on both DNA strands of the target, but the oxidation is significantly more efficient to the 3' side of the triplex, over 25-38 base pairs.

When intercalators were tethered directly to the 5' terminus of the triplex-forming strand as opposed to the center, significant amounts of oxidative damage was generated only in the immediate vicinity of the intercalation site, suggesting that the base stack is distorted at the 5' end of the triplex region in the duplex/triplex junction. Targeting of photooxidative damage by triplex formation extends previous studies of long-range charge transport to significantly longer DNA sequences through a strategy that does not require covalent attachment of the photooxidant to the DNA being probed.

Charge transport can also promote another reaction from a distance: the repair of a thymine cyclobutane dimer lesion (10). Long-range oxidative damage to guanine doublets in DNA is shown to compete for oxidation with this thymine dimer repair on oligonucleotide duplexes with covalently-tethered rhodium intercalators. When both thymine dimer lesions and guanine doublets are present, both can be oxidized by a photoexcited rhodium complex, although each in lower yield than in the absence of the other. This competition is interesting because the 5-GG-3' is by far the thermodynamically favored site for oxidative reaction, but repair of the thymine dimer appears to be kinetically more favorable. Therefore, electronic "holes" generated on genomic DNA might not of necessity cause DNA damage, but could also be funneled onto proteins or other oxidizable sites that are accessible via the DNA base stack. Furthermore, an electronic "hole" generated as an intermediate by the oxidation on the DNA cannot merely hop from guanine base to guanine base along the DNA, but must at least transiently be associated with the pyrimidine orbitals as well as it migrates.

Since DNA is intimately associated with a large number and variety of proteins *in vivo*, it is of critical interest for us to examine their effect upon long-range charge transport. Using a variety of DNA-binding proteins, it was shown that protein binding to DNA can sensitively modulate charge transfer through the

helix, depending on its effect on π stacking (11). Within eukaryotic cells most DNA is packaged as nucleosome core particles, made up of ~146 base pairs of DNA wrapped around a core of histone proteins (12). Photoexcited rhodium complexes were also used to explore charge transport through DNA within reconstituted core particles *in vitro*. Although histone proteins inhibit intercalation of a noncovalent rhodium complex, they do not prevent oxidation of 5'-GG-3' sites, the signature of oxidative charge transport through DNA. Furthermore, some of these sites are not directly accessible to a solution-bound oxidant due to histones in the major groove, and thus they must be oxidized from a distance. Therefore, although the structure of the nucleosome core particle generally protects DNA from damage from solution-borne molecules, it does not protect the DNA from charge transfer damage through the base pair stack. In support of this assertion, guanine bases within nucleosomal DNA were oxidized at a distance of over 23 base pairs from a covalently-tethered rhodium intercalator, and the efficiency of this long-range oxidation was not significantly changed by the binding of the DNA to histone proteins within the nucleosome core particle.

The environment within the cell nucleus contains a variety of other proteins and small molecules that could potentially influence the migration of charge through DNA. Using the rhodium photochemistry, the oxidation of guanine by photoexcited rhodium complexes inside of nuclei from cultured human cells was examined and compared with the oxidative damage on bare genomic DNA. As on oligonucleotides, restriction fragments, and nucleosomes, oxidation occurs preferentially at the 5'-guanine of 5'-GG-3' sites, indicative of base damage by DNA-mediated charge transport chemistry. Moreover, oxidative damage occurs at multiple-guanine sites which are inaccessible to the rhodium complex due to the binding of transcription factors in the major groove. Thus,

DNA-mediated charge transport acts to induce base damage from a distance even within nuclei.

DNA can be modified in a staggering variety of ways, leading to any number of different kinds of damage lesions. Radicals can be generated on the DNA bases using ionizing radiation, high-energy ultraviolet light, reactive oxygen species, or photosensitizing oxidants (13). Oxidative damage to DNA by long-range charge transport was described here, wherein an electron is abstracted from the DNA at one place but damage is ultimately localized to a remote site. Given the number of different pathways in which a radical can be generated on the DNA bases, charge transport through DNA may in fact be a common mechanism by which DNA is damaged. It is therefore critical to re-examine other DNA damage agents to determine whether charge transport is involved in their mechanism of damage, and to reconsider the design of DNA-based drugs and therapies to take into account this powerful mechanism for DNA modification. Furthermore, all of these observations indicate that charges can migrate along DNA within the cell, spreading damage away from an initial site to divergent distal sites, potentially within transcriptionally inactive or packaged regions of the DNA. This distribution of damage to divergent or less-accessible sites is likely to adversely affect the ability of the repair machineries to find and remove damaged bases from the genome. It will be interesting to see what role DNA charge transport is ultimately revealed to play in DNA damage inside the cell.

7.2 References

1. D.D. Eley, D.I. Spivey, *J. Chem. Soc, Faraday Trans.* **58**, 411 (1962).
2. S. O. Kelley, J. K. Barton, *Metal Ions in Biological Systems* **26**, 211 (1998).
3. M. E. Núñez, J. K. Barton, *Curr. Op. Chem. Biol.* **4**, 199 (2000).
4. D. B. Hall, R. E. Holmlin, J. K. Barton, *Nature* (London) **382**, 731 (1996).
5. D. B. Hall, J. K. Barton, *J. Am. Chem. Soc.* **119**, 5045 (1997).
6. M. R. Arkin, E. D. A. Stemp, S. Coates Pulver, J. K. Barton, *Chem. Biol.* **4**, 389 (1997).
7. D. B. Hall, S. O. Kelley, J. K. Barton, *Biochemistry* **37**, 15933 (1998).
8. G. B. Schuster, *Acc. Chem. Res.* **33**, 253 (2000).
9. I. Saito, M. Takayama, *J. Am. Chem. Soc.* **117**, 5590 (1995).
10. P. J. Dandliker, R. E. Holmlin, J. K. Barton, *Science* **275**, 1465 (1997).
11. S. R. Rajsiki, J. K. Barton, *Biochemistry* **40**, 5556 (2001).
12. B. Lewin, *Genes VII*, Oxford University Press, Oxford, England (2000).
13. E. Friedberg, G. Walker, W. Siede, *DNA Repair and Mutagenesis*, ASM Press, Washington, D.C. (1995).